Dynamic Approach to Behavior-Based Robotics

Design, Specification, Analysis, Simulation and Implementation

Dissertation submitted by
Estela Bicho
to the University of Minho
for the Degree of Doctor on Industrial Electronics
in the Branch of Automation and Control

Guimarães, Portugal

September, 1999

Scientific adviser:

Dr. Gregor Schöner
Directeur de Recherche
Centre de Recherche en Neurosciences Cognitives
Centre National de la Recherche Scientique (CNRS)
Marseille, France

Defense committee:

Prof. Werner von Seelen
Institut für Neuroinformatik
Ruhr-Universität Bochum
Germany

Prof. Isabel Ribeiro
Institut of Robotic Systems
Technical University of Lisbon
Portugal

Prof. Carlos Couto
Department of Industrial Electronics
University of Minho
Portugal

Prof. Francisco Vaz
Department of Electronics and Telecommunications
University of Aveiro
Portugal

Dr. Gregor Schöner
Directeur de Recherche
Centre de Recherche en Neurosciences Cognitives
Centre National de la Recherche Scientique (CNRS)
Marseille, France

Defence's date:

10^{th} December 1999

To Wolfram...

Acknowledgements

I am indebted to many people for their contribution to my knowledge and for their help in many ways during these past years.

I wish to express my sincere gratitude to my scientific adviser Dr. Gregor Schöner, from the CRNC-CNRS in Marseille, who initiated me into science and who has accompanied me during the past years. I had the pleasure to experience and profit from his brilliance, his friendship and his unconventional ideas. Furthermore, traveling and discussing with him around the world was a deep pleasure.

I want to thank Prof. Francisco Vaz, from the Department of Electronics and Telecommunications at the University of Aveiro, for his humanity and for making my scientific life possible at first place.

Thanks are also due to Prof. Carlos Couto, from the Department of Industrial Electronics at the University of Minho, for his interest and continuing institutional support.

I wish to express my respect to Prof. Keith Doty and Scott Jantz, from the Machine Intelligence Laboratory at the University of Florida in Gainsville, for their knowhow in building autonomous robots. I am indebt for their contribution to my knowledge in behavior-based robotics.

Pierre Mallet, who worked with me in the "Equipe de Dynamique" at the CRNC-CNRS in Marseille, deserves my deepest thanks for constructing Robodyn and for his continuing support and confidence. I also thank him for his careful reading of the manuscripts.

I am grateful to Prof. von Seelen for his generous hospitality at the "Institut für Neuroinformatik" in Bochum. The stays in his institute and the interactions with my "dynamical peers" were fundamental for the final phase of my thesis.

I am indeed indebted to Wolfram Erlhagen, Rainer Menzner and Axel Steinhage for careful proof-reading, for their interest and their helpful comments on this thesis. They were always there to help in any situation. Thanks also due to Martin Giese.

My thanks also go to Michael Neef for his quick and excellent assistance in technical issues.

I am grateful to the members of the "Dynamikgruppe" for making my participation possible in the Friday meetings.

At the CRNC-CNRS in Marseille I would like to express my gratitude to Dr. Catherine Thinus-Blanc, Francesca Acerra, Françoise Joubond, Nicolas Mathian, Michelle Coulmance and Alexa Riehle.

The institutional support provided by Profs. Hendler and Krisnhaprasad at the University of Maryland, USA, are gratefully acknowledged.

My thanks also go to my Portuguese colleagues and friends Jorge Cabral, Paula Cravo, Graça Minas, Teresa Peixoto, Fernando Ribeiro, João Rodrigues, Cristina

Santos and Ana Seca who helped me in many ways.

To Wolfram, more words of gratitude are spoken from my heart. I thank him for his extensive support, companionship and for the adventure that our life is. His help has been fundamental during the final phase of this thesis. Furthermore, I have the privilege of having a husband with such an immense knowledge in Neural Field Dynamics. To our families I wish to express my gratitude for their endless support.

Grant support was provided through the "Fundação para a Ciência e a Tecnologia" of the Portuguese Ministry of Research (grant PRAXIS XXI/BD/2949/94) and the "Groupement d'Intérêt Scientifique 'Cognition' " of the French Ministry of Research.

Bochum, 26 de Setembro de 1999

Contents

Chapter 1

Introduction

The aim of this thesis is to investigate how behavior-based robots can be modeled by non-linear dynamical systems. Taking the example of navigation as a case study, dynamic control architectures are developed and implemented on low-level vehicles. These architectures combine a number of behaviors and lead to flexible and smooth overt behavior which is stably coupled in closed loop with sensory information. Moreover, these architectures also comprise dynamical representations of information which enable the vehicles to exhibit cognitive behaviors such as decision making, memory, forgetting and robustness against noisy sensory information. The design of the individual behaviors, of the representations of particular types of information, as well as of their coupling is based on the qualitative theory of dynamical systems and dynamic field theory. These provide a general theoretical language in which autonomous robot architectures can be built.

1.1 Autonomous robotics

A *robot* is frequently viewed as an artificial worker that executes tasks traditionally performed by humans based on detailed action plans. In modern industrial robots these action plans take the form of digital computer programs. Control and sensing is used primarily to assure the precise execution of these plans. The programming of a robot is done by the engineer and/or the operator through various programming interfaces, including, in their most advanced form, highly interactive interfaces.

From the very beginning of robotics, the idea of *autonomous robots* has fascinated researchers. An autonomous robot would essentially program itself, that is, develop adequate action plans based on sensory information acquired by the robot itself. Autonomous robots would come close to a machine version of intelligently acting human operators. In particular, operation in non-engineered or natural environments as required in many maintenance, construction, repair, or supervision tasks, necessitates some degree of autonomy of the robot. Because of the elevated anticipated cost of such "intelligent" agents, their use has been initially projected to be primarily in areas where human operation is either extremely expensive or

dangerous such as in underwater, outer space, or radioactive environments. It is, however quite thinkable, that such robots, once viable, would find a large field of applications right down to the classical "household" robot that has been the topic of so many amusing science fiction fantasies and science fact.

For researchers the challenge has been to enable a machine to emulate the behavioral, perceptual, and cognitive skills of humans and animals, and to investigate how an artifact can successfully interact, in real time, with an uncertain, dynamic environment.

The classical approach to the problem of autonomous robotics has been developed since the fifties in close alliance with the discipline of artificial intelligence (McCarthy, Minsky, Rochester and Shannon, 1955; Nilson, 1969). The basic idea is that an intelligent robot requires an abstract model of the environment where it is supposed to operate. In this approach a robot is structured along the stream of information through the system, from sensing and sensory processing, through a central representation of the world (often symbolic in nature) that is to be derived from the processed sensory data, to a planning stage, which is read out to a layer of controllers that bring about the actual execution of the action plan. In these systems behavioral responses emerge from the interplay of the planner with given goals, and the particular world model that has been constructed from the sensory data. The main strength of this approach is the high degree to which it has been formalized theoretically. Its main drawback remains the frustratingly limited practical success of robots based on this idea when the goal is to behave autonomously in dynamic, non-engineered environments. The problem of deriving a general purpose representation of the world as well as of devising action plans within such a representation have turned out to be exceedingly difficult to solve. For example, it turned out that an accurate metric or symbolic model of the environment is very hard to obtain from noisy sensor data. In addition, building such representations is extremely time consuming.

1.2 Behavior-based robotics

Since the mid-eighties, an initially radical alternative has been proposed that has since gradually become one of the main stream views. This approach has become known as *behavior-based robotics* [1] (review e.g., Brooks, 1991; Mataric, 1992; Brooks, 1997; Mataric, 1998; Arkin, 1998). Brooks proposed that autonomous robot architectures should be organized in a manner that is essentially orthogonal to the classical architecture: Rather than structuring the system along the information stream into stages of feed-forward information processing, the system is divided into multiple behavioral modules, each of which entails all stages of information process-

[1] Although radical at the time this approach was not in fact entirely new. The work of Walter (1953) on building electronic machines as a tool to unravel the intricacy and complexity of the brain is prototypical of this approach to robotics.

ing, but each with a particular different task or behavior in mind. The individual behaviors would not by themselves possess any form of "intelligence". However, by providing an architecture that couples the various behavioral modules, the complete system would exhibit the property of flexible reorganization under the influence of its own sensory information that is the defining feature for an autonomous robot. The architecture of elementary behavioral modules and their interaction is therefore the backbone of behavior-based robots. Representations when needed are adapted to the specific ability of a behavioral module.

The main argument in favor of this approach was its impressive and rapid practical success. Tasks that were previously considered very difficult, such as navigation of a walking machine in an environment containing non-geometrical obstacles, were solved by relatively small and inexpensive robots that had been developed within a few months (Brooks, 1989). As the field matured it became apparent, however, that there are also a number of serious problems that must be solved for the approach to be ultimately viable for real world applications. The main source of trouble seems to be the rather untheoretical nature of the entire approach. This makes it very hard to design such robots other than by having extensive experience with the prototype. This also severely limits, of course, the generalization of the architectures beyond the simple experimental robots that have been produced and studied. This problem is exacerbated by the intrinsic difficulty encountered when attempting to debug and diagnose failures in an autonomous robot: The artifact will react non-trivially and non-locally by reorganization to errors in any of its modules, not unlike nervous systems do. Another drawback of this approach is the surprise emergence of unpredictable overt behavior. Although emergent behaviors might be interesting in the study of artificial organisms, is an objectionable feature when the robot must behave in a particular and desired purposive way. Such emergent phenomena arise because the internal behavior structure of the system does not necessarily mirror its externally manifested behavior. Behaviors are activated in response to external and/or internal conditions, that is, sensory inputs and internal state. The system as a whole activates subsets of behaviors so that parallelism can be exploited in the resulting dynamics. As pointed out by Mataric (1998) in a recent review this is still a critical aspect of behavior-based control: as multiple behaviors or modules are active, dynamics of interaction arise both within the system itself (from the interaction among the behaviors) and within the environment (from the interaction of the behaviors with the external word). Still another problem is how dedicated representations appear within the architecture of an autonomous robot and how they couple to behavioral modules to which they are dedicated.

This dissertation aims to contribute to the solution of these central problems of the behavior-based approach to autonomous robotics. The motivation comes from recent studies which show that methods from dynamical systems theory can be used as a tool, conceptual framework and theoretical language to describe the dynamic coupling between the robot and its environment (Schöner, Dose and Engels, 1995; Beer, 1995; Smithers, 1994). The potentiality of these approaches to

develop autonomous robotic systems became not yet fully evident nor accepted. Brooks (1997), in his paper "From earwigs to humans", when referring to these approaches writes:

"The jury is still out as to whether these analysis tools will lead to great conceptual or practical advances."

The goal of this thesis is therefore to investigate how dynamical systems can be used in the design, specification, analysis, simulation and implementation of behavior-based robots.

1.3 The Dynamic Approach: Aims of this dissertation

The work presented in this thesis is based on the so called *Dynamic Approach to Robotics* proposed by Schöner and Dose in 1992 (see Schöner, Dose and Engels, 1995, for a review). The basic ideas of this approach are:

a) Describe and parameterize behaviors through task-related variables, called *behavioral variables*, that abstract from effector degrees of freedom and peripheral sensor coordinates and in addition have an appropriate degree of invariance under changes in the environment the system interacts with.

b) Generate behavior in time as attractor solutions of dynamical systems, which take the form of ordinary differential equations.

c) Erect these dynamical systems from sensory information or from internal representations.

d) To generate representations the dynamics take the form of dynamic fields.

The approach was developed initially as a method of planning within representations of the navigable space (Schöner and Dose, 1992; Engels and Schöner, 1995). Previous implementations involved large scale platforms with several onboard and off-board computer systems. Sensory information was visual and provided high precision information. The implementations required extensive computations and were not always realized in closed loop with sensory information. More recently, surprisingly complex behavior has been achieved but only at the simulation level (Steinhage, 1998).

Implementations on low-level platforms is a non-trivial task and has not been attempted before. Some questions concerning the extension of the Dynamic Approach to low-level robots are:

- Is the approach essentially limited to high-level systems, more in the line with the classical approach, or conversely, can it be made to function in computationally weak systems based on very low-level sensory information, more in the line with the behavior-based approach?

  How can this approach be applied to lower level vehicles, which know nothing about external reference frames, nothing about objects resting in the world, but have only their own low-level (noisy and uncalibrated) sensory information to generate behavior?

- What is the capacity of the dynamic approach to generate cognitive properties in low-level robotic platforms? Specifically, can continuous metric representations be derived from low-level sensory information, decisions be stabilized on such representations, sub-symbolic memory and processes operating on memorized information (e.g. suppression of outdated information) be implemented?

- How can integration of representations with stable action planning and control be achieved within the dynamic approach?

- How can different goals be derived from the same sensors?

- How can this approach solve the architectural problem of the behavior-based approach? How can multiple and goal-conflicting behaviors be combined in a way that leads to smooth and stable overt behavior, and in a away such that the internal state of the system is observable and hence overt behavior mirrors the internal state?

This dissertation describes a project in which these questions are systematically investigated. As a case study we choose the classical problem of navigation in ordinary non-engineered environments. This problem contains control-like behaviors, for instance obstacle avoidance, target acquisition and wall-following. It also contains basic cognitive behaviors like: Detection of a target only if sensory information is sufficiently consistent and persistent in time, target localization through interpolation of sensory data, selection of one target out of multiple detected targets; moving toward an occluded target, forgetting about a target if renewed sensory information is not received within a particular time span, detection of a wall only if sensory information is convergent, wall orientation estimation and wall selection.

1.4 Outline of the dissertation

The remainder of the dissertation is organized as follows:

Chapter 2 gives an overview of the main concepts and principles of the dynamic approach to behavior generation as it is applied in the domain of robotics.

Chapter 3 presents the two robotic vehicle platforms and the simulator we worked on.

Chapter 4 demonstrates that attractor dynamics can be used to control motion based on low-level distance sensors such as infra-red sensors and sonars.

Chapter 5 proves that the dynamic approach can be implemented in computationally very weak platforms. Obstacle avoidance and photo-taxis are implemented on an 8-bit micro-controller. As a technical novelty, we demonstrate the integration of dynamics of two different levels of temporal derivative.

Chapter 6 presents a dynamic field model for target representation based on low-level sound sensors. We show how dynamic fields can be used to interpolate sensory information. We also show how the robotic system stabilizes decisions in the presence of multi-valued sensorial information, and how it activates and deactivates memory. Integration of target representation with target acquisition, in the form of phono-taxis, and obstacle avoidance is demonstrated.

Chapter 7 presents a dynamic field module for sub-symbolic wall representation based on low-level distance sensors such as infra-red detectors and sonars. It endows a robot with the following capabilities: wall detection, wall orientation estimation, insensibility to noisy sensor data and wall selection. This representation is integrated with a behavioral dynamics for wall-following. Results show the ability of the vehicle to follow walls with various shapes and to steer at a constant distance to the wall.

Chapter 8 addresses the integration of the wall-following module with the module for phono-taxis and obstacle avoidance. Results that demonstrate the stability of the complete control architecture are shown.

Finally, a summary of the results, conclusions, relation to other works and future work are given in Chapter 9.

Chapter 2

The dynamic approach to behavior generation

The dynamic approach to behavior generation, presented in detail by Schöner, Dose and Engels (1995), provides a number of concepts and principles that are based on the mathematical theory of dynamical systems and on the elements of neural networks. These concepts can be used as a theoretical language in which autonomous robotic architectures can be built. The basic ideas of this language are: **(1)** The concept of *behavioral variables*, which consist of variables that can describe a particular behavior and define behavioral dimensions along which behavior can change. Specific values of these variables correspond to task constraints; **(2)** The concept of *behavioral dynamics* according to which behaviors are generated as attractor solutions of dynamical systems; **(3)** Neural field dynamics extends the previous principles to the concept of *neural representation of information*.

In this chapter we provide a brief review of the main concepts and principles of this approach as it is applied in the domain of robotics.

2.1 Basic principles

2.1.1 Behavioral variables

To design a behavior in the context of the dynamic approach, the first step is to find variables that can describe, parameterize and internally represent the behavior (state of the system). These variables are called *behavioral variables*. They define *behavioral dimensions* along which behavior can change. A specific instance of the behavior corresponds to a point in the space of the behavioral dimensions. Behavioral variables must be chosen such that the following requirements are fulfilled:

a) At any time a behavior must be associated with particular values of its corresponding behavioral variables and task requirements must be expressed as values or set of values of these variables.

b) The specified values for a behavioral variable, that express the task, must be independent of its current value.

c) It must be possible to specify the values by the on-board sensors or by another behavioral model (for example a representation system).

d) Finally, and very important, the behavioral variables must enable the design of control systems that impose their values on an effector system.

Now we give an example that aimes to clarify these requirements. In the task of autonomous robot navigation in the plane the movement must be controlled such that locations of obstacles are avoided while a particular target position is reached. To express the behavior that this movement represents the heading direction, ϕ, in the world (i.e. relative to some arbitrary but fixed world axis), is an adequate variable since (see Figure 2.1):

First, task requirements of moving toward the target while avoiding collisions with obstacles can be expressed as particular independent values of the heading direction. The direction Ψ_{tar} represents the orientation at which the target lies from the current view point relative to the world axis, while Ψ_{obs} represents the direction at which the obstacle is seen. Moving toward the target, which is a desired behavioral state, is associated with $\phi = \Psi_{\text{tar}}$. Conversely, moving toward an obstacle is associated with $\phi = \Psi_{\text{obs}}$, and is of course an undesirable behavioral state.

Second, if the robot turns on the spot the specified values Ψ_{tar} and Ψ_{obs}, either desired or to be avoided, for the heading direction are kept invariant, i.e. the specified values Ψ_{tar} and Ψ_{obs} do not depend on the current value of the behavioral variable (i.e. ϕ). Since the values expressing the task to be performed ($\phi = \Psi_{\text{tar}}$ expressing target acquisition and $\phi \neq \Psi_{\text{obs}}$ expressing obstacle avoidance) are independent from the current value for the heading direction the individual behaviors can be designed independently from each other.

Third, on-board sensors may specify the values Ψ_{obs} and Ψ_{tar} as long as an estimate of the current orientation of the robot in the world is maintained (in reality, the correct calibration of this value is not fundamental as long as the calibration drift is slow, this will be demonstrated later in Chapters 4 and 6).

Finally, the heading direction can be easily controlled by providing incremental commands to the vehicle's motors or to a steering module.

Path velocity and angular velocity are also appropriate behavioral variables for the example given above (Neven and Schöner, 1996; Bicho and Schöner, 1997a; Bicho and Schöner, 1997b; Bicho, Mallet and Schöner, 1999a; Bicho, Mallet and Schöner, 1999b). This will become clear as we present the material in this dissertation.

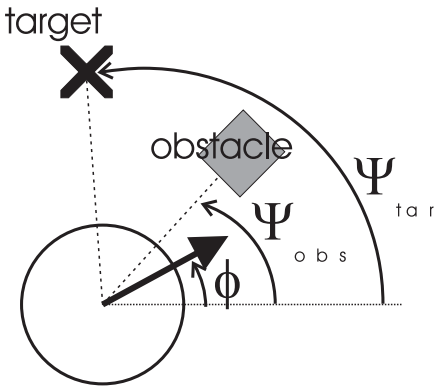

Figure 2.1: An adequate behavioral variable for the task of moving in the plain toward a target location while avoiding to run into obstacles.

2.1.2 Behavioral dynamics

The next step is to generate values for the behavioral variables in time, which control the robot's action. For this purpose a dynamical system for the behavioral variables is designed. Mathematically such dynamical system is time-continuous and is defined by a differential equation in which the dynamical state variables are the behavioral variables. For example, for the heading direction, ϕ, a dynamical system defines the temporal rate of change of the heading direction as a function of the current value, i.e.

$$\frac{d\phi(t)}{dt} = f\left(\phi(t), \text{parameters}\right) \tag{2.1}$$

The function $f(\cdot)$ defines a *vector field*; i.e. to each point in the state space it assigns a vector $f(\phi)$. Each of these vectors determine the direction in which and the rate with which the system will move from the point where the vector is anchored.

Fixed points: Attractors and repellers

As a design principle, we are interested in a particular type of solutions of dynamical systems called *fixed points* or *equilibrium solutions*. These are the points at which the vector field is null,

$$\frac{d\phi}{dt}|_{\phi=\phi_{\text{fixed point}}} = f(\phi_{\text{fixed point}}) = 0 \tag{2.2}$$

Fixed points are, in other words, constant solutions of the dynamical system: The system does not change state in time. But the system being "stuck" in a state does not mean that it is stable. This is depicted in Figure 2.2.

For a dynamical system in one variable the stability of the fixed points can easily be investigated graphically. This is illustrated in Figure 2.3.

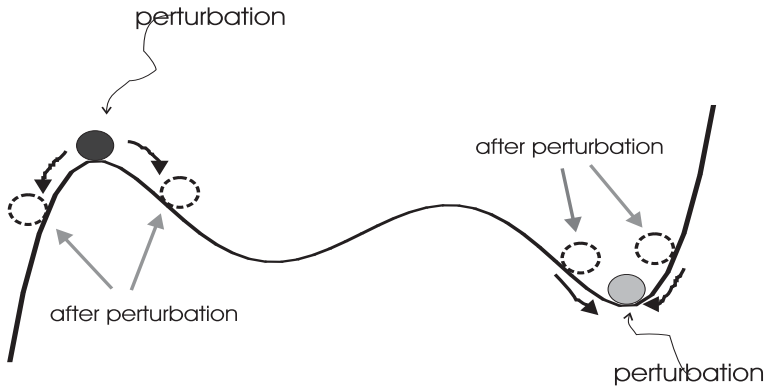

Figure 2.2: Unstable and stable equilibrium points. Initially the two balls are in rest. The black ball is at an equilibrium point at the top of a hill. This is an unstable equilibrium point since a very small perturbation will send it down. By contrast the grey ball is at stable equilibrium point. Once the perturbation ceases to act the ball returns to its initial point.

Panels A and B in Figure 2.3 depict a linear and a non-linear dynamical system, respectively. These two dynamical systems exhibit a fixed point at $\phi = \phi_{\mathsf{A}}$. Because the slope at this fixed point is negative, the fixed point is an asymptotically stable state. In this case the fixed point is also called an *attractor* because it attracts the behavioral variable to the value specified by the fixed point. To see this consider a value slightly to the right of the fixed point ϕ_{A}, i.e. ϕ_1. At this point because the rate of change of the behavioral variable is negative the system is driven toward decreasing values of the behavioral variable, i.e. toward the fixed point. Analogously, at points starting to the left of this fixed point, for example ϕ_2, the rate of growth is positive thus driving the system toward increasing values, i.e toward the fixed point again. When the system arrives at this fixed point it stays there. The vectors fields of both these dynamical systems behave as attractive forces that drive the system to the state specified by $\phi = \phi_{\mathsf{A}}$. Thus, for example, in the target acquisition behavior in which the direction at which the target is seen is a desired value for the heading direction of the robot, we can make that direction an attractor by erecting a *attractive force-let* (vector-field) with a zero at that direction and a negative slope. The range of the behavioral variables over which a force-let exerts its attractive influence can be unbounded (Panel A) or limited (Panel B). Thus, an important concept related to the idea of attractors is the *basin of attraction*. For a given attractor this refers to the region in the state space in which all initial conditions will converge to the attractor.

Conversely, when the slope at a fixed point is positive, (Panels C and D in Figure 2.3), the fixed point is an unstable state and is called a *repeller* because it repels the system from its value. This can be read on the phase plots of the dynamics: consider a value slightly to the left of the fixed point ϕ_{B}, i.e. ϕ_3. At this

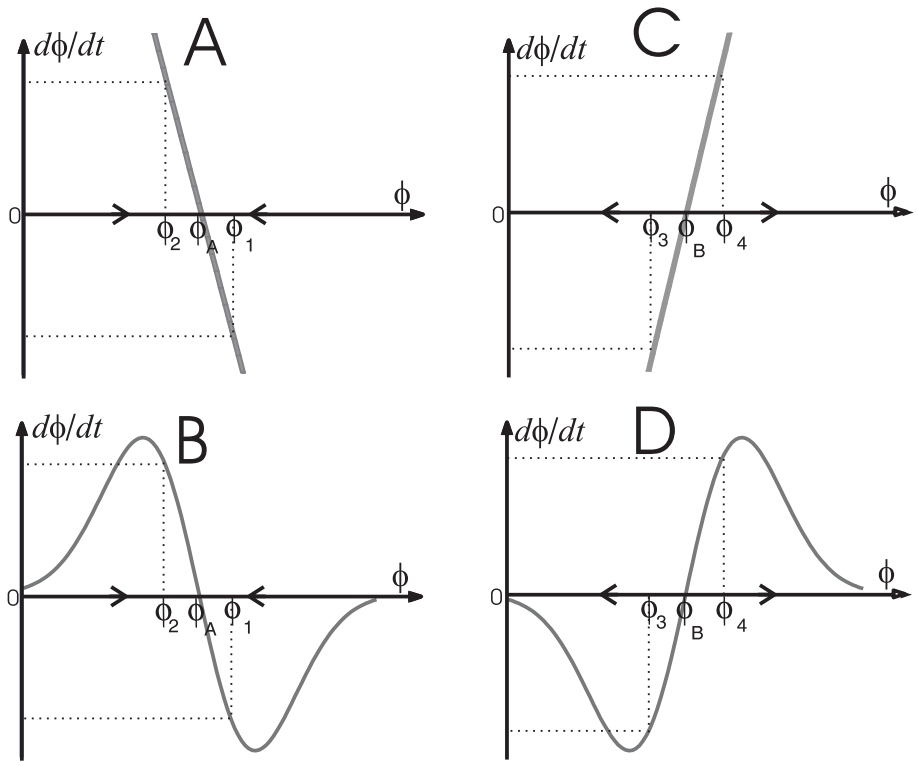

Figure 2.3: Four *phase plots* of one dimensional dynamical systems: the rate of change $d\phi/dt$ is plotted as a function of ϕ. The points at which $d\phi/dt$ is zero (ϕ_{A} and ϕ_{B}) are the fixed points of the dynamics and the slope of $d\phi/dt$ there indicates their nature. Panel A: The system is linear with a fixed point at $\phi = \phi_{\mathsf{A}}$. The slope at this fixed point is negative. This makes that fixed point an attractor. The system converges in time to the state defined by the fixed point. Panel B: A non-linear system with a fixed point attractor also at $\phi = \phi_{\mathsf{A}}$. As for the linear case, the system converges in time to ϕ_{A}. Panel C: The system is linear with a fixed point at $\phi = \phi_{\mathsf{B}}$. The slope at this fixed point is positive thus making this fixed point a repeller. The system diverges away in time from the state specified by the fixed point. Panel D: A non-linear system with a fixed point repeller also at $\phi = \phi_{\mathsf{B}}$. As for the linear case, the system diverges from ϕ_{B} as time increases. The direction of the arrows indicate the evolution of the behavioral variable as time increases.

point negative rate of growth for the behavioral variable drives the system toward decreasing values, thus driving the system away from the fixed point. Analogously for a value of the behavioral variable starting to the right of the fixed point, ϕ_4, the system is driven toward increasing values because the rate of change is positive. Once again the system is driven away from the fixed point. In such a case the vector field is called a *repulsive force*. At the value of the fixed point the rate of change is zero but an arbitrary small perturbation immediately causes the system to diverge from the state (unstable) defined by the repeller. Now for example, an obstacle can be modeled by erecting a repulsive *force-let* at the direction at which the obstacle

lies, because one has to prevent the heading from taking that direction.

The range of repulsion, i.e. the region of points over which a repulsive force-let wields its influence, can be unbounded (Panel C) or limited (Panel D).

Stability measures or strength of fixed points

For a linear dynamical system (Panels A and C in Figure 2.3) the slope determines how strongly attractive or repulsive a fixed point is. When the fixed point is an attractor the steeper this slope, the stronger the restoring force and the faster the system relaxes to the attractor after a perturbation. For a repeller the steeper the slope the faster the system relaxes away from the repeller after a perturbation. Thus the slope represents the stability of the system in the fixed points.

Since relaxation is exponential it can be characterized by a *time scale*. For instance, if an initial perturbation puts the linear system depicted in Panel A at point ϕ_1, then the system evolves in time according with the solution

$$\phi(t) = \phi_{\mathsf{A}} + (\phi_1 - \phi_{\mathsf{A}})e^{-\frac{t}{\tau}} \tag{2.3}$$

where τ determines the *relaxation time* with which the systems approaches the fixed point ϕ_{A}. When shifted to a distance $|\phi_1 - \phi_{\mathsf{A}}|$ from the attractor, the system reduces this distance by a factor of e (e is the natural number) in a time interval of τ. Relaxation is faster, the smaller the time scale τ is. Therefore, τ can be used to characterize quantitatively the stability of the system in the fixed points. τ can be obtained from the reciprocal of the slope of the linear vector field at the fixed point

$$\tau = -\left[\frac{df(\phi)}{d\phi}|_{\phi=\phi_{\text{fixed point}}}\right]^{-1} \tag{2.4}$$

Negative values for τ indicate that the corresponding fixed point is a repeller. $\tau = 0$ denotes that the fixed point is *semi-stable*.

For non-linear dynamical systems (Panels B and D in Figure 2.3) with hyperbolic fixed points [1] we can use the linearization method to characterize the stability of the fixed points (Perko, 1991; Crawford, 1991). For example, a stability measure of the attractor ϕ_{A} of the non-linear dynamical system depicted in Panel B may be obtained by approximating this system to a linear system near ϕ_{A}. This approximation represents in essence the behavior of the non-linear system in the neighborhood of the attractor. Expanding the vector field $f(\phi)$ in a Taylor series around the fixed point ϕ_{A} and keeping only the terms up to first order yields a dynamics with a linear vector field,

$$\frac{d\phi}{dt} = f(\phi) \approx \left(\frac{df(\phi)}{d\phi}|_{\phi=\phi_{\mathsf{A}}}\right)(\phi - \phi_{\mathsf{A}}) \tag{2.5}$$

the solution of which has the form of Equation 2.3 and where the time scale, τ, is again given by the inverse of the slope of the (non-linear) vector field at the fixed

[1] Fixed points are called hyperbolic when they have no eigenvalues on the imaginary axis.

point as for the linear case. Thus, τ as given by Equation 2.4 can also be used to characterize quantitatively the local stability of the fixed points of a non-linear dynamical system. Strong behavioral states have very short local relaxation times.

Integration of elementary behaviors

The complete behavioral dynamics is build up from individual contributions (i.e. force-lets), which are added to shape the complete vector field. Each force-let represents a constraint on the behavior that we are designing. Because the range of the force-lets are limited the resulting dynamical system in non-linear. By design one makes the system to be at all times in, or very near, an attractor so that the overt behavior is really generated by attractor solutions of the dynamical system. This way powerful theoretical tools from the qualitative theory of dynamical systems (Perko, 1991; Crawford, 1991; Scheinerman, 1996), such as local bifurcations analysis, can be used to design autonomous robot architectures and quantitatively evaluate their compliance with specifications.

Each force-let models an elementary behavior. The time scale of each elementary behavior determines how strongly that behavior contributes to the vector field of the behavioral variables. Thus the hierarchy of time scales also determines the hierarchy of behaviors. Prior behaviors have smaller time scales.

Moving attractors

When attractors are static the requirement that the system must be in or near an attractor at all times is trivially fulfilled. For a robot moving around in the environment the specified values either desired (e.g. Ψ_{tar}) or to be avoided (e.g. Ψ_{obs}) as well as of their strength of attraction or repulsion vary. Thus the individual contributions to the vector field change in time and as a consequence the attractors from the resulting dynamical system move. Since by design the system must be in or near a stable state (attractor) at all times, the rate with which the attractors move must be controlled so that the system is able to track the moving attractors. This is accomplished by making the relaxation time of the dynamics much faster than the time associated with the moving attractors. This will be discussed in detail in Chapter 4 where a solution is proposed.

Bifurcations

The shape of the vector field in Equation 2.1 is dependent on the parameters. Thus changing the parameter values in time may lead to *bifurcations* in the underlying behavioral dynamics. Bifurcations correspond to qualitative changes in the number, nature or stability of fixed points. Local bifurcation theory helps to make design decisions around points at which the system must switch from one type of behavioral state to another. By driving the system through bifurcations the robot is able to flexibly "decide" the appropriate behavior at any given time.

2.2 Principle of neural representation

More abstract forms of behavior or processes, like for example representations of information and memory, cannot be realized with attractor dynamics of the type described above. Dynamical systems of the type presented above have a unique state at all times (each variable has exactly one value) and change state continuously in time, i.e. to attain a new value each variable must pass through all intermediate values. Such dynamical systems are thus incapable of representing graded amounts of information about a behavioral variable. For instance:

- The absence of any knowledge about a particular variable cannot be expressed.
- Nor can the presence of ambiguous, multi-valued information be expressed in a manner that does not yet reflect a decision.

The principal of neural representation was proposed to overcome this limitation (see Engels and Schöner, 1995; Schöner, Dose and Engels, 1995, for a review). We present the main ideas next.

2.2.1 Field dynamics

The first idea is that behavioral variables are now conceived of as behavioral dimensions, spanning a space of possible values of these variables. Over that space of behavioral dimensions a field of activation is defined. At each location along a behavioral dimension, the level of activation represents the extent to which the particular value of the behavioral variable is presently specified. Well defined states of the behavioral variable are thus represented by peaks of activation, centered over the appropriate location in the field, that is, at the specified values on the behavioral dimension. For instance, the direction, ψ, at which a target lies as viewed from the robot but referenced to an external frame can be used as a behavioral dimension (taking values in the interval $[0, 2\pi]$ rad). An activation variable, $u(\psi)$, can be defined for each possible value of target direction, ψ. The function $u(\psi)$ is now the dynamical state variable and represents if a target in direction ψ is present. Positive values of activation, $u(\psi) > 0$, indicate that a target near ψ is detected, negative values of activation, $u(\psi) <= 0$, indicate that no target was detected near ψ. The larger the activation, the more certitude about the detection of a target at direction ψ. A single target is represented by a single localized distribution of activation in the neural field centered over the value at which the target lies. This conceptualization also permits to deal with the absence of information ($u(\psi) <= 0 \;\; \forall\psi \in [0, 2\pi]$) about a target and the representation of multiple instances. This is illustrated in Figure 2.4.

The second idea is to evolve the activation, $u(\psi)$, continuously in time as a dynamical system:

$$\tau \frac{du(\psi, t)}{dt} = F\left[u(\psi, t), \text{parameters}\right] \tag{2.6}$$

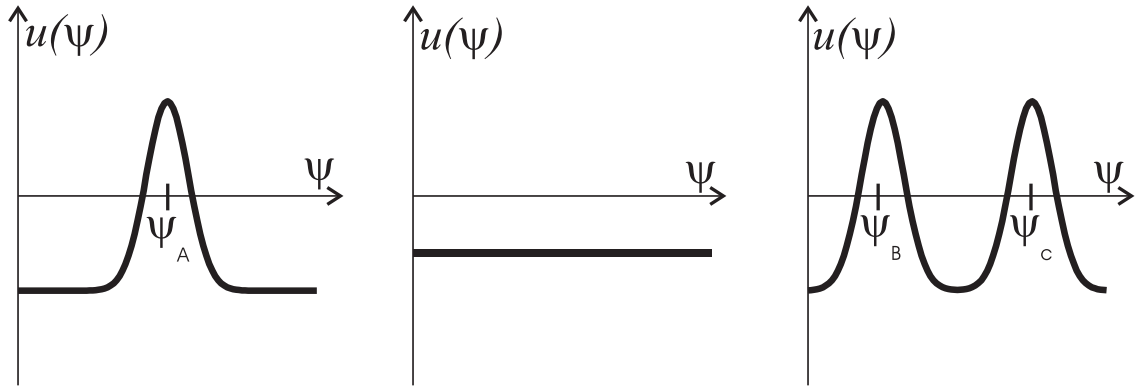

Figure 2.4: The principle of neural representation: the behavioral variable defines a behavioral dimension, ψ. An activation variable, $u(\psi)$, represents the extent to which values along the behavioral dimension are present. Left: The presence of one target is represented by a localized peak of activation centered over the direction value, ψ_{A}, at which it is detected. Middle: The state of negative activation along the entire field represents that no target is present. Right: Multiple targets are represented by multiple peaks along the behavioral dimension. Two targets at directions ψ_{B} and ψ_{C} are represented.

The concepts of attractor dynamics and bifurcation are now implemented at the level of a dynamics of the entire field. Particular patterns of activation (like the ones depicted in Figure 2.4) are made attractor solutions by choosing particular types of interaction in the field, i.e. making the activation $u(\psi, t)$ at a point ψ, dependent on the activation $u(\psi', t)$ at other points ψ' in the field.

2.2.2 Amari neural field model: a biological inspiration

A convenient form for the dynamics of the activation variable is given by the following non-linear integro-differential equation:

$$\tau \frac{du(\psi, t)}{dt} = -u(\psi, t) + S(\psi, t) + \int w(\psi, \psi')\Theta(u(\psi', t))d\psi' + h. \qquad (2.7)$$

This equation was first proposed in the seventies to model activity patterns in the cortical surface, in which a large number of interacting neurons creates a network that is almost homogeneous along the cortical surface and can thus be approximated as a continuous field of neural activation (Wilson and Cowan, 1973; Amari, 1977). Because in Chapter 6 we present a detailed analysis of the use of this equation in building dynamic representations of information we give here just a brief description.

The linear part of this dynamics defines the time scale, τ, of the field. $S(\psi, t)$ is the input activation and excites ($S(\psi, t) > 0$) regions of the field for which values in the behavioral dimension are defined and inhibits ($S(\psi, t) \leq 0$) sites of the field where no value is specified. The integral term introduces interaction within the

field. The type of interaction is determined by the shape of the interaction kernel $w(\psi, \psi')$. A typical form of interaction that guarantees the existence of localized peaks of activation is a local excitatory and longer ranged inhibitory process. $\Theta(\cdot)$ is a non-linear threshold function and makes that only points of the field that are above a certain threshold can contribute to the interaction. Parameter h determines the resting level (always negative) of the field, which together with the non-linear threshold function, also controls the number of sites that actually contribute to the interactions.

The qualitative behavior of the field of activation changes with a change of the parameters on which the field depends. In Chapter 6 we discuss how the parameters resting level h, strength of input, shape of input (mono-modal or multi-modal) affect such behavior. The equation has been analyzed mathematically by Amari (1977) and then by Kishimoto and Amari (1979). Their studies provide valuable insights about the different regimes of stability and the role of the different parameters for the existence and stability of localized activity patterns.

Chapter 3

The robotic vehicles and the simulator

Previous implementations of autonomous robot architectures based on the dynamic approach (Schöner and Dose, 1992; Schöner, Dose and Engels, 1995; Neven and Schöner, 1996) involved relatively large scale platforms with several on-board and off-board computer systems. Sensory information was visual, required extensive computation and potentially provided high precision information. By contrast the platforms used in this thesis project rely on computationally modest systems based on very low level sensory information. This chapter presents the two platforms we worked on. The first is one of the simplest platforms, a MIT *rug-warrior* type micro-controller based vehicle whose sensors consist of infra-red detectors and light dependent resistors. The second is a mid-size 486 PC based platform equipped with infra-red detectors, sonars and microphones.

The simulator used to test and/or illustrate relevant aspects of the designed dynamic control architectures is also presented in this chapter.

3.1 Rodinsky: An 8 bit micro-controller based platform

Rodinsky is a MIT *rug-warrior* (Jones, Flynn, 1993) type robot and it was built during a course on mobile robotics teached by Prof. Keith Doty (from the University of Florida in Gainsville, USA) at the University of Aveiro, Portugal, during the spring of 1995. Figure 3.1 presents this robot.

As we can see this is a very minimal platform. It fits approximately into a 20 by 20 by 15 cm "cube" and it has a cylindrical shape. Its chassis is made of wood. It is based on the MC68HCA11A0 (8 bits) micro-controller from Motorola, operating at 2 MHz with 32 Kbyte of RAM. It is programmable in Interactive C (compiler provided through the MIT Media Lab, written by Randy Sargent with the assistance of Fred Martin). The vehicle is propelled by two lateral wheels, each driven by a simple DC

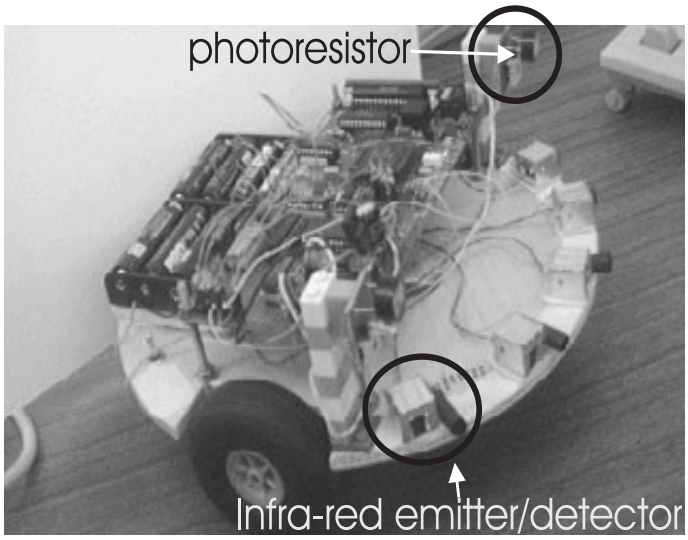

Figure 3.1: Rodinsky

motor, and stabilized by a passive caster wheel. An ensemble of eight 1.2 Volt NiCd batteries power the platform. This robot acquires sensory information through five pairs of infra-red emitters/detectors and two light sensors. The infra-red sensors serve to measure distances to obstructions. They have a distance range of 60 cm and an angular range of about 30 deg. They are mounted in the front part of the robot around its periphery. The angular separation between the infra-red sensors is 30 deg so that their sensitive cones slightly overlap. Two photo-resistors (i.e. light dependent resistors), one mounted on the left and another mounted on the right side of the vehicle, provide information about light targets. The output voltage at the terminals of these photo-resistors is a monotonically decreasing function of light intensity.

Neither motors nor sensors are calibrated other than through rough order-of-magnitude estimation.

3.2 Robodyn: A mid-size 486 PC based platform

Robodyn was designed and built by the Dynamical Robotics group responsible engineer Pierre Mallet at the CRNC-CNRS in Marseille, France. Figure 3.2 shows this robot.

It consists of a cylindrical platform with two lateral motorized wheels and a passive rear caster wheel. It fits approximately into a 40 by 40 by 40 cm cube. The robot has a single board computer system based on a 486DX4 processor operating at 100 MHz, equipped with 4 Mbytes of DRAM and 4 Mbytes of FLASH memory. The

operating system is DOS 6.22. A monochrome LCD monitor, a removable keyboard and a removable driver for 3 1/2 diskettes make the platform an autonomous workstation. All programming, control and computation are done on-board. The control architectures were implemented in Microsoft Quick basic V4.5 (the only compiler that could be installed on the 4 Mbytes of FLASH memory). The two lateral wheels are each driven by a DC brushless servo-motor, each separately controlled by electronic circuitry that guarantees accurate control of rotation speed without the use of external shaft encoders. The relationship between input voltage and rotation speed is approximately linear, so that generating desired robot speeds and turning rates is easy. The motors are powered by two 12 Volt batteries in line, with two separate 12 Volt batteries supplying the computer and the on-board electronics. This yields an average autonomy of about 1h 30 min (the computer being the bottleneck).

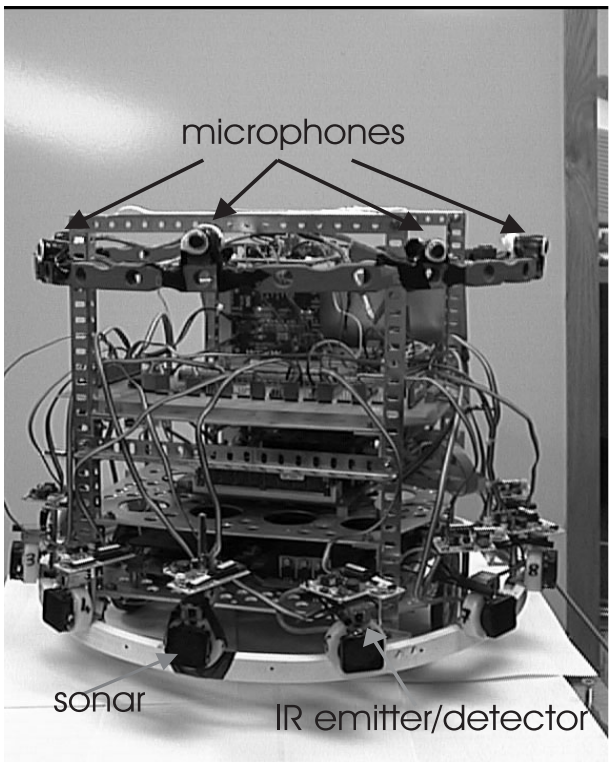

Figure 3.2: Robodyn

The robot is equipped with nine infra-red sensors (initially seven) and nine sonars (initially also seven), which are used to measure distance to obstructions. Additionally, it has five microphones which provide information about sound targets. The infra-red sensors are of the same type of those used in Rodinsky. Their signal is uncalibrated as it depends on surface reflectivity. The sonars distance range is from 45 cm to 175 cm. In both type of distance sensors the angular range over which distances are averaged is about 30 deg. They are mounted on a ring centered on the

robot's axis. The sensors are arranged such that their sensitive cones just touch, thus completely covering the forward semi-circle. The microphones are of the cardiod type. They are most sensitive to sound arriving from the direction at which they are pointing in space. Sensitivity decreases for sound impinging from other directions. Sensitivity loss (in the mounted configuration) is about 6 dB for sound sources sideways from the microphones and 20 dB for sound sources at the rear. Microphones are spaced 45 deg apart on the upper ring around the robot.

3.3 Kinematics

The path velocity, v, and the angular velocity, w, of this type of platforms are controlled by setting the rotational speeds of the two driving wheels as follows (l=left, r=right):

$$w_{\text{wheel,l}} = \frac{1}{R_{\text{wheel}}}\left(v + \frac{D_{\text{wheels}}}{2}w\right) \tag{3.1}$$

$$w_{\text{wheel,r}} = \frac{1}{R_{\text{wheel}}}\left(v - \frac{D_{\text{wheels}}}{2}w\right) \tag{3.2}$$

where R_{wheel} is the wheels radius and D_{wheels} the distance between the two driving wheels.

When path velocity and angular velocity can be accurately controlled the robot can perform dead-reckoning by using simple geometric equations to compute momentary position of the vehicle relative to a known starting position. The vehicle position in the plane, (x,y), relative to a starting point, and its heading direction, ϕ, can be computed by integrating the following equations

$$\frac{dx(t)}{dt} = vcos\left(\phi(t)\right) \tag{3.3}$$

$$\frac{dy(t)}{dt} = vsin\left(\phi(t)\right) \tag{3.4}$$

$$\frac{d\phi(t)}{dt} = w(t) \tag{3.5}$$

where v, ϕ, and w are obtained from the behavioral dynamics (cf. Chapters 4 and 5).

3.4 Simulator

Whenever considered important, simulations are used in this dissertation, to illustrate relevant aspects of a control architecture. The simulations were generated by a software simulator written in MATLAB. This simulator is depicted in Figure 3.3.

In the simulation a robot is represented as a triplet (x, y, ϕ), consisting of the two Cartesian coordinates and the heading direction. Cartesian coordinates are updated

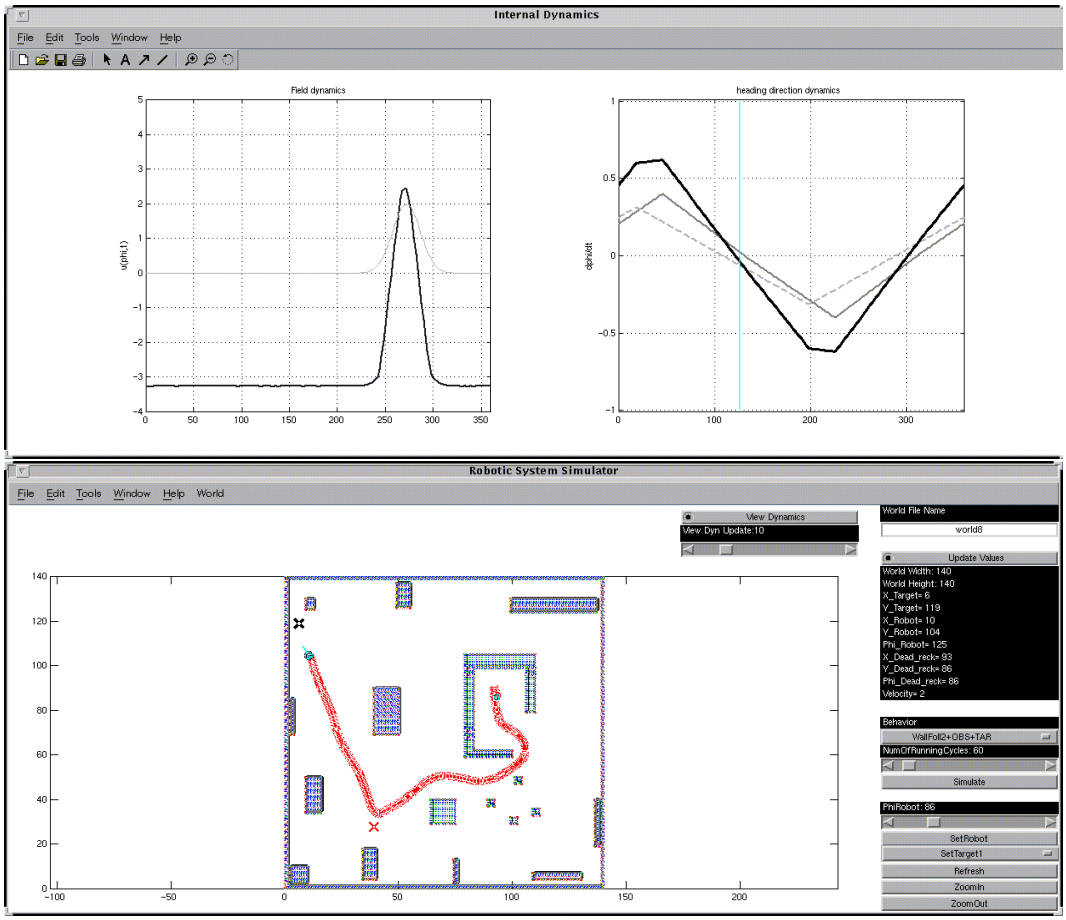

Figure 3.3: The simulator: Here a snapshot of the screen when a simulation is running is depicted. The window on the bottom of the screen depicts the simulated environment where the robot operates. The environment is represented by an occupancy grid recorded in a file (there exists one file for each simulated environment) which can be selected and loaded through the menu **World** on this window's tool bar. On the right side of this window a set of interactive buttons and control slices are displayed.These are used for setting the robot's position and heading direction (can be changed any time during a run), selecting and setting a target position (up to three different targets are possible and their position can be changed at any time), setting the number of cycles that the simulation will run, selecting the visualization of the internal dynamics (which is displayed on the top window), choosing the visualization of the behavioral variables values, and finally setting the control architecture to run (which can also be changed at any time). On the top window is displayed (when selected) the behavioral dynamics and the dynamic fields activity when these are part of the architecture.

by a dead-reckoning rule ($(\dot{x} = vcos(\phi),\ \dot{y} = vsin(\phi))$, see Chapter 4 for details) while heading direction, ϕ, and path velocity, v, are obtained from the behavioral dynamics. All dynamical equations are integrated with a forward Euler method

with fixed time step, and sensory information is computed once per each cycle.

Distance sensors are simulated through an algorithm reminiscent of ray-tracing. The target information can be provided into two different forms depending on the selected architecture. The target can be defined by a goal position in space when this information is supposed to be known a priori, or it can be a simulated light or sound source. Light targets are modeled as point sources with hyperbolic radiance decay (no reflections taken into account). Sound sources are also modeled as point sources assuming fixed frequency and exponential intensity decay (again no reflections taken into account).

Chapter 4

Using attractor dynamics to control motion based on low-level distance sensors

This chapter demonstrates (see also Bicho, Mallet and Schöner, 1999b) that the dynamic approach to path planning (Schöner and Dose, 1992) lends itself naturally to implementation on simple autonomous vehicles using only low-level sensory information such as distances sensed by infra-red detectors or sonars. It also shows how theoretical design and hardware implementation are enchained effortlessly. The chapter starts with a review of the literature in the domain of path planning so that we can position the dynamic approach to path planning with respect to the other approaches. Section 4.2 presents a dynamical system that generates a time series of the vehicle's heading direction. Each sensor is assumed to contribute a repulsive force-let to the vector-field of this dynamical system and their sum leads to obstacle avoidance. Movement toward the target is achieved by adding an attractive force-let. Next, Section 4.3 explains how the vehicle's path velocity can be controlled such that the system is near an attractor at all times. Section 4.4 presents some implementation details. Experimental results that demonstrate the properties of the path generating system and the velocity control system are presented in Section 4.5. Finally, the chapter ends with conclusions.

4.1 Introduction

Motion planning is an essential part of an autonomous robot system (Latombe, 1991). In the basic variation of motion planning for a mobile robot, the task is to generate a collision-free vehicle path that brings the robot system to a specified target location. The majority of the research in this domain has been conducted, in the field of robotics, under the title of path planning. Even-though motion planning has been studied for two decades and a large body of research reported in the

literature exists, the design of a simple and reliable path generating (planning and motion control) system is still a challenge.

The problem has been addressed in theoretical work by isolating the path planning aspect from the aspects of obtaining sensory information about the world and controlling vehicle motion to generate the path (review, e.g., in Latombe, 1991; chapters 4 and 7 in Cox, Wilfong, 1990; Kortenkamp, 1998; Pruski, 1998).

Classical theoretical approaches to the problem, also called model-based planning, assume that complete knowledge of the world's geometry is known prior to the planning stage (Lozano-Perez and Wesley, 1979; Schwartz and Sharir, 1983; Cameron, 1998). The objective is to find a connected sequence of collision-free spaces for a finite-size object (a robot), from an initial position to a target position, typically based on polygonal representations of the objects in the world. Some of these theoretical approaches propose algorithms that guarantee that kinematic and dynamic constraints are fulfilled and that a path is found if one exists (Gilbert and Jonhson, 1985; Shin and Mckay, 1985; Kim and Shin, 1985; Kedem and Sharir, 1988). A path is then generated by piecing together the free spaces or by tracing around the forbidden areas (Brooks, 1983; Singh and Wagh, 1987; Takahashi and Schilling, 1989) .

After the planning stage, the robot has to control its motion along the nominal path. The major difficulty here is due to the uncertainties because of unprecise world modeling and/or changes in the robot environment, e.g. appearance and disappearance of objects, and moving objects (Laumond, 1993; Hu and Brady, 1997). First, the path has been computed from unprecise geometric models of the environment. Either the planned path is guaranteed to be safe with respect to these uncertainties, or the robot has to check its safety in the real world. Second, the robot does not perfectly execute the nominal path. Motion planning in the presence of uncertainties and feedback control gave rise to the necessity of sensor based motion planning (Feng and Krogh, 1990). However, it is not possible to simply add a step to acquire sensory information, and then rebuilt the world model and re-plan a collision free path dynamically using these classical schemes (i.e. computational geometry methods) since they are very difficult to obtain and maintain in real time. This also poses the problem of the overall control-theoretic stability of the path generation systems, as the step-wise computation of representations of obstacles and targets is not characterized by a time scale. Thus it might be difficult to satisfy Brockett's necessary condition of systems controllable by smooth feedback (Brockett, 1983).

In contrast to the approaches described above, the potential field approach uses a scalar function to describe both objects and free space (Khatib, 1986). The target location is modeled with an attractive potential and the obstacles with repulsive potentials. Traditional potential field methods typically consider all obstacles at every point in the world. The path is then generated by following the negative gradient of the overall potential function. Although this approach can be computationally efficient (Barraquand and Latombe, 1991) and is suitable for on-line feedback

control (Feng and Krogh, 1992) it suffers from local minima, which may cause the path to terminate at a point other than the target location. Some solutions have been proposed that attempt to overcome this limitation (Cannolly, Burns and Weiss, 1990; Rimon and Koditschek, 1992).

The above approaches rely upon global representations of the world in which the robot operates. Another approach to the navigation problem is to define instead a local representation of the space around the robot (e.g. Lumelsky and Stepanov, 1986; Lumelsky and Stepanov, 1987). Still another possibility is the limit case where sensory information is used at low levels of parameter extraction which is not typically represented (Brooks, 1986; Borenstein and Koren, 1989; Zapata, Lepinay and Thompson, 1994; Fujimori, Nikiforuk and Gupta, 1997). This later approach is usually called sensor-based motion planning.

Among all the approaches, the potential field approach is one of the most popular to date. The main reason is that this approach is suitable for on-line feedback control (Arkin, 1989; Arkin, 1998).

The dynamic approach to path planning and control (Schöner and Dose, 1992) makes this linkage to control even stronger by replacing the transient solutions of the potential field approach with attractor solutions (asymptotically stable states) of a dynamical system, that therefore contributes to the asymptotically stability of the overall control scheme.

In the planning dynamics, that is, in the equations of motion, the vector field is specified so that it captures the task constraints as component forces that define attractors or repellers of the dynamical system. An attractive force serves to attract the system to the direction at which the target lies, and repulsive forces are used to avoid the directions at which obstacles are located. Since some of these forces have limited range from their superposition a non-linear dynamical system results. By design the system is tuned so that the planning variable is in a resulting attractor of this dynamics most of the time. Thus, the path is in fact generated by an attractor solution and not by a transient solution of the dynamical system.

This way one can avoid the difficult problem of designing a non-linear dynamical system all transient solutions of which fulfill multiple constraints. By contrast, designing a dynamical system, the attractors of which fulfill particular constraints, is possible by making use of the qualitative theory of dynamical systems (Perko, 1991). Qualitative changes in the robot's behavior arise through changes in the number, nature, and stability of fixed points. Such changes correspond to bifurcations in the vector field. Local bifurcation theory helps to make design decisions around points, at which the system must switch from one type of solution to another (Schöner, Dose and Engels, 1995). The values of model parameters can be chosen in part based on such analyses.

4.2 The attractor dynamics of heading direction

The dynamic approach to path generation in autonomous vehicles (Schöner and Dose, 1992; Schöner, Dose and Engels, 1995) employs the heading direction, ϕ, relative to some external world axis as the planning variable. The path plan is a time course of this variable which is obtained in time as attractor solutions of a dynamical system for the heading direction.

Task constraints are component forces which are cast together into the vector field of this dynamical system. For example, the directions $\phi = \psi_{obs}$ (relative to a fixed external world axis) in which obstacles lie from the view point of the robot, and similarly, the direction $\phi = \psi_{tar}$ in which the target lies are constraints that are represented by repulsive and attractive force-lets acting on the heading direction (see Figure 4.1). In isolation, each force-let erects an attractor (asymptotically stable state) or a repeller (unstable state) of the dynamics of the planning variable, ϕ. The attractive force-let serves to attract the system to the desired value of the heading direction (here the direction in which the target lies). A repulsive force-let is used to avoid that the system takes an undesired value (here the direction in which an obstacle lies). By design, the system is operated so that the heading direction is in or near a resulting attractor of this dynamics. As the vehicle moves, the directions to the obstacles and target in the world changes, so that the resulting attractor shifts, pulling the heading direction along (Figure 4.2).

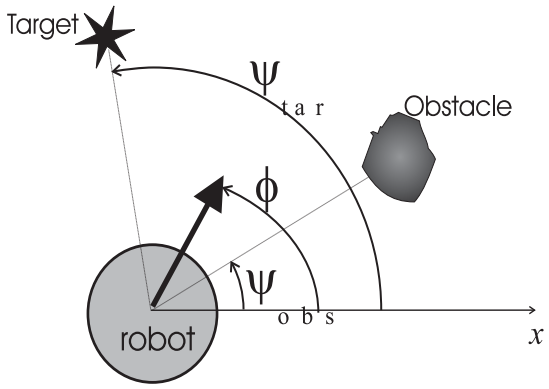

Figure 4.1: Constraints for the dynamics of ϕ are the directions at which obstacles and target lie from the current position of the robot, i.e. directions ψ_{obs} and ψ_{tar}.

Because all angles are measured in an external reference frame, the contributions of the obstacles′ and the target to the dynamical system of heading direction do not depend on the current orientation of the robot.

In Schöner and Dose (1992) and Schöner, Dose and Engels (1995) representations of the locations of obstacles in the external reference frame were obtained from a computer vision system, that employed the method of inverse perspective projection (Mallot, Bültoff, Little and Bohrer, 1991) based on a cali-

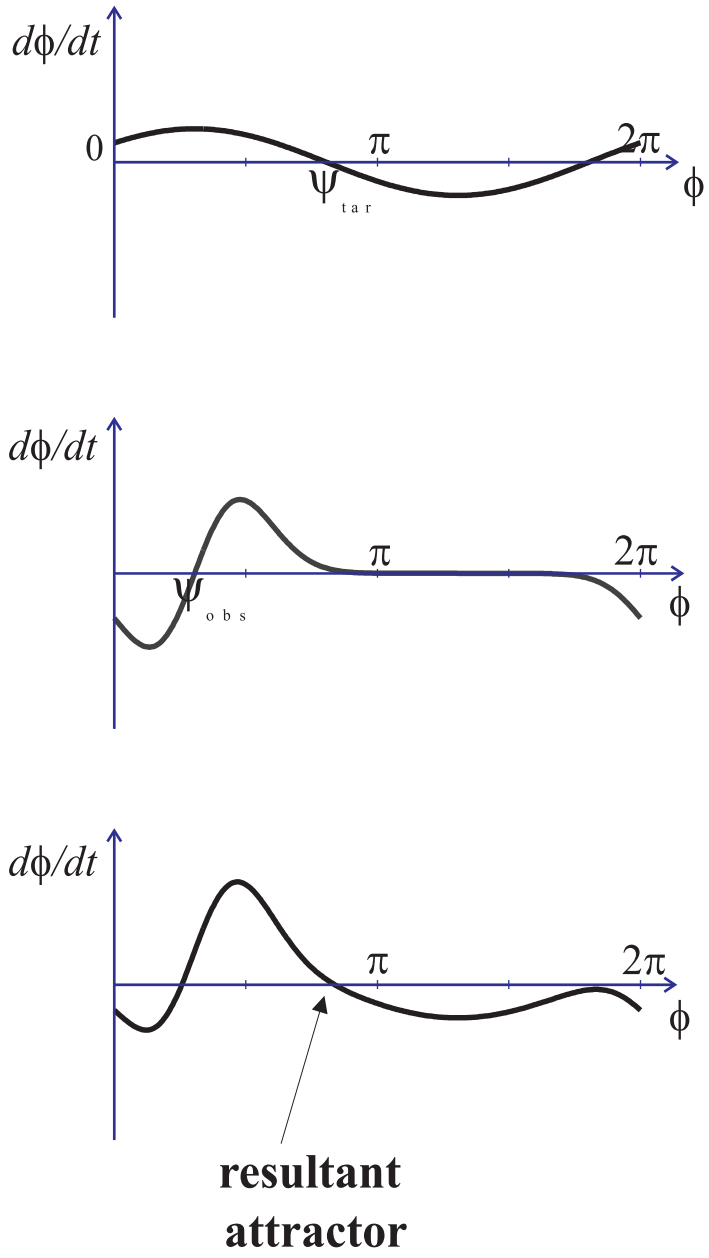

Figure 4.2: Resultant attractor (bottom Panel) from the superposition of the repulsive force-let (middle Panel) from obstacle constraints and attractive force (top Panel) due to the target constraint. Parameters must be tuned so that the system is relaxed in the attractor.

brated camera geometry. Thus, if the robot was rotated on the spot, the directions to the objects in the world did not change and thus the dynamics of heading direction was independent of the current value of heading direction. Only because this

was true did the resultant dynamics have attractors and repellers as designed.

The question we address here is how can this approach be applied to our lower level vehicles, which know nothing about external reference frames, nothing about objects resting in the world, but have only their own low-level sensory information to generate a dynamics of heading direction? We answer this question in the next subsection.

4.2.1 Obstacle avoidance

The vehicle used in this project has seven infra-red sensors mounted on a ring which is centered on the robot's rotation axis. These infra-red sensors are used to measure the distance to surfaces at the height of the ring (see Section 3.2).

On this low-level platform, each distance sensor points into a fixed direction, θ_i, in a reference frame fixed to the robot body. Thus each distance sensor looks into a direction, $\psi_i = \phi + \theta_i$, in an external reference frame if ϕ is the heading direction in such an external frame. This is illustrated in Figure 4.3.

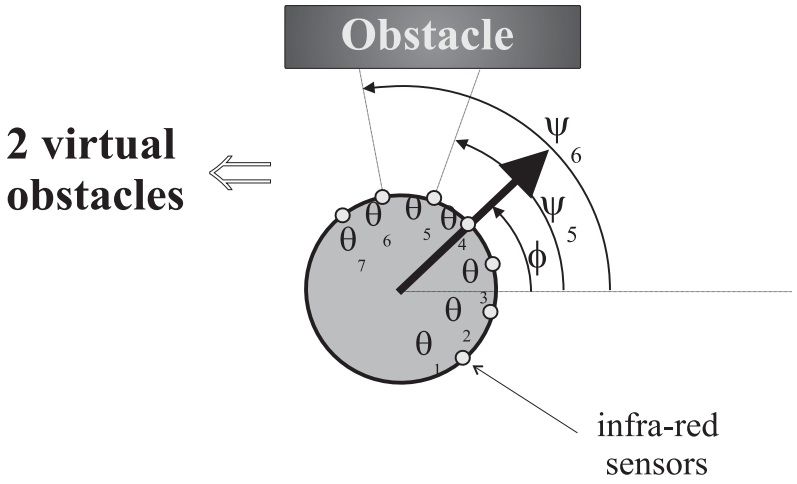

Figure 4.3: Each sensor i ($i = 1, \ldots, 7$), which is mounted at angle θ_i relative to the frontal direction, specifies an obstacle at direction $\psi_i = \phi + \theta_i$ in an external reference frame. In the figure, sensors 5 and 6 specify virtual obstacles at ψ_5 and ψ_6 respectively.

Our strategy is now simply to say that each sensor i ($i = 1, 2, \ldots, 7$) specifies a virtual obstacle in that direction ψ_i, if an obstruction is detected there, so that repulsive force-lets centered at these directions are erected. Each repulsive force-let reads (see Figure 4.4):

$$f_{\text{obs},i}(\phi) = \lambda_i(\phi - \psi_i) \exp\left[\frac{-(\phi - \psi_i)^2}{2\sigma_i^2}\right] \quad i = 1, 2, \ldots, 7 \tag{4.1}$$

In this equation only the difference $\phi - \psi_i = -\theta_i$, which is fixed and known,

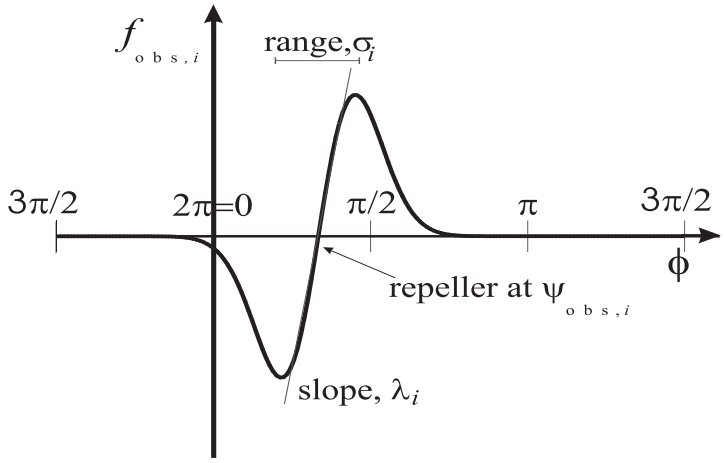

Figure 4.4: A contribution to the dynamics of heading direction expressing the task constraint "avoid moving toward obstacles" is a force-let with a zero-crossing at the direction, $\psi_{\text{obs},i}$ at which an obstruction has been detected. Every distance sensor ($i = 1, 2, \ldots, 7$) contributes such a force-let centered on the direction in which the sensor points. The positive slope of force at the zero-crossing makes that direction a repeller. By decreasing this slope with increasing measured distance, only nearby surfaces repel strongly. The range of the force-let is limited based on sensor range and on the constraint of passing without contact.

enters into the dynamics of the heading direction. This renders the performance independent from the calibration of the planning coordinate system. The strength of repulsion, $\lambda_i > 0$, from the virtual obstacle at direction ψ_i, is a decreasing function of the sensed distance, d_i:

$$\lambda_i = \beta_1 \exp\left[-\frac{d_i}{\beta_2}\right] \tag{4.2}$$

where β_1 controls the maximum repulsion strength of this contribution, and β_2 controls the rate of decay with increasing distance. Thus, when no surface is within the range of the distance sensor, then the corresponding force-let is zero and drops out of the dynamics of heading direction.

The angular range over which the force-let exerts its repulsive effect is determined by σ_i, which depends on the sensor sector, $\Delta\theta$ (= 30 deg), and also on the distance, d_i, because the angle subentended by half the vehicle at the sensed distance is added on each side of the sensor sector as a safety margin:

$$\sigma_i = \arctan\left[\tan\left(\frac{\Delta\theta}{2}\right) + \frac{R_{\text{robot}}}{R_{\text{robot}} + d_i}\right] \tag{4.3}$$

The first term reflects the angular range, $\Delta\theta$, over which the infra-red sensor may detect reflected light, while the second term expresses the additional angle required for the robot to pass next to an obstacle that would occupy maximally the entire sensor range. The further away the robot is from the obstacle, the smaller the angular safety margin, because the angle subentended by the robot itself when next to the obstacle decreases as is indicated. This is depicted in Figure 4.5.

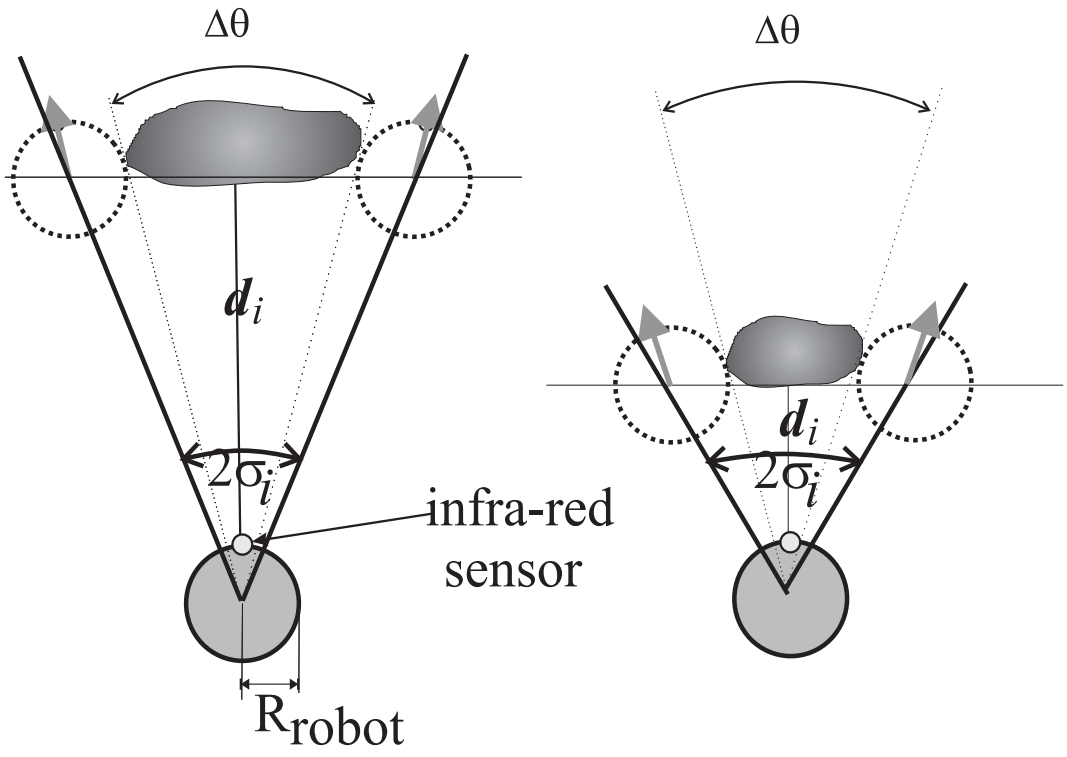

Figure 4.5: The range of the repulsive force-let is limited based on the sensor range and on the constraint of passing next to the virtual obstacle without contact.

The contributions from all the sensors are summed. Therefore, the overall obstacle avoidance dynamics reads:

$$\frac{d\phi}{dt} = F_{\text{obs}}(\phi) = \sum_{i=1}^{7} f_{\text{obs},i}(\phi) \tag{4.4}$$

Figures 4.6 and 4.7 illustrate that the summed obstacle contributions depend little on the current orientation of the vehicle.

In the situation depicted in Figure 4.3 two sensors respond to the obstacle. The sum of their contributions leads to a single repeller that covers the entire angular range subentended by the obstacle (see Figure 4.6). Figure 4.7 shows how at a different orientation of the sensors relative to the obstacle three sensors detect now

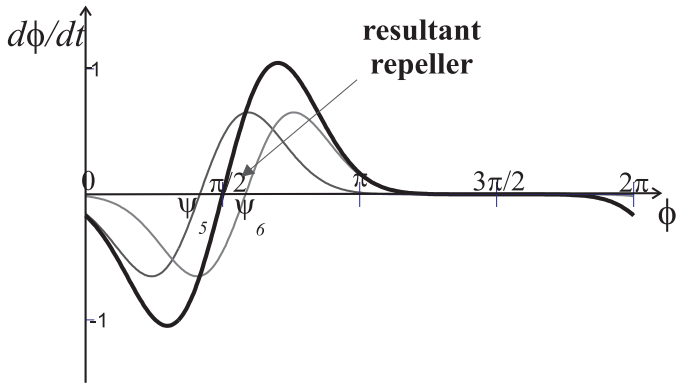

Figure 4.6: In the situation depicted in Figure 4.3 two virtual obstacles are detected, at directions ψ_5 and ψ_6. In that figure $\phi = \pi/4$ rad, $\psi_5 = 5\pi/12$ rad and $\psi_6 = 7\pi/12$ rad, the sensed distances are both 35 cm. Two repulsive force-lets centered at these directions are therefore erected (solid thin lines). The solid bold line shows the resultant obstacle dynamics. The resultant repeller is at $\pi/2$ rad.

the obstacle, leading to changed individual repulsive force-lets. However, their sum erects a repeller at approximately the same direction with respect to the external reference frame. This result thus shows that the dynamics for the heading direction has indeed the designed structure with the repellers and attractors at the right location, as it is invariant under rotations of the vehicle on the spot. This invariance is, of course, constrained by the number of sensors disposed around the robot. The more sensors are used the more invariant the dynamics is.

4.2.2 Target acquisition

As a simple variation of the "find-goal problem" we assume that the absolute coordinates of the target are known. A second, more higher level, variation of this problem is to leave for the robot the responsibility of determining the target location based on its own sensory information (see Chapter 6 and Bicho, Mallet and Schöner, 1999a).

For simplicity, because in this chapter we want to focus on the problem of path planning and motion control, the target is given in external coordinates (X_{target},Y_{target}). The robot keeps an estimate of its own location, ($X_{\text{robot}}, Y_{\text{robot}}$), in the external reference frame by integrating motor commands, through the dead-reckoning mechanism, from an initial reference position:

$$\frac{dX_{\text{robot}}}{dt} = v\cos(\phi) \tag{4.5}$$

$$\frac{dY_{\text{robot}}}{dt} = v\sin(\phi) \tag{4.6}$$

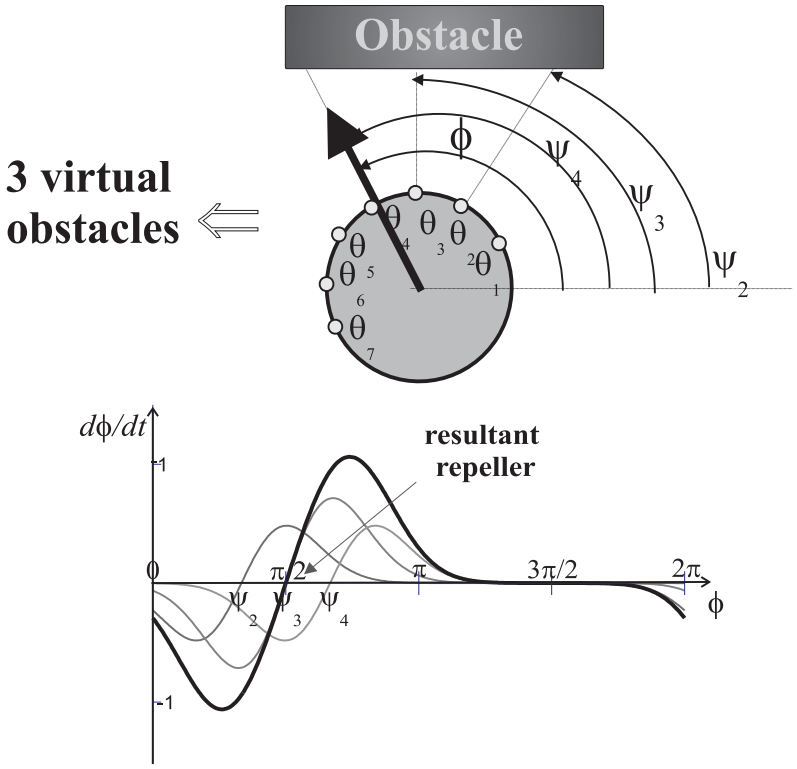

Figure 4.7: On the top: with respect to Figure 4.6 the robot turned left $5\pi/12$ rad. From this rotation three virtual obstacles at directions ψ_2, ψ_3 and ψ_4 result. In this figure $\phi = 2\pi/3$ rad, $\psi_2 = \pi/3$ rad, $\psi_3 = \pi/2$ rad and $\psi_4 = 2\pi/3$ rad. Distances are 40, 30 and 40 cm respectively. On the bottom: three repulsive force-lets are erected at these directions. The bold line represents the resultant obstacle avoidance dynamics. The resultant repeller is near $\pi/2$.

Where v is the path velocity and ϕ the heading direction as obtained from the planning dynamics. The direction, ψ_{tar}, relative to the x-axis, in which the target lies as "seen" from the current position of the robot is:

$$\psi_{\text{tar}} = \arctan\left(\frac{Y_{\text{target}} - Y_{\text{robot}}}{X_{\text{target}} - X_{\text{robot}}}\right) \tag{4.7}$$

The orientation toward the target, is specified by erecting an attractor at direction ψ_{tar} with strength λ_{tar}. Because target acquisition is desired from any starting orientation of the robot the range over which this contribution exhibits its attractive effect, over the heading direction of the robot, ϕ, is the entire full circle (i.e. from 0 to 2π rad). The simplest mathematical form for this attractive force-let is (see Figure 4.8)

$$\frac{d\phi}{dt} = f_{\text{tar}}(\phi) = -\lambda_{\text{tar}} \sin(\phi - \psi_{\text{tar}}) \tag{4.8}$$

For this module the calibration of the dynamic variable heading direction, ϕ, does matter.

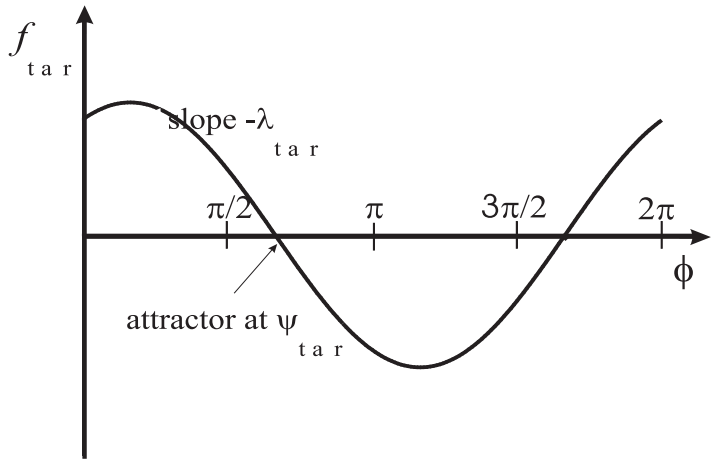

Figure 4.8: A contribution to the dynamics of heading direction expressing the task constraint "move toward targets" is a force with a zero-crossing at the specified direction toward the target, ψ_{tar}. The negative slope at the zero-crossing makes this an attractor of the dynamics. The target contribution is sinusoidal and extends over the entire range of heading direction. This leads to a repeller in the direction $\pi + \psi_{\text{tar}}$ opposite to ψ_{tar}.

4.2.3 Integrating the two behaviors

The integration of these two behaviors is obtained by summing obstacle and target contributions to the vector field:

$$\frac{d\phi}{dt} = F_{\text{obs}}(\phi) + f_{\text{tar}}(\phi) \tag{4.9}$$

Precedence of obstacle avoidance is accomplished making the strength of the obstacle contributions stronger than the target contribution. More sophisticated control over activation and deactivation of such contributions can be obtained using activation networks (see Steinhage and Schöner, 1997; Steinhage, 1998; Large, Christensen, Baczy, 1999) but is unnecessary here.

Figure 4.9 illustrates the simultaneous effect of target and obstacle constraints. In the depicted situation, the space between the two obstacles is not sufficient for the robot to pass between them. The target lies behind this opening, the most challenging situation for obstacle avoidance. The obstacle avoidance contribution

to the dynamics (solid thin line) generates a repeller at the direction in between the two obstacles, while the target contribution (dashed line) erects an attractor at this direction. The resultant dynamics (solid bold line) has a repeller at this direction because the obstacle contributions dominate.

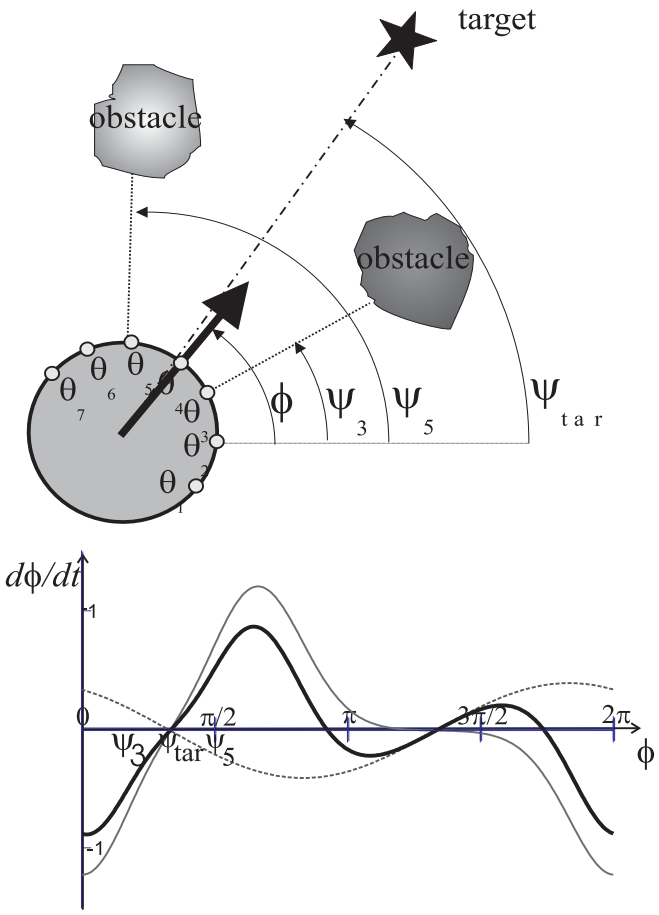

Figure 4.9: On the top: The distance between the obstacles is not sufficient for the robot to pass through, and the target lies in the direction pointing in between the two obstacles thus defying the obstacle avoidance behavior. On the bottom: Obstacle and target contributions for the dynamics are represented by the solid thin line and the dashed line respectively. The resulting dynamics is the solid bold line.

Qualitative changes of behavior arise if the number and stability of fixed points of the heading direction dynamics changes. These changes correspond to bifurcations of the vector field brought about by changing sensory information as the robot moves. For instance, an attractor pointing along a path leading between two obstacles may become unstable and turn into a repeller as the vehicle approaches the obstacles, and the obstacle contributions widen in angular range. At such bifurcations, the heading direction may come to lie exactly on a repeller (a former attractor that

turned unstable). To ensure escape from repellers within a limited time, the planning dynamics is augmented by a stochastic force

$$f_{\text{stoch}} = \sqrt{\mathcal{Q}}\xi_{\text{n}} \tag{4.10}$$

chosen as Gaussian white noise, ξ_{n}, of unit variance, so that $\mathcal{Q}$ is the effective variance of the force. This stochastic force is in addition to sensory and motor noise, which may vary as a function of environmental conditions. Since behaviors are generated by asymptotically stable states (attractors) the system is robust against noise.

The complete heading direction dynamics is therefore:

$$\frac{d\phi}{dt} = F_{\text{obs}}(\phi) + f_{\text{tar}}(\phi) + f_{\text{stoch}} \tag{4.11}$$

Planning decisions, i.e. qualitative changes in the behavior, arise through bifurcations in the vector field which are brought about as the vehicle moves or the environment changes.

4.3 Control of driving speed

As the robot moves sensory information changes and thus attractors (and repellers) shift. The same happens if obstacles move in the world. To keep the system stable, i.e. in or near an attractor at all times, the rate of such shifts must be limited to permit the system to track the attractor as it shifts. One way this can be accomplished is by controlling the path velocity, v, of the vehicle. This is because, the velocity with which the fixed points shift is determined by the relative velocity of the robot with respect to its environment. Let us analyze the rate of such shifts for the simplest case of the robot moving in a resting environment with constant velocity and heading direction. Figure 4.10 shows that for this case the maximal rate of change of obstacle or target bearing occurs when the corresponding objects are seen sideways.

We derive the relationship between the maximal rate of change, $\dot{\psi}_{\text{max}}$, and the vehicle's path velocity, v (see Figure 4.11): Let us assume that initially, $t = 0$ sec, the object (target or obstacle) is located exactly at a right angle to the current heading direction and at a distance d from the robot. At this instant in time the direction at which the object lies as seen from the current position of the vehicle and with respect to the external reference axis is $\psi_0 = 0$ rad. Δt later the vehicle has traveled a distance of $\Delta d_{\text{robot}} (= v\Delta t)$. Thus the object direction as seen from the new position of the robot is now

$$\psi_{\Delta\text{t}} = \arctan\left(\frac{\Delta d_{\text{robot}}}{d}\right) \tag{4.12}$$

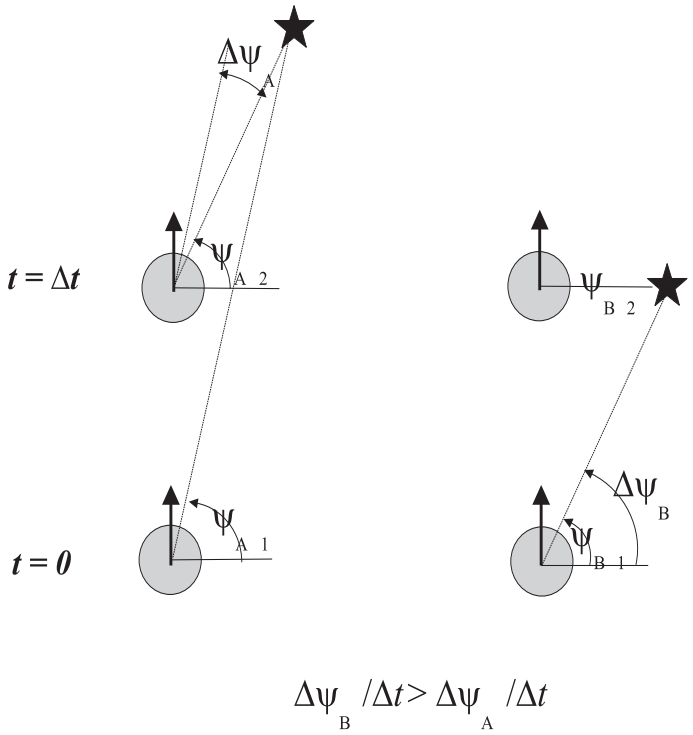

Figure 4.10: Rate of change of obstacle or target bearing (here represented by the black star) as the robot moves in a resting environment with constant movement direction. On the left: The obstacle or target lies far ahead. Initially, the robot is at the position indicated by $t = 0$. The direction at which the object is "seen" is ψ_{A1}. Later on the robot is at the position indicated by $t = \Delta t$. From this position the object is "seen" at direction ψ_{A2}. Thus, in the time interval Δt the rate of change of the object bearing is $\Delta\psi_{\mathrm{A}}/\Delta t$. On the right: The obstacle or target is "seen" sideways. In the same interval of time the rate of change of the object bearing is $\Delta\psi_{\mathrm{B}}/\Delta t$ and is larger than in the previous case.

For small $\Delta d_{\mathrm{robot}}/d$ we can write:

$$\psi_{\Delta \mathrm{t}} \approx \frac{\psi_0 - \psi_{\Delta \mathrm{t}}}{\Delta t} \approx \frac{v \Delta t}{d} \tag{4.13}$$

Therefore we can derive the maximal rate of shift of the fixed points as a function of the vehicle's velocity

$$\dot{\psi}_{\max} \approx \frac{\Delta \psi}{\Delta t} \approx \frac{v}{d} \tag{4.14}$$

This approximate description can be turn around to compute the desired path velocity as a function of distance with $\dot{\psi}_{\max}$ as a design parameter, that can be tuned

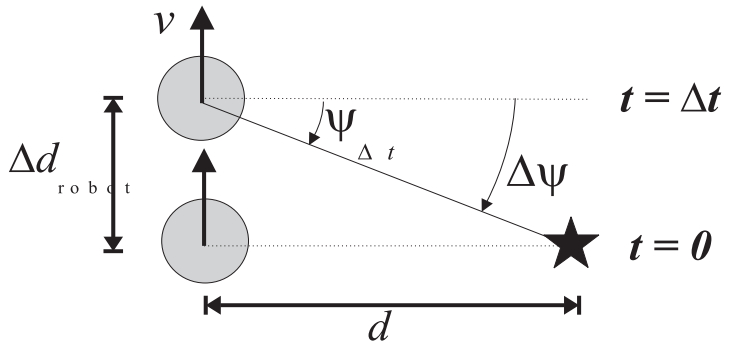

Figure 4.11: This figure illustrates the relationship between the maximal rate of change of obstacle or target bearing and the vehicle's path velocity, which occurs when the objects are seen sideways.

to obtain good tracking. We compute the desired velocity separately for each of the two constraints (i = tar or obs):

$$V_i = d_i \dot{\psi}_{\max} \tag{4.15}$$

The desired velocities are imposed through a very simple dynamics (Bicho, Schöner, 1997)

$$\begin{aligned} \frac{dv}{dt} = &-c_{\text{obs}} \left(v - V_{\text{obs}}\right) \exp\left[-\frac{(v - V_{\text{obs}})^2}{2\sigma_{\text{v}}^2}\right] \\ &-c_{\text{tar}} \left(v - V_{\text{tar}}\right) \exp\left[-\frac{(v - V_{\text{tar}})^2}{2\sigma_{\text{v}}^2}\right] \end{aligned} \tag{4.16}$$

The strengths, c_{obs} and c_{tar}, are adjusted such that in the presence of strong obstacle contributions the obstacle term dominates while in the absence of such contributions the reverse holds. A systematic way to construct a function that indicates if obstacle contributions are present, is to integrate the obstacle force-lets, from which a potential function of the obstacle avoidance dynamics results:

$$U(\phi) = \sum_{i=1}^{7} \left(\lambda_i \sigma_i^2 \exp\left[-\frac{(\phi - \psi_i)^2}{2\sigma_i^2}\right] - \lambda_i \sigma_i^2 / \sqrt{e} \right) \tag{4.17}$$

Positive values of this potential function indicate that the heading direction is in a repulsion zone of sufficient strength, λ_i, so $c_{obs} > 0$ and $c_{tar} = 0$ is required. Conversely, negative values of the potential indicate that the heading direction is outside the repulsion range or repulsion is weak, so now $c_{obs} = 0$ and $c_{tar} > 0$ is

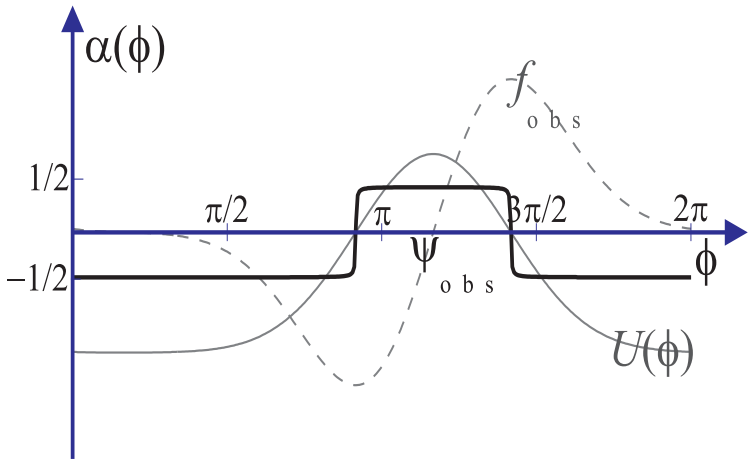

Figure 4.12: The dashed line is a repulsive force-let, f_{obs}. Its integral provides a potential (solid thin line), U, which is maximal near the heading direction to be avoided, i.e the resultant repeller. The thresholded potential (solid bold line), α, serves as an indicator function of those intervals of the heading direction from which obstacle forces repel.

required. The transformation of levels of the potential to the strengths of the two contributions to the velocity control makes use of a sigmoidal threshold function,

$$\alpha(\phi) = \arctan[cU(\phi)]/\pi \tag{4.18}$$

ranging from $-1/2$ to $1/2$ (see Figure 4.12). Finally we can write the following functions for the strengths of the two velocity contributions:

$$c_{\text{obs}} = c_{v,\text{obs}}\,(1/2 + \alpha\,(\phi)) \tag{4.19}$$

$$c_{\text{tar}} = c_{v,\text{tar}}\,(1/2 - \alpha\,(\phi)) \tag{4.20}$$

At sufficiently sharp sigmoids (c sufficiently large) this leads to the required transition behavior. The parameters, $c_{v,\text{tar}}$ and $c_{v,\text{obs}}$, determine the relaxation rate of the velocity dynamics in the two cases when either the obstacle or the target constraints dominate.

The following hierarchy of relaxation rates ensures that the system relaxes to the attractors and that obstacle avoidance has precedence over the target contribution:

$$\lambda_{\text{tar}} \ll c_{v,\text{tar}}, \quad \lambda_{\text{obs}} \ll c_{v,\text{obs}}, \quad \lambda_{\text{tar}} \ll \lambda_{\text{obs}} \tag{4.21}$$

4.4 Implementation on Robodyn

The complete dynamic architecture was implemented and tested on the mobile platform Robodyn.

In the implementation, the dynamics of heading direction, path velocity and the dead-reckoning equations are integrated numerically using the Euler method.

Sensory information is acquired once per computation cycle. The cycle time is measured and is approximately 50 ms. As the time step must be smaller than the fastest relaxation time on the system, this imposes minimal time scales on the entire dynamical architecture. Thus the computational cycle time is the limiting factor for determining the relaxation times of the dynamics in real time units and thus for the overall speed at which the robot's behavior evolves.

The rate of change of heading direction obtained from the dynamics of heading direction (Equation 4.11) directly specifies the angular velocity, w, of the robot for rotation around its center. This can be translated into the difference between left and right wheel rotation speed. The path velocity, v, specifies the average rotation speed of both wheels. Together, the rotation speeds of both wheels can be computed and are sent as set point to the velocity servos of the two motors (see Section 3.3).

4.5 Experimental results

We first discuss a number of results demonstrating the properties of the path planning system, then the velocity control system, and finally we present some sample trajectories of the vehicle in different scenarios.

4.5.1 Properties of the path planning dynamics

Decision making through bifurcations

The capability of the path planning system to make decisions is depicted in Figure 4.13, and discussed in more detail now. In the top Panel the robot faces two obstacles that are sufficiently far apart to pass in between. In this case the corresponding obstacle contributions to the vector field share little overlap. The resulting obstacle avoidance dynamics has repellers corresponding separately to each obstruction, and an attractor in between, which attracts the robot to pass between the obstacles. The target contribution also erects an attractor at the direction pointing in between the two obstacles. Obstacle and target contributions "cooperate" and give rise to a vector field with a strong attractor at that direction. Behaviorally this means that the behavior corresponding to proceed straight to the target becomes more stable, or put in another way, the decision to pass through the obstacles is reinforced. In the bottom Panel, the robot faces again two obstacles but this time they are positioned too close together for the robot to pass in between them. In the illustrated situation four obstructions (i.e. four virtual obstacles) are detected: two corresponding to the left obstacle while the other two to the right obstacle. The repulsive force-lets from these four virtual obstacles are sufficiently overlapping. Their superposition corresponds, therefore, to averaging among the repulsive

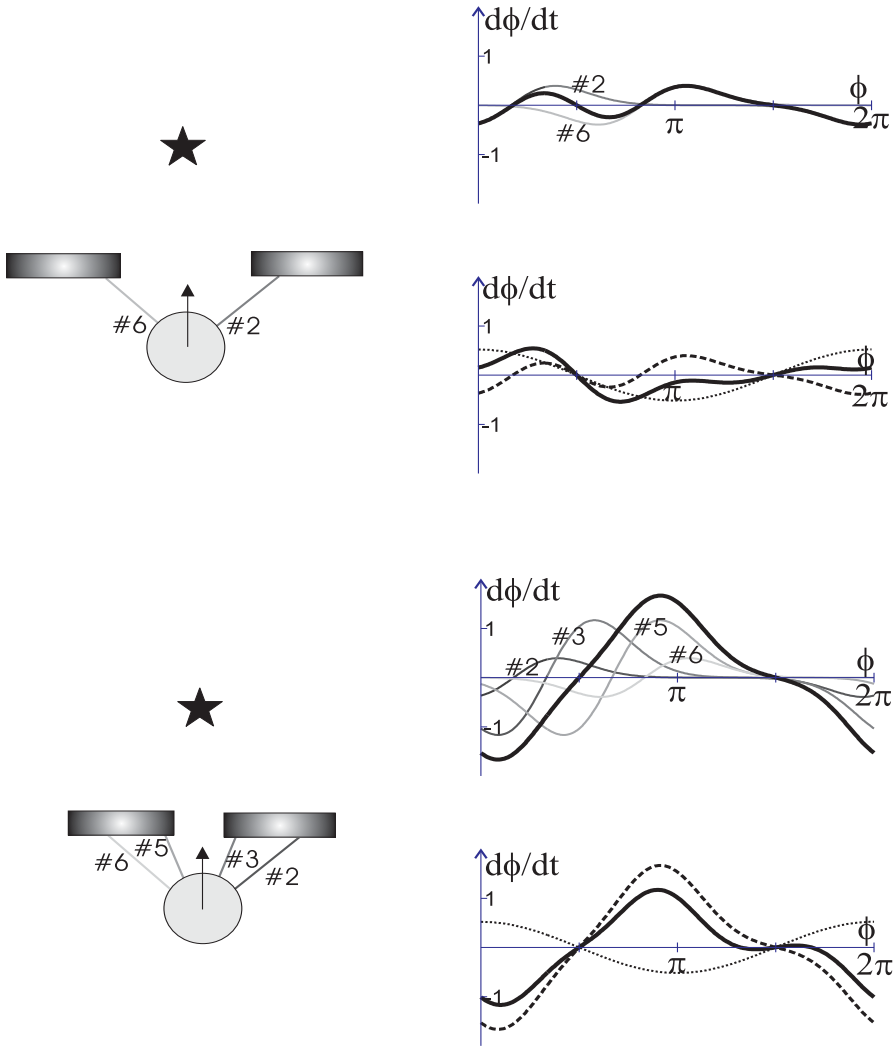

Figure 4.13: Demonstration of decision making by the path planning dynamics: The robot is placed at a distance 20 cm from the obstacles and facing them. The target lies behind the obstacles. The two pictures in the left column illustrate two situations: In the first (top of this column) the separation between the two obstacles is larger then the robot's size, while in the second (bottom of the column) the opposite holds. For each situation two plots are presented. The first plot shows the individual repulsive force-lets(grey lines) and their superposition (solid bold line). The second plot exhibits the resultant obstacles contribution (dashed line), target contribution (doted line) and the resultant dynamics of the heading direction (solid bold line). When the separation between the two obstacles is larger than the vehicle size the path planning dynamics forms an attractor at the direction pointing toward the passage. Conversely, the path planning dynamics erects a repeller at this direction when the distance between the obstacles is not sufficient for the robot to pass in between.

force-lets, which leads to a single repeller in the obstacle avoidance dynamics, positioned at their average location. These two obstacles (or four virtual obstacles) are thus behaviorally modeled as just one obstacle. The target contribution erects an attractor at that direction. However, since the repeller from the obstacle constraints is stronger than the attractor from the target constraint the resulting vector field keeps a repeller at that direction. Behaviorally this corresponds to the decision of steering away. Note that the resultant planning dynamics has two attractors, one on each side of the repeller, which reflect the two possibilities, turning right or left. If the robot turns left or right depends on which basin of attraction the heading direction is in. These decisions in the planning dynamics were investigated systematically for a continuum of distance values between obstacles ranging from 80 cm down to 0 cm when the robot is at a distance of 20 cm from the obstacles. The resulting fixed points are plotted in Figure 4.14 and their stability is indicated. When the obsta-

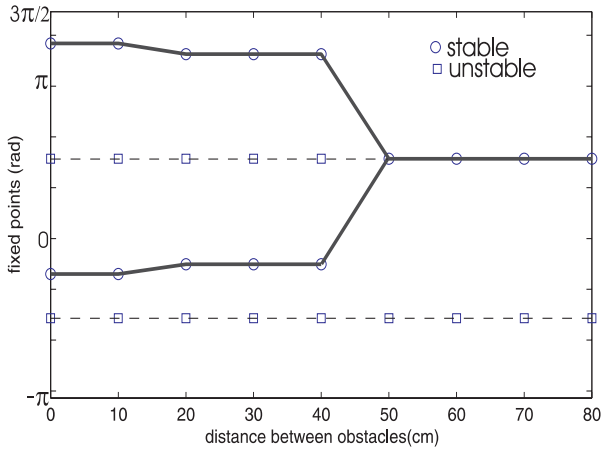

Figure 4.14: Bifurcation diagram of the path planning dynamics when the robot is at a distance of 20 cm from the obstacles. Stable and unstable fixed points are indicated by circles and squares, respectively. Pitch-fork bifurcation: The planning dynamics has an attractor at $\phi = \pi/2$ while the distance between obstacles is larger than 50 cm. For a distance value smaller than 50 cm this attractor becomes unstable (i.e. a repeller) and two new attractors appear. The value 50 cm is the bifurcation value and is the distance below which the vehicle (with size 45 cm) cannot pass between the two obstacles.

cles are 80 cm apart the planning dynamics exhibits an attractor at the direction in between the two obstacles. As the distance between obstacles is decreased a critical value is reached where a bifurcation in the planning dynamics takes place. This attractor becomes unstable and two new attractors appear (pitch-fork bifurcation[1]). The bifurcation point is at 50 cm and is the distance below which the robot (with size 45 cm) fails to pass physically between the two obstacles. Behaviorally, this bi-

[1]A bifurcation is called pitch-fork bifurcation when a stable fixed point becomes unstable and casts off two stable fixed points.

furcation leads to a qualitative change, i.e. a decision making, in the planned path. For distances larger than 50 cm the robot passes straight through the obstacles to reach the target while for smaller distances it turns around.

Decision making through bifurcations generated by the moving vehicle itself

The bifurcation we have just described was induced by changing the environment as sensed from the sensors, while the robot's position and orientation were kept fix. Now we show results where planning decisions arise during actual motion.

In Figure 4.15 the time course of the robot's position and corresponding planning dynamics, as the robot moves from an initial position toward the target location, is shown. The robot faces two obstacles that are separated by a distance (20 cm) smaller than the robot diameter. The target location lies behind the obstacles.

Initially (see Panel A) no obstructions are sensed by the infra-red sensors, thus the obstacle contributions to the vector field of the planning dynamics are null. Only the target contributes, the planning dynamics has therefore an attractor at the direction at which the target lies, as seen from the current position. The heading direction is relaxed in this attractor. As the robot approaches there is a distance for which it starts to detect obstructions (Panel B). The obstacle avoidance dynamics erects a repeller, at the average direction in between the two obstacles ($\pi/2$ rad), which is weakly repulsive since the obstacles are still far away. The resultant vector field maintains the attractor at about the same position although its strength of attraction is weakened. Behaviorally, the robot moves straight ahead. As the robot continues approaching the obstacles an instability takes place (Panel C). This because as the sensed distances to obstructions decrease the strength of the corresponding repulsive force-lets increase. Thus the strength of the repeller erected by the obstacle avoidance dynamics increases and eventually overrides the attractor, leaving a repeller there and two atractors, one on each side which correspond to the two possibilities, turning to the right or to the left. A bifurcation (subcritical pitch-fork bifurcation) in the path planning dynamics has taken place. The system has made a decision (no path is possible through the obstacles). As the distance decreases even further the strength of repulsion of this new repeller increases (Panel D) and strongly repels the heading direction of the robot from the direction it specifies. The robot circumnavigates then the entire area in which obstructions have been detected (Panel E). When it reaches the position indicated in Panel E another bifurcation takes place. An attractor replaces the repeller and the planning dynamics pulls henceforth the robot to move toward the target.

If there is no opening between the obstacles, so that a single broad obstruction is encountered (Figure 4.16), the same bifurcations take place and the robot follows a qualitatively similar path. A new challenge is posed however. When too many obstacle contributions are simultaneously activated, spurious attractors could hypothetically arise: the pull to the left exerted by one contribution could be cancelled by

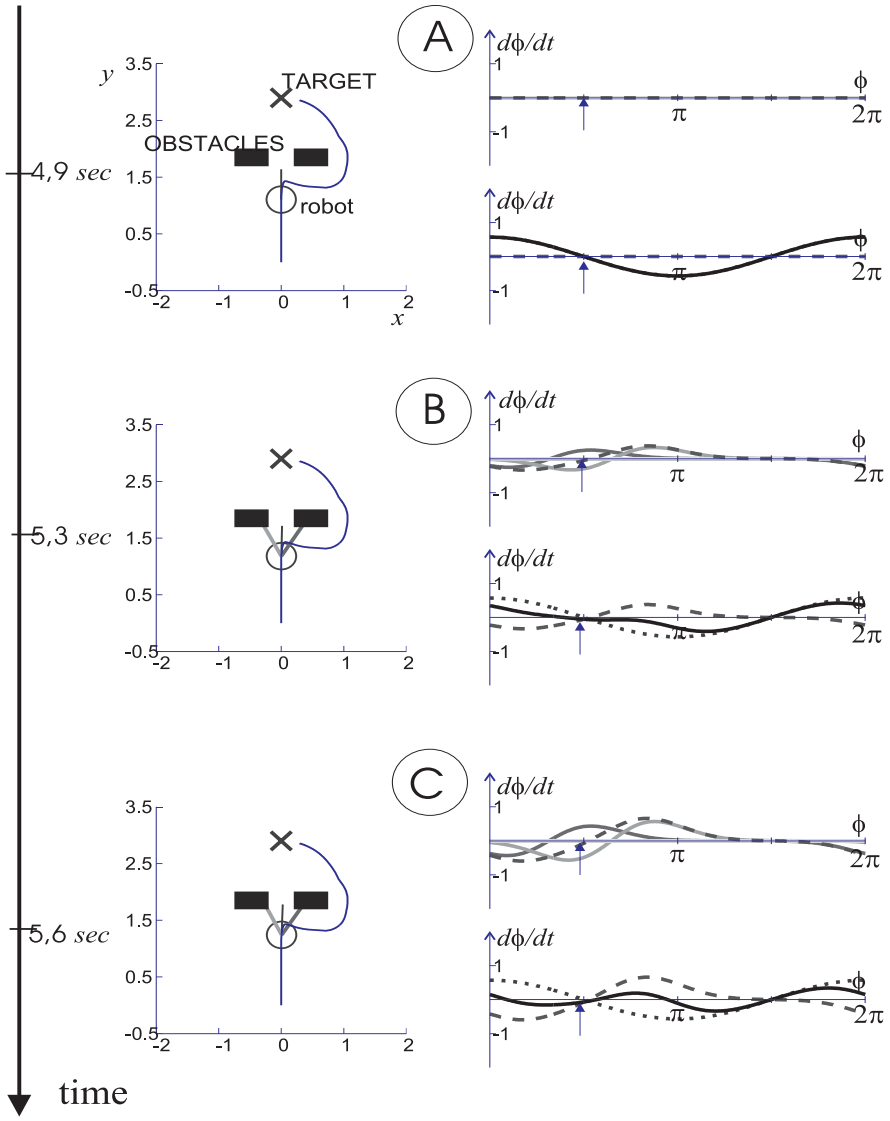

Figure 4.15: Evolution in time of the robot's position and corresponding heading direction dynamics as the robot moves toward the target. Initially the robot is positioned at coordinates $(0, 0)$ m facing two obstacles, which are separated by 20 cm (smaller than the vehicles size). The target position is at $(2.9, 0.0)$ m. Each picture in the left column shows the robot position at a certain instant of time. For each robot position two plots are presented. The first plot shows the individual repulsive force-lets (grey lines) and their superposition (dashed line). The second plot illustrates the resultant obstacle contributions (dashed line), the target contribution (doted line) and their sum (solid bold line). The arrow in the plots indicates the current value of the heading direction. The robot moves ahead, toward the target, until it detects the obstacles. Since the spacing between the obstacles is small the robot circumnavigates then both obstacles, through their right, and eventually reaches the target(cont.).

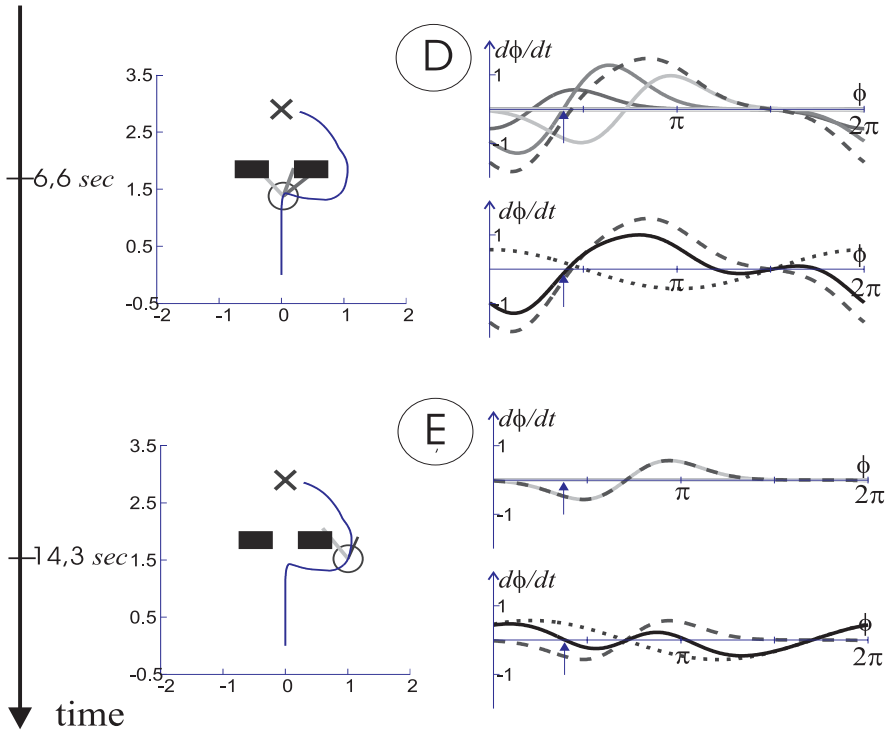

Figure 4.15: Continued.

the pull to the right of a next contribution. The figure demonstrates, however, that even when multiple contributions are simultaneously activated, spurious attractors need not arise.

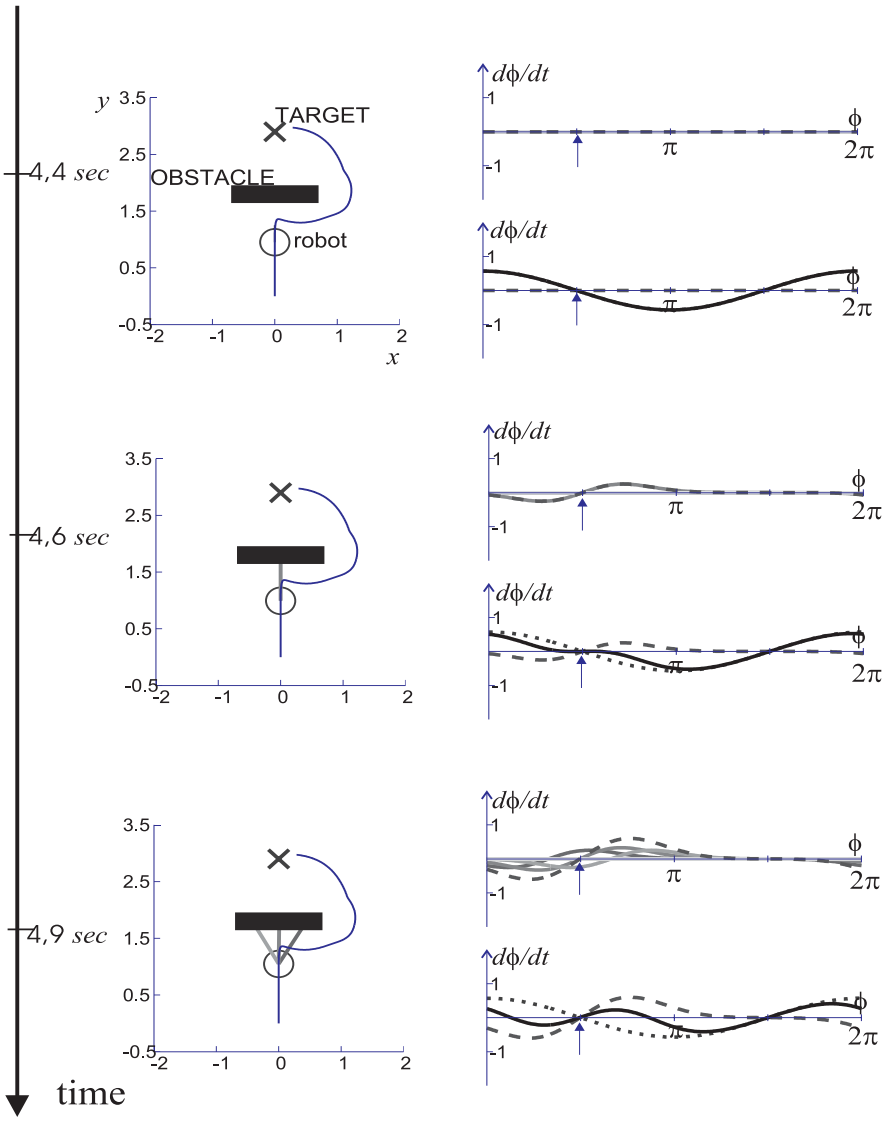

Figure 4.16: This figure is elaborated as explained in the Figure 4.15. The overture between the obstacles depicted in that figure is here closed. The robot follows a qualitative similar path. It circumnavigates the long obstacle and successfully reaches the target(cont.).

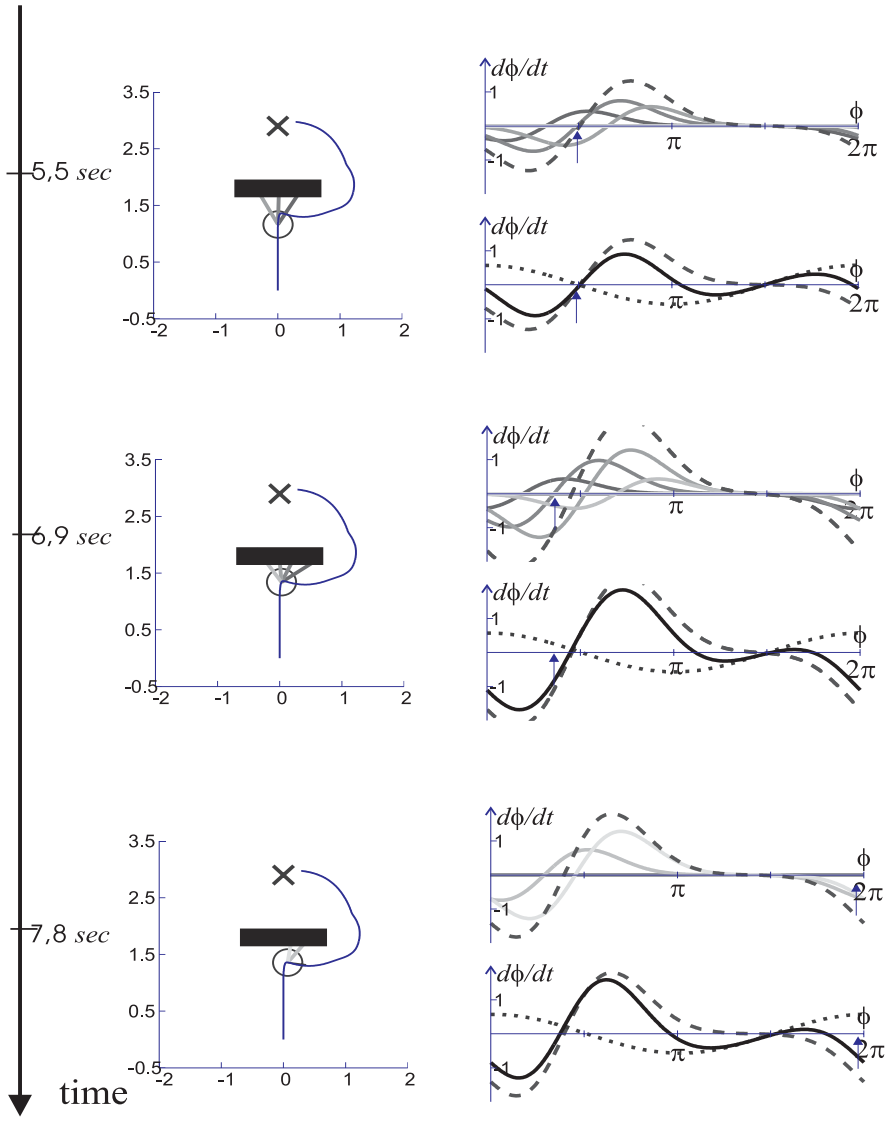

Figure 4.16: Continued.

When the separation between the obstacles is sufficiently large the path followed is qualitatively different. This is illustrated in Figure 4.17 where the overture between the two obstacles was made just slightly larger (55 cm) than the robot size. The time course of the robot position and corresponding planning dynamics is also depicted. While the distance of the robot to the obstacles is larger than the range of detection of the infra-red sensors no obstructions are detected and the resultant vector field has an attractor at the direction pointing toward the target (Panel A). The robot moves thus straight ahead. When the robot arrives at the position indi-

cated in Panel B it detects two obstructions. At this point the angular separation

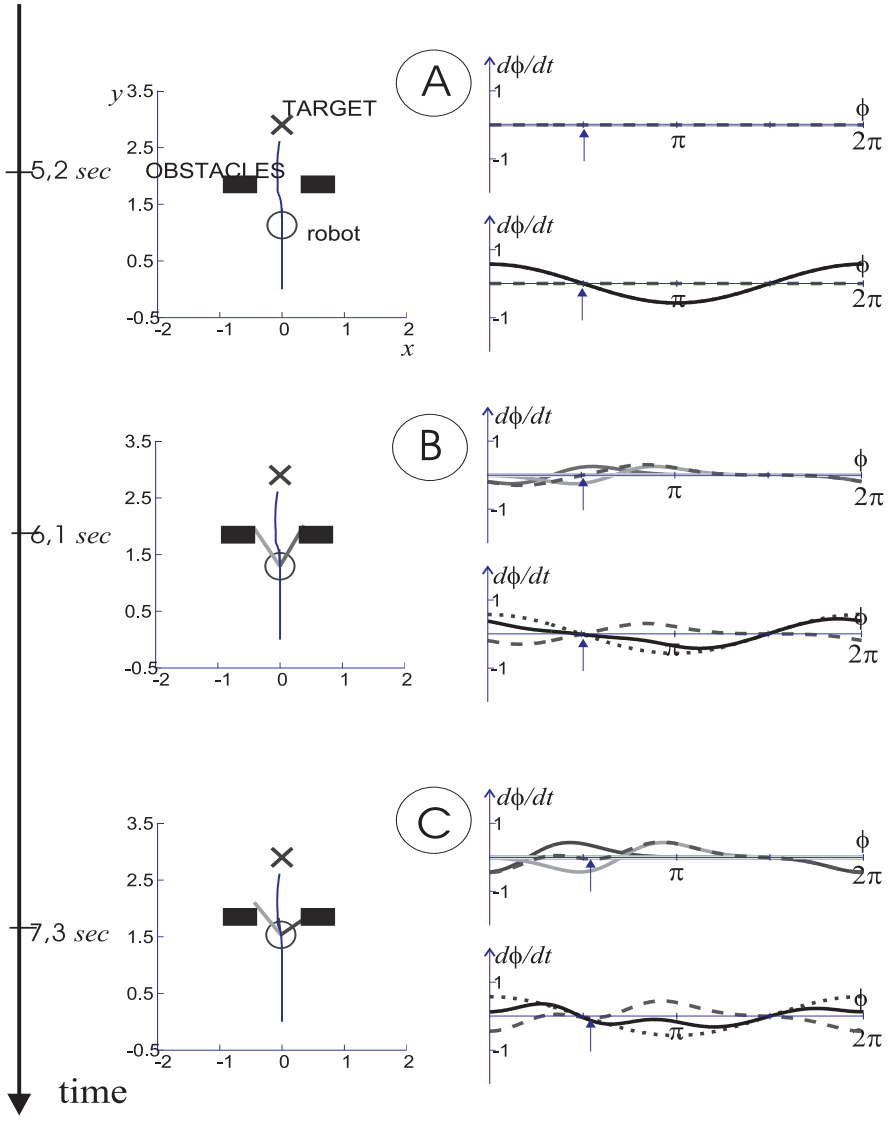

Figure 4.17: The obstacles depicted in Figure 4.15 are now placed at a distance of 55 cm which is larger than the robot's size. The qualitative path is therefore different. Here the path is more direct. The robot passes through the overture in between the obstacles to reach the target(cont.).

between the two obstructions, as detected from the current position of the robot, is relatively small. The corresponding repulsive force-lets are sufficiently overlapping and therefore these contributions are linearly dependent. Their superposition produces a repeller at their average angular distance. This repeller "competes" with the attractor from the target dynamics. Because the strength of the attractor is

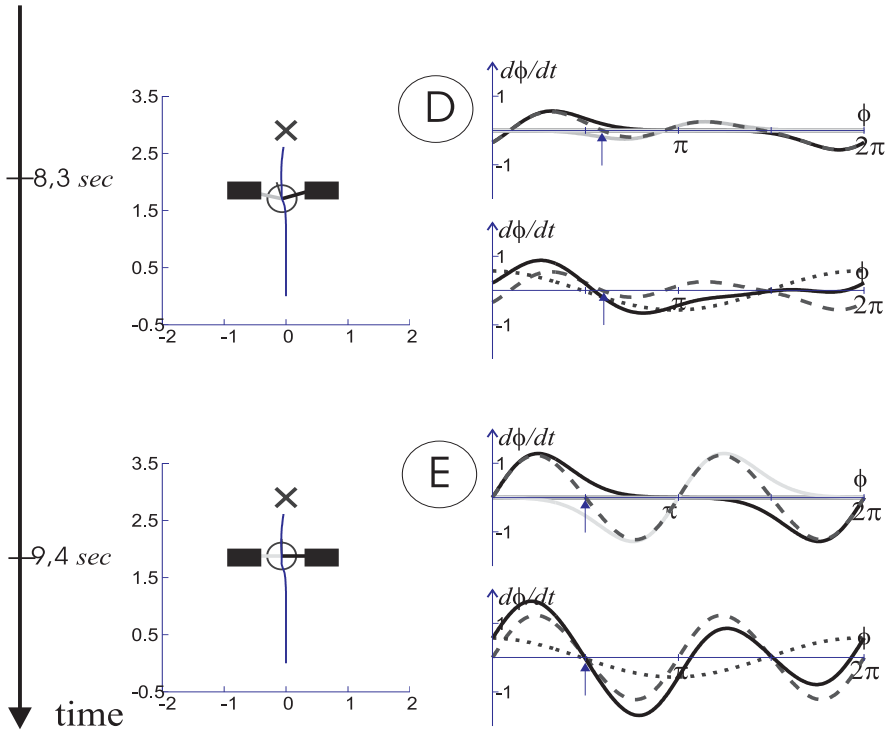

Figure 4.17: Continued.

stronger than the repulsion of the repeller the resultant vector field maintains an attractor, although less stable, at the direction at which the target is seen. The robot continues driving ahead. As the robot approaches the obstacles their angular separation, as detected from the current position of the robot, increases. The individual repulsive force-lets become less overlapping. At a certain distance a phase transition in the obstacle avoidance dynamics takes place. The sum of the repulsive contributions now forms an attractor at that direction (Panel C). From this point on, obstacle and target contributions cooperate and the resultant attractor is thus more stable. In spite of the fact that the obstacle dynamics went through a phase transition the complete vector field always produced a continuous varying attractor solution, which smoothly tuned the robot movement through the narrow passage toward the target.

Stability

We have just seen that as the vehicle moves the directions to the obstacles and the target in the world change, thus the resulting attractor of the planning dynamics shifts. Figure 4.18 shows, for the three examples presented above, how the time courses of the heading direction track the time courses of the attractor solutions of the heading direction dynamics. In each case, the system tracks one of the attractors closely, except for those moments in time, when a bifurcation occurs, and some time

is needed to relax to the nearest new attractor. These results demonstrate that the complete dynamic planning system is stably coupled in closed loop to the sensory information.

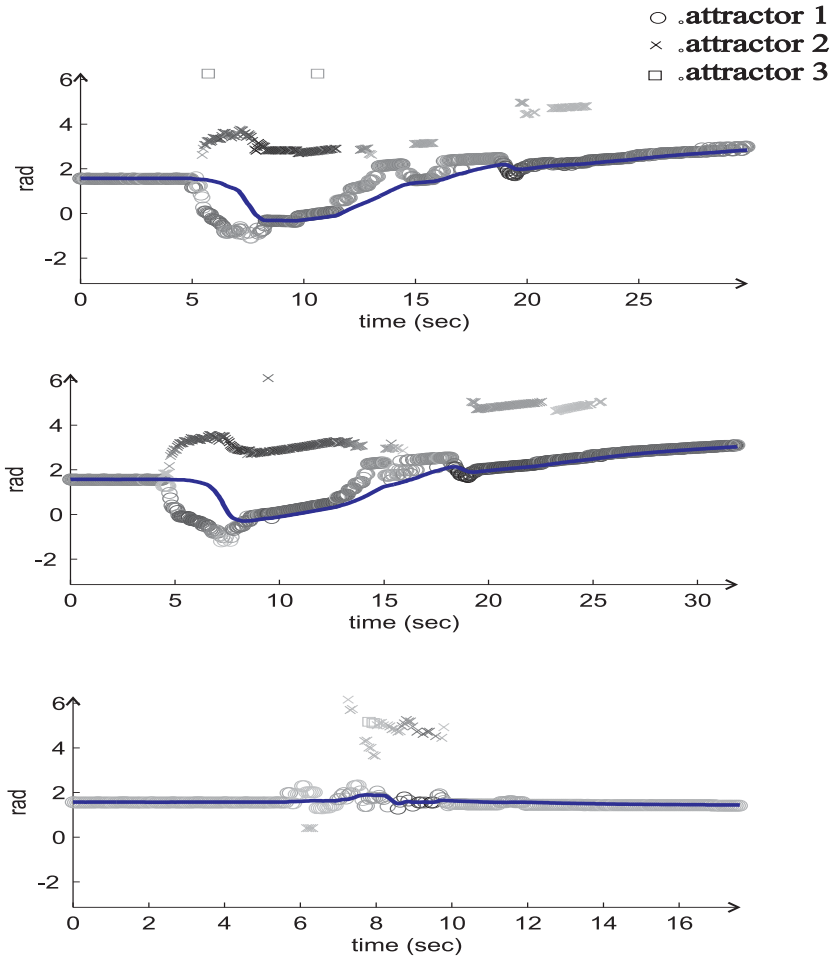

Figure 4.18: These three plots show the time course of the attractors and heading direction for each of the paths shown in Figures 4.15, 4.16 and 4.17 respectively. The attractors are represented by circles, crosses and squares. The color of these symbols gives information about the corresponding strength of attraction of the attractors they represent: The darker they are the more stable the attractors are. The time course of the heading direction is the black solid line.

4.5.2 Velocity control

To maintain the system stable, i.e. in or near an attractor, we guarantee that the vehicle drives sufficiently slow so that the rate of shift of the attractors occurs at a slower time scale than the time scale of the path planning dynamics. Figure 4.19

illustrates the path velocity dynamics as the sensed world changes.

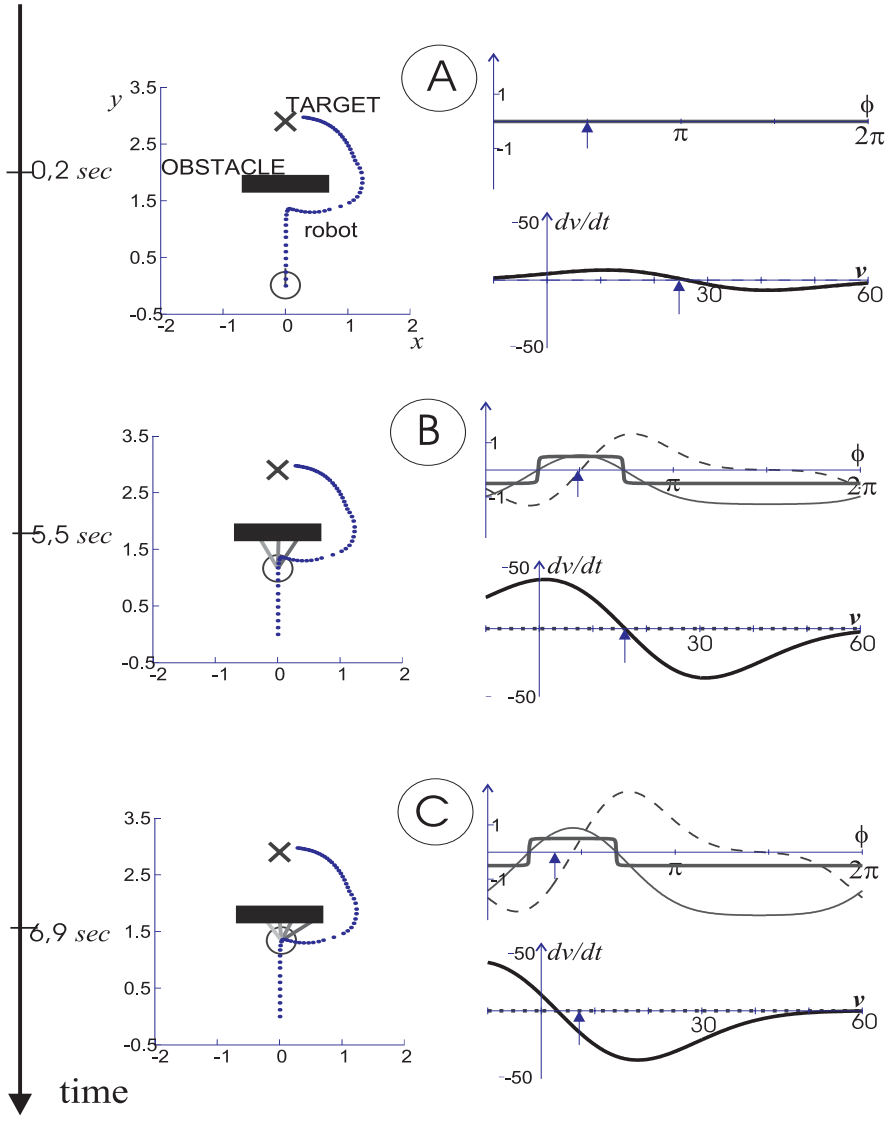

Figure 4.19: Evolution in time of the robot's position and velocity dynamics as the robot moves toward the target for the situation illustrated in Figure 4.16. Each picture in the left column shows the robot position at a certain instant of time. For each robot position two plots are presented. The first plot shows the resultant obstacle contributions F_{obs} (dashed line), the corresponding potential U (solid thin line) and thresholded potential α (solid bold line). The arrow indicates the current value of heading direction. The second plot depicts the velocity dynamics and the arrow indicates the vehicle's current velocity. The trajectory is depicted as a sequence of points. The time interval between two consecutive points of the trajectory is constant. Thus the plotted trajectory directly gives a perception of the robot's path velocity: The closer the points are the smaller the velocity is (cont.).

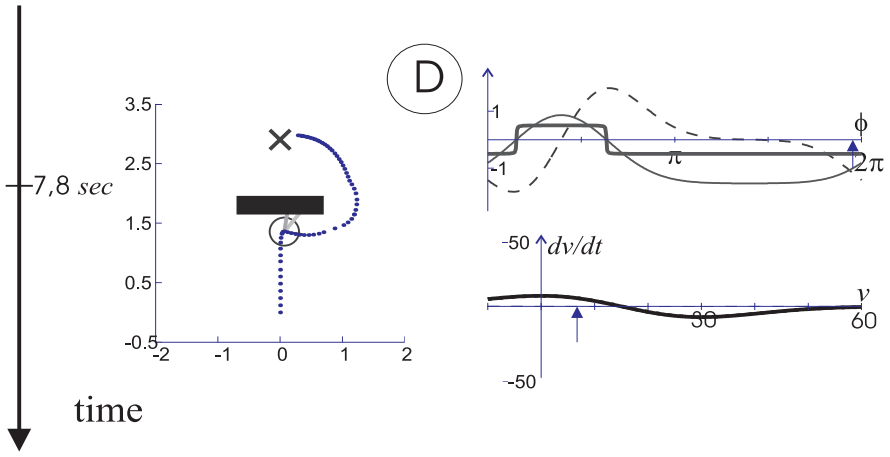

Figure 4.19: Continued.

Panel A shows that when no obstructions are detected (indicated by negative or zero $\alpha(\phi)$ at the current heading direction) the robot velocity is stabilized by an attractor, which is set proportional to the distance to the target, according to the target constraint imposed by Equation 4.15. Conversely when obstructions are detected (as illustrated in Panels B and C), $\alpha(\phi)$ is positive at the current heading direction, the velocity dynamics is governed then by an attractor whose value is proportional to the minimal sensed distance to the obstructions if this minimal distance is larger than 25 cm, otherwise its value is set proportional to $d_{\min} - 20$ cm. This way the obstacle constraints are satisfied. Panel D shows what happens in a situation where obstructions are detected but the robot's heading direction is outside the repulsion zone created by the obstructions ($\alpha(\phi)$ negative). In this case the velocity dynamics is dominated by the target constraint as we have just explained above. The strengths of the attractors, erected by target or obstacle contributions for the velocity dynamics, are adjusted according to Equation 4.21.

Again, as the vehicle moves the attractor for the path velocity dynamics, either erected by the target or obstacle constraints, shifts. The system is able to follow the attractor, however. This is depicted in figure 4.20.

4.5.3 Sample trajectories in complex environments

Figures 4.21 to 4.24 show sample trajectories of the robot as recorded by the dead-reckoned robot position. The initial position of the vehicle is always considered the referential point with respect to which the target coordinates $(X_{\text{target}}, Y_{\text{target}})$ are given. The vehicle stops running when the estimated distance to the center of the vehicle to the target is equal to 30 cm. The error in this estimated distance and the real distance varies between 10 and 20 cm depending on the length of the overall path.

In the run depicted in Figure 4.21 the robot is initially placed inside a box. The target position lies outside at coordinates $(X_{\text{target}}, Y_{\text{target}}) = (1.5, -1.5)$ m. As

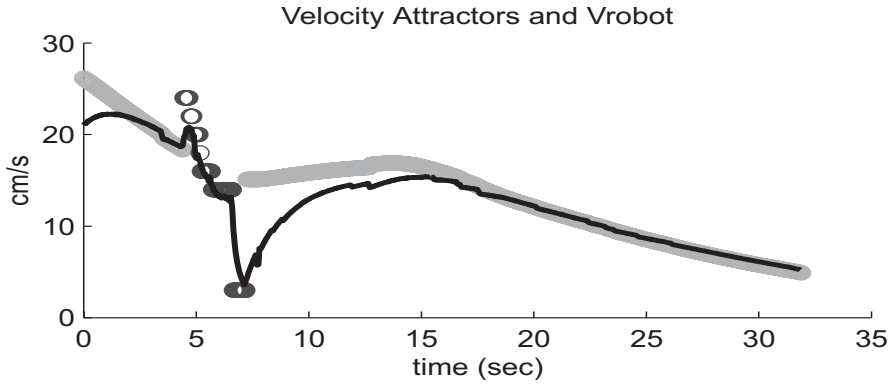

Figure 4.20: Time course of the attractor from the path velocity dynamics and robot's velocity along the path depicted in Figure 4.16. The attractor is represented by a circle. The color gives information about its strength of attraction. Darker color indicates stronger attractor. The time course of the path velocity is the black solid line.

one can see, the robot first turns toward the target direction and circumnavigates the detected obstacles that constitute the walls. It then finds the exit and continues moving toward the target until it is inside the neighborhood of the target coordinates.

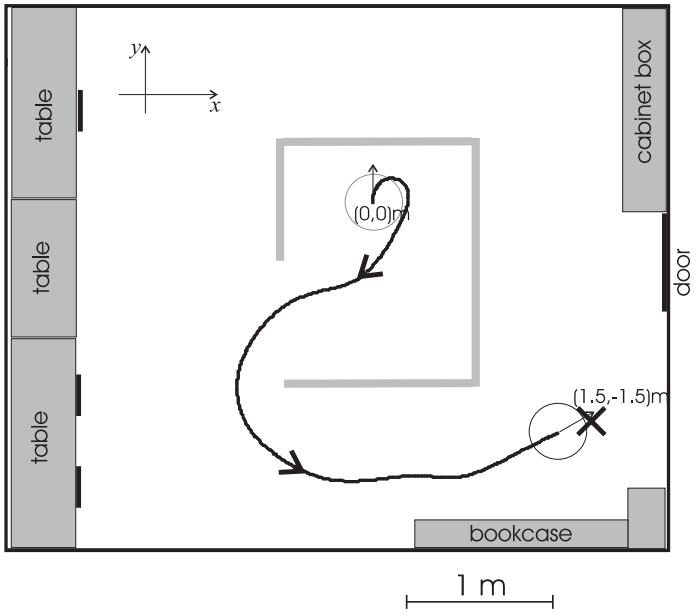

Figure 4.21: A sample trajectory of the robot as recorded by the dead-reckoned position. Robot initial position is considered the reference point. The target is placed at a position $(1.5, -1.5)$ m with respect the reference point.

The two runs depicted in Figure 4.22 demonstrate the flexibility of the path gen-

erating system. The results reported in subsection 4.5.1 have also demonstrated this property, of course, but here the environment is more complex. Initially the robot is positioned outside the box, in the bottom right corner. The target coordinates fall inside the box ($(X_{\text{target}}, Y_{\text{target}}) = (-2, 1.8)$ m). In the first run (top Panel) the robot circumnavigates the obstacles taking the top direction. It finds its way into the box while successfully avoiding the walls and finally ends up stopping near the target position. In the second run (bottom Panel) three obstacles indicated by A, have been placed in front of the robot with respect to its departure position. From this position the additional obstacles are not detectable, since they have been placed at a distance larger then the sensors range. Initially, the robot attempts to reach the target through the top direction as before. However, it detects that this way is a dead-end. Therefore, it changes the direction of driving and once again successfully reaches the target.

A longer run is illustrated in Figure 4.23. Initially, the robot is positioned in the corridor of our lab. The target position lies inside a box in one of the offices, $(X_{\text{target}}, Y_{\text{target}}) = (-3.2, 3.0)$ m. The robot drives along the corridor. Then, based on the target contribution and helped by obstacle avoidance, the robot moves through the office door. It circumnavigates the obstacles and eventually reaches the entrance of the box. Finally, it stops near the target position.

All the results presented till now were obtained using distance measures provided by infra-red sensors only, because it makes the computation cycle faster and thus larger path velocities are possible. We end this section by illustrating the simultaneous use of infra-red sensors and sonars and the concomitant implications in the generated path.

When infra-red sensors are used together with the sonars, sensory information is acquired in the following way: The signal of each infra-red sensor is read only once per each computation cycle as when they are used in isolation. In each computation cycle five measures for each sonar are taken. In this case the cycle time is approximately 70 ms. The distance estimate provided by a sonar is then taken as the average among the five measures. This way errors due to specular reflexions are reduced to a large extend. The "sensory fusion" between infra-red sensors and sonars is performed through a very simple algorithm. In the overlap distances interval (e.g from 45 to 60 cm) the minimum distance is taken as the estimated distance to a detected obstruction.

Figure 4.24 illustrates how sensors distance range affect the generated path. This figure shows two runs executed in the same scenario. The target position is at coordinates $(X_{\text{target}}, Y_{\text{target}}) = (-1.0, 2.2)$ m with respect to the vehicle's departure position. In the first run only infra-red sensors have been used to measure distances to obstructions. The maximal distance at which obstructions can be detected is 60 cm. Initially, the robot turns left in order to avoid the obstacles, indicated by A, which lie on its right side. Then the robot attempts to reach the target through the left direction. However it detects that this way is a dead-end (indicated by B). It changes therefore its direction of driving and successfully reaches the target position.

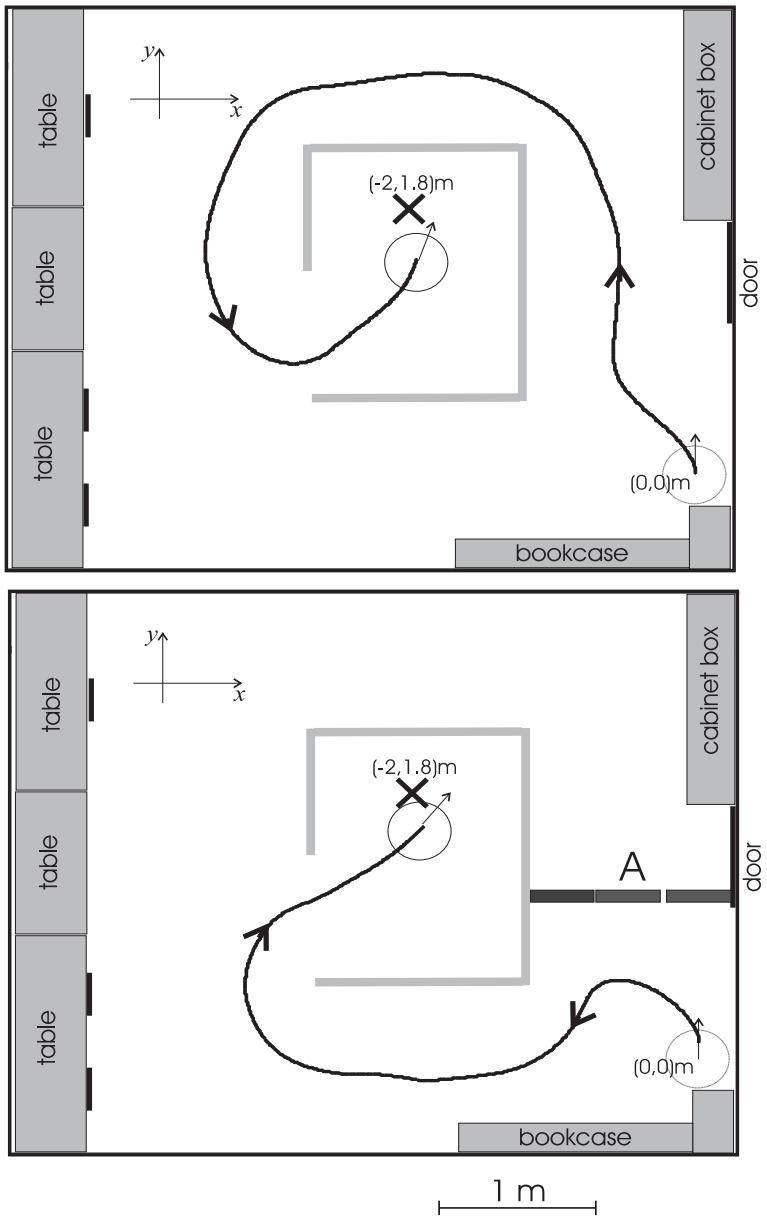

Figure 4.22: Flexibility of the path generating system is illustrated here. Top: the robot is positioned initially at the lower left corner as illustrated. The target lies inside the box at coordinates $(-2, 1.8)$m with respect to the departure position. The generated trajectory that brought the system from its initial position to the target location is depicted. Bottom: Here additional obstacles have been added to the configuration in a form that blocks the previous path. The resultant trajectory takes a different course.

In the second run (depicted on the right side of the figure) both infra-red sensors and sonars are used. The maximal distance at which obstructions can be detected is now 175 cm. The robot starts detecting obstacles for larger distances and as a

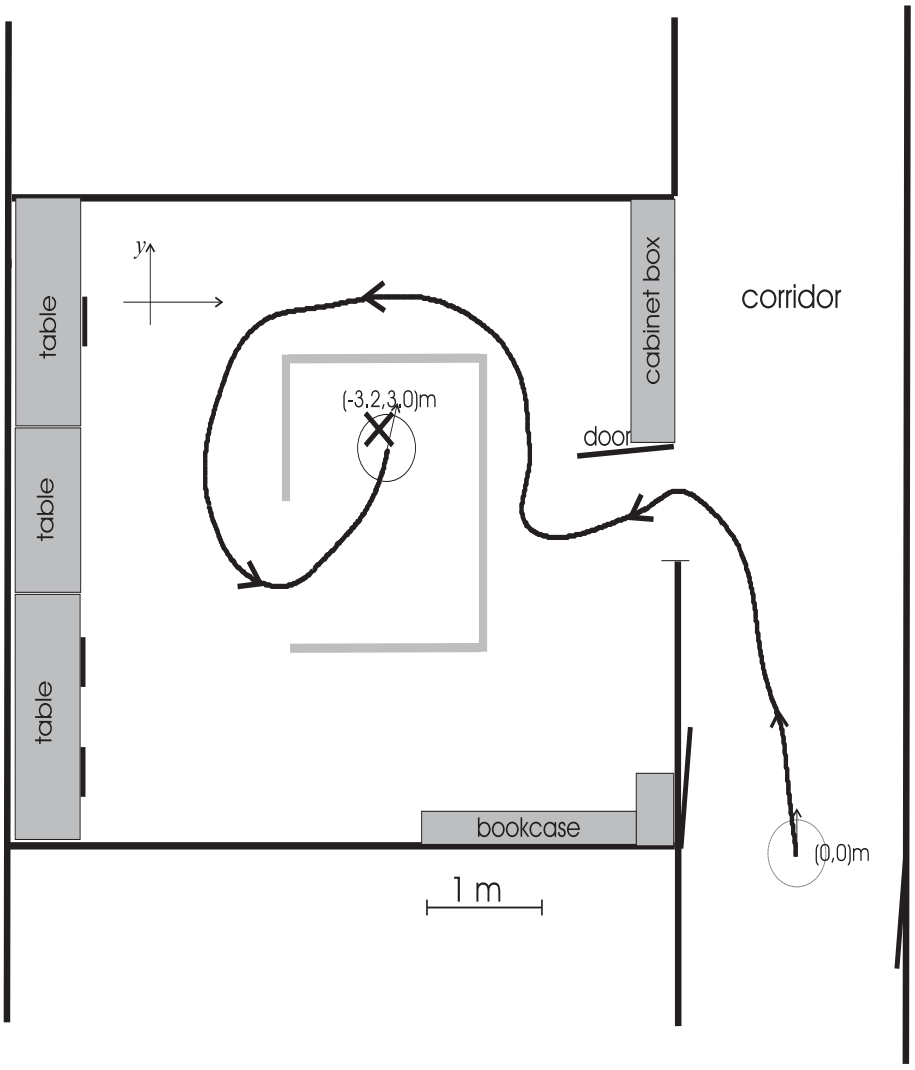

Figure 4.23: Another and longer trajectory is depicted here. The robot is initially placed at the corridor. The target location is inside an office at coordinates $(-3.2, 3)$m relative to the departure position.

consequence it can anticipate which direction to move. The dead-end is detected earlier.

As we can see from the results the dynamic path planning system leads to smooth collision free trajectories to the target. The result is valid for both types of sensors.

4.6 Conclusion

In this chapter we have demonstrated that the dynamic approach to path generation can be used even in the absence of veridical representations of obstacles as objects

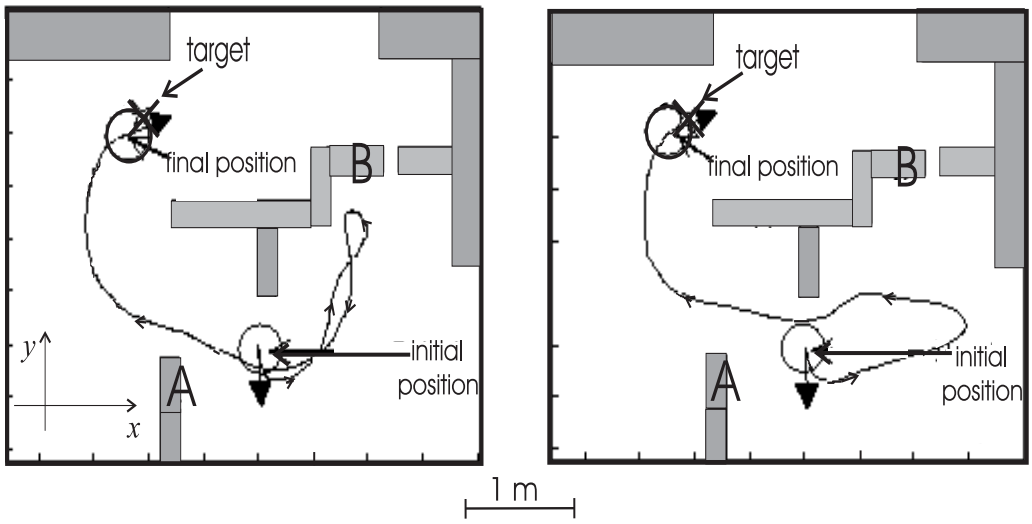

Figure 4.24: Two sample trajectories of the vehicle as recorded by the dead-reckoned position are depicted. The target is placed at coordinates $(-1.0, 2.2)$ m with respect to the robot's initial position. Left: Only infra-red sensors have been used to measure distances to obstructions. Right: Distance measures to obstructions have been provided by infra-red sensors and sonars.

in the world. The information from distance sensors is directly used to define contributions to a dynamical system of path planning. Heuristically, the sum over such contributions has attractors that specify collision free directions toward the target. Target and obstacle constraints also define contributions to a dynamical system of path velocity. The generated trajectories are smooth. Flexibility is achieved in that as the sensed environment changes, the system may change its planning solution continuously, but also discontinuously.

Because this dynamic path generation system is a local form of path planning one cannot guarantee that the trajectories toward a target are optimal with respect to the overall traveled path.

The proposed solution involves explicit design and all system parameters can be specified rationally based on the qualitative theory of dynamical systems and bifurcation theory. The system never entered into spurious attractors.

Although we did not show here it for technical reasons, the dynamic architecture works for dynamic environments, as long as the rate of change of the environment is slow compared with the relaxation time of the planning dynamics. No conceptual difference exists between stationary and moving obstacle avoidance. Avoiding moving obstacles is shown on a video demonstration.

Since motion planning is just a piece in the way robots interact with their world, a next direction is to integrate this motion planning system with the related problem of target detection and localization.

Chapter 5

Demonstrating the dynamic approach on the 8-bit micro-controller based platform

We have seen that the dynamic approach proposes a set of concepts with the help of which autonomous systems can be specified and designed. While the approach builds systems from elementary behaviors driven by behavior-specific sensory information, it also represents behaviors internally in terms of the state of dynamical systems, thus positioning itself somewhere between classical and behavior-based approaches.

This chapter demonstrates that the dynamic approach also lends itself naturally to implementation on computationally very weak platforms, such as an 8 bit micro-controller based vehicle, working with very low level sensory information.

Obstacle avoidance and target acquisition are implemented on Rodinsky. Obstacle avoidance is based on using the five infra-red detectors as distance sensors. Target acquisition consists of *photo-taxis* and is based on two photo-resistors.

We show how theoretical design, software simulation, and hardware implementation are tied effortlessly.

As a technical novelty we demonstrate the integration of dynamics at two different levels of temporal derivative (see also Bicho and Schöner, 1997a).

5.1 Photo-taxis

As a simple form of sensory driven target acquisition we implement the task of *photo-taxis*, that is, the task of moving toward light sources (see Schone, 1984, for the biological background). This obviates the need for explicit representation of ego-position and its updating through dead-reckoning or other means (but see Steinhange and Schöner, 1997) for a dynamic approach toward such ego-position representation). The idea is, essentially, to provide a dynamic version of Braitenberg's proposal (Braitenberg, 1984). Braitenberg pointed out, that the mere

feed-forward connection of two light sensors, mounted side by side, to two motors, driving the wheels of a single axle vehicle, can be organized to generate *photo-taxis*. For instance, the left light sensor might be connected to the left wheel such as to drive the wheel the faster the less light is sensed, and, correspondingly, the right light sensor would drive the right wheel the faster the less light is sensed. This leads to that wheel turning faster, on the side of which less light is sensed, so that the vehicle turns toward the brighter side. The result is orientation toward light sources, that is, *photo-taxis*.

This proposal can be implemented quite directly using, for instance, simple feed-forward neural nets. However two problems must be addressed. First, such simple taxis behavior must be integrated with other behavioral constraints, here for instance, with obstacle avoidance. Second, and relatedly, the properties of the taxis behavior must be characterizable so as to determine parameter values on a rational basis and to specify the temporal and spatial limits within which performance can be guaranteed. Both problems are solved by implementing the Braitenberg proposal within the dynamic approach. Integration with obstacle avoidance is discussed in the next section. The resultant behavior can be characterized in terms of linear stability theory. Because these dynamics in isolation do not undergo bifurcations, the result is equivalent to standard control theoretic solutions. The present formulation lends itself to integration with the obstacle avoidance module (cf. Section 5.2).

Light intensity is sensed by the two photo-resistors, one mounted on the left, one on the right side of the vehicle (see Figure 3.1). The output voltage of these photo-resistors, I_i (i =left or right), is a monotonically decreasing function of light intensity. Because the intensity of the light source, the geometry of surfaces in the surround and their reflectances all are unknown, the photo-resistors cannot be said to specify a direction in space in which the target lies. Translating Braitenberg's proposal into dynamics, we can say, however, that each light specifies a turning rate. For instance, the left photo-resistor can be constructed to specify turning to the right, while the right photo-resistor, correspondingly, specifies turning to the left. These turning rates increase with voltage (that is, decreasing with light intensity),

$$\omega_{\text{left}} = -c_{\text{target}} I_{\text{left}} \tag{5.1}$$

$$\omega_{\text{right}} = c_{\text{target}} I_{\text{right}} \tag{5.2}$$

(keep in mind that ϕ is mathematically positive, so that negative $\omega = \dot{\phi}$ means turning right). Thus, when the left sensor receives more light than the right sensor, I_{left} is smaller than I_{right} and hence the rate of turning right is smaller than the rate of turning left. The vehicle would turn left toward increasing light intensity.

The averaging among the two specified turning rates is done by a dynamical system

$$\frac{d\omega}{dt} = g_{\text{taxis}}(\omega) = g_{\text{left}}(\omega) + g_{\text{right}}(\omega) \tag{5.3}$$

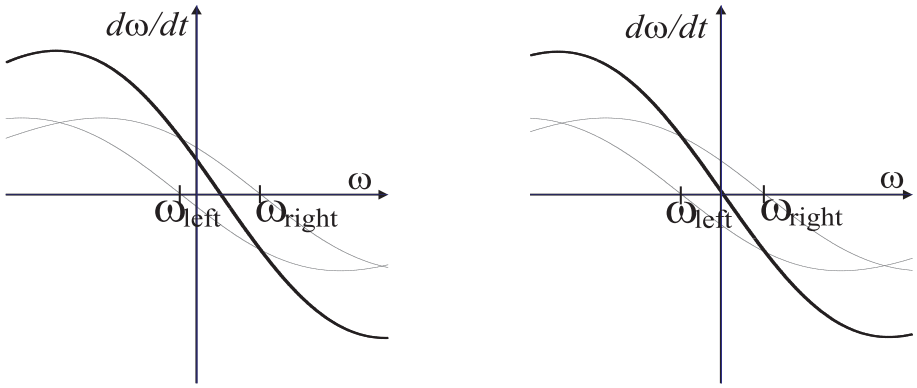

Figure 5.1: Two contributions for *photo-taxis* to the dynamics of turning rate are superposed (bold curve) leading to an attractor at an averaged turning rate because we use rather broad range functions. On the left, the right sensor receives much less intensity than the left sensor, which leads to an attractor at positive turning rates. On the right, both sensors are similarly stimulated leading to an attractor close to zero turning rate.

with two additive contributions, each defining an attractive force-let (i = right or left) centered at the turning rate value specified by the corresponding light sensor:

$$g_i(\omega) = -\frac{2}{\tau_{\text{taxis},\omega}}(\omega - \omega_i)\exp\left[-\frac{(\omega-\omega_i)^2}{2\Delta\omega^2}\right] \tag{5.4}$$

The time scale of this taxis dynamics, i.e. the relaxation time to the resultant attractor, is specified by $\tau_{\text{taxis},\omega}$. As illustrated in Figure 5.1, we use a broad range function ($\Delta\omega$ larger than the maximal values of ω_i) to average these two forces so that the resulting dynamics exhibits only one attractor, at positive or negative turning rates depending on which sensor detects more light intensity. For instance, when the left sensor receives more light intensity than the right sensor, the resulting dynamics leads to an attractor at positive turning rates, which implies turning to the left (left side in Figure 5.1). Conversely, when the right sensor receives more light intensity than the left sensor, the resulting dynamics exhibits an attractor at negative turning rates, which implies turning to the right. When both sensors are stimulated by similar light intensity the resulting dynamics has an attractor close to zero turning rate (right side in Figure 5.1).

5.2 Obstacle avoidance dynamics defined at the level of turning rate

In Chapter 4 we have defined a dynamics for obstacle avoidance using the heading direction of the vehicle, ϕ, in an arbitrary but fixed world reference frame as a behavioral variable. As we have just analyzed in the previous section, it turns

out to be difficult to express *photo-taxis* at this level since the difference of light intensity sensed on either side of the vehicle does not specify a direction, in the world, toward which to move in the absence of a world model (of the light source and the surrounding reflective surfaces). Nevertheless, we have shown how a dynamics for the turning rate, $\omega(=\dot{\phi})$, can be defined that has the adequate attractor to achieve *photo-taxis*. Thus, integrating an obstacle avoidance dynamics as it was specified in Chapter 4 with *photo-taxis* dynamics which was defined at the level of turning rate involves integration of dynamics at two different orders of temporal derivative of the dynamical system. To achieve this, we must find a way to lift the dynamics for obstacle avoidance from the level of ϕ to the level of $\dot{\phi}$ (i.e. ω).

This lifting can again be based, of course, on the basic concepts of the dynamic approach. We must ask which state at the level of ω is specified by the obstacle contributions and then we use bifurcation analysis to select the adequate functional form. Quite simply, while the heading direction is outside the repulsion zone created by the obstacles or when obstacles are very far way ($\lambda_i \approx 0$, in Equation 4.2), obstacle contributions (given by Equation 4.1) are small ($F_{\text{obs}} \approx 0$) and do not specify any change of heading direction. This can be expressed by specifying an attractor for a dynamics of ω at $\omega = 0$ ("move straight ahead"). Inside the repulsion zone at sufficient strength of the contribution, the attractor at $\omega = 0$ must turn into a repeller ("do not move straight ahead"). This transition can be modeled by a pitchfork bifurcation, which stabilizes two new attractors at positive and negative turning rates $\pm\omega \neq 0$. Its normal form

$$\frac{d\omega}{dt} = \alpha_{\text{taxis}}\omega - \gamma_{\text{taxis}}\omega^3 \tag{5.5}$$

is illustrated in the top row of Figure 5.2. (See e.g., Perko, 1991), for the mathematical background). At $\gamma_{\text{taxis}} > 0$ fixed, the dynamics is switched by α_{taxis} from a regime with a single fixed point attractor at $\omega = 0$ ($\alpha_{\text{taxis}} < 0$, top left in Figure 5.2) to a regime with two fixed point attractors at $\pm\sqrt{\alpha_{\text{taxis}}/\gamma_{\text{taxis}}}$ (turning either left or right) ($\alpha_{\text{taxis}} > 0$ top right in Figure 5.2). Thus, α_{taxis} must change sign as function of whether the obstacle contributions are sufficiently weak or not and as a function of whether or not the current heading direction is in the repulsion zone of the obstacle contributions.

Applying a sigmoid threshold function to the potential function, U, of the obstacle avoidance dynamics at the level of heading direction (i.e. Equation 4.17) such as

$$\alpha_{\text{taxis}}(\phi) = \frac{\arctan[cU(\phi)]}{\pi} \tag{5.6}$$

therefore generates the desired transition behavior. The parameter c determines the size of the transition zone. This function is depicted in Figure 4.12.

This analysis was entirely local to $\omega = 0$. It did not take into account that in the presence of repulsive forces these also specify something beyond the immediate

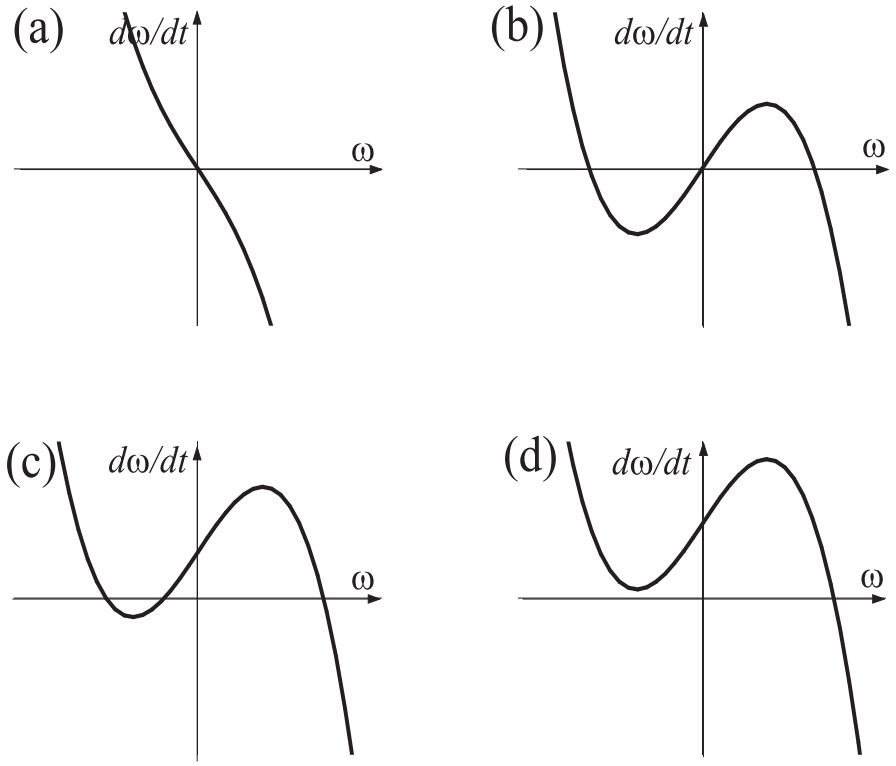

Figure 5.2: The dynamics of turning rate for obstacle avoidance are shown, on top, in the form of Equation 5.5 and, on bottom, in the form of Equation 5.7. (a) The single attractor at $\omega = 0$ for negative α_{taxis} bifurcates in a pitchfork bifurcation into (b) two symmetric attractors for turning left or right at positive α_{taxis}. This bistability generates hysteresis, which ensures that a decision to turn either way persists sufficiently to suppress oscillations. The symmetry of this dynamics is reduced by adding a constant term proportional to the obstacle forces, F_{obs}. In (c) this constant is positive, enlarging the basin of attraction of the attractor at positive turning rate, but maintaining bistability. In (d) the obstacle forces are so large and positive that the attractor at negative turning rate has undergone a tangent bifurcation and the system is now exclusively governed by the attractor at positive turning rate.

vicinity of zero turning rate. In fact, from the sign of the obstacle forces, F_{obs} given by Equation 4.4 (see Figures 4.6 and 4.7), we can read off, whether an attractor at positive turning rate or an attractor at negative turning rate should be stabilized.

When F_{obs} is positive at the current heading direction means that the obstacles are to the right and the robot must therefore turn left. Conversely, when the obstacles are to the left F_{obs} is negative and the robot turns right.

Again, it is useful to think of the limit in which a bifurcation is generated: For sufficiently positive obstacle forces we want to eliminate the attractor at negative turning rates so that only an attractor at positive turning rates remains. Conversely, for sufficiently negative obstacle forces the attractor at positive turning rate must

disappear. These bifurcations can be modeled by *tangent bifurcations* induced by the obstacle forces:[1] For positive and increasing obstacle forces we can make the attractor at negative turning rates and the repeller at zero turning rate to move in the direction of each other such that they eventually collide and eliminate each other. Similarly, for negative and increasing obstacle forces the attractor at positive turning rates and the repeller at zero turning rate can be made to approach each other and finally cancel each other.

To integrate the tangent bifurcations with the pitch-fork bifurcation, we only need to add a term which is a function of the obstacle forces. To compute this term, we multiply the obstacle forces, F_{obs} with $\alpha_{\text{taxis}}+1/2$, which is infinitely close to zero wherever the obstacle contributions fall below a threshold. This way the attractor at $\omega = 0$ is not shifted unnecessarily when obstacle contributions are weak. The resultant obstacle avoidance dynamics

$$\frac{d\omega}{dt} = g_{\text{obs}}(\omega) = (\alpha_{\text{taxis}} + \frac{1}{2})c_{\text{w,obs}}F_{\text{obs}} + \alpha_{\text{taxis}}\omega - \gamma_{\text{taxis}}\omega^3 \tag{5.7}$$

is illustrated in the bottom row of Figure 5.2 for two different positive values of F_{obs}. On the left, the positive obstacle forces enlarge the basin of attraction of the attractor at positive turning rate. The attractor at negative turning rate continues to exist, however, so that the system is stabilized by hysteresis if it arrives at this situation while turning right. For even larger positive obstacle forces, the attractor at negative turning rate is eliminated by a tangent bifurcation (the dynamics lifts off the ω-axis) and only the attractor at positive turning rate remains. The system is thus mono-stable.

Figure 5.3 summarizes the situation by showing the four regimes arising from a single, finite strength force-let:

1. Outside the range of repulsion of the force-let the dynamics of turning rate is mono-stable with an attractor at $\omega = 0$ ("move straight ahead").

2. To the right of the direction, ψ_{obs}, into which the obstacle lies, negative values of f_{obs} specify turning right, corresponding to an attractor at a negative value of $\omega < 0$.[2]

3. To the left of that direction, positive values of f_{obs} specify turning left, corresponding to an attractor at a positive value of $\omega > 0$.

[1] A bifurcation in which occurs a sudden appearance and then splitting of a fixed point (or conversely) is called a tangent or saddle node bifurcation. It is called a tangent bifurcation because the curve $d\omega/dt = g_{\text{obs}}(\omega)$ becomes tangent to the ω axis at the bifurcation value.

[2] Note that we use the mathematical convention for direction so that heading direction increases for counter-clockwise rotation (turning left).

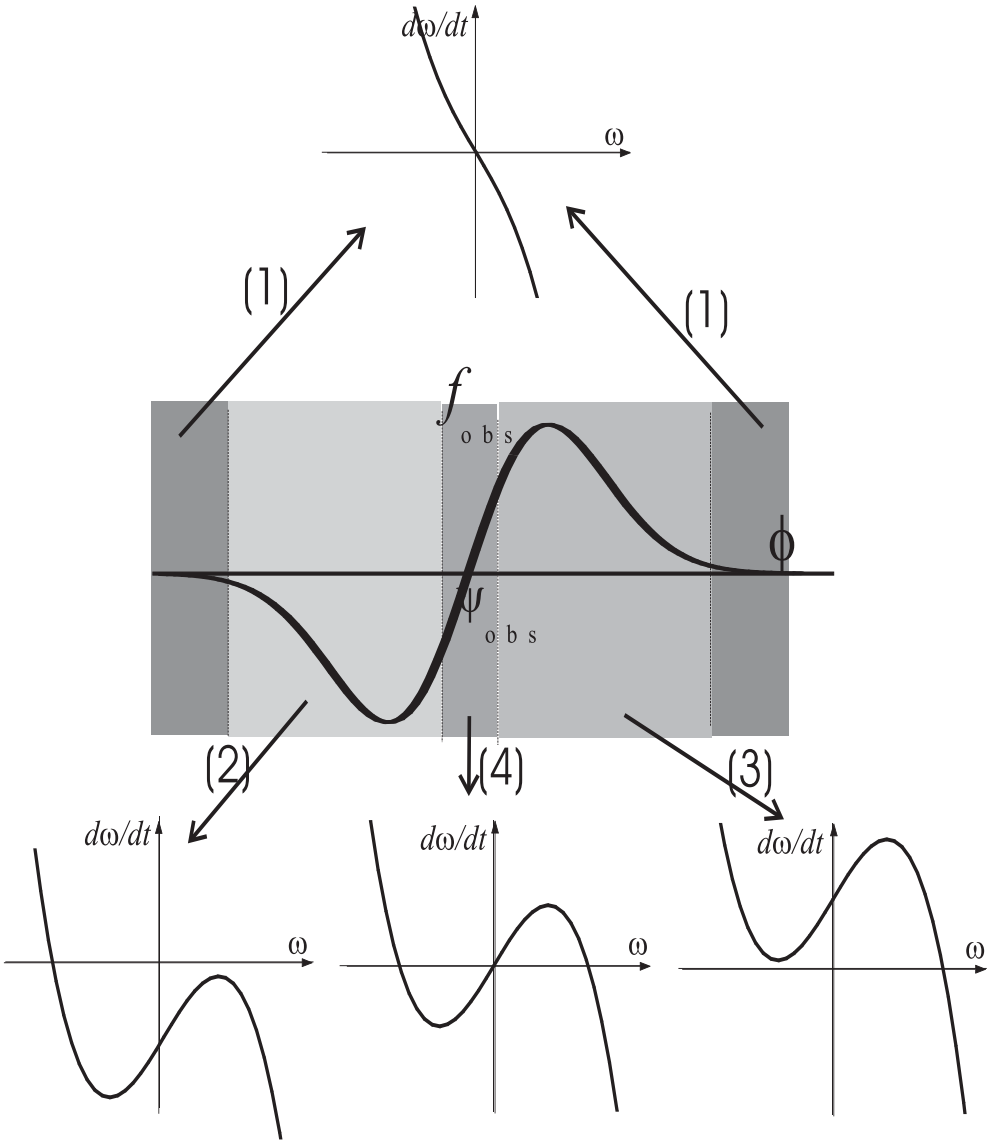

Figure 5.3: This figure illustrates how the different regimes of a single repulsive obstacle "force-let" (depicted at the center) are modeled at the level of turning rate. The outer regime far from the specified direction leads to a mono-stable dynamics of turning with an attractor at zero turning rate (top). For the direction in which the obstacle lies (center region) a bistable dynamics with attractors at a positive and a negative turning rate, and a repeller at zero turning rate is erected (bottom center). In the regime of negative obstacle force (left) a dynamics with an attractor at negative turning rates is defined (bottom left). Correspondingly, for positive obstacle force an attractor at positive turning rate is defined (bottom right).

4. In the center zone, that is, for heading directions close to ψ_{obs}, turning either left or right is specified as a bistable dynamics of turning rate with attractors

at finite $\pm\omega \neq 0$.

The transition from the center zone into either of the neighboring zones (i.e. transition from (4) to (2) or (4) to (3)) is a tangent bifurcation, while the transition to the outer zone (i.e. transition from (2) to (1) or (3) to (1)) is continuous and does not involve an instability. The pitch-fork bifurcation (i.e. from (4) to (1)) emerges as the strength of repulsion, λ_i (in Equation 4.1), decreases with increasing sensed distance (as defined by Equation 4.2).

The design is completed by a formal analysis of the phase diagram of the complete second order dynamics. The heading direction, ϕ, itself is always marginally stable. Turning rate, ω, is stable at either zero or one of the non-zero values. The attractor at zero turning rate has a relaxation time specified by $\tau_{\text{obs},\omega=0} = 1/\mid \alpha_{\text{taxis}}\mid$, while the relaxation rate of the non-zeros values, $\tau_{\text{obs},\omega=\pm\omega}$, is slightly larger than $1/(2 \mid \alpha_{\text{taxis}}\mid)$.[3] The parameters are constrained by the requirement that relaxation be sufficiently fast so that the system is close to its attractor at all times. At first sight, this might appear to be a vacuous condition, since the time units of the behavioral dynamics are really arbitrary. This requirement, nevertheless, constrains the system because the time units of the dynamics are limited by the realizable sensory throughput and by the computational cycle. Specifically, time scales must be chosen such that given the computational cycle (during which sensory information must be updated), the dynamics is numerically stable. Therefore, relaxation times must be larger than the computational cycle time. The constraint that the dynamics has relaxed then in turn limits the achievable turning rates of the vehicle.

5.3 Behavior integration

Because we have formulated both behaviors at the level of turning rate, integration of these two behaviors simply consists of adding the corresponding contributions to the vector-field

$$\frac{d\omega}{dt} = g_{\text{obs}}(\omega) + g_{\text{taxis}}(\omega) \tag{5.8}$$

Precedence of obstacle avoidance is expressed by adjusting the time scale of obstacle avoidance to be faster than the time scale of photo-taxis.

Because the system moves or the environment changes, sensory information is time dependent and thus the value of turning rate at which the resulting attractor is erected is also time dependent. Relaxation to the attractor can be enforced only if we have some handle on the rate at which sensory information might change. That rate of change can be specified by controlling the path velocity, v, of the vehicle such that it drives sufficiently slow. This way the attractor shifts on a much slower time scale than the characteristic relaxation time of the system and thus we can

[3] This is the relaxation time of the attractors, $\pm\sqrt{\alpha_{\text{taxis}}/\gamma_{\text{taxis}}}$, of $\dot{\omega} = \alpha_{\text{taxis}}\omega - \gamma_{\text{taxis}}\omega^3$ when α_{taxis} is negative.

guarantee that the system tracks the moving attractor. The velocity is controlled by the velocity dynamics presented in the previous chapter.

Finally, the following hierarchy ensures that the system is close to the attractor and that obstacle avoidance has precedence over the photo-taxis contribution:

$$1/\tau_{\text{taxis},\omega} \ll c_{v,\text{tar}}, \quad 1/\tau_{\text{obs},\omega} \ll c_{v,\text{obs}}, \quad \tau_{\text{taxis},\omega} \gg \tau_{\text{obs},\omega} \tag{5.9}$$

where $c_{v,\text{tar}}$ and $c_{v,\text{obs}}$ are the parameters that determine the relaxation rate of the velocity dynamics in the two cases when either the obstacles or the target constraints dominate (see Section 4.3).

5.4 Simulations

Equivalence of obstacle avoidance behaviors

Figure 5.4 shows runs generated from a software simulation. The vehicle is depicted by a circle with a hair indicating its heading direction. The initial robot position is indicated by a small circle inside the box with a single entrance. The outer perimeter and the shaded regions are simulated obstacles. The path is shown as a sequence of points. The left side of the figure shows a run based on the obstacle avoidance dynamics defined at the level of heading direction, ϕ, as it was specified by Equation 4.4 in Chapter 4. On the right side we illustrate that this second order obstacle avoidance dynamics works in simulation equally smoothly and in similar fashion as the first order dynamics first implemented.

Complete system

Figure 5.5 shows a simulation run of the complete system which demonstrates the smooth behavior consistent with all imposed constraints.

5.5 Implementation on Rodinsky

For implementation of the dynamical equations a simple Euler algorithm was written in Interactive C. Note that the dynamics at the level of heading direction does not need to be integrated. Because the system operates close to attractors of known stability, the maximal permissible step-size can be computed from the relaxation times of the attractors (time scales of the two contributions). The required cycle time needed to make one computational step delimits the time scales of the dynamics that can be realized by the system in real time. The transformations from sensor readings to the various distance dependent strengths, ranges and speeds were stored in lookup tables. A single computational step was made for each loop of sensory information acquisition. The cycle time in this form of operation is approximately

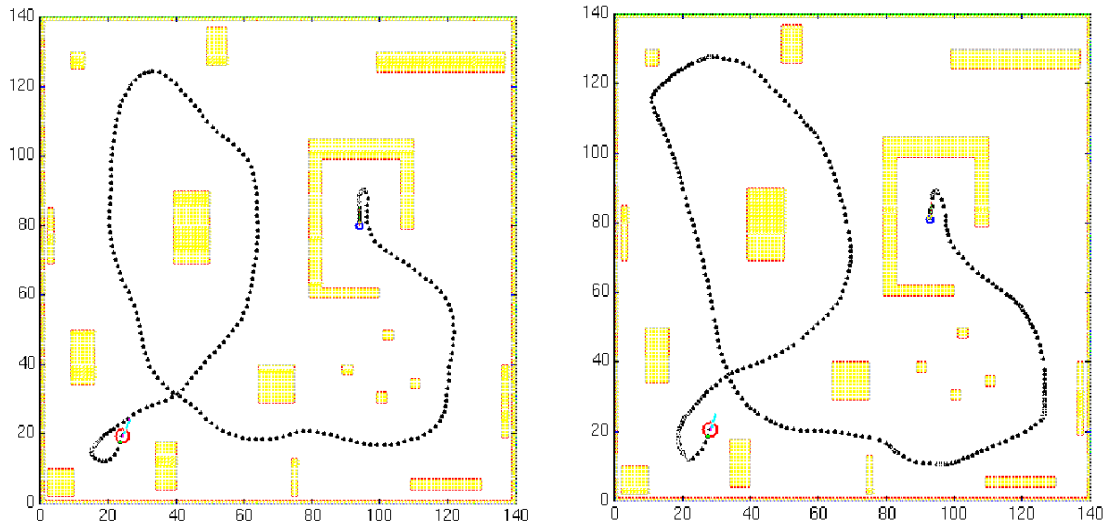

Figure 5.4: Runs generated from a software simulation of the obstacle avoidance dynamics are shown. The sensor model here consisted of measuring directly the distances from the robot to obstacle surfaces, through ray-tracing, in the directions of the five vehicle mounted infra-red sensors. The outer perimeter and the shaded regions are simulated obstacles. The vehicle is represented by a circle with a hair indicating its heading direction. The initial robot position is depicted by the small circle inside the box with a single entrance. Initial heading direction is 90 deg. The left part of the figure shows a run based on the first order dynamics given by Equation 4.4, the right part shows a run based on the dynamics lifted to second order as defined by Equation 5.7.

157 msec. We used the parameter settings obtained from analytical work and tested in the simulations. The system worked immediately.

5.6 Results of the implementation

The most striking feature of the system is its smooth behavior which seems to react anticipatorily to upcoming changes. This is due to how the dynamic approach permits information from various sources to affect in a graded fashion the generated behavior.

We filmed the robot motion as viewed from top in a few simple situations (which were limited by the space available within the viewing range of the camera). Figure 5.6 illustrates the robot's behavior through a sequence of video images. The situation is the simplest scenario testing the obstacle avoidance behavior by setting it in conflict with the target acquisition component: Initially, the robot is separated from the target (light source) by a row of obstacles, which consisted in four inverted plastic glaces. The robot moves along a curved path around the obstacles to reach the target.

In Figure 5.7 we illustrate a more complex scenario. Initially, the robot is posi-

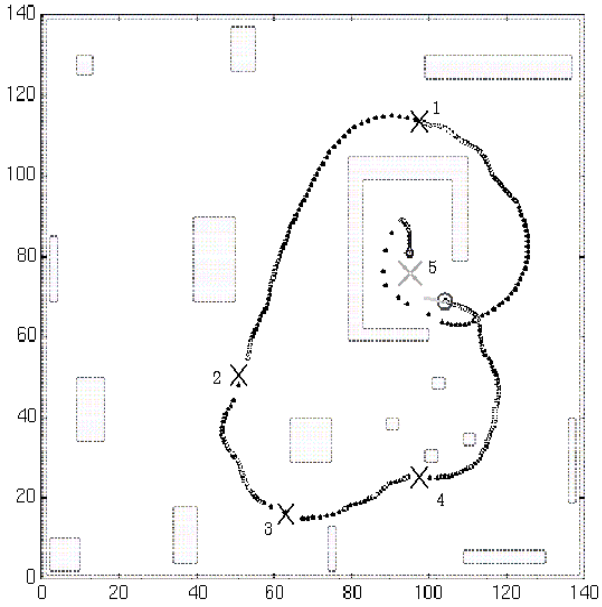

Figure 5.5: This figure shows a run of the complete behavioral dynamics implemented in software simulation. The same conventions as in Figure 5.4 apply. The light sensor is modeled by assuming that within an angular range of 75 deg, light intensity falls off hyperbolically with the distance between the light sensor and light source. The sensors are assumed to be mounted at a distance of R_{robot} symmetrically and forward-looking. Initially, the robot is inside the "box" heading toward a light source indicated by a cross marked "1" outside the box. The obstacles are assumed not to block vision. The obstacle avoidance contribution steers the vehicle out of the box toward the target. Once the target is reached, the simulated light source is shifted to the position marked by a cross labeled "2", and so on, until target number "5" is reached again inside the box. Note, that in addition to escape from a box, this simulation illustrates successful navigation in cluttered environments when moving from position "4" to position "5".

tioned in a box heading toward the right (white arrow), so that it is pointing away from the only exit from the box (at the lower left corner of the box). The light source is off during that period. The robot finds the exit and, in this case, roams around in the absence of a luminosity gradient. At some point, the light inside the box is turned on. The robot finds its way back into the box, while successfully avoiding the side walls. It ends up stopped in front of the light source. Stopping comes about due to the velocity control dynamics.

We also tested for oscillations near narrow passages and for escape from U-shaped obstacles. For both, performance is very good, due to the stabilization of zero-turning in the second order dynamics. The absence of memory is a limitation, leading to meandering paths in complex obstacle arrays.

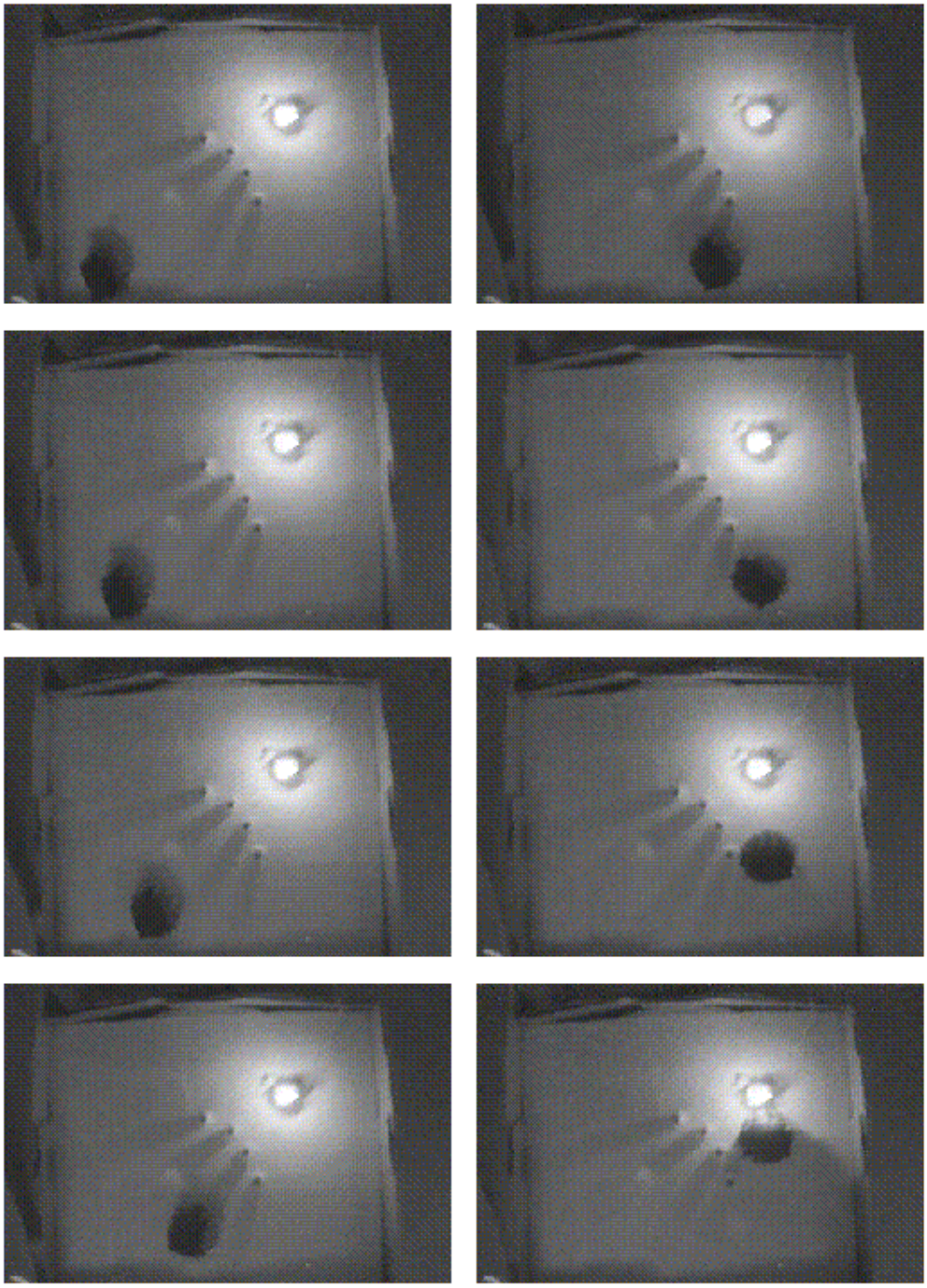

Figure 5.6: A sequence of video images filmed from above illustrates the motion of the real robot. Time increases from top to bottom, first along the left column, then along the right column. The vehicle is the dark round object, located in the first frame in the lower left corner. A light source is visible in the top right corner. Four plastic cups are obstacles blocking the direct path for the robot toward the light source. The images show these cups as black dots, but the shadows are visible as well. The work space is delimited by pieces of cardboard, which are likewise detected as obstacles. The robot moves smoothly around the obstacles toward the light source, stopping in the final frame in front of the light source.

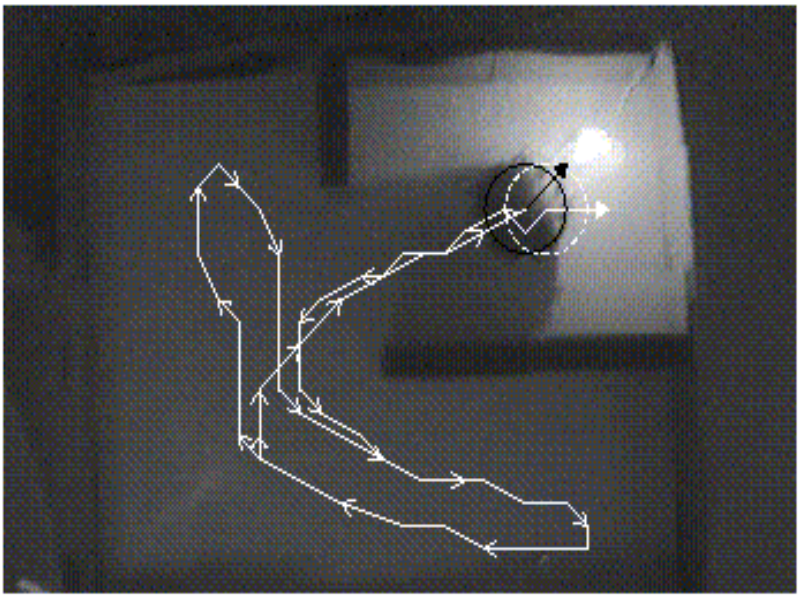

Figure 5.7: This video image illustrates a more complex scenario. The initial position of the robot is shown by a dashed white circle, with a white arrow indicating its initial heading. The dark fuzzy shades are cardboard walls, enclosing the robot except for an opening near the center of the image. Initially, the light source visible in the upper right corner is off. The trajectory of the robot was reconstructed using a PC based video tracking system. The white solid line tracks out the robot trajectory, with arrows indicating the direction in which the trajectory is run through. After leaving the enclosure, the robot wanders around until the light source within the half-open box is turned on. The robot then finds its way back into the box and stops in front of the light source. The final configuration of the robot is indicated by the solid black circle and black arrow.

5.7 Conclusion

We have demonstrated that the dynamic approach can be implemented to work with very low level sources of sensory information, here five infra-red sensors and two photo-resistors. This is in spite of the conceptual commitment of the dynamic approach to explicit representation of the internal behavioral state and of the behavior specified by sensory input. Moreover, a dynamic architecture including control of turning rate and driving velocity based on constraints from obstacle avoidance, target acquisition and the requirement to stabilize a maximum rate of change of the attractors positions was implemented on a slow 8 bit micro-controller with only 32 KByte of memory (the code takes up 8 Kbyte). The results demonstrate that computational cost is not a limiting factor of the dynamic approach.

Chapter 6

Dynamic field model for target representation based on low-level sound sensors

How can low-level autonomous robots with only very simple sensor systems be endowed with cognitive capabilities? Specifically, we consider a system which uses 7 infra-red sensors and 5 microphones to avoid obstacles and acquire sound targets. The cognitive abilities of the vehicle consist of representing the direction in which a sound source lies. This representation supports target detection, estimation of target direction, selection of one out of multiple detected targets, storage of target direction in short-term memory, continuous updating of memory, and deletion of memorized target information after a characteristic delay. We show that the dynamic approach employed to control the motion of the robot can be extended to the level of representation by using dynamic fields to interpolate sensory information. We show how the system stabilizes decisions in the presence of multi-value sensorial information, and how it activates and deactivates memory. Smooth integration of this target representation with target acquisition, in the form of *phono-taxis*, and obstacle avoidance is demonstrated.

6.1 Introduction

Autonomous vehicles are robotic systems that are not only able to control their motion in response to the sensory information acquired by themselves, but are also able to act intelligently (or flexibly) in their environment. Acting in an intelligent way requires the system to exhibit some cognitive capabilities. This means that the system must be able to behave autonomously even in response to environmental constraints not directly linked to online sensory information. Moving toward an occluded target, for instance, requires memory. That memory must be updated when sensory information is again available, or must be deleted if such information

continues to be unavailable over a characteristic period of time. Making and stabilizing a decision in the presence of multi-valued or ambiguous information is another form of cognitive capability, in that such decisions are not directly dictated by the incoming sensory information. We speak of representations of information when the processing of sensory information generates such cognitive capabilities.

Over the last decade or so, some controversy has existed regarding the appropriate role of representations within robotic systems. At one extreme, the use of symbolic representations has been viewed as an impediment to efficient and effective control of autonomous robots, by roboticists subscribing to a behavior-based approach (Brooks, 1991; Connell, 1990). On the other hand, it has long been assumed and argued that strong forms of representation are needed when robots are aimed at, that perform in ways that go beyond the purely reactive (Chatila, 1991). A consensus, which appears to emerge now, does no reject representations as such, but emphasizes their integration within the architecture of an autonomous robot (Arkin, 1998).

The dynamic approach to autonomous robotics was developed initially as a method of planning within representations of the navigable space (Schöner and Dose, 1992). The first implementations involved relatively high-level systems with ample computing power and vision as primary source of sensory information (Schöner, Dose and Engels, 1995). For such systems it has been shown, that the approach is not limited to the realization of relatively simple control behaviors, such as obstacle avoidance and target acquisition, but may generate sub-symbolic memory (Engels and Schöner, 1995), or the representation of computed metric information and its association with sensory input (for ego-position estimation see Steinhage and Schöner,1997, for instance).

That there is nothing in the approach that actually requires us to work at such a relatively high level of abstraction has been demonstrated in the two previous chapters (see also Bicho and Schöner, 1997a; Bicho, Mallet and Schöner, 1998) where we have implemented obstacle avoidance and target acquisition on two low-level platforms with very modest computational power and low level sensorial information. These systems were reactive, however, lacking cognitive capabilities.

In this chapter we are exploring the extent to which the dynamic approach can be used to generate cognitive properties in lower-level platforms. Specifically, can continuous metric representations be derived from low-level sensory information, decisions be stabilized on such representations, sub-symbolic memory and processes operating on memorized information (e.g. suppression of outdated information) be implemented? This transfer to lower levels of sensory information is not trivial. The high-end systems deal with such cognitive functions essentially by compressing large amounts of sensory information as obtained from computer vision into reduced representations. The dynamic decision making and memory operations could be viewed as sophisticated forms of noise removal and model-based estimation. By contrast, low-level sensors typically provide very limited amounts of sensory information. For instance, a small set of microphones provides a very *coarse-grained* sample of the

ambient distribution of sound intensity. From this sample, a stable and graded representation must be derived. The nature of the problem is thus changed from information compression and noise removal towards interpolation. In both cases, integration of the representations with stable action planning and control must be achieved.

We answer these questions in the affirmative by demonstrating the cognitive properties of a simple target representation system where targets are defined as sound sources (see also BICHO, MALLET AND SCHÖNER, 1999). A dynamic field representation of the spatial direction in which sound targets are detected is constructed. The robot receives sensory information from five weakly directional microphones that scan the forward 180 degree semicircle. Input to the field is thus a two dimensional sound panorama (intensity versus direction). A dynamic neural field representing sound target direction is endowed with the capacity to make and stabilize decisions in response to multi-valued sensory information (such as when two sound sources lead to a bimodal input distribution). Strong recurrent connections in the dynamic field lead to sub-symbolic memory that enables the robot to continue moving toward a sound source even when it is temporarily silenced. A process of adaptation is constructed which gradually reduces the stability of memorized information so that a memorized target orientation is deactivated if no confirmatory sensory information is received within a particular time span. This dynamics of target representation is coupled into the dynamic architecture for target acquisition and obstacle avoidance that has been previously established in Chapter 4 (see also BICHO, MALLET AND SCHÖNER, 1998; BICHO, MALLET AND SCHÖNER, 1999b). Results obtained from the implementation prove the capacity of the system to perform target detection and localization, target selection, and to exhibit temporary knowledge (memory and forgetting). Smooth overt behavior and the ability to track and follow moving sound sources are also demonstrated.

This chapter is structured as follows: In section 6.2 we review some related work. Dynamic fields for behavior representation are presented in section 6.3. Next, in section 6.4 the dynamic field representing sound targets is specified. Its integration with the movement control architecture is explained in section 6.5. A view of the implementation details of this architecture on a robot platform are given in section 6.6. Experimental results are described in section 6.7. The chapter ends with discussion and conclusions in section 6.8.

6.2 Related work

Moving toward sound sources is called *phono-taxis* in biology (BRAINTENBERG, 1984) and one may think of our system as a simple, although cognitive, realization of this basic behavior of organisms. Phono-taxis is exhibited by quite simple nervous systems. For example, in cricket mating, the male cricket attracts a female by generating noise. Successful mating entails detection, recognition and localization

in space of the mating sound, and movement toward the sound source (Cade and Cade, 1992). This example illustrates that there are two fundamental problems solved by the female cricket: The incoming sound signal must be detected and recognized as the call of a male member of the species. This detected signal must then be used to locate the source of the sound. This biological example has inspired work on low-level robots to test hypothesized control mechanisms that account for phono-taxis in crickets (Webb, 1995). An interesting robot model is reported in Lund, Webb and Hallam (1997). They tested their robot in a number of experiments based on cricket research. They reproduce a set of behaviors including signal choice, which have often been taken as evidence for complex mechanisms that go beyond purely peripheral nervous control. In their model, however, phono-taxis is implemented through a simple control-system-like mechanism. The model therefore does not have any cognitive capabilities (e.g., no memory, no representation of direction other than by physically rotating the robot). The model also does not address integration of phono-taxis with other behaviors such as the avoidance of obstacles during movement toward the sound source.

A simple realization of taxis behaviors can be based on the rule of turning left if left-looking sensors detect more signal than right-looking sensors and conversely. Using nonlinear dynamical systems, this qualitative form of control can be integrated with other behaviors, in particular, with obstacle avoidance (Chapter 5, Bicho and Schöner, 1997a). Such a solution fails, however, to explicitly represent the spatial direction toward the target source. That direction is only represented implicitly by the physical orientation of the robot once the control mechanism has stabilized. The presence of other constraints such as obstacle avoidance, distorts even this implicit representation. It is therefore not possible, based on this simple algorithm, to perform additional computations on the target information, such as memorizing that information, or steering at a given angle relative to the sound source (in order to permit, for instance, multiple sound emitting robots to drive in formation). Moreover, this simple mechanism does not support explicit decision making and stabilization of decisions when sensory information is ambiguous, for instance, because sound from two different sources impinges on the sensors with comparable intensity.

There is a considerable amount of modeling work on sound localization by higher level nervous systems, including models of spatial hearing in humans (Mills, 1972; Shamma, Shen and Gopalaswamy, 1989; Blauert, 1996; Duda, 1996). Binaural processing is the mechanism through which humans (and some animals, like for example the Barn Owl) localize sound. In humans, this entails exploiting inter-aural intensity differences (for the estimation of the elevation of the source) and inter-aural time differences (for the estimation of the horizontal orientation of the source). Some technical systems for sound localization have used arrays of microphones measuring differences between the signals received at the different microphones. An example, which was aimed at robotics as its major application, is described in Guentchev and Weng (1998). This system does not deal with multiple sources.

The approach adopted in this chapter is very close to mathematical models of

biological systems for target localization and selection, in which the prey localization and selection by frogs and toads (Chipalkatti and Arbib, 1987; House, 1988) has been described using neural fields (Amari, 1977). In these species, prey catching is triggered by very low level visual cues (Ewert, 1974). These models remained somewhat limited at the time as they did not deal with continuous updating of the target representation in time, nor with the integration of such a representation into other ongoing behaviors (the goal of the models was not, of course, to create autonomous robots).

Outside the particular angle provided by analogies with biological systems, related problems are addressed in robotics in the domain of target tracking. The location, velocity and other attributes of multiple moving objects are estimated from sensor data. Modern systems for target tracking often use multiple physically distributed sensors of different types to provide complementary and overlapping information about targets. Thus fusion is necessary to extract the relevant information on the targets and integrate that information across different sensor systems. Functional architectures for tracking thus require the two operations of data association, establishing which sensory measurement belongs to which target, and estimation (Liggins, Kadar and Vannicola, 1997). A wide array of established methods of estimation exist. In most cases estimates of the state of each target (e.g., position and velocity) are based on a model of the target and its motion.

Such methods have, to our knowledge, not been directly applied to the problem of estimating the direction in which a sound source lies. This may be due, in part, to the limited practical importance of this problem for the target tracking community. A more fundamental problem may be, however, that a good model of sound propagation is difficult to establish without taking recourse to a substantial amount of measurements to establish the geometry and reflective properties of the environment.

6.3 Dynamic fields for representation

More abstract forms of behavior or processes cannot be realized with attractor dynamics of the type described in the previous chapters. Examples in the present context are:

1. Target detection, in which a target is indicated only if sensory information is sufficiently strong and convergent while the absence of a target is signaled for weak or disperse sensory information.

2. Interpolation, that is, the capacity to make continuous estimates of the target location when sensory information is provided by a discrete array of sensors.

3. Computations on distributed representations of sensory information in which multiple instances of a sensed quality exist or sensory information is ambiguous.

4. Memory, that is, the representation of information about a target location, during transient occlusions from the sensors, so that overt behavior can be generated that continues to move the robot toward the target.

5. Forgetting, that is, the gradual deactivation of a memorized target location if no confirmatory sensory information is received within a particular time span.

Such processes, which we continue to refer to as behaviors although they do not necessarily involve overt movement, entail representations of information.

For phono-taxis, we want to represent the direction, ψ, in which a sound source lies, as viewed from the robot but referenced to an external frame. This variable can take on values in the interval $[0, 2\pi]$ rad. We define an activation variable, $u(\psi)$, for each possible value of target direction, ψ. The function $u(\psi)$ is considered a dynamical state variable and "codes" the presence of a target in direction, ψ. Positive values of activation, $u(\psi) > 0$, indicate that a target near ψ is detected, negative values of activation, $u(\psi) \leq 0$, indicate that no target was detected near ψ. The amount of activation corresponds to the certainty about the detection of a target. A single target is thus represented by a single localized peak of activation in the field (Figure 6.1 top). The absence of information on a possible target is expressed through a state of the field in which activation is negative everywhere ($u(\psi) \leq 0 \ \ \forall\psi \in [0, 2\pi]$) (Figure 6.1 bottom).

Next, the ideas about attractor dynamics and bifurcations are implemented at the level of a dynamics of the entire field. Localized peaks of activation are made attractor solutions by a particular pattern of interactions in the field. Sensory information provides input to the field. We develop these ideas step by step.

The readings of the sound sensors at time t provide an input sound distribution, $S(\psi, t)$. In practice, the sensor readings at a small number of field locations, ψ, are convolved with a Gaussian filter so that they activate continuous regions of the field (cf. Section 6.4). The simplest dynamics is one in which all sites of the field evolve independently of each other toward a level of activation, $u(\psi, t)$, that reflects the amount of input at each site:

$$\tau \frac{du(\psi, t)}{dt} = -u(\psi, t) + S(\psi, t) \tag{6.1}$$

This linear dynamics makes the field relax to the current input pattern, $u(\psi) = S(\psi)$, with a low pass characteristic. This dynamics is thus not yet useful by itself, as it merely reproduces the shape of the input pattern. What we need are mechanisms that make that activation in the field becomes positive only when a critical amount of input is given (detection), that activate only one site if multiple sites receive similar or even identical input (selection), and that are capable of retaining activation after input is removed (memory). In the last case it becomes particularly clear that such mechanisms involve *interaction*, that is, the evolution of activation at one site of the field depends on the level of activation at other sites of the field. An interaction mechanism that does the job has three characteristics:

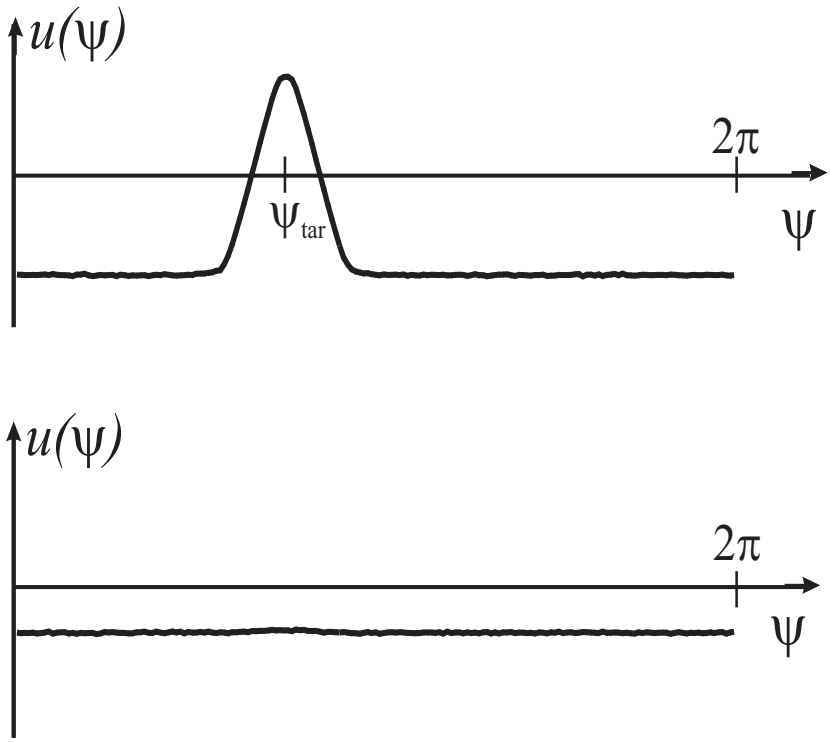

Figure 6.1: A field of activation is defined over the *behavioral dimension*, ψ, of the direction in which a target is detected. Top: A localized peak of activation represents a single target in the direction, ψ_{tar}, corresponding to the location of the peak. Bottom: A flat, sub-zero level of activation represents the absence of target information.

1. Neighboring field sites provide each other with positive input ("local excitation").

2. Field sites at larger distances provide each other with negative input ("global inhibition").

3. Only field sites with positive activation contribute to interaction ("sigmoid threshold").

Localized peaks of activation develop due to the interplay between the inhibitory and excitatory processes. These interactions enable the field dynamics to sustain localized peaks of activation even once input has been removed. That is the basis of memory. Moreover, when input creates a localized peak, there is a critical amount of activation when the local excitation first sets in and beyond which the peak can be self-sustained. This is the basis of detection. If there are multiple sites that receive input, global inhibition sets in. As soon as one field site has gained even only a minute advantage in activation, it wins the competition and suppresses other

sites more than it is suppressed itself. This is due to the sigmoid, which weakens the influence of sites with lower levels of activation.

A convenient mathematical format of this interaction mechanism is

$$\tau \frac{du(\psi,t)}{dt} = -u(\psi,t) + S(\psi,t) + \int_0^{2\pi} w(\psi-\psi')\Theta(u(\psi',t))d\psi' + h \tag{6.2}$$

Interaction collects input from all field sites, ψ'. The non-linear threshold function

$$\Theta(u) = \begin{cases} 0 & \text{for } u < 0 \\ u & \text{for } 0 < u < 1 \\ 1 & \text{for } u > 1 \end{cases} \tag{6.3}$$

makes that only sites of the field with positive activation contribute to interaction and that sites with larger activation contribute stronger to the interaction (the threshold avoids that activation "explodes" to infinite).

The interaction kernel

$$w(\Delta\psi) = \begin{cases} k_p & \text{for } -l_{\text{coop}} < 2\Delta\psi < l_{\text{coop}} \\ -k_n & \text{else} \end{cases} \tag{6.4}$$

only depends on the distance, $\Delta\psi = \psi - \psi'$, between field sites. It is positive ($k_p > 0$), if the two sites are closer to each other than the cooperativity length, l_{coop}, and is negative ($k_n > 0$) for larger distances. The kernel is shown in Figure 6.2. Finally, the negative constant, $h < 0$, determines the resting level of the field without input: $u = h \quad \forall\psi \in [0, 2\pi]$. This controls how much input field sites need before they first contribute to interaction.

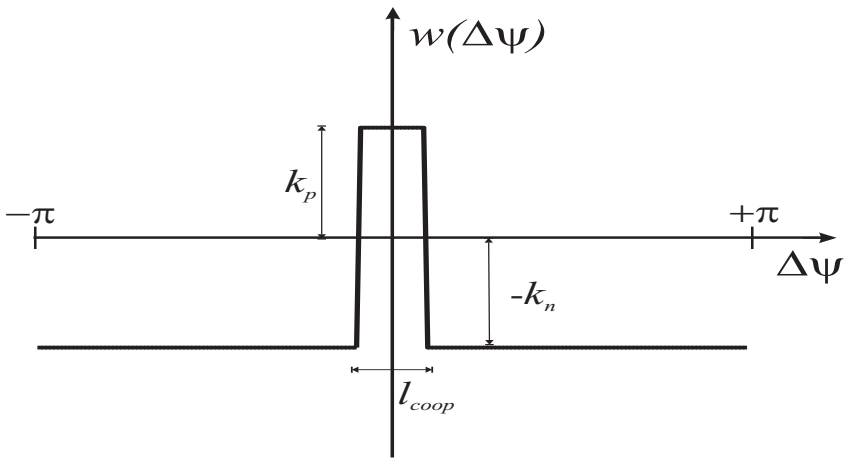

Figure 6.2: The interaction kernel is positive ("excitatory") for sites that are closer to each other than the cooperativity length, l_{coop}, and is negative ("inhibitory") for larger distances between the sites.

The particular form of the equation we are employing has been analyzed mathematically by Kishimoto and Amari (1979). Their studies provide valuable information about the different parameter regimes for the existence and stability of

localized peaks of activation. Next, we discuss the role of the different parameters in the field dynamics (see Appendix A for more details).

Detection

The resting level, $h < 0$, makes that interaction kicks in only when sufficient input is applied. For an input, $S(\psi)$, localized around one location, for instance, this means that while that input has a small amplitude, the flat state of the field is deformed by input but remains negative everywhere: $u(\psi) = h + S(\psi)$, as illustrated in Figure 6.3 on the left. The field codes absence of information (no target detected).

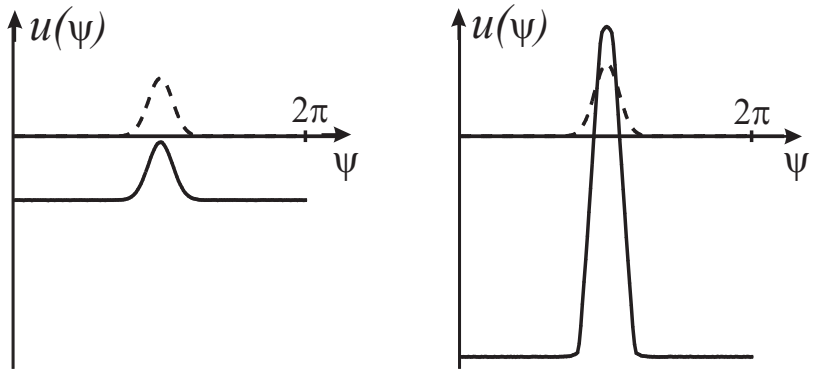

Figure 6.3: A single localized input, $S(\psi)$, is applied to the field (dashed line). Left: When the amplitude of that input is below a critical level, the stable state of the field is the homogeneous resting level with the input profile superposed: $u(\psi) = h + S(\psi) < 0$ (solid line). Right: Beyond a critical input amplitude, activation in the field becomes positive and interaction sets in. The stable state that emerges (solid line)is a localized peak of positive activation, which is largely self-sustained, but positioned over the location of maximal input. The transition between these two states is hysteretic and represents the detection mechanism.

When the amplitude of input is sufficiently strong, interaction becomes important. The stable state of the field is now a localized peak of positive activation, the size of which reflects not only input strength, but is also determined in large part by local self-excitation. The transition between the sub-threshold peak and the self-sustained peak as a function of input strength involves a dynamical instability and is the mechanism used here for detection. Detection means that input needs to be of sufficient size over a sufficient period of time in order to generate a self-sustained peak. The location of the self-sustained peak is determined entirely by input, however. The peak is positioned over the location of maximal input.

Memory

Once a localized, positive peak of activation has been generated, the local self-excitation within the peak is so strong, that a peaked pattern of activation remains stable even after input is removed (Figure 6.4). This is the dynamic field mechanism for memory. This form of memory is sub-symbolic. Within the category of memory, defined by the behavioral dimension, ψ, an instance of memory is identified simply by its location. There is not need to label peaks. When input information is reapplied, the position of the stable peak is readjusted so as to be centered exactly on the location of maximal input. Thus, memory is updated automatically without the need for an explicit input-to-memory matching process.

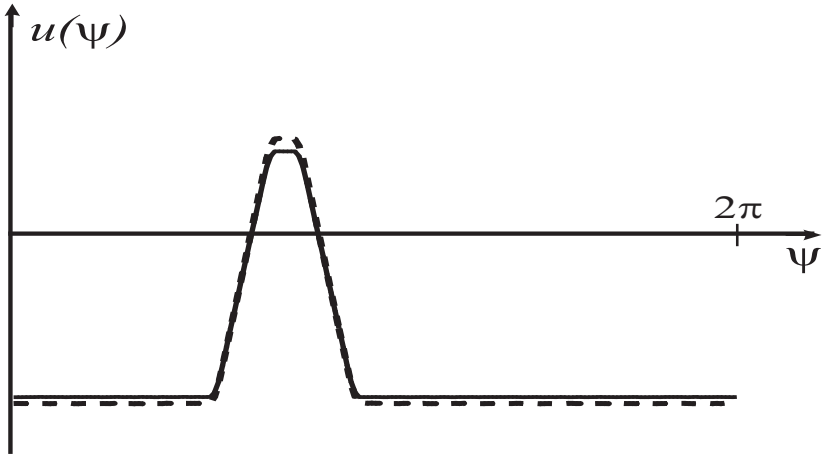

Figure 6.4: A localized positive peak of activation (dashed line) is stable in the presence of input. It remains stable if input is removed (solid line). The peak is sustained by local self-excitation. Its lateral diffusion is limited by global inhibition. This is the memory mechanism in the dynamic field. The position of the peak within the field is marginally stable, however, so that the contents of memory may slowly degrade with time.

Over the longer term, memorized information may become obsolete. Angular information may become incorrect because the robot moved. Targets may actually have been removed. Even the memory mechanism itself is subject to degradation as the peak position within the field is only marginally stable in the absence of input. A mechanism for forgetting must suppress positive localized peaks of activation if no confirmatory sensory input arrives within an appropriate time interval. The resting level, $h < 0$, provides such a mechanism. When the resting level is made sufficiently negative, activation in the field is generally so low, that the local self-excitation is no longer sufficient to sustain a positive peak of activation. In fact, mathematically, the field dynamics without input goes through an instability when the resting level is varied (Amari, 1977). At levels of h below but close to zero, the field dynamics is bistable: the homogeneous "off" state of the field coexists with the state in which a

localized positive peak of activation is positioned somewhere within the field. This is the regime in which memory is operational: If input has induced a positive peak of activation and is then removed, the system maintains a localized peak of activation. If no input has been present, the homogeneous "off" state persists. When the resting level is lowered below a critical value ($h < -W_m = -\max_\psi\{\int_0^\psi w(\Delta\psi)d\psi\}$) the localized positive peak solution becomes unstable and the field dynamics is mono-stable, only the homogeneous "off" state remains. Thus, a localized memory peak can be deleted by lowering the resting level below this critical level. The two regimes of the field dynamics are illustrated in Figure 6.5.

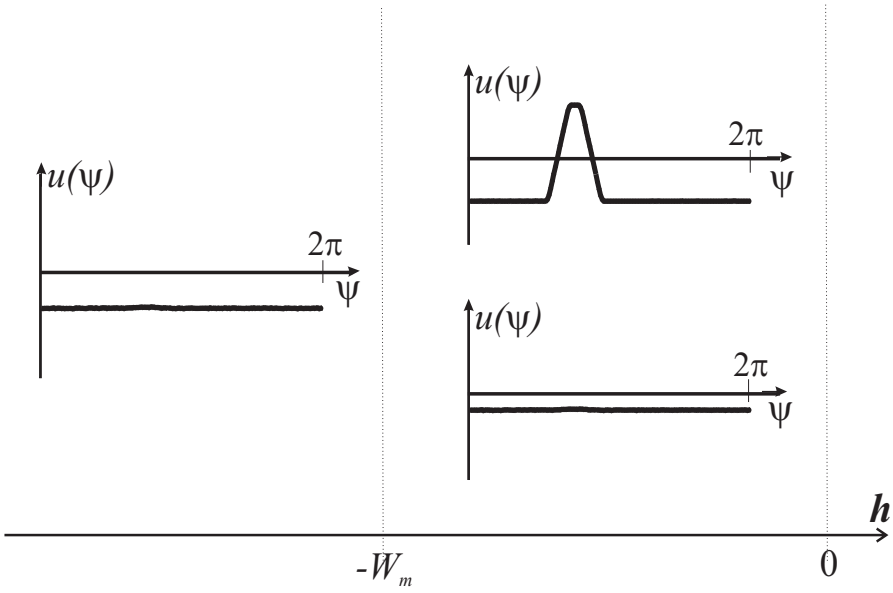

Figure 6.5: The different stable states of the field dynamics without input are illustrated as a function of the resting level, h. Below a critical level of h ($-W_\mathrm{m}$), only the homogeneous "off" state of the field is stable. All sites have the same negative level of activation. Above the critical level (but still below zero), two types of stable states coexist. The homogeneous state persists, but a positive localized peak of activation is likewise stable (irrespective of where it is positioned). This bistable regime serves the memory function, while the mono-stable regime induces forgetting or resetting of memory. Memory peaks are set by applying sufficiently strong input (see detection mechanism).

Interpolation *versus* decision making

When more complex shapes of input distributions are considered, additional properties of this strongly interactive field come into play. The top of Figure 6.6 shows that bimodal input patterns may lead to a single localized peak of activation that is positioned over the mean of the two locations of maximal input. This is, in fact, a

weighted mean as different amplitudes of the two input peaks lead to bias of the resulting position of the localized peak of activation toward the site receiving stronger input (left). This fusion or integration of input information results from the local excitatory interaction. Roughly, when the two peaks of the input distribution are within the cooperative length, l_{coop} of the dynamic field, then fusion takes place as shown.

If, by contrast, the two peaks of the input distribution are separated by more than the cooperative length, then a decision is made as to which peak to activate. The field is bistable. A positive localized peak may be positioned over either of the two sites. The other site remains more activated than the background, but is suppressed below zero (bottom of Figure 6.6). Which of the two sites of maximal input "wins" depends on two factors:

(a) The initial state of the field may bias the competition toward maintaining positive activation where there has previously been positive activation. This leads to hysteresis, in which a decision once made is stabilized in the face of multi-valued or ambiguous information.

(b) If the two input peaks have different amplitude, then the site receiving stronger input is more likely to be activated.

6.4 The dynamics of target representation

To build a dynamic field representation of the sound sources we use the direction, ψ, in which the sound source lies as viewed from the current position of the vehicle. The angle is taken relative to a fixed, but arbitrary reference orientation, so that it would not change if the robot were to turn on the spot. In implementation this requires integrating heading direction in time to maintain this reference frame. While the absolute calibration of this reference frame is irrelevant, its drift contributes to degradation of memorized information, but not of currently sensed information. A much more limiting factor of this form of target representation is that memorized angular information becomes obsolete as the robot moves over distances comparable to the distance to the target. The main advantage of this representation is, however, that distance information is not needed for detection, estimation, decision making and short term memory of targets.

A dynamic field, as defined in the previous section, represents information about the orientation of a potential sound target. Sensory input to the field is provided by the time-varying signals, M_i, from 5 microphones ($i = 1, 2, \ldots, 5$), each pointing into a different sector on the forward field of view of the vehicle (angles (-90, -45, 0, 45, 90) deg from the main axis of the vehicle, see Figure 6.7). These signals reflect the sound pressure measured by each microphone. They increase from zero with increasing sound pressure. Their angular characteristic is described approximately by a cone of about 60 deg opening, so that neighboring microphones have overlapping

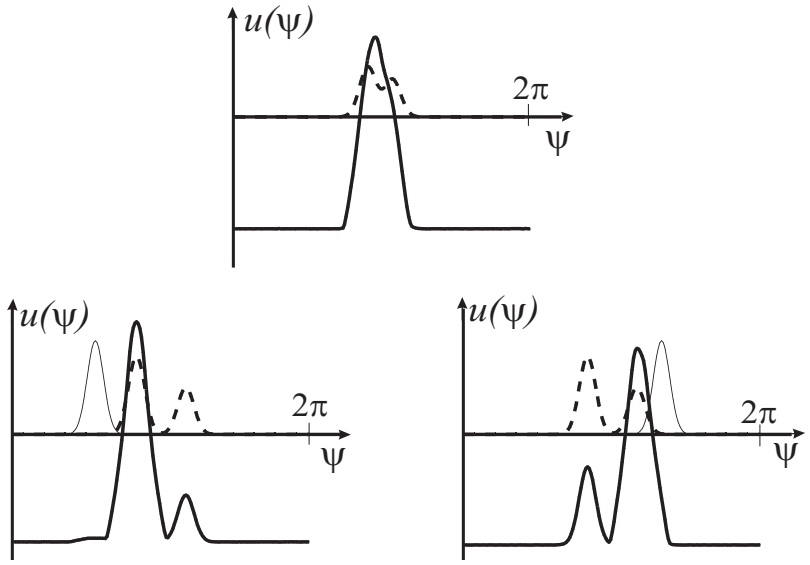

Figure 6.6: A bi-modal input, $S(\psi)$, is applied to the field (dashed line). Top: when the distance between the two peaks of the input distribution is within the cooperative distance, the stable state of the field is a localized peak of activation (solid bold line) positioned over the weighted mean of the input distribution. The field thus fuses input information. Bottom: when the distance between the two peaks of the input distribution is beyond the cooperative distance competition takes place. The field is bistable, in the sense that it can evolve a peak of activation centered at either one of the two sites receiving input (solid bold line). On the left, the site receiving stronger input "wins". On the right, the initial state of the field (solid thin line) has a peak of activation at a distance to the smaller peak, within the cooperative distance, the competition is thus biased toward the selection of the smaller input peak.

sensitivity cones. Thus, these sensors specify target orientation in the sense that a single sound source induces a graded pattern of detected sound pressure, with a maximum at the sensor pointing in the direction closest to the one in which the sound source lies (except for reflections, cf. Section 6.7). Interpolation is based on spreading the contribution of each microphone over a range in the field by convolving with a Gaussian kernel of width, $\sigma = 0.4$ rad (± 23 deg):

$$S(\psi, t) = \left(\sum_{i=1}^{5} M_i \exp \left[-\frac{(\psi - \psi_i)^2}{2\sigma^2} \right] - 0.25 \right) H(\sum_{i=1}^{5} M_i) \tag{6.5}$$

Here, $H(\cdot)$ is the Heaviside step function. Multiplying with this step function applied to the sum of all microphone signals turns input entirely off when no sensor receives input (background sound below sensor threshold).

The parameter h is set so that the field operates in the memory mode. Thus,

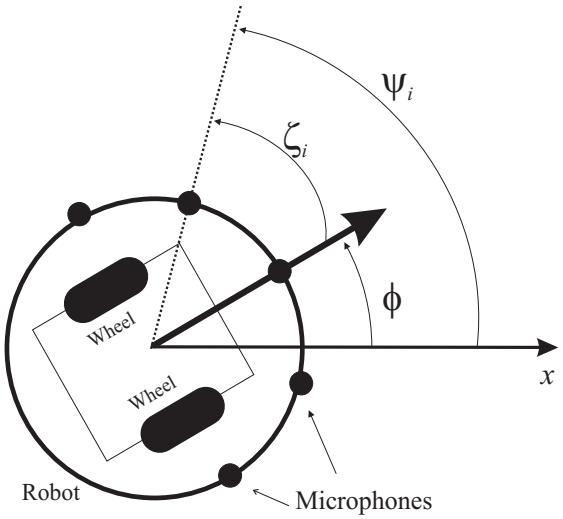

Figure 6.7: Sensory information about sound targets is acquired by five microphones, each pointing into a direction ζ_i (=-90, -45, 0, 45, 90 deg), with respect to the heading direction, ϕ, of the robot. The direction in the world at which microphone i is pointing is $\psi_i = \phi + \zeta_i$.

once sufficient input (detection) has induced a single localized peak of positive activation (decision), that peak persists when input is removed (e.g, because the sound source is momentarily silent or its volume is reduced due to occlusion). The memorized target orientation is maintained for a time interval that permits the robot to continue moving in the target direction. This memory peak must be deleted if no renewed sensory input arrives within a particular period of time, because memorized angular information becomes obsolete as the robot moves. This forgetting behavior is modeled by making the resting level, h, a dynamical variable with the following dynamics:

$$\frac{dh}{dt} = -r_{h,\min} c_h (h - h_{\min}) - r_{h,\max}(1 - c_h)(h - h_{\max}) \tag{6.6}$$

Here, $h_{\max} = -0.25 W_m$ and $h_{\min} = -1.1 W_m$ are the two limit values of the resting level within the bistable and the mono-stable regime, respectively (see previous section and Figure 6.5 for significance of W_m). This dynamics lowers the resting level (destabilizing memory) at the rate $r_{h,\min}$ while a memorized peak exists ($c_h = 1$). It restores the maximal resting level (to enable memory) at the rate $r_{h,\max}$ otherwise. The destabilization (forgetting) process is slower than the restoring process, so that after forgetting, the field is immediately able to again detect and memorize a new target. The presence of a memorized peak is represented by

$$c_h = [H(N_u) - H(N_s)]H(N_u) \tag{6.7}$$

where

$$N_u = \int_0^{2\pi} H(u(\psi))d\psi \tag{6.8}$$

is the total positive activation in the field and

$$N_s = \int_0^{2\pi} S(\psi)d\psi \tag{6.9}$$

is the total input activation (positive by construction). $H(\cdot)$ is the Heaviside step function. The function c_h is equal to one if there is positive activation in the field ($N_u > 0$), but no input ($N_s = 0$). It is zero if there is no peak in the field or if there is a peak but also input.

6.5 Coupling the dynamics of target representation with the attractor dynamics of heading direction

Now we address how the direction, ψ_{tar}, in which a target lies, can be computed from the activation on the dynamic field. Because the time scale, τ, of the field is chosen faster than that of the heading direction and velocity dynamics, the field has typically relaxed to a stable pattern on the time scale on which the movement plans of the robot evolve. Directly reading out the location in the field of maximal activation is not a very good solution, as the maximum of the stable state may jump and thus destroy the carefully constructed stability properties of the system. Moreover, such a procedure does not deal consistently with the absence of target information. A better and elegant solution has been proposed by Kopecz and Schöner(1995) and used in an earlier implementation of dynamic fields on vehicles (Bicho and Schöner, 1997b). Because the field has by construction only a single peak of positive activation, the peak location could be computed as a mean, if the distribution of activation is interpreted as a probability density

$$\psi_{\text{tar}} = \frac{\int_0^{2\pi} \psi H(u(\psi))d\psi}{N_u} \tag{6.10}$$

where division by the total positive activation, N_u, is needed to normalize the distribution. The normalization poses a problem when no positive activation exists in the field (devision by zero).

This problem can be solved once it is realized, that what we actually need in the dynamics of heading direction for target acquisition, is not necessarily ψ_{tar} itself, but $-\lambda_{\text{tar}}(\phi - \psi_{\text{tar}})$, an attractive force-let centered at that angle. The strength of attraction must be zero if no target is represented. Thus, λ_{tar} should be replaced by $\lambda'_{\text{tar}} N_u$ with a new constant, $\lambda'_{\text{tar}} > 0$. This leads to: $-\lambda'_{\text{tar}}(N_u\phi - N_u\psi_{\text{tar}})$, in which the normalization factor cancels and division by zero never occurs. Thus, we redefine the target contribution in Equation 4.8 as

$$f_{\text{tar}} = \begin{cases} -\lambda'_{\text{tar}}(N_u\phi - \int_0^{2\pi}(H(u(\psi))\psi)d\psi) & \text{for } \psi_{\text{tar}} - \pi/2 < \phi \leq \psi_{\text{tar}} + \pi/2 \\ \lambda'_{\text{tar}}(N_u(\phi - \pi) - \int_0^{2\pi}(H(u(\psi))\psi)d\psi) & \text{for } \psi_{\text{tar}} + \pi/2 < \phi \leq \psi_{\text{tar}} + 3\pi/2 \end{cases} \tag{6.11}$$

where ϕ is mapped into the listed cases through a *modulus* 2π operation. This contribution is then used in Equation 4.11 together with the obstacle contributions to generate the time course of the robot's heading direction. The path velocity is controlled as explained in Section 4.3.

Finally, the following hierarchy of relaxation rates ensures that the system relaxes to the stable solutions, that obstacle avoidance has precedence over the target acquisition and that the relaxation of the field is faster than the relaxation of the target acquisition dynamics:

$$\lambda_{\text{tar}} \ll 1/\tau, \quad \lambda_{\text{tar}} \ll \lambda_{\text{obs}}, \quad \lambda_{\text{obs}} \ll c_{v,\text{obs}}, \quad \lambda_{\text{tar}} \ll c_{v,\text{tar}} \tag{6.12}$$

6.6 Implementation on Robodyn

The dynamic architecture was implemented and tested on the mobile platform Robodyn (see Figure 3.2). In the implementation, the field dynamics as well as the dynamics of heading direction and of path velocity are integrated numerically using the Euler method.

The field is sampled spatially with a sampling distance of 8 deg. It is important that the discretized form of the interaction kernel, $w(\Delta\psi)$, is, like the exact kernel, symmetrical around zero. Deviations from symmetry generate a tendency for localized memory peaks to drift in one direction. Sensory information is acquired once per computation cycle. The cycle time is measured and is approximately 110 ms. As the time step must be smaller than the fastest relaxation time on the system, this imposes minimal time scales on the entire dynamical architecture. Thus the computational cycle time is the limiting factor for determining the relaxation times of the dynamics in real time units and thus for the overall speed at which the robot's behavior evolves.

6.7 Experimental results

In this section we first present results that document the properties of the dynamical field for target representation. These were obtained when the field evolved in response to actual physical stimulation by sound sources, but the robot did not move. Next we show how the robot behaves in a number of experimental scenarios that challenge particular aspects of the architecture. In all cases, all behavioral modules are integrated and work together.

6.7.1 Cognitive properties of the dynamic field representing targets

A set of experiments with fixed robot used a sound source that emitted a pulse modulated wave with a fundamental frequency of 440 Hz. Pulse modulation makes that this sound had high frequency harmonics that fell into the most sensitive range of the microphones. In experiments involving multiple targets a sound generator emitting a 2.5 KHz harmonic wave was used as a second sound source. Loudspeakers were placed 100 cm from the periphery of the robot. The robot was pointing in the 180 deg direction relative to the external reference frame in which we provide information about the real direction to the sound source.

Detection

Figure 6.8 shows how the field evolves when the intensity of the test sound is increased gradually. Initially, the entire field is "off" ($u(\psi) = h < 0$ everywhere). While sensory input is weak, positive activation cannot arise and the field continues to code for absence of a sound source. At time $t \approx 55$ sec the strength of sensory input becomes sufficiently strong to trigger generation of a peak of positive activation centered over the location that receives maximal input. From this point on a target is detected and the peak of activation maintains its shape almost invariant due to the strong interactions within the field. This result shows that the dynamic field behaves nonlinearly in response to ambient sound of different intensities.

Interpolation

In the presence of a single sufficiently strong sound source, input is mono-modal, although broad, and a single, localized positive peak of activation is stable in the dynamic field (Figure 6.9). The peak is positioned over the maximum of the broad input distribution, and thus unaffected by input that is further apart from the peak than the kernel width. The estimated sound orientation, ψ_{tar}, is 115 deg, very close to the actual target orientation, which was 112.5 deg. Repeating this experiment for a number of different orientations of the sound source we evaluated the quality of the interpolation of sound input by the dynamic field. Figure 6.10 summarizes the result. The estimated values of target direction are very close to the real values across a wide range from 110 to 250 deg. The two extreme configurations have a small bias (still less than 10 deg), which is caused by the unsymmetric sampling of these values due to the limited angular range of our microphone array.

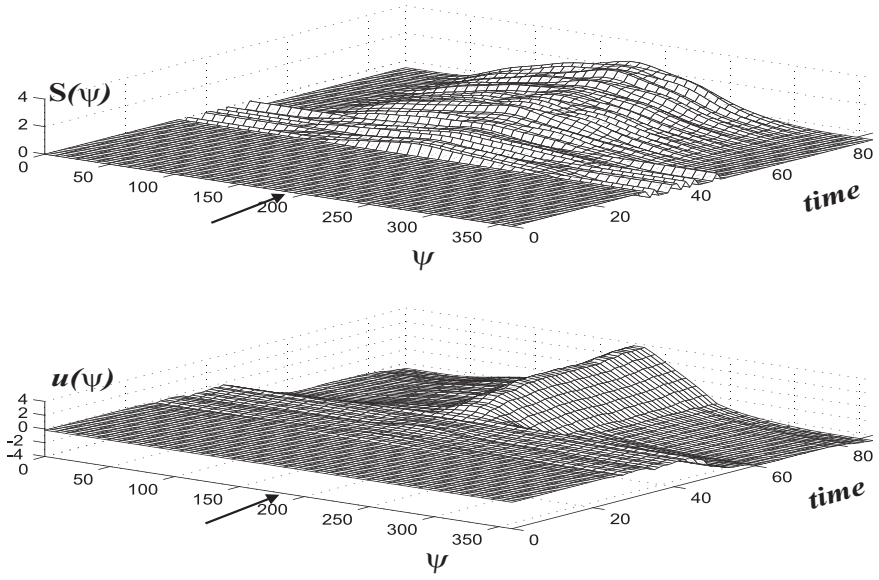

Figure 6.8: Here, the target detection behavior of the field is shown. Direction is in degrees (deg) and time in seconds (sec). The sound source was placed in the forward direction of the robot (indicated by the arrow) and sound intensity was increased from 0 to 2.5. Robot position and orientation (180 deg with respect to the world axis) in space was kept fix. Top: the input to the field, $S(\psi)$, is mono-modal and its strength increases in time. Bottom: while the input is weak the field is in the state in which it is all off and thus no target is detected. At time $t \approx 55$ sec the input strength is sufficiently strong to trigger the detection of the sound source. From this point on the stable state of the field is a localized peak of positive activation centered over the location of maximal input.

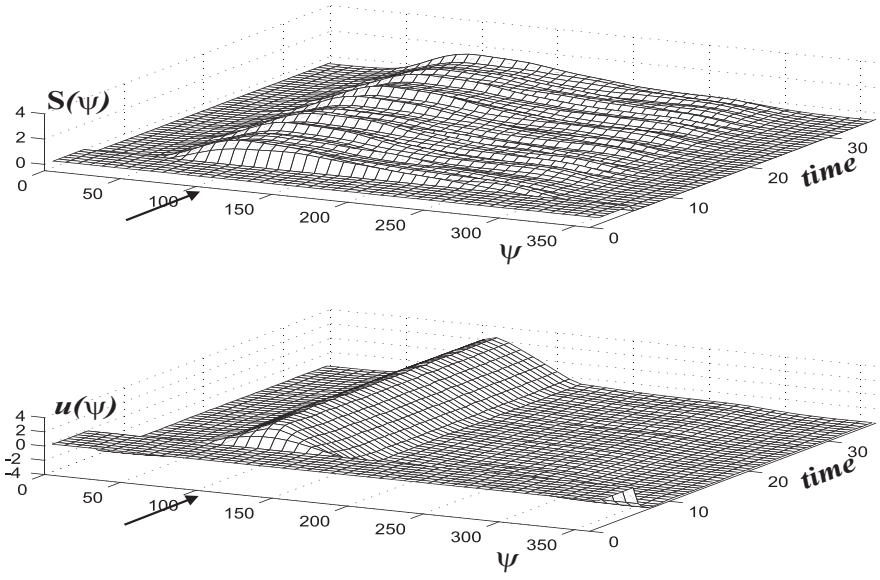

Figure 6.9: A sound source was placed at an angular position of 112.5 deg (the location indicated by the arrow) with respect to the world axis. Robot orientation was 180 deg, the five microphones where thus pointing in the directions 90, 135, 180, 225, 270 deg. Top: sensory information leads to a broad mono-modal input distribution. Bottom: the field activation relaxes to a stable localized peak centered over the maximum of the input. The estimated sound orientation is 115 deg.

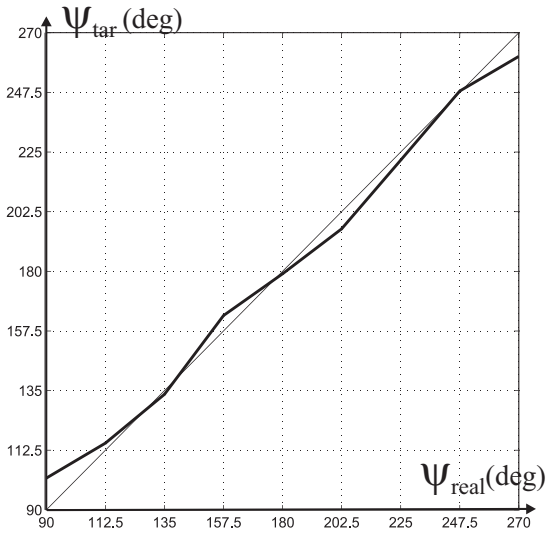

Figure 6.10: The experiment illustrated in Figure 6.9 was repeated for a number of different directions of the sound source. These directions can be read on the abscissas. On ordinates one can read the corresponding estimated target directions.

Tracking

Figure 6.11 shows how a moving sound target is tracked. The loudspeaker was moved more or less continuously from an initial orientation at 90 deg all the way to 270 deg. As a consequence sensory input has a moving peak. The dynamic field responds to such moving input by evolving a peak of activation which tracks and follows the moving input peak. The maximum of the field activation moves continuously with the angular location of the target. The estimated target location thus varies monotonically from approximately 102 deg to 261 deg.

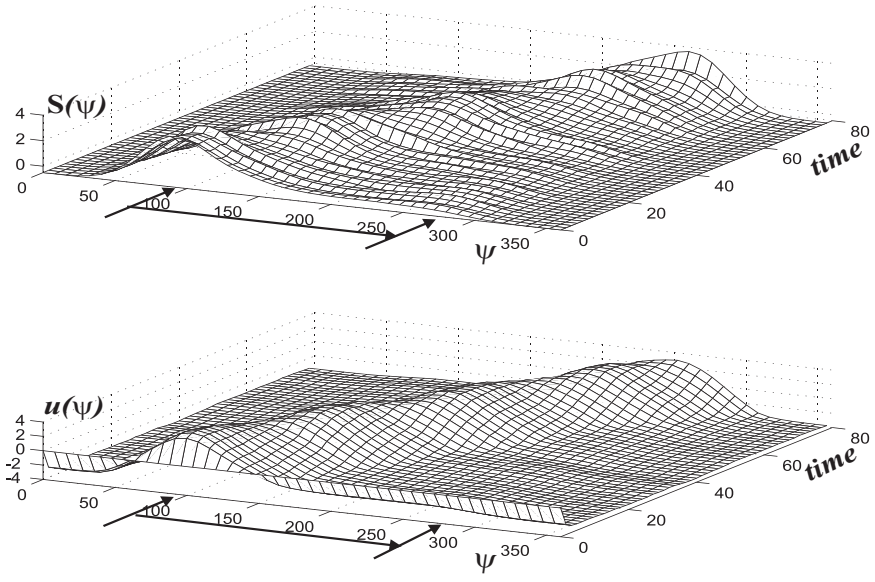

Figure 6.11: The robot was positioned with an orientation of 180 deg with respect to the external axis. The sound source was moved continuously from an initial direction of 90 deg (indicated by the left arrow) all the way to 270 deg (indicated by the right arrow). Top: sensory information is mono-modal and its maximal location varies continuously. Bottom: the field evolves a peak of positive activation which tracks and follows the moving input peak.

Target selection

To test the capacity of the field to select one of multiple targets, two loudspeakers were placed as illustrated in Figure 6.12. The loudspeaker on the left of the robot emitted the pulse modulated test sound while the loudspeaker on the right emitted the harmonic wave of 2.5 KHz. Both signals were played at similar intensity. Input is bi-modal under these conditions. The interaction enables the field to make a decision, in this case, selecting the site receiving stronger input. The field evolves a single localized peak of positive activation centered near the input peak located at 270 deg. The input information pertaining to the alternate site is discarded and

does not bias the estimation of target position.

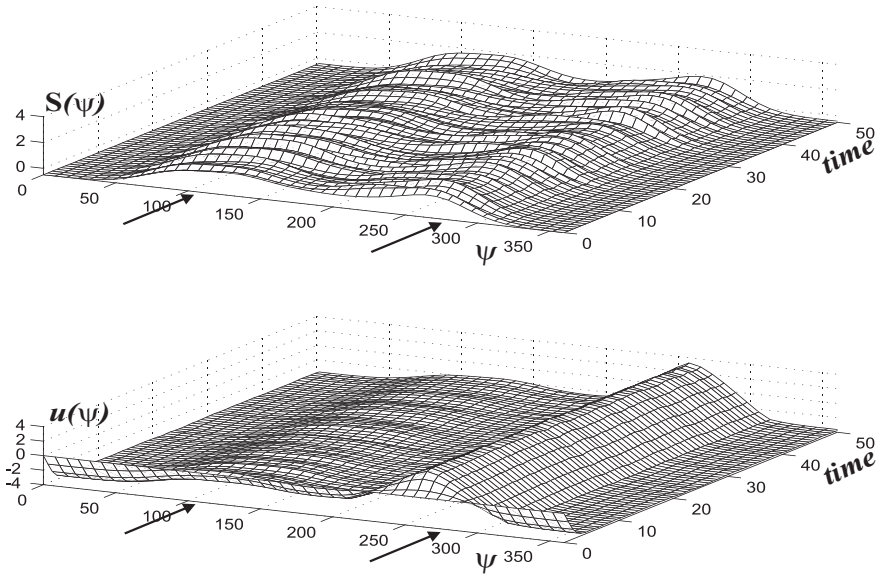

Figure 6.12: The robot was placed with a heading direction of 180 deg with respect to the external axis. Two sound sources, the pulse modulated wave and the harmonic wave, were placed at angular positions 112.5 deg and 270 deg (as indicated by the arrows), respectively. Top: under such experimental set up the sensory input to the field is bimodal. Bottom: competition takes place and as a result the field makes a decision. The field evolves a single peak of positive activation centered near the input peak located at 270 deg. Thus, the left target is selected.

Memory and forgetting

In Figure 6.13 we demonstrate memory and forgetting. A loudspeaker was placed in front of the robot (it could have been any other orientation). After a brief moment of silence, the sound source was turned on, emitting the pulse modulated test sound. As expected, the field evolves a stable peak of positive activation centered over the input peak (the estimated target orientation is 183 deg). About 10 sec later the sound source was turned off. Although sensory input was thus removed, the localized peak persists, albeit somewhat weakened, for a certain time interval. During this time interval the adaptive dynamics of the resting level, h, drives the resting level down, and thus progressively destabilizes the memorized information. Since no renewed sensory information is provided again the memorized peak eventually dies out. The target orientation is "forgotten". At this point the adaptive dynamics of h changes and its value is quickly restored to the value at which the target representation dynamics operates in the memory mode again. The field is once again sensitive to new (or the same) sound targets, which can be detected, selected and memorized.

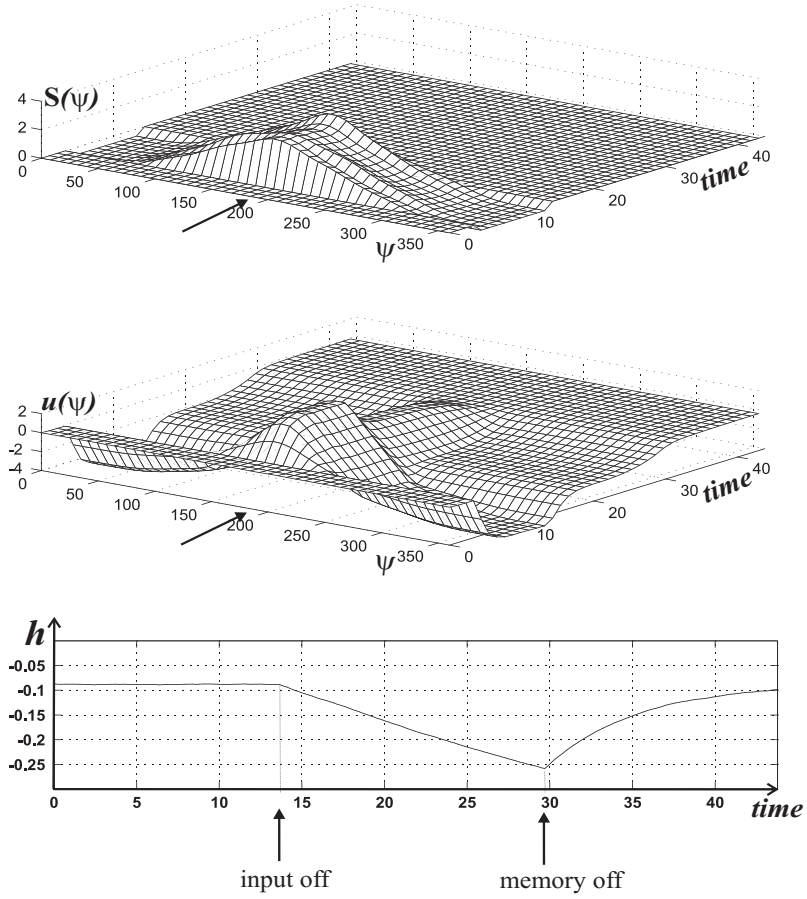

Figure 6.13: A loudspeaker was placed in front of the robot heading direction (indicated by the arrow). Top: 3 sec later the sound source was turned on. The sensory input to the field is mono-modal. About 10 sec later the sound source was turned off. The sensory input becomes zero everywhere. Center: while the sound source is on, the state of the field is a localized peak of positive activation centered over the location of maximal input. This peak solution persists (even though somewhat reduced in amplitude) even when the input to the field is turned off ($t \approx 13$ sec). The field is thus in the memory regime. At time $t \approx 29$ sec this peak solution becomes unstable due to the adaptation of the resting level, h. Target orientation is thus "forgotten". From this point on, the field remains in the state in which it is off (negative activation everywhere). Bottom: the resting level is in its maximum value until the input is turned off, which occurs at time $t \approx 13$ sec. After this instant and while there exists positive activation in the field the adaptive dynamics of h reduces its value. At time $t \approx 29$ sec the resting level reaches the value for which the peak solution in the field corresponding to the memorized information becomes unstable. Thus, the memorized peak is turned off. At this point the adaptive dynamics of h changes again and its value is restored to the value at which the field dynamics operates in the memory regime again.

Memory together with the adaptation of the resting level thus endows the robot with temporary knowledge about the target location.

6.7.2 Phono-taxis and obstacle avoidance on moving robot

In all the experiments reported here the sound source consisted of a loudspeaker emitting CD music. The particular piece we used (Vivaldi, Printemps, Allegro) not only provides sound at the higher frequencies to which our microphones are sensitive, but also has moments of silence that give occasion to test the memory capability of the target representation. To demonstrate target selection the music was played through two loudspeakers.

Scenario with a single sound source

Figure 6.14 illustrates the robot's behavior in the simplest scenario testing obstacle avoidance in conflict with the phono-taxis behavior. The target was a single loudspeaker placed behind a barrier (from the point of view of the initial position of the robot). The robot moves along a smooth, curved path around the obstacle to reach the target. It is the temporary knowledge about target direction retained in the dynamic field that enables the robot to continue moving in the correct direction during the periods of silence of the music. Two runs in the same scenario are shown. On one occasion the robot goes around the obstacle to the right, on the other to the left. The heading direction dynamics is bistable in this case and small fluctuations in sensory information can bring about either of the two paths. Once heading direction is in one of the two attractors, however, this decision is stabilized. In both cases the target is reached and the robot comes almost to rest near the loudspeaker.

Scenario with two sound sources

Figure 6.15 shows target selection based on different input strengths. Two speakers were fed with the same input signal. The robot was placed initially at position A with the sound sources switched off. The robot moves straight ahead. At point B, the sound sources are turned on. When the sound sources are at different distances from the robot the closer one is always selected. Figure 6.16 shows that when both sound sources are at quite exactly the same distance, the decision may depend on random fluctuations of the input stream.

Target selection based on prior activation patterns (hysteresis) is demonstrated in Figure 6.17. Two sound sources are both located behind obstacles (as seen from the initial position of the vehicle). In one run, the robot is initially closer to the sound source on the left. The field therefore establishes a peak at the leftmost target direction. The obstacle configuration forces the robot to pass through a position in which the robot receives symmetric input from the two sound sources. The preexisting peak on the left makes the robot retain the leftmost target. Analogously, when the robot starts out closer to the right target, that target is represented in the

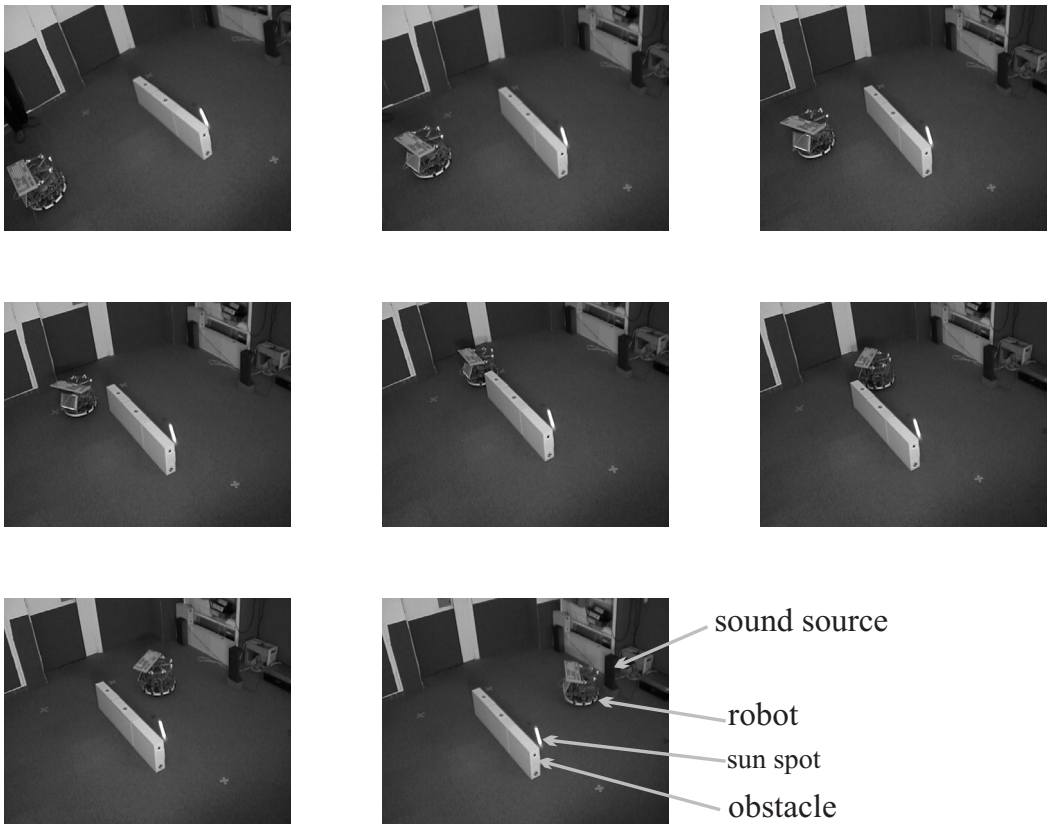

(a)

Figure 6.14: A sequence of video images illustrates the motion of the robot. Time increases from top to bottom, first along the first row, then along the second row and so on. The robot is the cylindrical object, located in the first frame in the lower left corner. A loudspeaker is visible in the top right corner. A long obstacle makes a barrier in between the robot's initial position and the loud speaker. The sound source is on all the time but exhibits some moments of silence. Part (a) shows that the robot moves smoothly around the obstacle, to the left, toward the sound source, coming to rest in the final frame in front of the loudspeaker. Part (b) shows a new run. This time the robot turns around the obstacle to the right, steering toward the sound source and it comes to rest near the loudspeaker.

dynamic field. The robot persists in the selection while it passes through the same position as in the first run with approximately symmetric input.

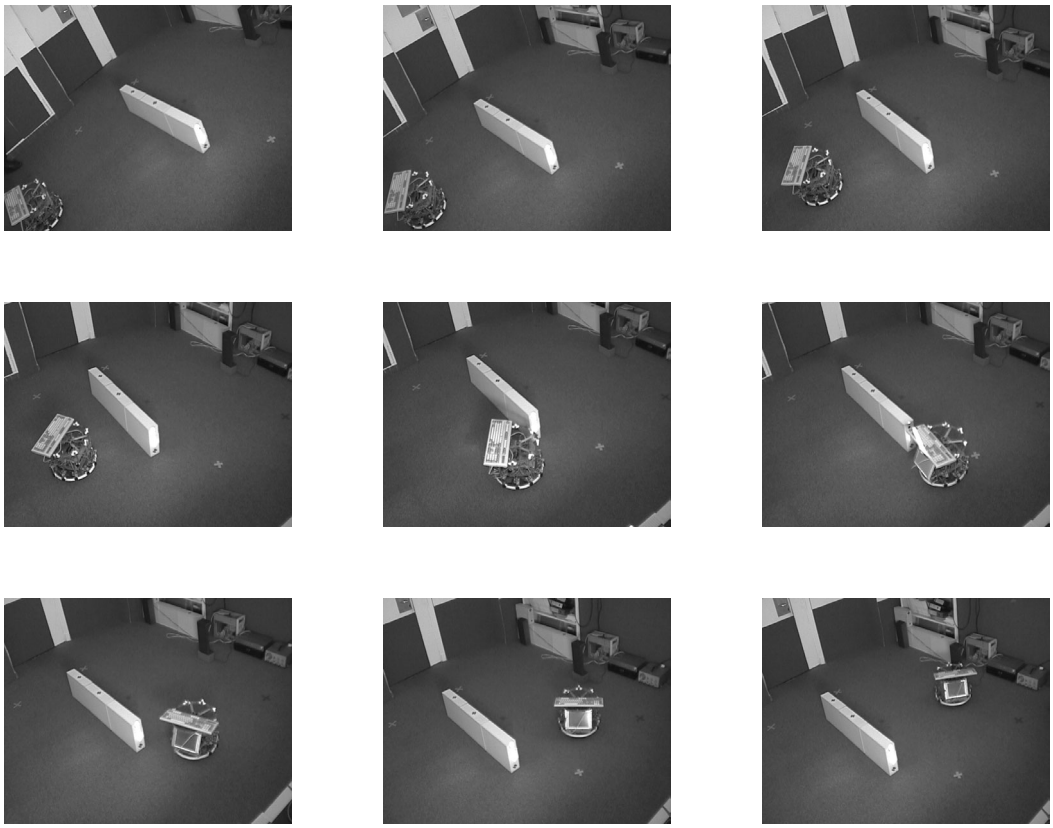

(b)
Figure 6.14: Continued.

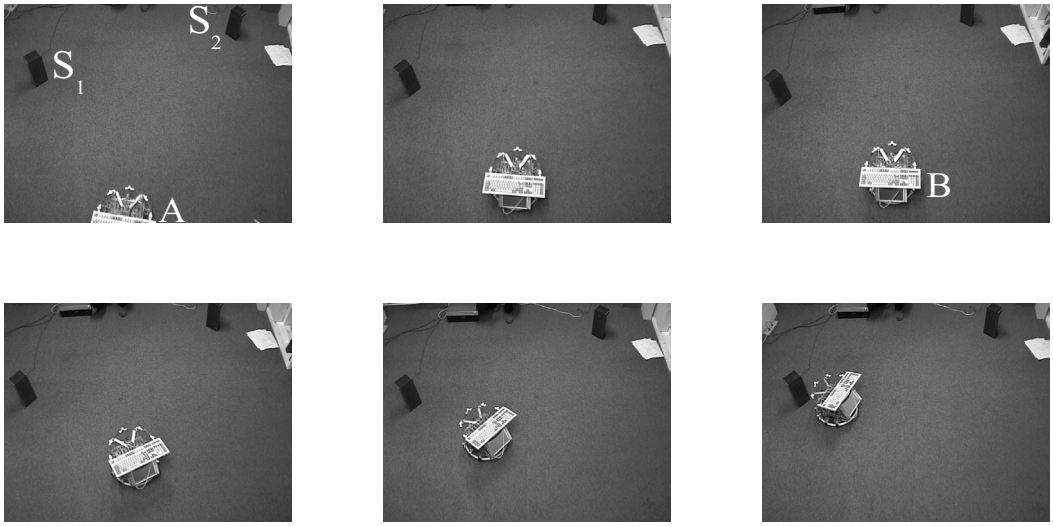

(a)

Figure 6.15: Two sequences of video images show the robot behavior in the presence of two loudspeakers emitting the same sound and in an asymmetric configuration. Time increases as announced in Figure 6.14. The robot is first located as depicted in the first frame. Two loudspeakers, S_1 and S_2, are located near the left and right top corners respectively. Initially, the sound sources are turned off, thus the robot moves straightforward. When it has traveled a distance of one meter both sound sources are switched on. In part(a) the loudspeaker on the left, S_1, is closer to the robot. This sound source is thus selected (it is visible in the 4th frame) and the robot moves smoothly toward it, coming to almost stop near the loudspeaker S_1. On part (b) another run is shown. Here the loudspeaker on the right, S_2, is closer to the robot. Analogously, the robot selects the closest sound (the decision can be seen in frame 4) and moves toward it.

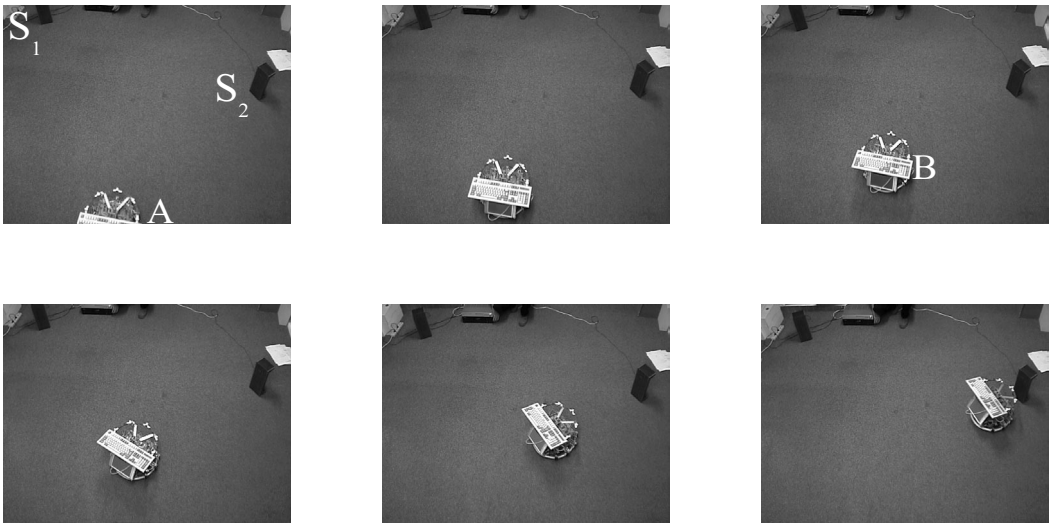

(b)

Figure 6.15: Continued.

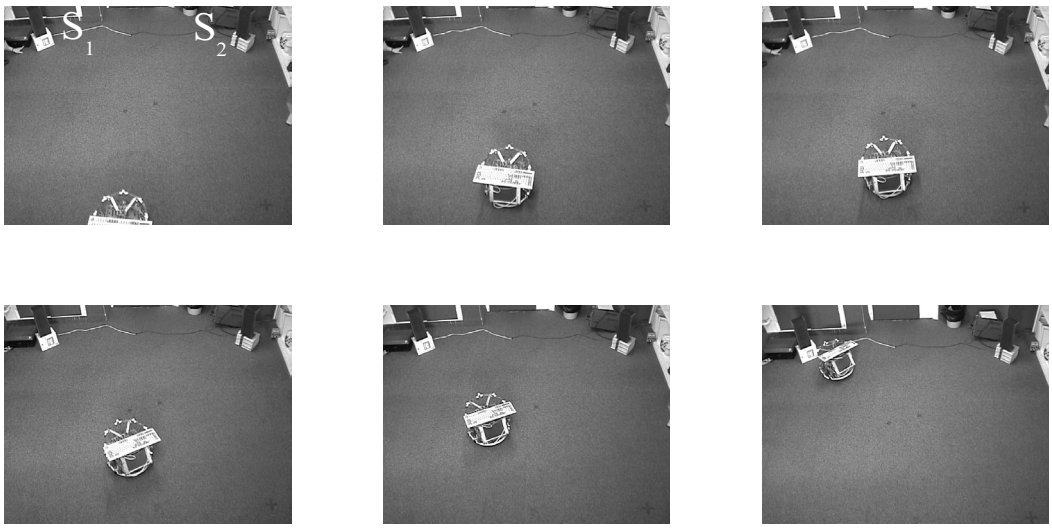

(a)

Figure 6.16: The two loudspeakers are now placed at exactly the same distance to the robot. In the run illustrated in part (a), the random fluctuations favor the selection of the left most target, S_1. The decision starts being visible on the third frame. The robot moves toward S_1 and finally stops in front of the loudspeaker (final frame). Part (b) shows a new run. This time the random fluctuations favor the selection of the right target, S_2. This decision becomes visible on the third frame. Again the robot moves toward the selected sound source and comes to rest in front of it.

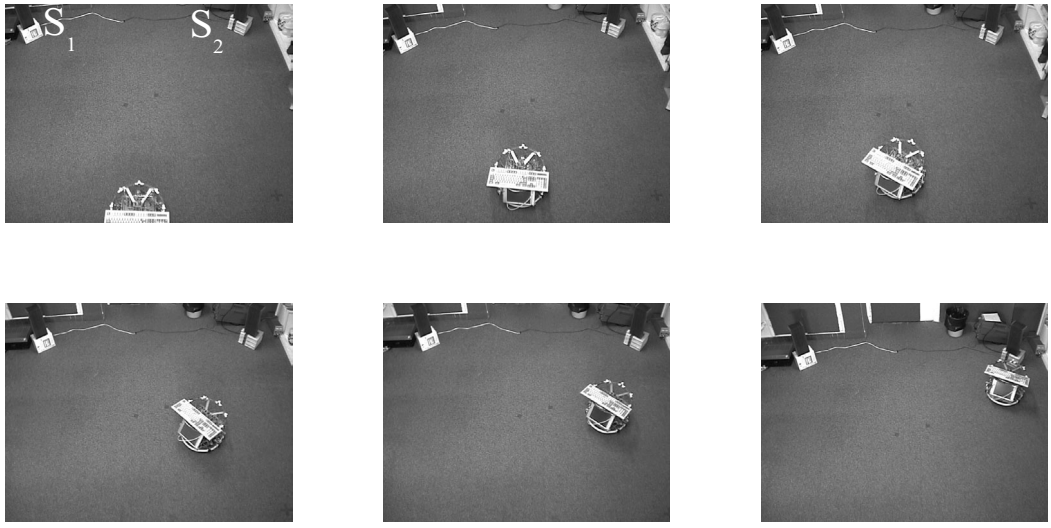

(b)

Figure 6.16: Continued.

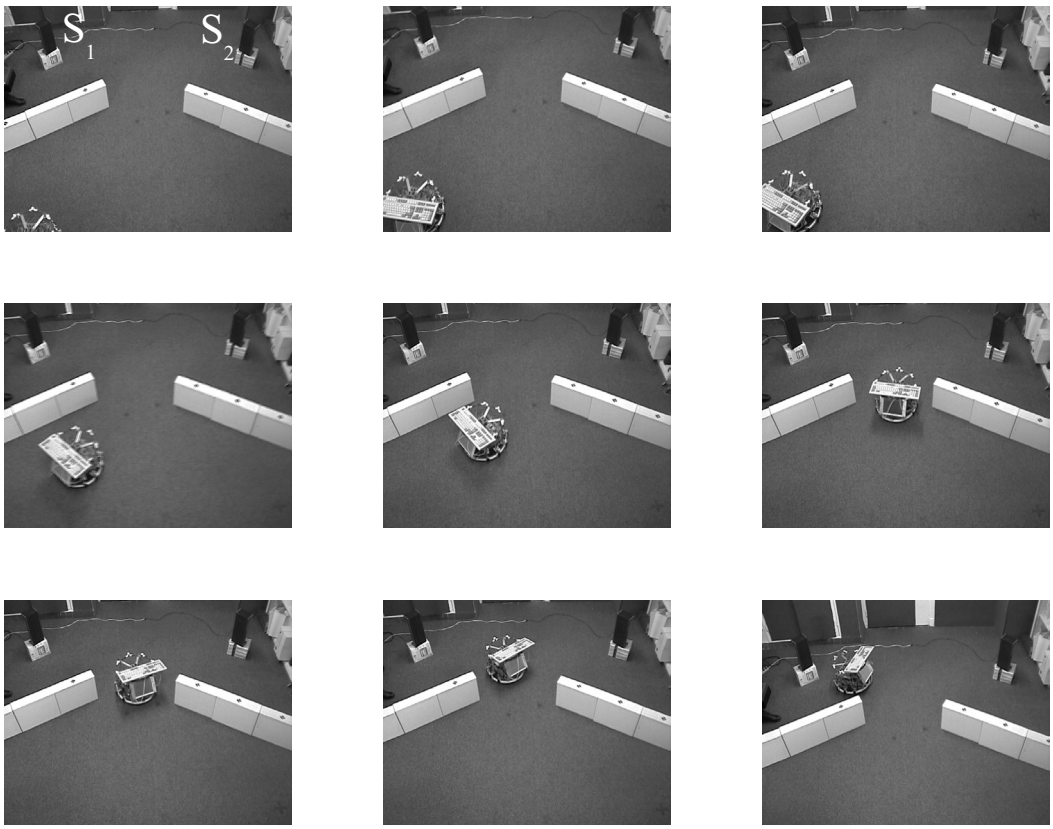

(a)

Figure 6.17: This figure shows that hysteresis enables to maintain a decision stable. Two sequences of video images are presented. The two identical sound sources, S_1 and S_2, are now placed behind obstacles as can be seen in the first frame. In part (a) the robot initial position is the left bottom corner in the first frame, i.e. in this run the robot is initially closer to the sound source on the left, S_1. Thus, the field evolves a peak of activation at the left most target direction. While moving toward S_1, due to the obstacle configuration, the robot is forced to pass through the opening in between the two barriers. At this time (frame 6) the sensory information received from the two sound sources is symmetric and the input to the field is bimodal with two input peaks of equal amplitude. The preexisting peak on the field corresponding to the selection of the left target bias the competition toward retaining the left most target. Thus the decision of moving toward S_1 is maintained stable. Part (b) shows a similar run. The robot now is closer to the right most target (see first frame). The robot starts moving toward the location of this sound source (but constrained of course by the obstacles). This decision is maintained stable when the robot is confronted with symmetric bimodal sensory input (frame 6). The robot comes to rest in front of the loud speaker S_2 (frame 9).

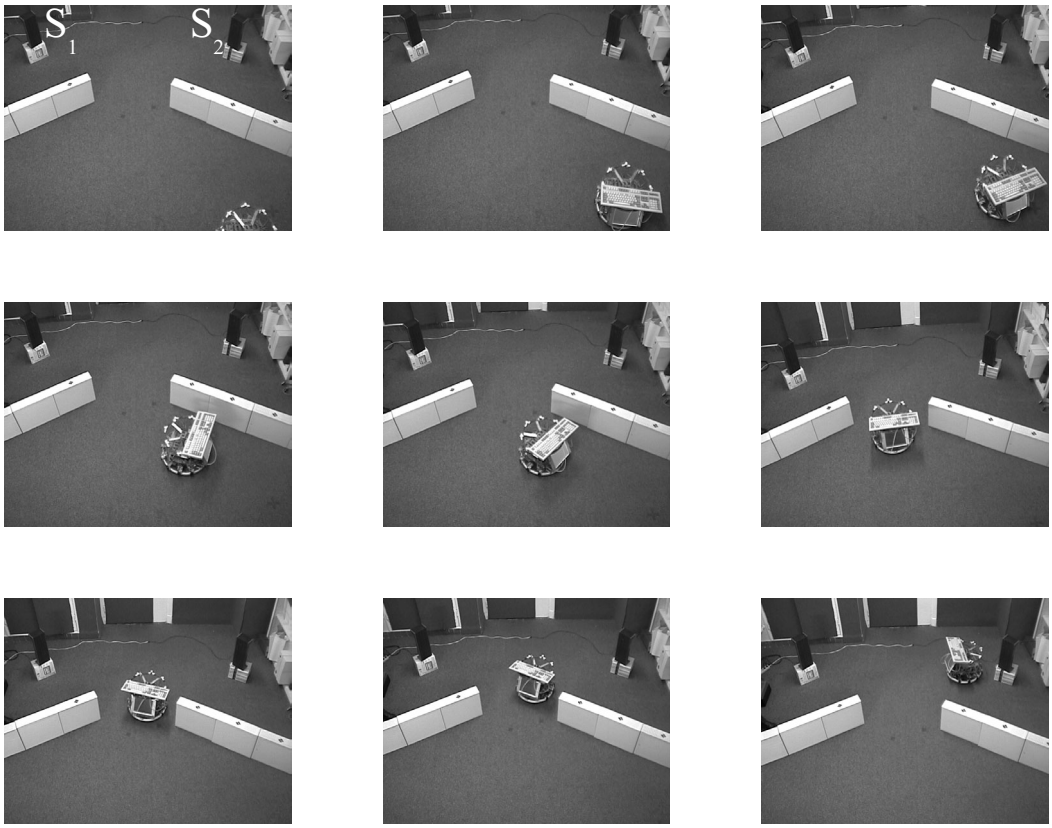

(b)

Figure 6.17: Continued.

Global behavior

In Figure 6.18 we illustrate behavior in a more complex environment. Initially, the robot is positioned in the corridor of our lab. The target is a loudspeaker placed inside one of the offices. Even while the robot moves along the corridor, its target representation already engages an approximate representation of the sound source. Based on that representation and aided by obstacle avoidance, the robot moves through the office door. It circumnavigates a number of additional obstacles and eventually finds the sound source, which is "hidden" inside a box with only a single entrance. It stops in front of the sound source (controlled by the velocity dynamics). Thus, although the architecture does not have global plans and finding a path is not theoretically guaranteed, the robot finds a remote target by moving along surfaces with the help of obstacle avoidance, until an "entry" is found. In our practical experience we have found it difficult to create scenarios in which the robot does not find its way even to quite intricately hidden sound sources.

6.8 Conclusion

We have demonstrated how dynamic fields can provide robotic systems with subsymbolic representations that rely on low-level sensory information. These representations enable the robot to show the simplest forms of cognitive capabilities, such as detecting targets, estimating direction to a target through interpolation, stabilizing a decision as to which of multiple targets to track, maintaining targets in short-term memory during momentary removal of pertinent sensory information, and deleting memory items after a characteristic delay to clear the memory of obsolete information. In the implementation, the dynamic field enabled a small autonomous vehicle to find sound sources while avoiding obstacles. Memory helped with intermittent sound, decision making enabled tracking of a sound source even if obstacle avoidance increased momentarily the distance from the sound source. Detection led to stable behavior near the sensor threshold.

The demonstrated robotic system has a number of obvious applications. We played, for instance, with the human voice as a sound source and demonstrated that the robot can follow or move toward a human operator who voices an utterance every now and then. The memory capacity of the dynamic field keeps the direction toward the human operator active during the intervals of silence. This robot system thus demonstrates an interesting interface, which could have multiple uses. Toys are an obvious example. An autonomous platform carrying tools and being operated by calling out is another example. Household devices to support handicapped people could be another domain in which such a simple interface could be of use. By installing particular filters at the auditory level, this system could be made sensitive to only particular types of sound (e.g., human voices rather than ambient sound).

The principle of representing direction information obtained from low level sensors could also be used to generate more complex movement behaviors of robotic

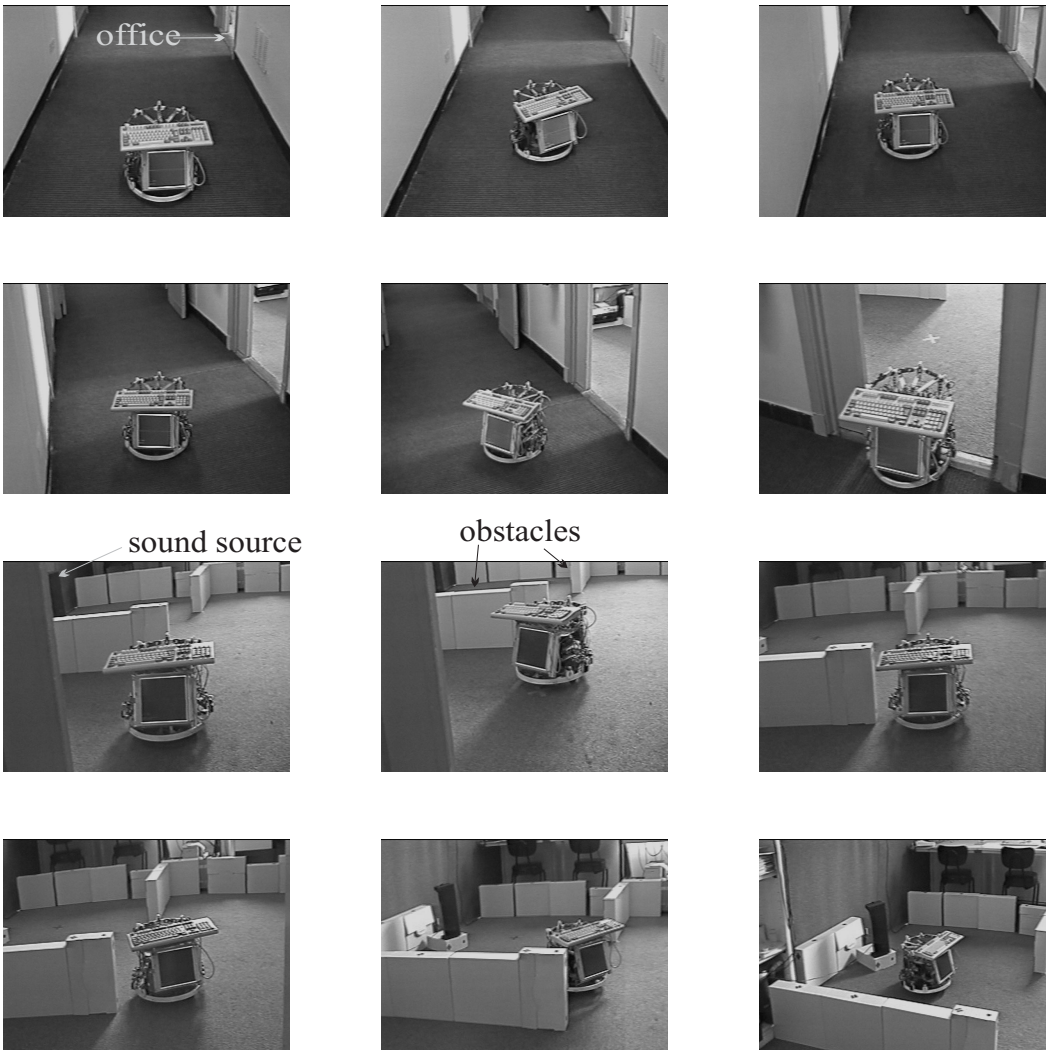

Figure 6.18: This figure shows a video sequence of the robot behavior in a more complex environment. The robot is initially positioned in the corridor. A sound source is inside one of the offices as indicated in the first frame. The robot moves along the corridor (frame 1 to frame 4). When the robot approaches the office door the phono-taxis behavior makes it enter into the room (frame 6). In frame 7 the robot is faced with a barrier of obstacles in between it and the sound source. The sound source is visible on the left top corner of this frame. The robot moves around the obstacles toward the target and finally comes to near rest in front of the loudspeaker (last frame).

platforms. For instance, the vehicle can be made to steer at a particular angle with respect to a sound source. In this way, a group of robots could drive in formation, if each robot emits a sound. Maneuvers in front of a docking station could be based on this mechanism. The representation of direction could also be used as a means of re-calibrating robot orientation without the need for actual movement of the robot

into a particular position or orientation. Finally, the fact that the sensed angle is explicitly represented could be used to communicate that information among robots or to an operator, which makes it possible to integrate such information into more complex strategies, for instance, for multi-robot environments.

Sound is only one sensory channel on which this approach can be based. We have tested a similar architecture that was based on light sensors (3 light dependent resistors). That system was able to orient toward light sources (Bicho and Schöner, 1997b). The fact that there is typically much more ambient light than ambient sound in work environments makes this a useful architecture only for work in near darkness, however. Chemo-detection is another potential sensor system that could be enhanced through a dynamic field (Kuwana and Shimoyama, 1998).

One limitation of the system as it stands come from the computational demands of dynamic fields. The cycle time obtained for a computational step on the order of 100 ms leads to reasonably fast behavior, but one could be much faster. If more complex architectures were tried with multiple dynamic fields for different representations, then this could become a serious limitation. One solution might be to implement the computationally critical parts in Assembler code. Another approach might be to use more optimal numerical procedures.

There are, of course, limitations that come from the low-level sensor system. The robot may select, for instance, sometimes an echo rather than the real sound source. This is not severe, however, as echos do not persist as the robot changes position. Once the robot has latched onto the real target, the stabilization of decision making provided by the dynamic field makes sure that the robot does not get sidetracked by new echos it encounters on the way to the target.

Chapter 7

Detecting, representing and following walls based on low-level distance sensors

Wall-following is an important behavior in navigation since in office environments, as well as in maze like environments, corridors and long wall ways (in various shapes) are very common. Thus, much of the work to bring a robotic vehicle from one location to another consists of driving along a series of walls or corridors. So, when a robot senses a wall it is very often useful to be able to follow the wall smoothly instead of turning away from it.

In this chapter the problem of following walls with different shapes and keeping a constant distance from the wall is analyzed. A solution is proposed which is based on a sub-symbolic representation of walls and on a behavioral dynamics that controls the distance from the wall. The wall representation system is built making use of the dynamic field concept. It endows the robot with the following capabilities: wall detection, wall orientation estimation, insensibility to noisy sensory data and wall selection. Simulation results and experimental results are presented.

7.1 Introduction

Following our previous work (Chapter 6; Bicho, Mallet and Schöner, 1999a) we continue to speculate, in this chapter, that in order for a low-level robot vehicle to be endowed with cognitive capabilities, which are the background for intelligent and flexible behavior, it may need to have representations. Such representations are not general purpose descriptions, though. Instead, each representation is associated with a particular behavior of the robotic system.

In Chapter 6 we have demonstrated how a dynamic field can provide a robotic vehicle with a sub-symbolic target representation system that relies on low-level sensory information. Specifically, the system used 5 microphones to provide information

about sound targets. That representation enabled the robot to show the simplest forms of cognitive capabilities, such as detecting targets, estimating direction to a target through interpolation, stabilization of a decision as to which of multiple targets to track, maintaining targets in short-term memory during momentary removal of pertinent sensory information and forgetting items after a characteristic delay to clear the memory from old and therefore obsolete information.

As a case study, we address here the problem of representing information about walls based on low-level distance sensors (e.g. infra-red sensors and sonars). These sensors provide distance measures to objects at the directions at which they are pointing in space. We assume that each pair of neighboring distance sensors defines a wall segment whenever both detect obstructions (see Figure 7.1). Our goal is to built a sub-symbolic wall representation system, from this sensory information, that permits to endow a robot vehicle with a wall-following behavior which exhibits the most basic cognitive capabilities: detecting walls , estimating the orientation of a wall through averaging of sensory data, robustness against noisy sensory information and wall selection.

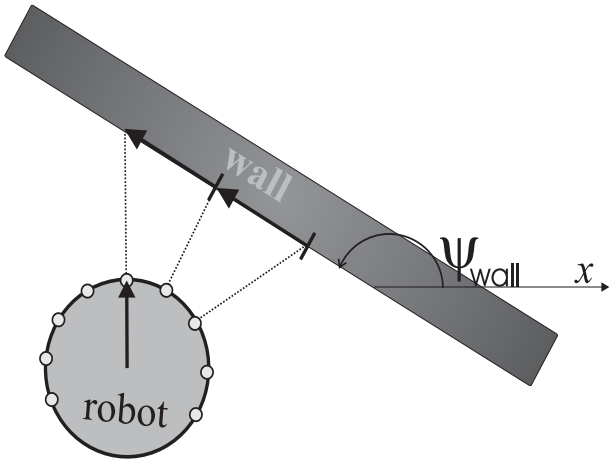

Figure 7.1: A wall with orientation ψ_{wall} is to the right of the robot. Each pair of neighboring distance sensors defines a wall segment whose orientation ideally is the orientation of the wall.

In order to generate the basic cognitive elements enumerated above, a dynamic field representation of the spatial orientation in which a wall is detected is defined. Input to the field is provided by the orientation of each detected wall segment. The dynamic field is endowed with the ability to suppress outliers in the input pattern distribution (due to inaccurate sensory information), as well as of making and stabilizing decisions in response to multi-valued sensory information (such as when two walls lead to a bimodal input distribution).

This dynamic wall representation is coupled with a dynamics which generates the overt wall-following behavior in the world. This overt behavior also exhibits

decision making in the sense that the robot can follow a wall keeping it to its right or to its left side. Results prove the capacity of the system to perform wall detection, robust wall orientation estimation and wall selection. Results also show the ability to follow walls in various shapes.

The robot has no a priori information about the environment, that is, no information about position or shape of the walls or obstacles.

This chapter is structured as follows: In Section 7.2 we review some related work. Section 7.3 and Section 7.4 present the dynamics of wall-following and the dynamics of wall representation, respectively. In Section 7.5 explains the coupling of the dynamics of wall representation with the behavioral dynamics of wall-following. Next, in section 7.6 some simulation results are presented to illustrate the properties of the dynamic field for wall representation. Section 7.7 discusses some implementation details of the dynamic architecture on the robotic platform. Experimental results are described in Section 7.8 and finally the chapter ends with discussion and conclusions in Section 7.9.

7.2 Related work

Wall-following has been a problem of interest in robotics research and a large body of references can be found in the literature (Bauzil, Briot and Ribes, 1981; Brooks, 1992; Iijima, Yuta and Kanayama, 1983; Giralt, 1984; Turennout, Honderd and Schelven, 1992; Koza, 1994; Ando, Tsubouchi and Yuta, 1996; Yata, Kleeman and Yuta, 1998; Meng, Liu, Zhang and Sun, 1999).

The problem of wall-following has been examined as a case study both in model based (Giralt, 1984; Cox, 1991) and behavior-based approaches to robotics (Brooks and connel, 1986; Mataric, 1990; Brooks, 1992).

In the first approach sensor readings are taken to build straight lines (wall segments). For estimating the orientation of these straight lines robust methods exist based on filtering techniques, if the error models are accurate. Then these straight lines are matched against line segments in a model of the environment (either CAD or self-learned), and finally a trajectory is planned toward the closest wall found (Bauzil, Briot and Ribes, 1981; Giralt, 1984). The main drawback of this approach is that models of the environment are difficult to obtain and maintain in real time, thus limiting its application for navigation in unstructured and dynamic environments, and the error models might not be sufficiently accurate.

In contrast, behavior-based approaches make no special assumptions and use sensory information at low levels of parameter extraction. Wall-following is generated as a continuous link between sensing and acting (Brooks and Connell, 1986). This raises the difficulty to generate behavior that is not directly linked to on-line sensory information. For example, the ability to keep the behavior stable against noisy sensory data or to decide which wall to follow when two walls are detected. This last problem is usually alleviated by algorithmically switching to a

corridor following behavior so that the robot navigates along the center of the corridor (Balkenius, 1995). This might not be the most adequate solution, however, especially if other vehicles or persons share the same physical space. The vehicle should instead select one of the two walls and move along it in order to leave maximum space available.

Mataric (1990) presents a wall-following behavior which is generated as an emergent activity which results from the interaction between four mutually exclusive behaviors and the environment. We argue that if a robot is supposed to navigate along walls in order to improve its navigating performance its behavior should be purposive.

Wall-following has been also an attractive problem for behavior based approaches using Fuzzy control algorithms (Meng, Liu, Zhang and Sun, 1999) and genetic algorithms (Ross, Daida, Doan, Begey and McClain, 1996) and good solutions have been proposed. The drawback here is that the integration with other behaviors requires the redesign of the overall control architecture.

Ando, Tsuboushi and Yuta (1996) as well as Chen and Luo (1998) present results of a robot following walls in various shapes. The algorithm is reactive and very simple. The results show that their algorithm for wall-following is robust even though its success is much dependent on the specular reflections. An important limitation of this algorithm is that the robot must be in the neighborhood of an object at the initial time. These authors neither reported integration with other movement behaviors nor the problem of having more than one wall. Based on this simple algorithm it is difficult to support explicit decision making and stabilization of decisions when sensory information is ambiguous or inaccurate.

7.3 Wall-following dynamics

Two possible wall-following behavioral modes must be distinguished: Right-mode, where the robot follows a wall on its right, and Left-mode, where the robot follows a wall on its left. In either behavioral mode, the robot must steer such as to follow the wall contour at a fixed pre-defined distance. We design wall-following as a behavioral dynamics of heading direction

$$\frac{d\phi}{dt} = F_{\text{wall}}(\phi) = \gamma_{\text{r}} F_{\text{wall,r}}(\phi) + \gamma_{\text{l}} F_{\text{wall,l}}(\phi) \tag{7.1}$$

where $F_{\text{wall,r}}(\phi)$ represents the Right-mode and $F_{\text{wall,l}}(\phi)$ the Left-mode. The strengths γ_{r} and γ_{l}, when adequately tuned, select the behavioral mode that must dominate the heading direction dynamics. We will explain later how this selection (i.e. decision making) is brought about.

The Right-mode term is a sum of two contributions

$$F_{\text{wall,r}}(\phi) = f_{\text{inwards,r}}(\phi) + f_{\text{outwards,r}}(\phi) \tag{7.2}$$

each defining an attractive force (i = inwards, outwards):

$$f_{i,\mathrm{r}}(\phi) = \begin{cases} -\lambda_{i,\mathrm{r}}(\phi - \psi_{i,\mathrm{r}}) & \text{for } \psi_{i,\mathrm{r}} - \pi/2 < \phi \leq \psi_{i,\mathrm{r}} + \pi/2 \\ \lambda_{i,\mathrm{r}}(\phi - \psi_{i,\mathrm{r}} - \pi) & \text{for } \psi_{i,\mathrm{r}} + \pi/2 < \phi \leq \psi_{i,\mathrm{r}} + 3\pi/2 \end{cases} \tag{7.3}$$

where ϕ value is mapped into the listed cases through a *modulus* 2π operation.

The first contribution, $f_{\mathrm{inwards,r}}(\phi)$, erects an attractor at a direction

$$\psi_{\mathrm{inwards,r}} = \psi_{\mathrm{wall}} - \Delta\psi_{\mathrm{w}} \tag{7.4}$$

pointing inwards the wall. This direction is obtained subtracting an angle $\Delta\psi_{\mathrm{w}}$ (because the wall is to the right) to the estimated wall orientation, ψ_{wall}, relative to the external reference frame. The strength of this attractor increases with distance, d_{r}, to the wall on the right of the robot

$$\lambda_{\mathrm{inwards,r}}(d_{\mathrm{r}}) = \frac{1}{1 + \exp\left(-(d_{\mathrm{r}} - d_{\mathrm{wall}})/\mu\right)} \tag{7.5}$$

Here d_{r} is the minimum distance measure given by the distance sensors on the right side of the robot and d_{wall} is the desired distance to the wall. The second contribution, $f_{\mathrm{outwards,r}}(\phi)$, sets an attractor at a direction pointing outwards (obtained summing $\Delta\psi_{\mathrm{w}}$ to the orientation of the wall because the wall is on the right side)

$$\psi_{\mathrm{outwards,r}} = \psi_{\mathrm{wall}} + \Delta\psi_{\mathrm{w}} \tag{7.6}$$

with a strength that decreases with distance, d_{r}, to the wall

$$\lambda_{\mathrm{outwards,r}}(d_{\mathrm{r}}) = 1 - \lambda_{inwards,\mathrm{r}}(d_{\mathrm{r}}) \tag{7.7}$$

Because the two attractive forces, $f_{\mathrm{inwards,r}}(\phi)$ and $f_{\mathrm{outwards,r}}(\phi)$, are overlapping only one attractor results from their superposition. The direction at which the resulting attractor is formed depends on the distance to the wall. This is illustrated in Figure 7.2.

The Left-mode term in the vector field of heading direction dynamics (Equation 7.1), which represents the behavior of following a wall to the left, is formally equivalent to the Right-mode. It is a sum of two attractive forces

$$F_{\mathrm{wall,l}}(\phi) = f_{\mathrm{inwards,l}}(\phi) + f_{\mathrm{outwards,l}}(\phi) \tag{7.8}$$

each with the same piecewise form of Equation 7.3. The first force erects an attractor at a direction pointing inwards the wall on the left with a strength that increases

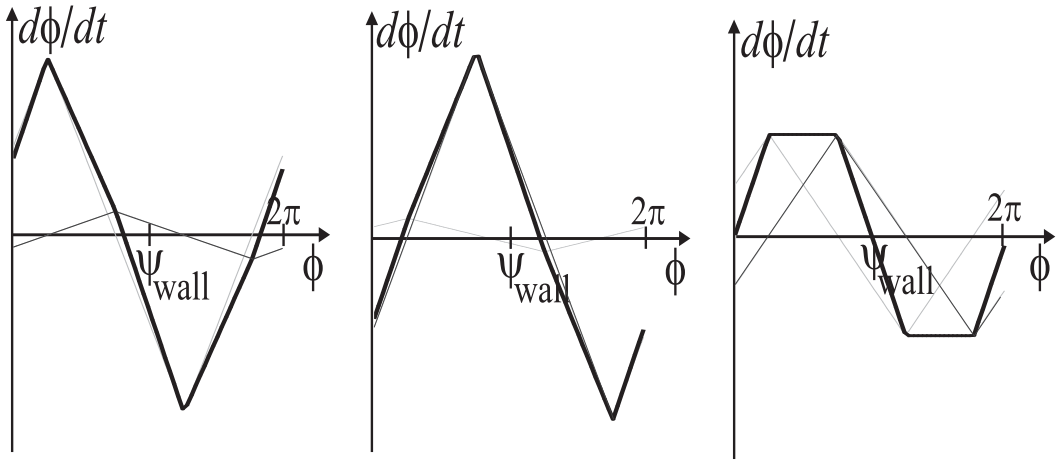

Figure 7.2: This figure shows the two contributions to the wall following dynamics (when the wall is to the right) and their superposition for the three different physical situations. $f_{\text{inwards,r}}$ and $f_{\text{outwards,r}}$ are depicted by the dark grey and light grey thin lines respectively. Their superposition, i.e. $F_{wall,\text{r}}$, is indicated by the bold black line. Left: When the robot is at a distance to the wall larger than the desired distance the attractive force erected at direction $\psi_{\text{inwards,r}}$ is stronger than the attractive set at direction $\psi_{\text{outwards,r}}$. Their superposition leads to an attractor at a direction still pointing into the wall, i.e. smaller than ψ_{wall}. Middle: Conversely, when the robot is closer to the wall than the desired distance, the reverse holds, i.e. the attractive force set at direction $\psi_{\text{outwards,r}}$ is now stronger than the attractive force at direction $\psi_{\text{inwards,r}}$. The resulting dynamics exhibits an attractor at a direction pointing away from the wall. Right: When the robot is at the desired distance to the wall the two attractive forces have the same strength which leads to a resultant attractor at the orientation of the wall, i.e. ψ_{wall}.

with distance. The second force sets an attractor at a direction pointing outwards the wall with a strength that decreases with distance. Since we assume that ψ_{wall} is the orientation of the wall estimated in the counter-clock direction the values of the attractors are

$$\psi_{\text{inwards,l}} = \psi_{\text{wall}} + \pi + \Delta\psi_{\text{w}} \tag{7.9}$$

$$\psi_{\text{outwards,l}} = \psi_{\text{wall}} + \pi - \Delta\psi_{\text{w}} \tag{7.10}$$

The strengths of these attractors are given by Equation 7.5 and Equation 7.7 respectively, where the distance is now the distance to the wall on the left side, of course. Similarly to $F_{\text{wall,r}}$, $F_{\text{wall,l}}$ exhibits one attractor only.

We now explain how the dominance of the Right-mode or the Left-mode in the dynamics of the heading direction is brought about by adjusting the strengths, γ_{r} and γ_{l}, in Equation 7.1.

The strengths γ_{r} and γ_{l} are tuned such that $F_{\text{wall,r}}$ dominates when the detected wall is to the right of the robot, while $F_{\text{wall,l}}$ dominates when the wall is to the left.

A function that indicates if a wall is to the right or to the left of the robot can be constructed by making use of the repulsive force-lets from the obstacle avoidance dynamics. In fact, from the sign of the obstacle forces, $F_{\text{obs}}(\phi)$ (Equation 4.4), we can read off if a wall is to the right or to the left of the robot (see Figures 4.3 and 4.7 in Chapter 4). Positive values of $F_{\text{obs}}(\phi)$, indicate that the wall is to the right, so $\gamma_{\text{r}} > 0$ and $\gamma_{\text{l}} \approx 0$ is required. Conversely, negative values of $F_{\text{obs}}(\phi)$ indicate that the wall is to the left, thus $\gamma_{\text{r}} \approx 0$ and $\gamma_{\text{l}} > 0$ is required. Applying a sigmoid threshold function to $F_{\text{obs}}(\phi)$

$$T\left(F_{\text{obs}}(\phi)\right) = \frac{2\arctan\left(C_{\text{w}} F_{\text{obs}}(\phi)\right)}{\pi} \tag{7.11}$$

ranging from -1 to 1, we can write the functions for the two strengths:

$$\gamma_{\text{r}} = c_{\text{r,w}}\left[1 + T\left(F_{\text{obs}}(\phi)\right)\right] \tag{7.12}$$

$$\gamma_{\text{l}} = c_{\text{l,w}}\left[1 - T\left(F_{\text{obs}}(\phi)\right)\right] \tag{7.13}$$

For a sufficiently sharp sigmoid (i.e. C_{w} sufficiently large) this leads to the selection of the required behavioral mode. The parameters $c_{\text{r,w}}$ and $c_{\text{l,w}}$ determine the relaxation rate of the wall following dynamics in the two cases where the wall is to the right or to the left respectively. They are tuned so that the heading direction is in or near the resultant attractor of this dynamics. As the estimate of the wall orientation changes (e.g., when the vehicle circumnavigates a curved wall) and/or the distance to the wall changes, the resultant attractor of the wall following dynamics shifts attracting the heading direction along.

7.4 The dynamics of wall representation

To compute the orientation of a wall we make use of the following strategy: Each pair of neighboring distance sensors (of the same type) define a wall segment as illustrated in Figure 7.3. Knowing the direction at which sensors are pointing in the world and their distance measures we can compute the orientation, Ψ_i, of wall segment number i through the trigonometric equation:

$$\Psi_i = \arctan\left[\frac{(d_{i+1} + R_{\text{robot}})\sin(\psi_{i+1}) - (d_i + R_{\text{robot}})\sin(\psi_i)}{(d_{i+1} + R_{\text{robot}})\cos(\psi_{i+1}) - (d_i + R_{\text{robot}})\cos(\psi_i)}\right] \quad i = 1, 2, \ldots, 8 \tag{7.14}$$

here ψ_i and ψ_{i+1} are the directions in the world in which sensors i and $i+1$ are pointing, respectively. The vehicle's heading direction, ϕ, is defined relative to the same reference frame and sensor k is mounted at an angle θ_k relative to the forward direction of the robot, thus $\psi_k = \phi + \theta_k$. In the implementation this requires integrating heading direction in time to maintain the reference frame. The absolute calibration of this reference frame is irrelevant, however.

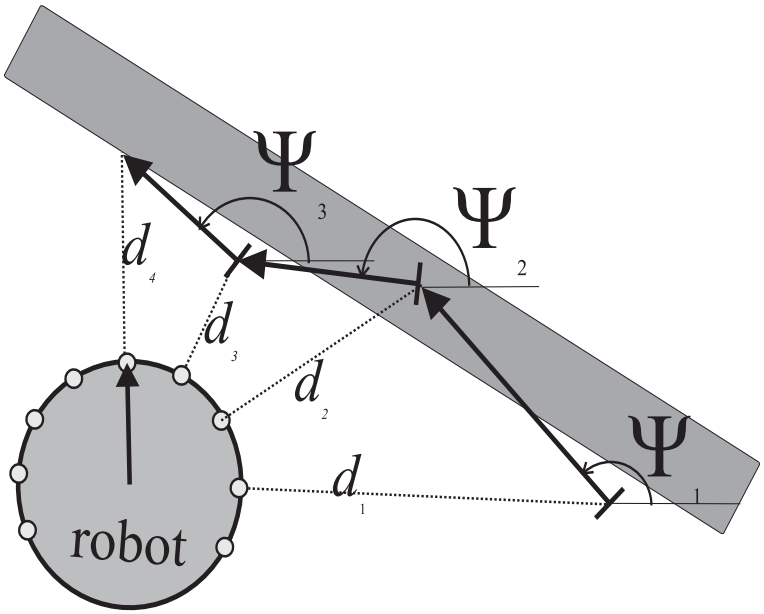

Figure 7.3: Problem associated with noisy and low resolution distance sensors: The orientations of the individual wall segments differ from the orientation of the wall.

Given a distribution of measures $(\Psi_1, \Psi_2, \ldots, \Psi_N)$ for the orientation of a wall (one per each detected wall segment) the next step is to estimate the wall orientation. The standard mean does not give a good estimate because it is very sensitive to outliers, which are a real problem when dealing with noisy and low resolution sensors. Robust estimation methods exist that are not affected by outliers. But we still have to deal with two more problems that can not be solved by these methods:

i) When does a wall exist? That is, when is sensory information consistent enough for the robot to "decide" that a wall is present and thus when to induce the wall-following behavior? For the situation depicted in Figure 7.4 on the left, should a wall be detected or just an obstacle?

ii) What should the robot do if two or more walls with different orientations exist? Which wall should the robot follow? This problem is illustrated in Figure 7.4 on the right and rises the necessity for wall selection.

Given these problems our challenge is to represent information about walls for an autonomous vehicle moving in the plane such that the following abstract behaviors are realized:

1. Wall detection, in which a wall is signaled only if sensory information is sufficiently convergent while the absence of a wall is indicated for weak or disperse sensory information.

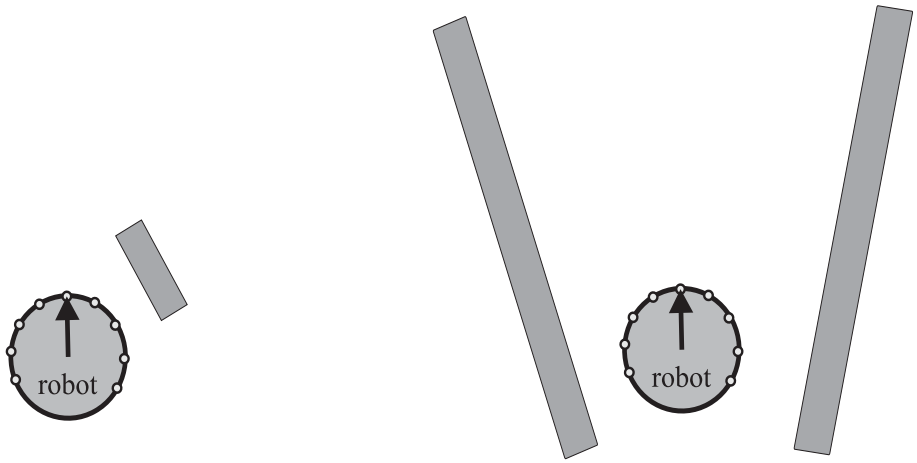

Figure 7.4: Two more problems in wall-following. Left: Sensory data define a wall segment. Should a wall be detected or not? Right: Sensors provide information about two walls. The problem to be solved is thus wall selection and, simultaneously, computation of a wall orientation estimate even in the presence of multi-valued sensory information.

2. The ability to make continuous estimates of the wall orientation, i.e. ψ_{wall}, when sensory information is provided by an array of distance sensors.

3. Insensibility to noisy sensory data, i.e. elimination of outliers (robust estimation).

4. Wall selection, i.e. computations on distributed representations of sensory information in which wall segments with different orientations are detected.

These information processing behaviors imply working with representations of information, here the orientation of a wall. To generate the wall representation system we make use, again, of the concept of a dynamic field of activation, as presented in Section 6.3.

For wall-following we represent the orientation, ψ, in the counter-clock direction, in which a wall lies, relative to an external reference frame. This variable can take values in the interval $[0, 2\pi]$ rad. An activation variable $v(\psi)$, is defined for each possible value of wall orientation, ψ. The variable $v(\psi)$ is a dynamical state variable and represents if a wall with orientation ψ is detected. The value ψ where a peak of positive activation is centered indicates the estimated value for the orientation of the wall. When sensory information does not specify a wall this is expressed in the field through negative activation everywhere ($v(\psi) \leq 0 \;\; \forall \psi \in [0, 2\pi]$).

Information processing takes place as the activation in the field evolves in time as described by the Amari equation:

$$\tau_{\text{w}} \frac{dv(\psi, t)}{dt} = -v(\psi, t) + S_{\text{w}}(\psi, t) + h_{\text{w}} + \int_0^{2\pi} W_{\text{w}}(\psi - \psi')\Theta(v(\psi', t))d\psi' \qquad (7.15)$$

$S_{\mathrm{w}}(\psi, t)$ represents input activation, which excites sites of the field for which sensory information defines wall segments.[1] If the data provided by the distance sensors indicate a wall segment with orientation ψ at time t, then input activation at this location is positive, $S_{\mathrm{w}}(\psi, t) > 0$, else input activation is zero, $S_{\mathrm{w}}(\psi, t) = 0$. The contribution (i.e. the orientation) of each wall segment is spread in angular range by a Gaussian kernel, such that near contributions from segments with close orientations overlap for some amount

$$S_{\mathrm{w}}(\psi) = \sum_i \exp\left[-(\psi - \Psi_i)^2/(2\sigma_{\mathrm{w}}^2)\right] \tag{7.16}$$

In this equation σ_{w} was kept constant and equal to 0.25 rad ($\approx$ 15 deg). The linear part of the Equation 7.15

$$\tau_{\mathrm{w}} \frac{dv(\psi, t)}{dt} = -v(\psi, t) + S_{\mathrm{w}}(\psi, t) + h_{\mathrm{w}} \tag{7.17}$$

makes the field relax to the pattern of activation

$$v(\psi, t) = S_{\mathrm{w}}(\psi, t) + h_{\mathrm{w}} \tag{7.18}$$

with a low-pass characteristic. If the input varies in time the field activation follows the input with a certain inertia (depending on τ_{w}). This linear dynamics *per se* is not useful because an estimate of a wall orientation based on Equation 7.18 is not robust, since each individual measurement of the wall orientation is taken equally and contributes to the final estimate. When dealing with noisy sensory information this is a serious drawback because outliers are frequent. We need a mechanism that suppresses or inhibits wall orientation measures, that are far away from the "actual" value, to contribute to the final estimate. This mechanism is provided by the integral term in Equation 7.15, which endows the field with interactions.

The typical form of interactions that fulfills our necessities/requirements is local excitation and global inhibition. Thus, we choose again, a rectangular interaction kernel with local excitation and global inhibition

$$W_{\mathrm{w}}(\Delta\psi) = \begin{cases} k_{p,w} & \text{for } -l_{\mathrm{coop,w}} < 2\Delta\psi < l_{\mathrm{coop,w}} \\ -k_{n,w} & \text{else} \end{cases} \tag{7.19}$$

which only depends on the distance, $|\Delta\psi|$, between field sites and makes that sites that are closer to each other than the cooperativity length, $l_{\mathrm{coop,w}}$, interact excitatorily ($W_{\mathrm{w}}(\Delta\psi) = k_{\mathrm{p,w}} > 0$), while for larger distances they interact inhibitorily ($W_{\mathrm{w}}(\Delta\psi) = -k_{\mathrm{n,w}} < 0$). The non-linear transfer function, $\Theta(\cdot)$, is given by Equation 6.3.

We now discuss how the different behaviors enumerated above can be realized by the field dynamics.

[1] Concretely, it is the orientation of each sensed wall segment that contributes to the input activation.

Wall detection

We want a wall to be signaled only if sensory information is sufficiently convergent. Our criterion is that a wall is present only when two or more wall segments have neighboring orientations. The size of the neighborhood is determined by the parameter $l_{\text{coop,w}}$. The resting level, $h_{\text{w}} < 0$, permits to control the value of the input strength above which a detection is triggered. For an input, S_{w}, localized around one location in the field, this means that while input has small amplitude ($S_{\text{w}} \leq |h_{\text{w}}|$), the state of the field is the solution $v(\psi) = h_{\text{w}} + S_{\text{w}}(\psi)$ which is negative everywhere. The field codes absence of a wall. When the amplitude of the input is sufficiently strong and lasts over a sufficient period of time, contributions from interaction within the field start to dominate the dynamics. The stable state of the field is now a localized peak of positive activation. The peak is positioned over the location of maximal input. The position over which the peak of positive activation is centered represents the wall orientation estimate, ψ_{wall}.

Weighted averaging *versus* decision making

In Chapter 6 we have seen that depending on the shape of the input distribution the field exhibits different properties.

When the input distribution is multi-modal[2] and has input peaks that are sufficiently close (i.e. within the cooperative length $l_{\text{coop,w}}$) the field evolves a peak of positive activation that is positioned over the weighted mean of the two locations of maximal input. The mean is weighted because different amplitudes of the input peaks lead to a bias of the position of the resulting peak of activation toward the site receiving stronger input. This fusion of input information results from the local excitatory interactions.

By contrast, if the input peaks are separated by more than the cooperative length, $l_{\text{coop,w}}$, then activation at these sites interact mutually inhibitory so that one site suppresses the others. The field evolves only one peak of positive activation. The site that wins the competition depends on the prior state and on the relative amplitudes of the peaks (as discussed in Section 6.3). The field dynamics exhibits hysteresis, in which a decision or an estimate once made is stabilized, in the face of multi-valued information (e.g. when two walls are present) or ambiguous information due to noisy sensor data.

Robust estimation

The ability of the field to self-generate and self-stabilize peaks of activation through cooperative interactions is used to endow the field with robust estimation properties (see Neven, 1997; Giese, 1999, for a study of dynamic fields as robust estimators). The estimate, ψ_{wall}, is robust in the sense that wall orientation measures which are

[2]Multi-modal input occurs when more than one wall are present and/or sensory information is noisy.

far away from the actual selected estimate are strongly inhibited such that they contribute weakly to the final estimate, i.e. to the resultant pattern of positive activation in the field. As a consequence these measures are effectively discarded as outliers.

7.5 Coupling the dynamics of wall representation with the behavioral dynamics of wall-following

By design the time scale of the field dynamics, τ_{w}, is set much faster than the heading direction and velocity dynamics such that we can assume that the field for wall representation has relaxed to a stable pattern on the time scale on which the movement plans of the robot evolve. Moreover, by design the field has only a single peak of positive activation. Thus, to compute the orientation, ψ_{wall}, of the wall from the activation in the field we can employ the same solution used in the previous chapter (see Section 6.5). The activation in the field is considered as a probability density and ψ_{wall} is computed as a mean like indicated by Equation 6.10. We have seen that this solution runs into trouble, however, when there is no positive activation in the field. We have also seen how this problem can be solved. We make the strength of each attractive force-let defined by Equation 7.3 also a function of the total activation

$$N_v = \int_0^{2\pi} H(v(\psi))d\psi \tag{7.20}$$

in the field,[3] so that in the absence of activation (i.e. situation in which ψ_{wall} is undefined) the attractive forces that compose the wall-following dynamics have strength zero. We therefore redefine each attractive force-let (Equation 7.3) by multiplying each by N_v. This amounts to defining:

$$f_{\mathrm{inwards},r}(\phi) = \begin{cases} -\lambda'_{\mathrm{inwards},r}\left(N_v(\phi + \Delta\psi_{\mathrm{w}}) - P_v\right) & \text{for } \psi_a < \phi \leq \psi_b \\ \lambda'_{\mathrm{inwards},r}\left(N_v(\phi + \Delta\psi_{\mathrm{w}} - \pi) - P_v\right) & \text{for } \psi_b < \phi \leq \psi_c \end{cases} \tag{7.21}$$

$$f_{\mathrm{outwards},r}(\phi) = \begin{cases} -\lambda'_{\mathrm{outwards},r}\left(N_v(\phi - \Delta\psi_{\mathrm{w}}) - P_v\right) & \text{for } \psi_d < \phi \leq \psi_e \\ \lambda'_{\mathrm{outwards},r}\left(N_v(\phi - \Delta\psi_{\mathrm{w}} - \pi) - P_v\right) & \text{for } \psi_e < \phi \leq \psi_f \end{cases} \tag{7.22}$$

$$f_{\mathrm{inwards},l}(\phi) = \begin{cases} -\lambda'_{\mathrm{inwards},l}\left(N_v(\phi - \pi - \Delta\psi_{\mathrm{w}}) - P_v\right) & \text{for } \psi_g < \phi \leq \psi_h \\ \lambda'_{\mathrm{inwards},l}\left(N_v(\phi - \Delta\psi_{\mathrm{w}}) - P_v\right) & \text{for } \psi_h < \phi \leq \psi_i \end{cases} \tag{7.23}$$

$$f_{\mathrm{outwards},l}(\phi) = \begin{cases} -\lambda'_{\mathrm{outwards},l}\left(N_v(\phi - \pi + \Delta\psi_{\mathrm{w}}) - P_v\right) & \text{for } \psi_j < \phi \leq \psi_l \\ \lambda'_{\mathrm{outwards},l}\left(N_v(\phi + \Delta\psi_{\mathrm{w}} - \pi) - P_v\right) & \text{for } \psi_l < \phi \leq \psi_m \end{cases} \tag{7.24}$$

[3] $H(\cdot)$ is the Heaviside step function

where the limits are presented in Appendix B. P_v reads

$$P_v = \int_0^{2\pi} H(u(\psi))\psi d\psi. \tag{7.25}$$

The robot's driving velocity is controlled by the same dynamics defined in Section 4.3.

Finally, the following hierarchy of relaxation rates ensures that the system relaxes to the stable solutions, and that the relaxation of the field is faster than the relaxation of the wall-following dynamics:

$$c_{\mathrm{r,w}},\ c_{\mathrm{l,w}} \ll\ 1/\tau_{\mathrm{w}}, \quad c_{\mathrm{r,w}},\ c_{\mathrm{l,w}} \ll c_{v,\mathrm{obs}} \tag{7.26}$$

7.6 Simulations

We illustrate in simulation how the dynamic field for wall representation evolves as the robot moves along walls with different shapes.

Following a circular wall

Figure 7.5 and Figure 7.6 show a simulation run in which the wall representation dynamics exhibits detection, continuous wall orientation estimation and hysteresis. Figure 7.5 depicts the trajectory and Figure 7.6 shows snapshots of the dynamics.

As can be seen in Figure 7.5, the robot is initially positioned in the bottom center of the arena and facing upwards ($\phi = 90$ deg). From this position no obstructions are sensed. No wall is thus detected and the robot moves forward. When the robot reaches the position indicated by A sensory information defines a wall segment. Input to the field is still weak, no positive activation arises and the field continues to code for absence of a wall (see Panel A in Figure 7.6). The robot continues moving ahead and when it arrives at position B, input to the field is sufficiently strong to trigger generation of a peak of positive activation centered over the maximal input. The field now codes the detection of a wall with an orientation of 180 deg, in the counter-clock direction (Panel B in Figure 7.6). Because obstructions are detected to the right and to the left of the robot the two behavioral modes for wall-following (Right-mode and Left-mode) contribute to the dynamics of wall-following. The resultant dynamics for the heading direction exhibits an attractor at 45 deg which pulls the robot to turn right.

As the robot moves the orientation of the sensed wall segments varies continuously. This leads to an input to the field with a moving peak. The peak of positive activation in the dynamic field tracks and follows the moving input peak. The estimated wall orientation thus varies monotonically from 180 deg (at position B) to 30 deg (at the end of the depicted trajectory, indicated by the small grey circle with a hair), in the counter-clock direction. This can be seen in the plots of the field activation (Panel B to Panel H in Figure 7.6). The wall representation field

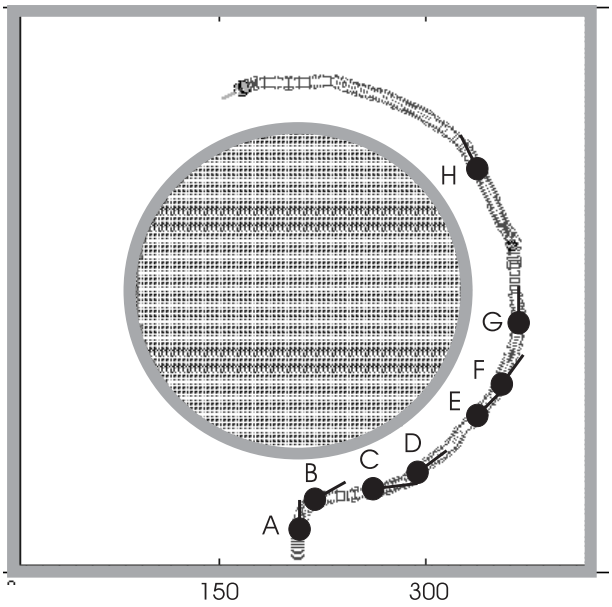

Figure 7.5: The robot (black circle with hair) moves from an initial position at the bottom center toward the circular obstacle and then it follows the contour of the circular wall at a distance of 30 cm. The dynamics at the eight points marked by the letters from A to H is depicted in Figure 7.6.

exhibits a single peak of positive activation, which moves continuously, from right to left (i.e. toward increasing values of orientation), although its input is bimodal during some periods reflecting the influence of the walls that make part of the outer square boundary that delimits the robot's workspace. For example, near point C obstructions due to the bottom wall of the boundary are sensed which in turn induce a second input peak centered over 360 deg (Panel C in Figure 7.6). Although this second input peak is stronger than the the first input peak the field keeps the representation of the "circular" wall stable. This is due to the strong interaction effects in the field that endow the field with hysteresis. A similar case happens near point G (see dynamics in Panel G in Figure 7.6). Here the second input peak arises centered over 90 deg corresponding to the orientation of the right wall belonging to the square boundary.

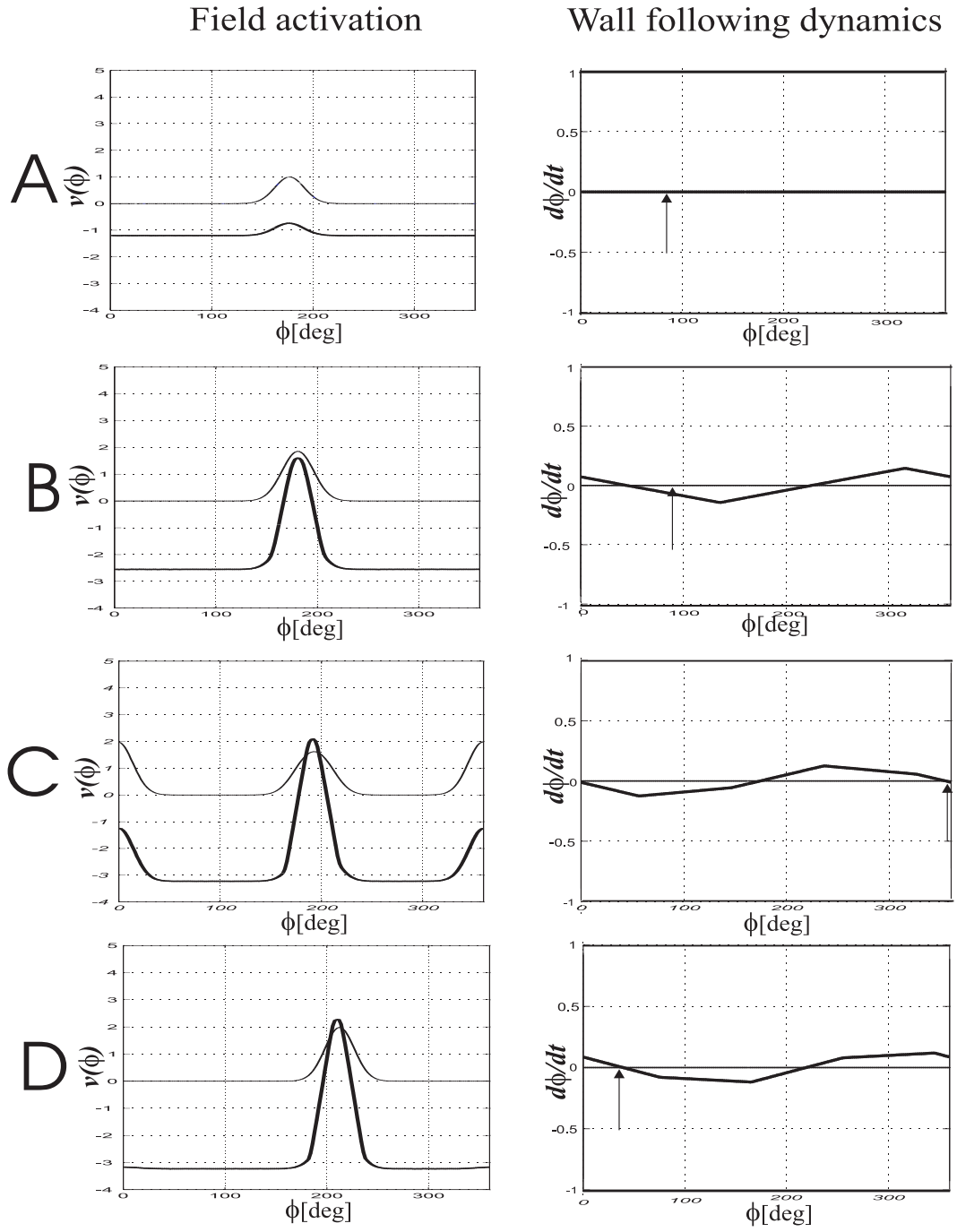

Figure 7.6: The wall representation dynamics (left column) and the wall-following dynamics (right column) for the positions signalled by the letters in Figure 7.5. Input to the field is the thin line, the activation in the field is the bold line. The vertical arrow on the plots of wall-following dynamics indicates the current orientation of the robot. Note that the system is relaxed in or very near the attractor (cont.).

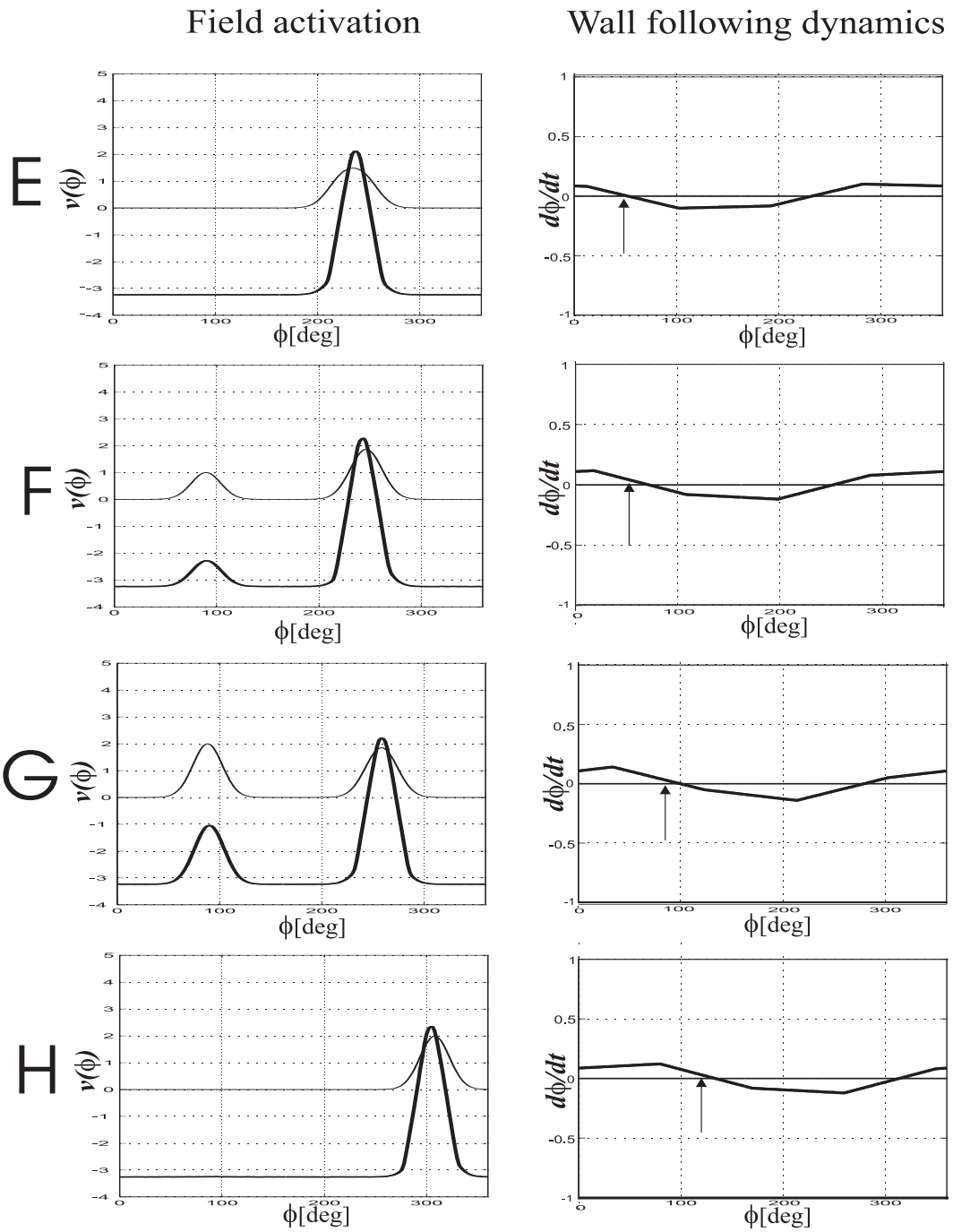

Figure 7.6: Continued.

Following a concave corner

How the field behaves when the robot is following a wall and then it encounters a concave corner is illustrated in the simulation run depicted in Figure 7.7 and Figure 7.8. The first figure depicts the trajectory while the second shows snapshots of the dynamics.

The robot initially is following the vertical wall on its right side (i.e. right boundary of the arena). The activation in the field represents this wall with an orientation near 90 deg (see Panel A in Figure 7.8). When it arrives near point B the forward distance sensor detects an obstruction which corresponds to the horizontal wall. The neighboring right sensor still detects the obstruction caused by the wall on the right. These two sensors together define a wall segment with an orientation in between the two walls orientations (i.e. between 90 deg and 180 deg). The input to the field is now bimodal. The field keeps the old wall orientation estimate (Panels B and C in Figure 7.8). The robot continues moving forward (i.e. following the vertical right wall). As the robot continues to approach the horizontal wall (top boundary of the arena) the number of wall segments with orientations closer to 180 deg augments while the number of wall segments with orientations near 90 deg decreases. In the left column of Figure 7.8 (Panels D to G) we can see how the input to the field evolves concomitantly. The field responds keeping the previous wall representation until the input peak corresponding to the horizontal wall (i.e. input peak centered over 180 deg) is sufficiently strong to dominate over the field hysteresis. This happens at point G (see dynamics on Panel G in Figure 7.8). At this point in time a sudden change takes place and the dynamic field now evolves a peak of positive activation centered over 180 deg. The field now represents a wall with an orientation of 180 deg. As a consequence the attractor of wall-following dynamics changes its value thus attracting the robot to turn left. At point H the input is again mono-modal, the input only reflects the contribution of the horizontal wall, and the robot's heading direction is relaxed near the attractor.

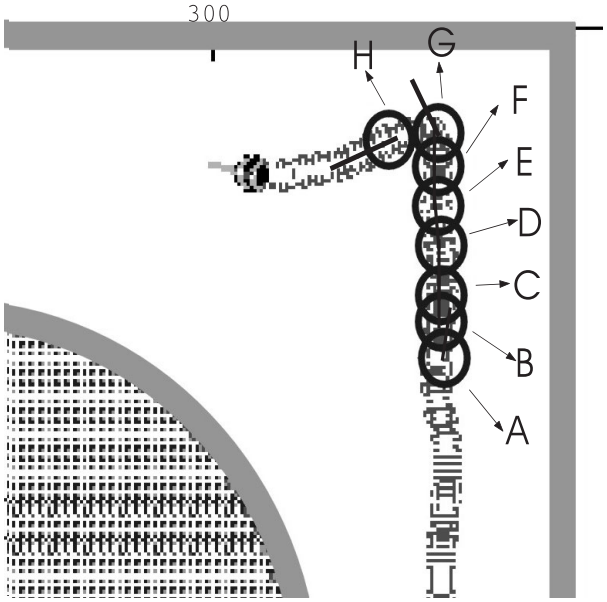

Figure 7.7: The robot (black circle with hair) is following the right wall at a distance of 30 cm. When it arrives at position B its sensors start sensing the obstructions due to the horizontal wall. The dynamics at the eight points indicated by the letters from A to H is shown in Figure 7.8.

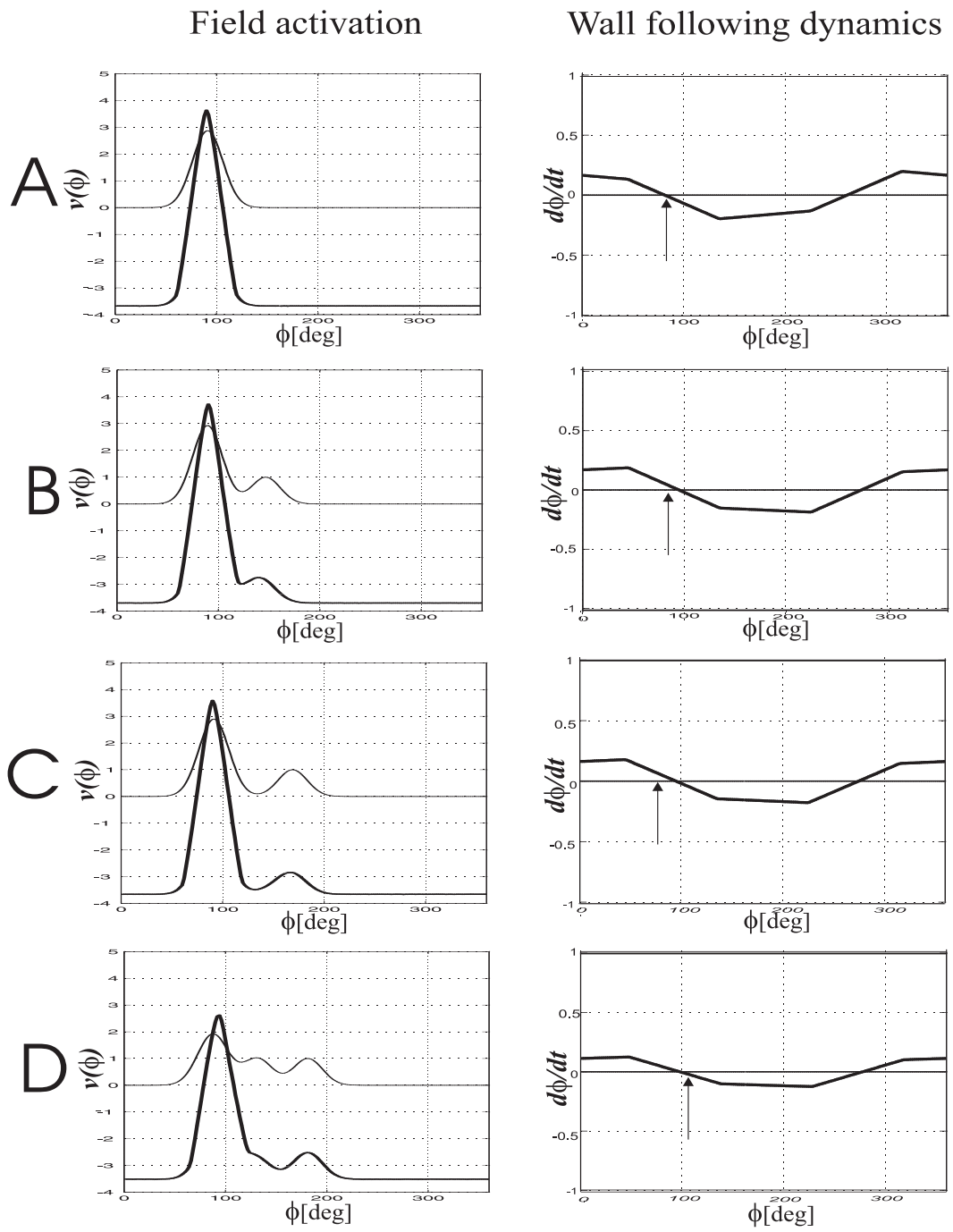

Figure 7.8: Snapshots of the wall representation dynamics (left column) and the wall-following dynamics (right column) for the positions signaled by the letters in Figure 7.7. Input to the field is the thin line, the activation in the field is the bold line. The vertical arrow on the plots of wall-following dynamics indicates the current orientation of the robot. Note that the system is relaxed in or very near the attractor (cont.).

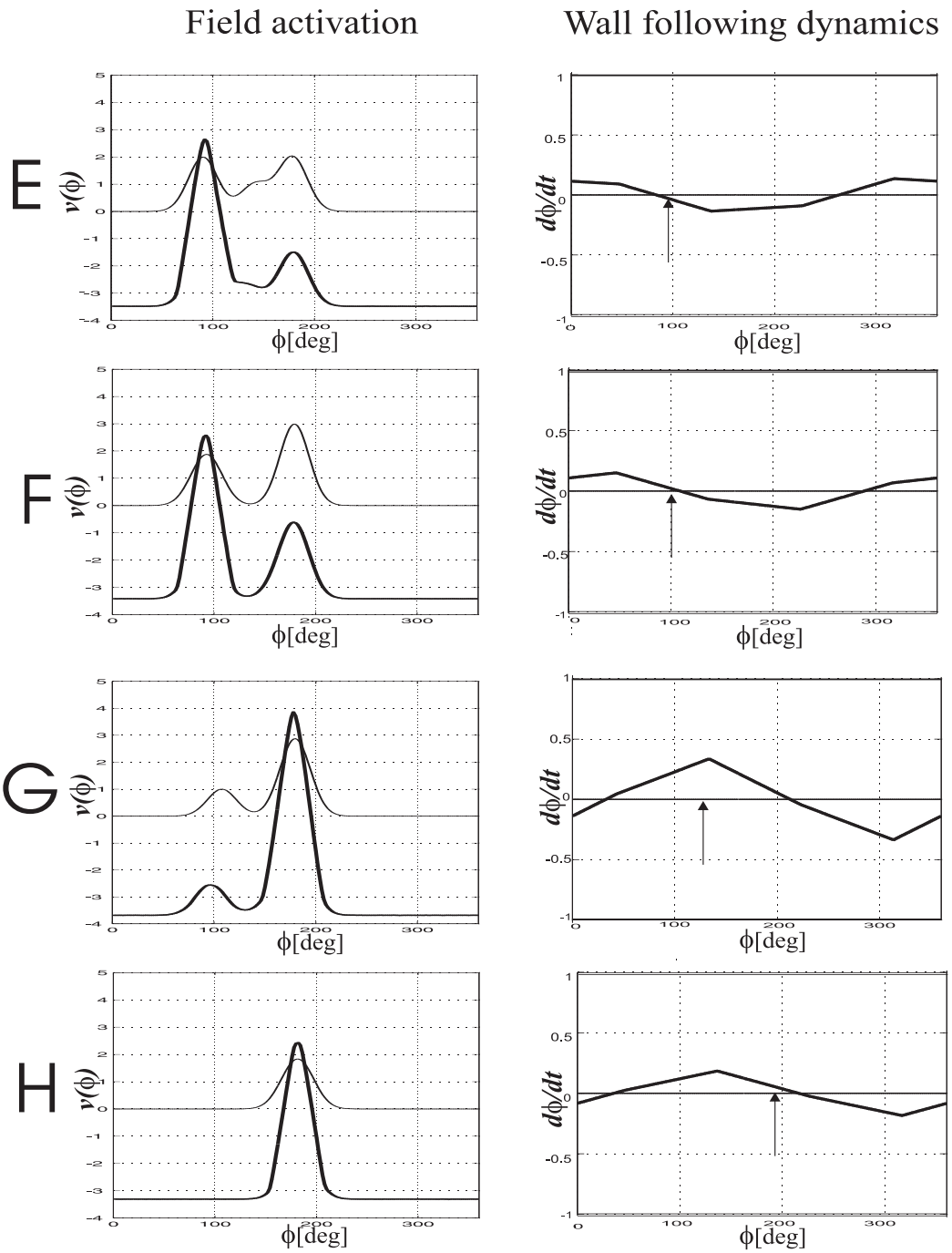

Figure 7.8: Continued.

The simulation results have demonstrated that the wall-following module is able to drive the robot along the obstacles contour when their configuration is such that they define a wall. Next, we present results obtained from the actual implementation on the vehicle platform.

7.7 Implementation on Robodyn

The dynamic architecture comprising wall representation and wall-following was implemented and evaluated on the mobile platform Robodyn. Sensory information about distance to obstructions is acquired by nine infra-red sensors or nine sonars. In the implementation, the neural field dynamics for wall representation, as well as the behavioral dynamics of wall-following and of path velocity are integrated numerically using the Euler method. The field is sampled spatially with a sampling distance of 8 deg. Sensory information is acquired once per computation cycle. The cycle time is measured and is 120 ms, when distance measures are obtained from infra-red sensors, or 150 ms, when sonars are used instead. These values delimit the time scales of the dynamics in real time units and thus determines the overall speed at which the robot's behavior evolves in the world.

7.8 Experimental results

In this section we start by presenting results that document the properties of the dynamical field for wall representation. These were obtained when the field evolved in response to actual physical stimulation induced by the presence of one or two walls, but the robot did not move. Next we show the robot following walls in various shapes.

7.8.1 Properties of the dynamic field representing walls

In the set of experiments reported in this section the robot was pointing in the 180 deg direction relative to the external reference frame and walls with different orientations were constructed (using card boxes) in its vicinity. The dynamic field for wall representation provides information about the real orientation of a wall.

Averaging

Figures 7.9 and 7.10 show that in the presence of a single wall and steady sensory information, input is mono-modal and a single localized positive peak of activation evolves in the dynamic field. In Figure 7.9 sensory information about the wall was provided by sonars while in Figure 7.10 sensory information was obtained by infra-red sensors. As one can read on these two figures the wall orientation estimates are very close to the actual values.

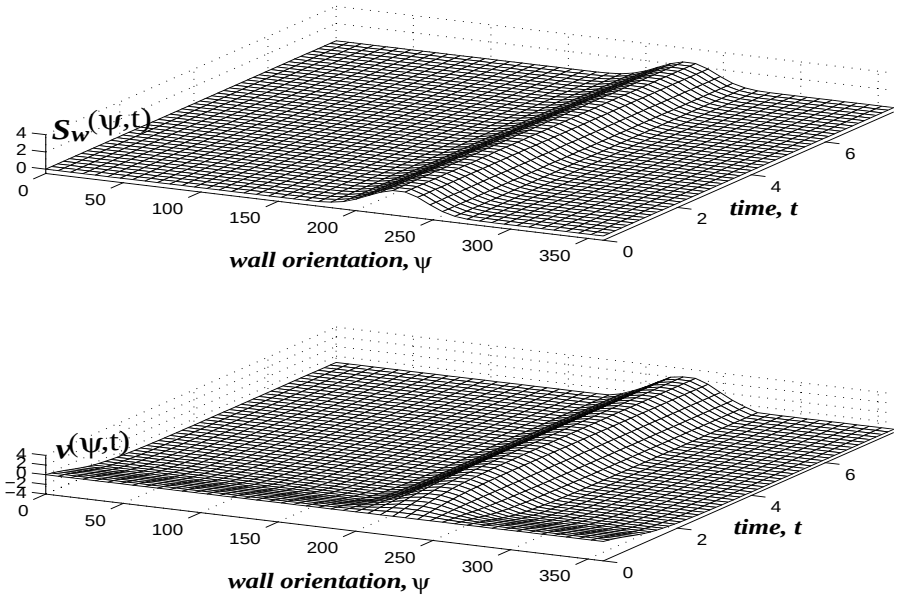

Figure 7.9: **Based on sonars**: A wall with orientation 225 deg, in the counter-clock direction and with respect to the world axis, was built to the right side of the robot, 100 cm away. Top: sensory information leads to a mono-modal input distribution. Bottom: The field activation relaxes to a localized-peak centered over the maximal input. The estimated wall orientation is 226 deg.

Repeating these experiments for a number of different orientations of the wall we evaluate the capacity of the the dynamic field to perform estimation based on sonars and infra-red sensors. Results are presented in Figure 7.11. The results show that even though wall orientation estimates based on sonars are accurate, this type of sensors exhibits a serious drawback. For some wall orientations specular reflections occur. For this reason, no obstructions are detected and thus no wall segments are defined by the sensory information. The input to the field is null everywhere or weak and the field codes therefore absence of wall. This happens when the wall diverges from the forward direction of the robot with an angle of 45 deg or the wall is perpendicular to the robot's heading direction. These problems can be avoided by choosing a value for the desired distance to the wall inside the range of detection of the infra-red sensors. These are not so accurate but they are certainly more reliable.

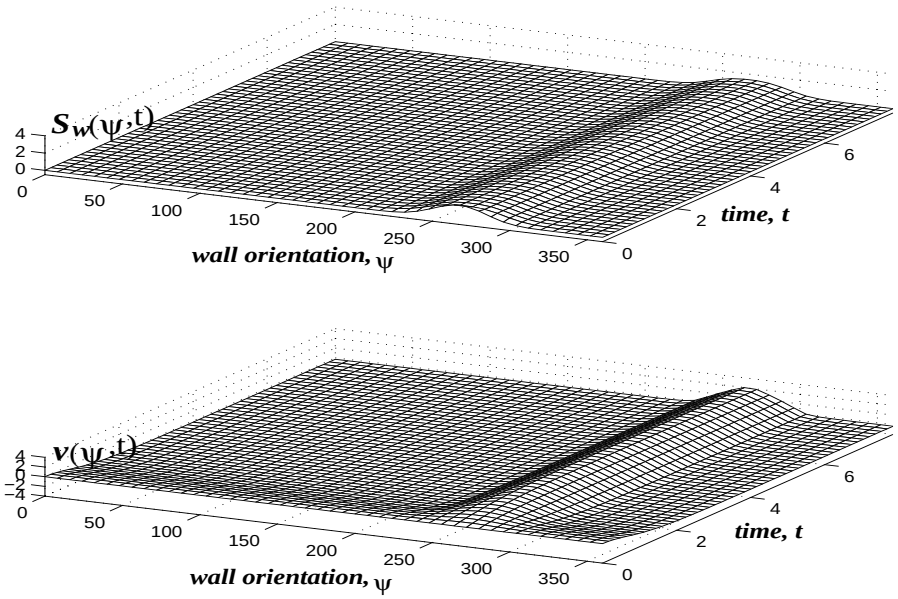

Figure 7.10: **Based on Infra-red**: A wall perpendicular (orientation 270 deg in counter-clock direction) to the robot heading direction was built at a distance 35 cm. Top: Sensory information is less convergent than in Figure 7.9 which is reflected by an input peak with smaller amplitude. Sensory information leads to a mono-modal input distribution. Bottom: The field activation relaxes to a localized-peak centered over the maximum of the input. The estimated wall orientation is 267 deg.

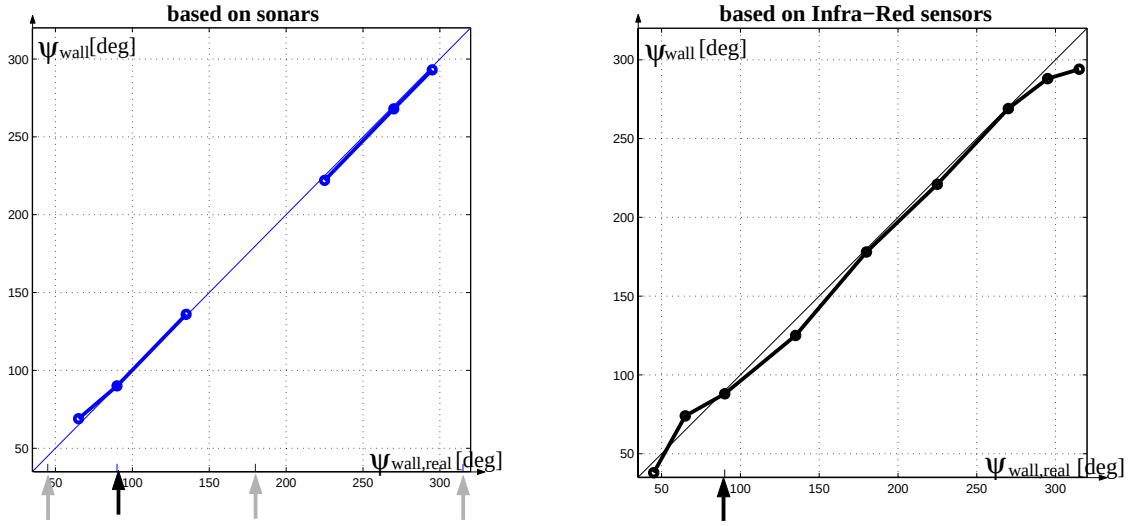

Figure 7.11: The experiments illustrated in Figures 7.9 and 7.10 were repeated for a number of different wall orientations. These orientations can be read on the abscissas. Here the vehicle was heading in the direction of 90 deg. The black arrow in both plots indicates the robot's heading direction. On ordinates we can read the corresponding estimated wall orientation. Left: Sensory information provided by sonars. There are a number of orientations for which no wall is detected. The arrows with grey color signal these directions. Right: Wall orientation estimates based on infra-red sensors.

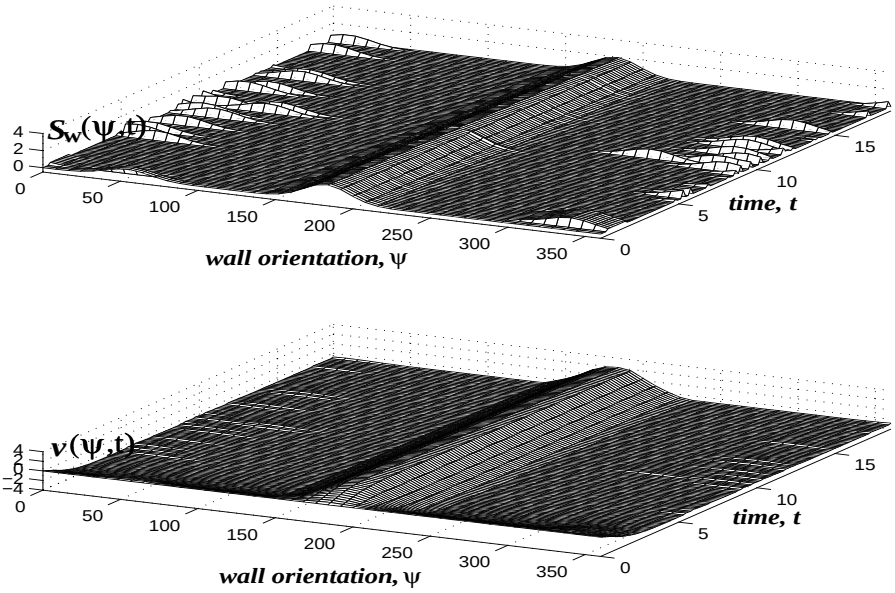

Figure 7.12: Top: Sensory input to the field has a stable peak centered over 180 deg but "corrupted" with outliers. Bottom: The field evolves and stabilizes a peak centered over 180 deg. Through inhibition the contribution of the outliers for the wall orientation estimation is annihilated.

Field behavior in the presence of noisy sensory data

In Figures 7.12 and 7.13 we illustrate how the dynamic field for wall representation behaves in presence of noisy sensory information.

In a first experiment, a wall was built parallel to the robot (orientation 180 deg) on its right side at a distance 100 cm. The distance measures were based on sonars. On the left side of the robot there were moving obstacles. Figure 7.12 shows that the estimate, ψ_{wall} (= 180 deg), computed by the dynamic field is robust against wall orientation estimates which are far away from the actual selected estimate because they are weighted, through inhibition, such that they do not contribute to the resultant pattern of positive activation. As a consequence these measures are effectively discarded. This result shows therefore that the field behaves as a robust estimator for wall orientation.

Figure 7.13 depicts how the field behaves when the orientations of the segments, originated from the same wall, vary due to time changing sensory information. A wall was constructed on the right side of the robot with an orientation of 220 deg and at a distance of 40 cm from the robot. Distance measures were provided by the infra-red sensors. The environment is static but sensory information changed in time though. Input distribution to the field is mono-modal with a jitter peak centered over either 176 deg or 220 deg (which correspond to the averages of the orientations of the sensed wall segments). The field behaves evolving a positive peak of activation, centered over 213 deg, and stabilizes it against the jumping input peak. The error,

7 deg, is relatively small and does not cause problems because the wall-following dynamics also controls the distance to the wall.

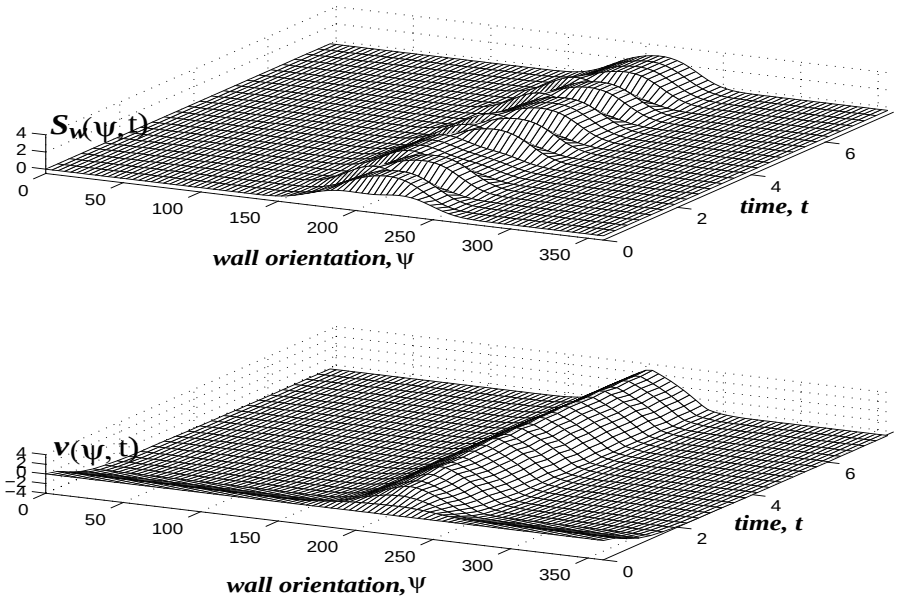

Figure 7.13: Top: Sensory input to the field exhibits a peak whose center oscillates between 176 deg and 220 deg. Bottom: The field evolves and stabilizes a peak centered over 213 deg. The local excitatory interactions within the field stabilize the peak of activation against the jumping input peak.

Wall selection

The ability of the field to select one of multiple walls is illustrated in Figure 7.14. Two walls are constructed to the right and to the left of the robot with orientations 160 deg and 20 deg, respectively. Input to the field is bimodal under this condition. The interactions within the field enable decision making. The field evolves a single localized peak of positive activation. Results demonstrate that the field is bistable. In a first run the field selects the wall to the right and gives an estimate of 156 deg. In a second run the field selects the wall to the left giving an estimate of 17 deg for the orientation of this wall. In both cases the estimates are very close to the real values.

Decision making in the presence of noisy and time varying sensory information is depicted in Figure 7.15. The robot was faced with two walls. One to the right side with orientation 220 deg, the other to the left with orientation 330 deg. Henceforth, the input to the field is bimodal. For this scenario the sensory information is time varying even if the environment is static. Despite these conditions the dynamic field is able to generate and stabilize a single peak of positive activation. This is because it is endowed with cooperative interactions. The right wall is selected and the estimate

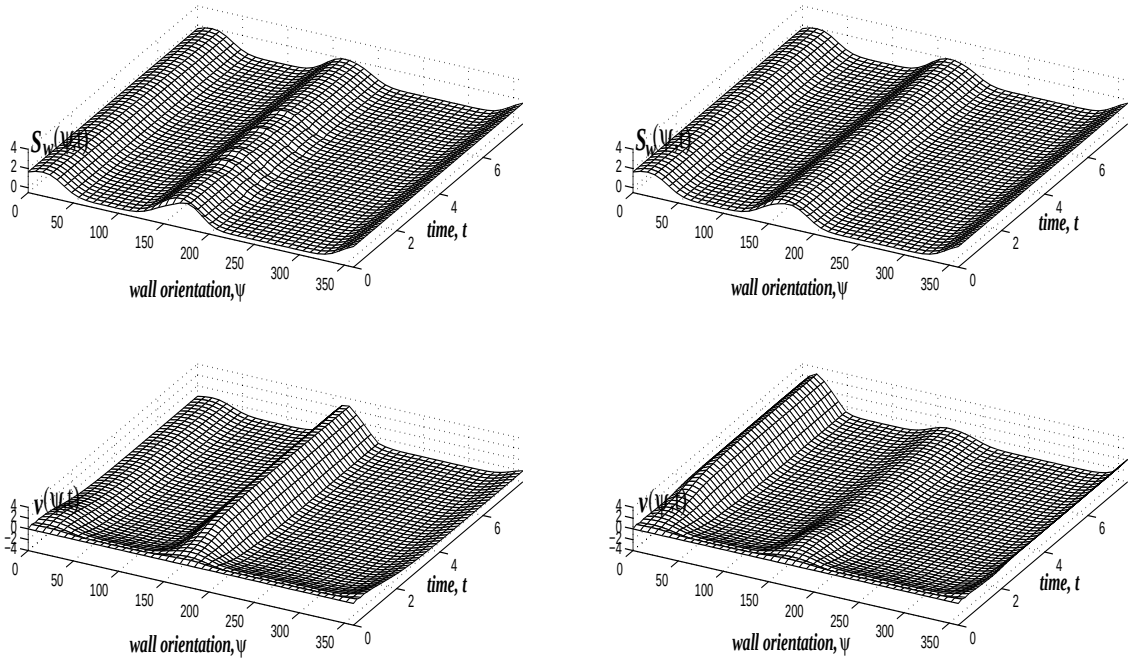

Figure 7.14: This figure shows the ability of the wall representation system to perform wall selection and proves that the dynamic field is bistable. Input distribution is bimodal (top row). Competition takes place and as a result the field makes a decision. The field evolves a single localized peak of positive activation centered at one of the input peaks. Bottom left: The field evolves a peak of positive activation centered over 156 deg. Thus the right wall is represent on the field. Bottom right: Here the left wall is selected by the field dynamics. This wall is represented by peak of positive activation centered over 17 deg.

for its orientation is 316 deg. The error between the real wall orientation and the estimate is due to the influence of the second wall. This error is not problematic since the control of the distance to the wall helps to compensate as we will show in the next section.

7.8.2 Following walls with different shapes

Figures 7.16 to 7.19 show sample trajectories of the robot as recorded by the dead-reckoned robot position for different scenarios. The initial heading direction of the robot is $\phi = 180$ deg. The times courses of the wall orientation estimate and the robot's heading direction are also depicted. The desired distance to the wall is 35 cm.

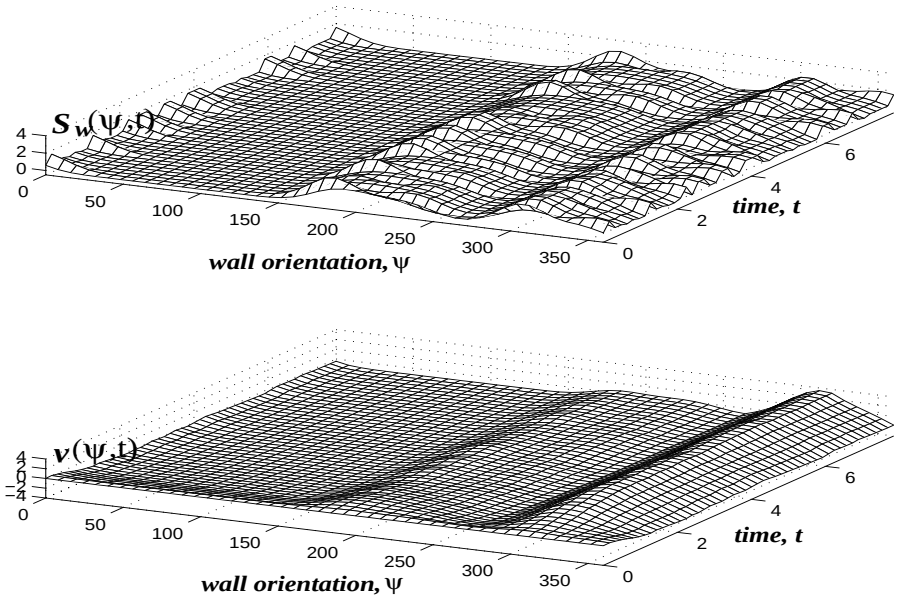

Figure 7.15: Here is illustrated that the dynamic field for wall representation is able to make and stabilize a decision in the presence of a bimodal and very noisy input. Top: Input induced by two walls with orientations 220 deg (right wall) and 330 deg (left wall). Bottom: The field evolves and stabilizes a peak of positive activation centered over the maximal input. The peak is centered over 316 deg which corresponds to the selection of the wall to the left of the robot.

Scenario with a planar wall

Figure 7.16 illustrates the robot's behavior in the simplest scenario testing the wall-following behavior. The wall is planar with orientation 215 deg in the counter-clock direction (or $215 - 180 = 135$ deg clockwise). Initially, the robot is placed at a distance to the wall smaller than the desired distance and heading in the 180 deg direction. The robot moves along a smooth and initially curved path in order to orient itself parallel to the wall and to steer simultaneously at the desired distance from the wall.

Scenario with a concave corner

Figure 7.17 shows the robot's behavior in slightly more complicated scenario. The robot faces a concave corner. Initially, the robot is placed closer to the wall than the desired distance. It steers as to follow the contour of the concave corner at the desired distance.

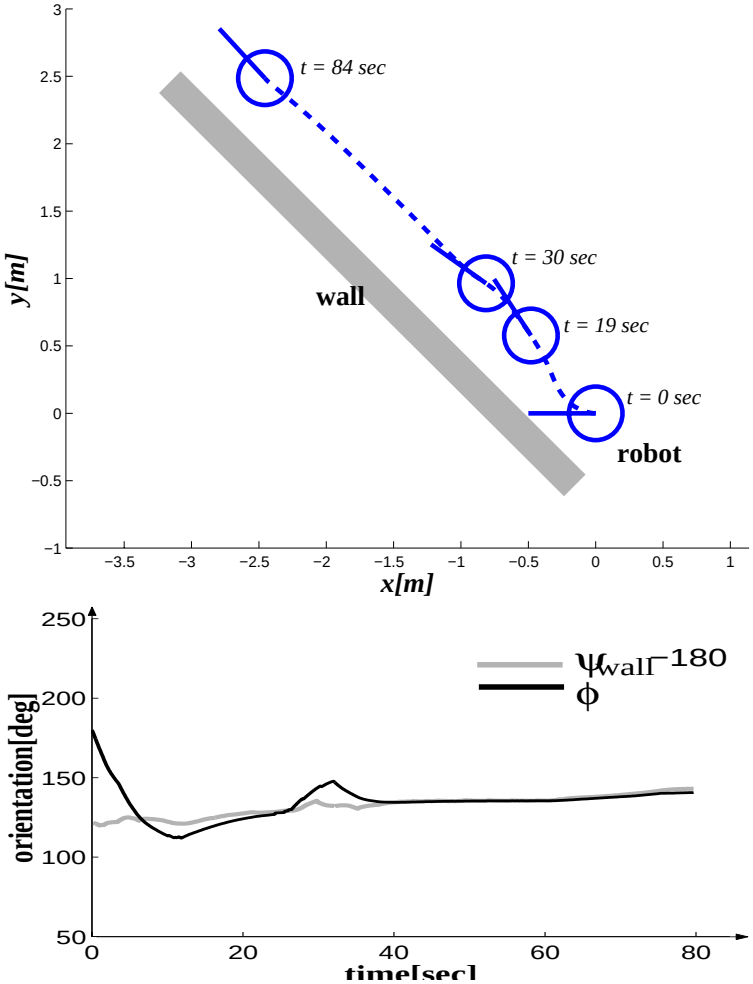

Figure 7.16: Top: The wall has an orientation of approximately 215 deg in the counter-clock direction (135 deg in the clockwise direction). Initially, the robot is placed at a distance to the wall smaller than the desired distance and heading in the 180 deg direction. The heading direction dynamics steers the robot to follow the wall based on the estimated wall orientation and with the constraint of imposing a desired distance. Bottom: The plot shows the time course on the heading direction and the time course of the wall orientation estimate in the clockwise direction, i.e. $\psi_{\text{wall}} - 180$ deg, because it makes the interpretation easier when the wall is to the left. The estimate for the wall orientation ($t = 0$ sec) is 123 deg. The error between the estimate and the actual value decreases as the robot steers to follow the wall. When the robot is at the desired distance ($t \approx 40$ sec) the value $\psi_{\text{wall}} - 180$ deg directly specifies the attractor for the heading direction dynamics.

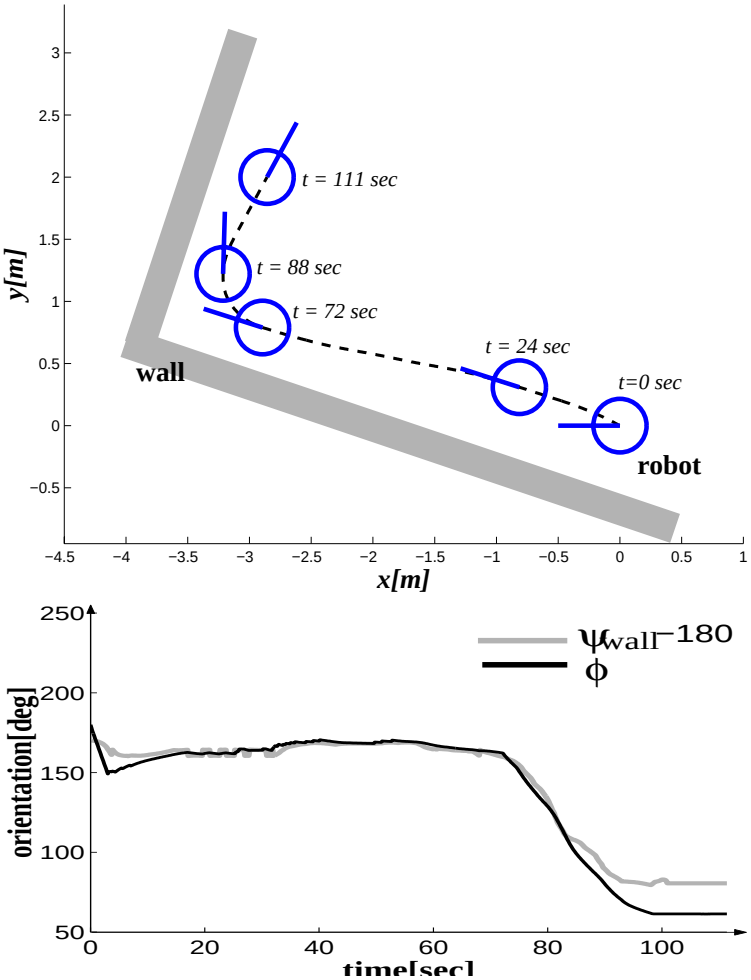

Figure 7.17: Top: Robot's trajectory as it steers to follow the contour of a concave corner at the desired distance. Bottom: Time courses of the heading direction and wall orientation estimate (plotted in clockwise direction, i.e. $\psi_{\text{wall}} - 180$ deg). Note that the difference between the estimated values for the orientation of the two perpendicular walls is 85 deg which is close to the actual value (90 deg).

Scenario with a circular wall

In Figure 7.18 we depict the robot's trajectory for a circular wall. Initially, the robot is placed at the desired distance to the wall. The robot successfully circumnavigates the circle.

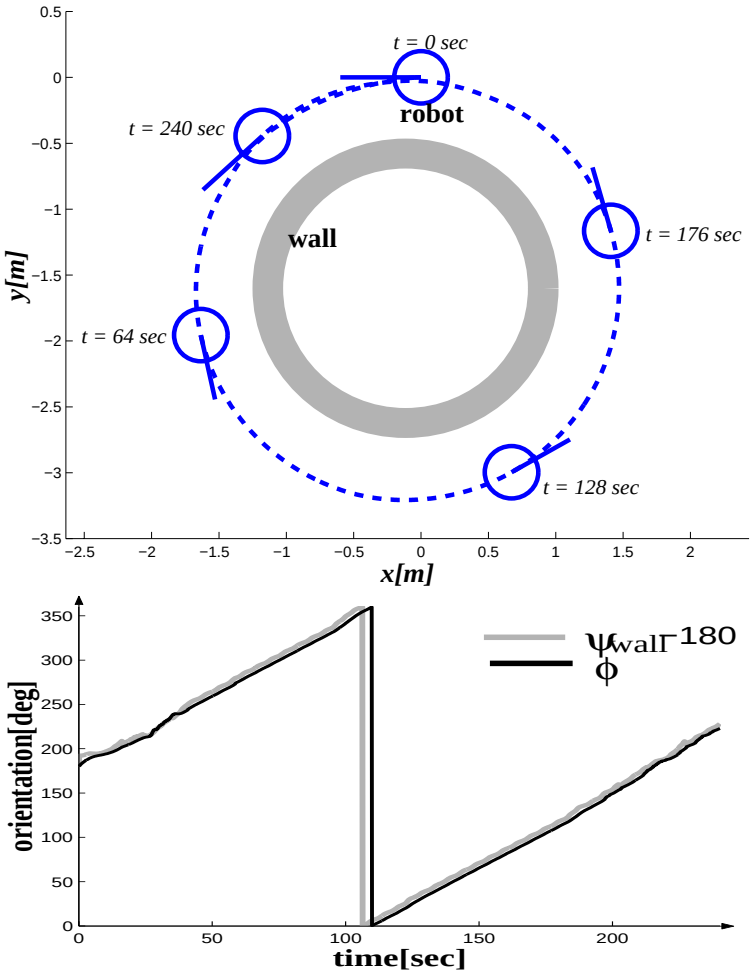

Figure 7.18: Top: Initially, the robot is positioned already at the desired distance to the wall at the position indicated by $t = 0$ sec. The robot makes a complete circumnavigation around the circular wall and is stopped at position marked by $t = 240$ sec. Bottom: the plot shows the time courses of the wall orientation estimate and heading direction. To make the interpretation easier the wall orientation estimate is here plotted in the clockwise direction (i.e $\psi_{\text{wall}} - 180$ deg). Because the robot was placed already at the desired distance the wall orientation estimate, $\psi_{\text{wall}} - 180$ deg, defines directly the attractor for the heading direction dynamics. This value varies monotonically from 180 deg at time $t = 0$ sec to 360 deg (= 0 deg) at time $t \approx 105$ sec, and then from 0 deg up to 245 deg at time $t = 240$ sec. As one can see the heading direction follows the moving attractor very closely, i.e. the system is always in a stable state.

Scenario with two walls

Figure 7.19 shows wall selection. The robot was placed at the middle distance between the two walls. Wall segments from both walls are sensed. The robot selects the wall to its left. First the robot steers to approach the wall and then follows the contour of the selected wall at the desired distance. The path is smooth.

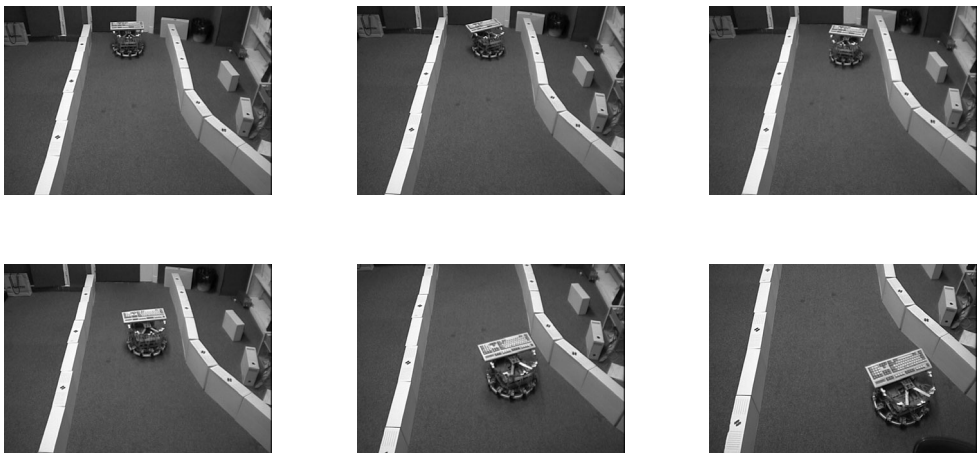

Figure 7.19: One sequence of video images show the robot behavior in the presence of two walls. Time increases first along the first row then along the second row. Initially, the robot located exactly in between the two walls. The robot selects the wall to its left and follows a smooth path along the wall contour.

7.9 Conclusion

In this chapter we have demonstrated how a dynamic field can provide a robotic vehicle with a sub-symbolic representation of walls based on low-level (i.e. noisy and low resolution) distance sensors. This representation enabled the vehicle to exhibit some basic cognitive abilities such as detecting a wall, robustness when confronted with noisy sensory information and to make and stabilize decisions as to which of two walls to follow. A behavioral dynamics of heading direction that enables a vehicle to follow a wall at a desired distance from the wall was proposed. Results have shown the ability to follow walls with different shapes. One limitation of our system is that when sensory information is based on sonars, walls with certain orientations are not detected (they are successfully avoided as obstacles, however, as we will explain in the next chapter). This is due to specular reflexions. Such problem can be prevented however, by choosing a distance from the wall that is inside the detection range of infra-red sensors.

The next chapter presents the integration of this wall-following dynamic module with phono-taxis and obstacle avoidance.

Chapter 8

Complete dynamic architecture

In this chapter we present the integration of the wall-following module with phono-taxis and obstacle avoidance. The complete dynamic architecture including sub-symbolic representations of sound targets and walls, control of heading direction and driving velocity is implemented on a vehicle platform. Simulation and experimental results that demonstrate the stability of the complete architecture are shown.

8.1 Integration of wall-following with obstacle avoidance and phono-taxis

Obstacle avoidance and phono-taxis have also been designed at the level of heading direction (see Chapter 6 and Bicho, Mallet and Schöner, 1999a). Thus, the integration of these two behaviors with wall-following may be obtained by adding the corresponding contributions to the vector field of the heading direction dynamics. However, when the robot is following a wall it should not avoid it simultaneously. Therefore, we make the strength of the obstacle contributions, F_{obs}, dependent on the total positive activation in the dynamic field for wall representation, such that, the larger the activation in this field the weaker the contributions of the obstacles to the heading direction dynamics. The complete vector field for the heading direction is

$$\frac{d\phi}{dt} = \mu_{\text{obs}} F_{\text{obs}}(\phi) + f_{\text{tar}}(\phi) + F_{\text{wall}}(\phi) + f_{\text{stoch}} \tag{8.1}$$

with

$$\mu_{\text{obs}} = \frac{\pi - 2\arctan\left[10\int_0^{2\pi} H(v(\psi))d\psi\right]}{\pi} \tag{8.2}$$

where $H(\cdot)$ is the Heaviside step function. The function μ_{obs} is one when no wall is detected, thus the obstacle avoidance dynamics fully contributes to the vector field. It is asymptotically equal to zero when a peak of positive activation is present in the

field for wall representation. In this situation the obstacle avoidance dynamics is essentially turned off and consequently the heading direction dynamics is governed by the wall and target contributions.

Some of the contributions in Equation 8.1 have limited range. The sum of all contributions leads therefore to a non-linear dynamical system, which may exhibit multiple attractors and repellers. These appear typically in a few number (cf. Section 8.2). The stochastic force, f_{stoch}, guarantees escape from unstable fixed points. By design we make the system to be in or near one of the attractors at all times. This is accomplished by the correct choice of parameter values and on the requirement of controlling the maximum rate of shift of the attractor solutions. As we have seen, this is possible by controlling the vehicle's path velocity by means of the dynamics presented in Section 4.3.

Finally, the following hierarchy of relaxation rates ensures that the system relaxes to the attractor solutions as they change due to varying sensory information and that obstacle avoidance and wall-following have precedence over phono-taxis:

$$\lambda_{\text{tar}} \ll c_{v,\text{tar}}, \quad \lambda_{\text{obs}} \ll c_{v,\text{obs}}, \quad \lambda_{\text{tar}} \ll \lambda_{\text{obs}}, \quad \lambda_{\text{tar}} \ll \lambda_{\text{wall}}, \quad \tau_{\text{w}} \ll 1/\lambda_{\text{wall}} \tag{8.3}$$

8.2 Simulation of the complete architecture

Figure 8.1 shows a simulation run of the complete system which demonstrates the smooth behavior consistent with all imposed constraints.

The sound sensors were modeled by assuming that within an angular range of 60 deg[1], sound intensity falls off exponentially with the distance between the sound sensor and the sound target. Distance sensors where simulated through a ray-tracing type algorithm. All dynamical equations and the dynamic fields were integrated with a forward Euler method with fixed time step. Sensory information was generated once per each Euler cycle.

Initially, the robot is at position marked "1" and the target lies at position marked "2". From position "1" to position "2" the robot is steered by wall-following and target acquisition. A snapshot of the dynamics at point A is illustrated in panel A on Figure 8.2. Once the target is reached, its position is shifted to position marked "3" to force the robot to travel the cluttered region between positions "2" and "3". Although sometimes wall segments are sensed the input to the wall representation field is not sufficient to trigger a peak of positive activation. The field thus codes absence of wall and the obstacle avoidance behavior steers the robot (see panel B in Figure 8.2). From position marked "3" to "4" the robot is driven again by the wall-following and target acquisition. Panel C in Figure 8.2 shows the dynamics at point C.

[1]Tests with the microphones performed in our lab have demonstrated that the angular range of the microphones is 60 deg.

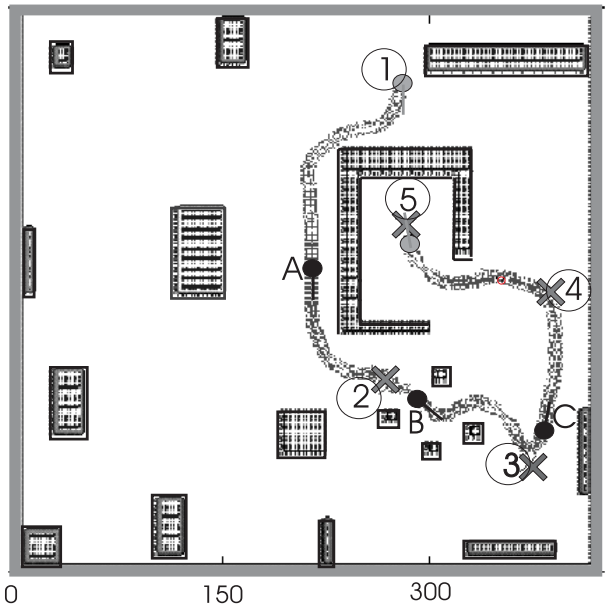

Figure 8.1: This figure shows the trajectory generated by the complete behavioral dynamics implemented in simulation. The target is indicated by a cross. Initially, the robot is at position marked "1" and the target lies at position marked "2". Once the target is reached, its position is shifted to position marked "3", and so on, until position marked "5" is reached. The wall representation dynamics and the heading direction dynamics at points A, B and C are presented in Figure 8.2.

8.3 Implementation on Robodyn

The complete architecture was implemented and evaluated on the mobile platform Robodyn. Sensory information about distance to obstructions is acquired by nine IR active sensors. Sensory information about sound targets is obtained by the five microphones of the cardiod type. In the implementation, the neural fields dynamics for target representation and wall representation, as well as the dynamics of heading direction and of path velocity are integrated numerically using the Euler method. Sensory information is acquired once per each computation cycle. The two fields are sampled spatially with a sampling distance of 8 deg. Sensory information (sound intensity and distance measures) is acquired once per computation cycle. The cycle time is measured and is 150 ms. This value delimits the time scales of the dynamics in real time units and therefore determines the overall speed at which the overt robot's behavior evolves.

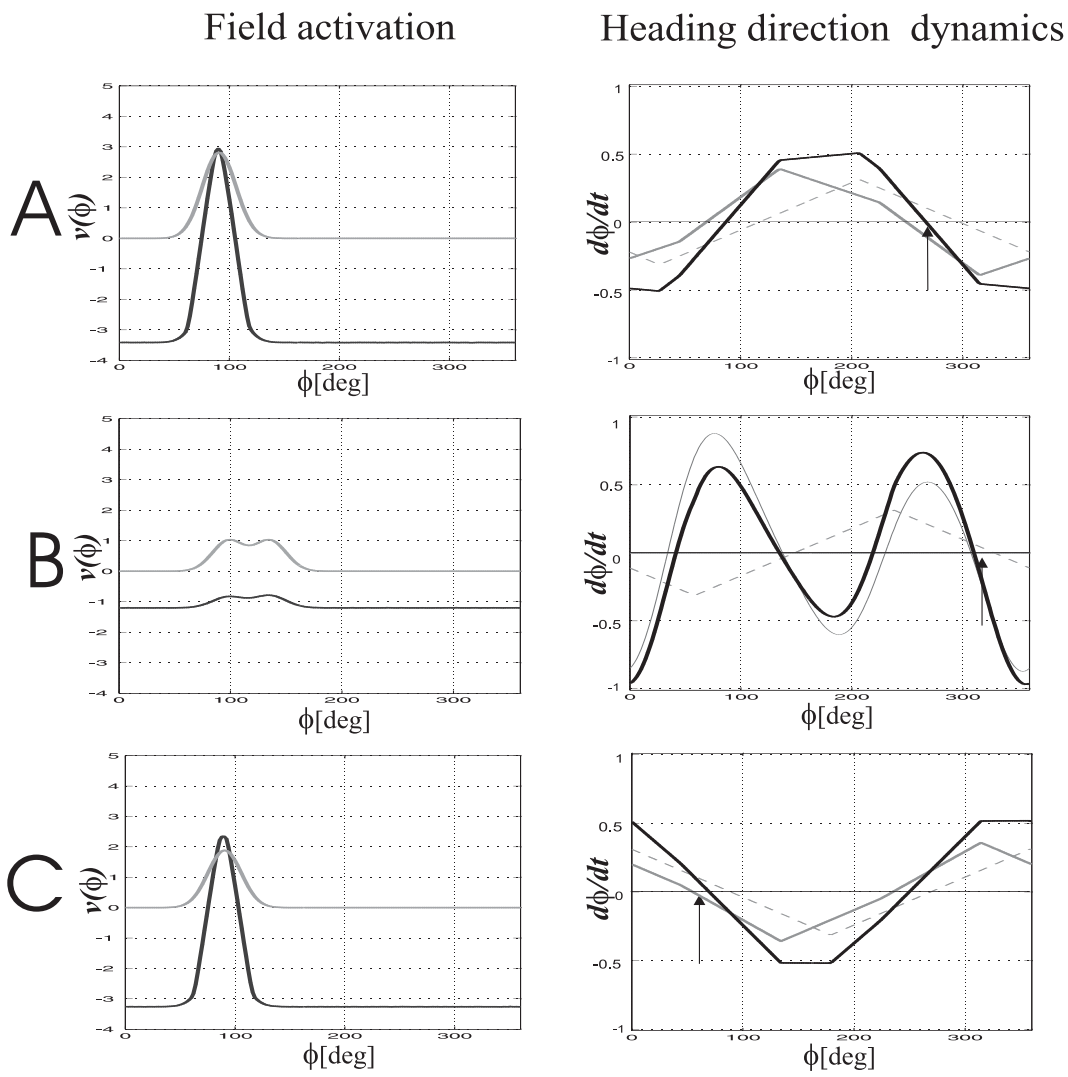

Figure 8.2: Snapshots of the wall representation dynamics (left column) and the heading direction dynamics comprising all constraints (right column) for the positions signaled by the letters in Figure 8.1. Input to the field is the line with grey color, the activation in the field is the black line. The wall-following contribution is indicated by the piecewise solid grey line. The target acquisition contribution is represented by the piecewise traced line with grey color. The obstacle contribution is the dotted thin line. The resultant dynamics is indicated by the bold black line. The vertical arrow on the plots of heading dynamics indicates the current orientation of the robot. Note that the system is relaxed in or very near the attractor.

8.4 Experimental results

In Figure 8.3 we illustrate the global behavior in a complex scenario. A sound source (i.e. the target) consisting of a loudspeaker emitting CD music (the same used in the experiments reported in Subsection 6.7.2) is placed inside one of the offices of

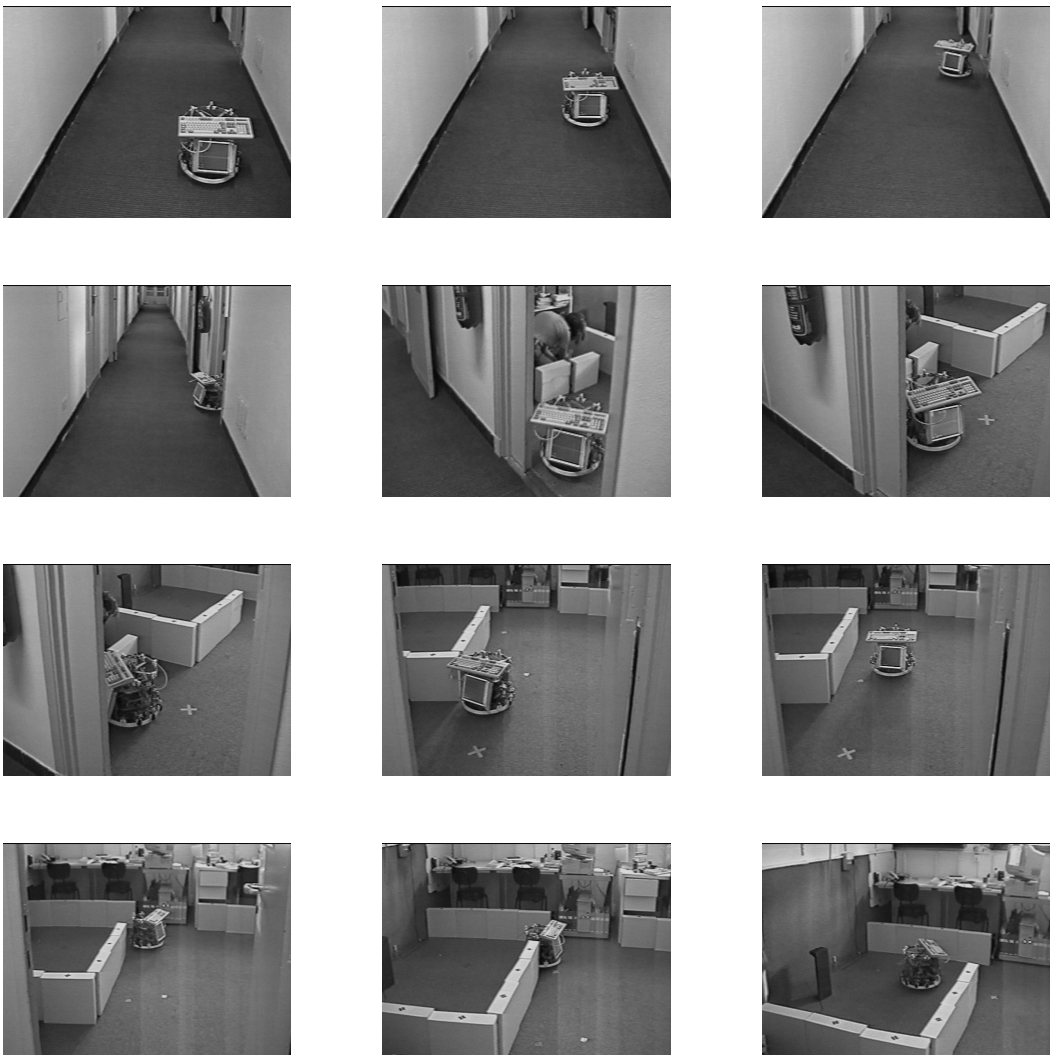

Figure 8.3: This figure shows a complex scenario challenging the complete dynamic architecture. Time increases from left to right on each row and from top to bottom. Initially, the robot is positioned in the corridor. A sound source lies inside one of the offices. The robot follows the wall to the right (frame 1 to frame 3). When it arrives near the office door the phono-taxis behavior, helped by obstacle avoidance, makes the robot to enter into the room (frame 4). From frame 5 to frame 7 the robot avoids the obstacles on its left side. Then the robot follows the wall to its left (frames 8 and 9). At the end of the this wall the robot finds the entrance to the place where the target is "hidden".

our lab. Initially, the robot is located in the corridor. The robot follows the wall to its right, at a distance 30 cm from the wall, until it arrives near the office door. Its target representation system provides an approximate representation of the sound source. The robot moves through the door helped by obstacle avoidance and target acquisition. Inside the office, the robot first avoids the obstacles on the left side and then it follows the wall to its left. The target is inside a square arena constructed

with boxes. The robot arrives at the entrance, it enters into the squared arena and finally finds the sound source.

8.5 Conclusion

We have demonstrated that a complex dynamic architecture can be implemented on a robotic vehicle with modest computation power and very low-level sensors. Specifically, the architecture integrates two dynamic fields for target and wall representation respectively, control of heading direction and path velocity based on constraints of obstacle avoidance, target acquisition, following walls and the requirement to stabilize the maximum rate of shift of the attractor solutions. Results demonstrate that the overt behavior is smooth and stable.

Chapter 9

Discussion

9.1 Summary

Dynamical systems theory was used as a theoretical language and tool to design, specify, analyze, simulate and implement behavior-based control architectures. The architectures were fully formulated in terms of dynamics and implemented on computationally modest vehicle platforms based on very low-level sensory information. The main ideas and achievements are the following:

1. **Attractor dynamics can be used to control motion based on low-level sensors**

   (a) Robot action can be generated in the manner of control systems, by assigning values to planning (i.e. behavioral) variables continuously in time. A process that can be formalized through dynamical systems. It was shown how an intelligent choice of such planning variables makes it possible to generate flexible behavior from asymptotically stable states (attractors) of such dynamical systems.

   (b) Generation of behavior is an intrinsically non-linear problem. Behavioral situations exist, in which a minor change in the configuration or sensory situation must elicit a qualitative change in the behavior. This is a simple form of decision making. This non-linearity poses a problem for the design of dynamical systems, as no general theory exists for such systems.

   (c) Bifurcation theory is one branch of the theory of non-linear dynamical systems that is very structured by powerful theorems. Local bifurcation theory helps to describe how attractors and repellers of dynamical systems may annihilate by collision or emerge through splitting at critical parameter values. Because the approach in this thesis made use of attractor solutions only, local bifurcation theory may be employed to design the dynamical systems such that an appropriate bifurcation is obtained when a behavioral decision must be made. Additional benefits are the

contribution of the behavioral dynamics to the overall control theoretic stability of the autonomous robot even when decision making takes place.

(d) Sensory information enters into the dynamical system by defining attractive or repulsive values of the planning variables, determining the strength of attraction or repulsion as well as the range of values over which theses forces act. Although the contribution of each individual sensor to the dynamical system is not invariant under change of the values of the planning variables, and neither necessarily generates the right postulated functional form nor necessarily generates the right attractors and repellers, the superposition of all contributions of all sensors does exhibit that invariance and thus generates the designed dynamics. This is ultimately true because the environment is invariant, for instance, under rotation of the vehicles on the spot, and the summed contributions sample that environment.

(e) We made a detailed presentation of how individual motion behaviors can be designed, how they can be integrated and moreover how they can be implemented on autonomous vehicles equipped with low-levels sensors like infra-red sensors, sonars, photo-resistors or microphones.

(f) Vehicle motion toward targets while simultaneously avoiding obstacles and/or following walls was generated from attractors of dynamical systems of heading direction and path velocity.

(g) Vehicle motion toward targets and avoidance of perceived obstructions also was generated from attractors of dynamical systems of angular and path velocities.

2. **Dynamic fields can endow robots with sub-symbolic representations based on low-level sensory information**

(a) We showed how the ideas of attractor dynamics employed to control the motion of the robots can be extended to the level of representation by using dynamic fields to interpolate sensory information.

(b) We have demonstrated how dynamic fields can provide robotic systems with sub-symbolic representations that rely on low-level sensory information. These representations enabled a robotic vehicle to exhibit the simplest forms of cognitive abilities. For instance:

- A dynamic field model for target representation based on low-level sound sensors was built. This permitted the robot to exhibit skills such as detecting targets only if sensory information was consistent, estimating direction to a target through interpolation, deciding which target to track when multiple targets were presented and stabilization of such decision, maintaining targets in short-term memory during momentary absence of pertinent sensory information, and deleting a

memory item after a characteristic delay to clear the memory from obsolete information.

- A dynamic field model for wall representation based on low-level distance sensors (infra-red sensors and sonars) was also built that supported wall detection, robust wall orientation estimation and wall selection.

3. **Representations can be integrated with stable action planning and control**

   (a) The pattern of activation in a dynamic field shapes continuously in time the vector field of the dynamics of the behavior to which it is dedicated:

      i. The value over which a peak of positive activation is centered defines an attractive value of the planning variable used to design the behavioral dynamics.

      ii. The amount of total positive activation in the field determines the attraction strength of that force.

      iii. Because the field dynamics is invariant under rotations of the vehicle on the spot so is the dynamics that brings about the motion of the vehicle.

   (b) The amount of positive activation in a dynamic field may also inhibit the contribution of other behaviors to the complete behavioral dynamics.

   (c) The time scale of the field dynamics is set much faster than that of the planning variables so that the field has typically relaxed to a stable pattern on the time scale on which the movement plans of the robot evolve. The resulting behavior is therefore stable.

   (d) Two examples are:

      - The dynamic field for target representation specifies the particular form of the target acquisition dynamics.
      - Analogously, the dynamic field for wall representation specifies the wall-following dynamics.
      - The dynamic field for wall representation inhibits the contribution of obstacle avoidance to the planning dynamics when a wall is detected.

4. **Navigation in non-engineered environments**

   (a) The smooth overt behavior generated when the systems are set to work in non-structured environments was documented.

   (b) The implementation of the dynamic field for target representation on a small autonomous vehicle enabled it to find sound sources while avoiding obstacles. Memory helped to keep it moving toward the target during

the periods when sensory information was not available. Decision making enabled the vehicle to track only one sound source. Hysteresis in the field dynamics enabled the vehicle to continue moving toward the selected sound target even when it approach a second sound source of equal intensity due to obstacle avoidance. Detection of a sound target with an intensity near the sensor threshold is stabilized through the cooperative forces within the field.

(c) The implementation of the dynamic field for wall representation on a small autonomous vehicle enabled it to follow walls with various shapes (e.g. planar, circular and concave corners). Decision making allowed to select a wall and hysteresis permitted to maintain the decision stable even when new walls were encountered during the motion course.

9.2 Related work

Work related to the individual points addressed throughout this dissertation was already discussed in the corresponding chapters. We focus now on reviewing projects which also applied the dynamic approach to behavior generation and which are therefore closely related.

Schöner and Dose (1992), simulated a dynamics of heading direction for obstacle avoidance and target acquisition and implemented the obstacle avoidance module on a mobile platform. A competitive non-linear dynamics was used to build a representation of the navigable space around the robot. Sensory information was visual. The path velocity was kept constant.

Engels and Schöner (1995) implemented a dynamics of heading direction for obstacle avoidance and target acquisition on a mobile platform equipped with vision. This dynamics was designed as a dynamic field. A dynamic field was used as a memory layer in world coordinates in which the positions of obstacles were stored. The path velocity was also kept constant.

Neven and Schöner (1996) implemented a dynamics of angular and path velocities that permitted a vision-guided mobile robot to exhibit obstacle avoidance and homing. Obstacle avoidance is based on extracting time-to-contact information from optical flow.

Steinhage (1998) developed and simulated a fully dynamic model of complex navigation behavior inspired on biological systems. Complex behavior is achieved through a non-linear competitive dynamical system of neural variables that activate and deactivated behaviors. This solution enables to generate sequences of behaviors without explicit representation of the entire sequence. The overall system is flexible and quite stable.

Bergener et al (1999) developed several behavioral skills for an anthropomorphic robot equipped with stereo vision. Dynamic fields are used to generate behavioral goals depending on the constraints of reaching a target and avoiding

obstacles: A one dimensional field specifies the next movement direction of the mobile platform and a two dimensional field determines the end-effectors' 3-d position. For technical reasons the control of the manipulator arm is not performed in close loop with sensory information. The behavior is impressively smooth and human-like (See also Bergener and Steinhage, 1998; Bruckoff and Dahm, 1998; Dahm, Bruckoff and Joublin, 1998).

Large, Christensen and Bajcsy (1999) simulated a dynamic model for cooperation between two agents. To control the strength of attractors they make use of a competitive non-linear dynamics.

The work presented in this dissertation has several aspects in common with these projects. Nevertheless, the following is unique to this thesis:

- Motion control through attractor dynamics in close loop with sensory information.
- The use of low-level sensory information to build dynamical systems the attractors of which generate the desired overt behavior.
- The use of dynamic fields to generate cognitive abilities based on low-level sensory information.
- To formalize these cognitive behaviors as asymptotically stable solutions of dynamic fields.
- The way dynamic fields are coupled with the behavioral dynamics that brings about the actual motion behavior.
- The implementation of fully dynamical architectures in robotic platforms.
- The use of computationally modest vehicle platforms.

It is worthwhile to finish this section by addressing concisely two other approaches to robotics which also make use of dynamical system theory albeit in a different form. Smithers (1994) and Beer (1995) are the proponents of two other dynamical systems approaches to robotics. Both place emphasis on the theoretical issues of the interchange of information between the agent and its environment. Beer uses dynamics as a theoretical tool for the analysis of systems rather than as a tool for design. To generate behavior he uses the transient solutions of neural networks. Smithers distinguishes between interaction and infrastructure dynamics. He proposes some principles of design which may enable a rational choice of system parameters and architectures.

The fundamental differences of these two approaches with our approach is that we insist on identifying adequate planning variables, which permit to design behaviors independently, on the principle of representation of information through dynamic fields and the on concept of mapping behaviors on attractor solutions.

9.3 Outlook

The work described in this dissertation offers various possibilities for further research. Therefore, we conclude with a prospect for future work.

In a project of multi-robot teams, at the department of Industrial Electronics at the University of Minho (Guimarães, Portugal), the idea of using dynamic fields to represent directional information obtained from low-level sensors will be explored to generate more complex movement behavior of robotic platforms. Two examples are: (a) Formation control: a vehicle can be made to steer at a particular orientation with respect to a leader vehicle which emits a specific signal (for example, a sound) or it is identified by a an intrinsic property (for instance, its color). To achieve successful formation control some basic cognitive abilities are required. (b) Cooperativity among robots: The fact that a direction is explicitly represented will be used to communicate that information among robots. Such information will be then integrated with other sources of information in order to achieve more complex strategies.

A project in the interface between cognitive science and psychology will make use of one of the autonomous robot architectures developed in this thesis to implement a model of infant spatial orientation behavior. This interdisciplinary project will be in collaboration with the *Equipe de Dynamique*, at the CRNC-CNRS in Marseille (France), and the *Infants motor lab* at the University of Indiana (Blomington, USA).

The transfer of the cognitive abilities, studied in this dissertation, to an anthropomorphic robot and to an industrial manipulator arm equipped with vision are planned. This will be a project in collaboration with the *Institut für Neuroinformatik* at the University of Bochum (Germany). The aim is to develop a dynamic field model that represents a reaching target in terms of the end-effector configuration required for a successful reach (movement direction and amplitude). Such representation must support target detection, target identification, estimation of target location, selection of one out of multiple detected targets, storage of target location in short-term memory, continuous updating of memory and deletion of memorized target information after a characteristic period of time. This cognitive target representation system will be based on different but convergent sources of sensory information.

We plan to extend the concepts of the dynamic approach to robotics toward the development of *Automatic Diagnostic Tools*, that is, to build an active and possibly autonomous system endowed with the ability to tune, monitor and diagnose the performance of the autonomous robot.

Appendix A

Appendix of Chapter 6: Dynamical properties of one-dimensional homogeneous fields of lateral-inhibition type

The dynamics of one-dimensional homogeneous fields of lateral-inhibition type was analyzed analytically by Amari (1977), and Kishimoto and Amari (1979). Their studies provide valuable information about the influence of the parameters on the existence and stability of certain types of equilibrium solutions.

Here we apply some of their studies to explore the particular dynamic properties of the field equation (Equation 6.2) we are using:

i) Rectangular interaction kernel with local excitation and global constant inhibition (i.e. Equation 6.4).

ii) Circular, and thus finite, behavioral dimension (i.e. $[0, 2\pi]$ rad).

iii) Ramp threshold function with saturation (i.e. Equation 6.3).

We first review some analytical results obtained for the case where the threshold function, $\Theta(\cdot)$, is a Heaviside step function. These results are then used to study the existence and stability of equilibrium solutions when the threshold function is a ramp function with saturation.

A.1 Dynamics of the field with Heaviside threshold function

When the threshold function, $\Theta(\cdot)$, is a Heaviside step function analytical results can be obtained. The dynamics of pattern formation within the field can be categorized

in different equilibrium solution types. The classes of equilibrium solutions that are interesting, in the context of the work presented in this dissertation, are the following:

(1) $\emptyset$-solutions which are characterized by $u(\psi) \leq 0 \;\; \forall \psi \in [0, 2\pi]$ rad (no excited region).

(2) a-solutions with $u(\psi) > 0$ in the interval (ψ_1, ψ_2). This corresponds to a pattern of activation with a localized peak of positive activation of length $a = \psi_2 - \psi_1 > 0$ in the field.

(3) N-b solutions which consist of a pattern of activation with N localized peaks of positive activation each with length b and separated by more than $l_{\text{coop}}/2$.

A.1.1 Existence and stability of equilibrium solutions

For simplicity we assume here a homogeneous input, $S(\psi, t) \equiv s_{\text{o}}$, and discuss the case of a space variant input pattern in Section A.1.2. The existence regimes of the three types of equilibrium solutions enumerated above are restricted by the following theorem.

Theorem A.1 (Existence of equilibrium solutions) *Let be* $W(\psi) = \int_0^{\psi} w(\psi')d\psi'$. *Then with constant input activation* $S(\psi, t) \equiv s_{\text{o}}$*:*

(1) There exists a $\emptyset$*-solution if and only if* $s_{\text{o}} + h < 0$.

(2) There exists an a*-solution (pattern of activation with a localized peak of positive activation) if and only if* $s_{\text{o}} + h < 0$ *and* $a > 0$ *satisfies*

$$W(a) + s_{\text{o}} + h = 0. \tag{A.1}$$

(3) There exists a N*-*b *solution if and only if* $s_{\text{o}} + h < 0$, $b > 0$ *and* $(\mathsf{N} - 1)k_{\text{n}} > 0$ *satisfies*

$$W(b) + s_{\text{o}} - (\mathsf{N} - 1)k_{\text{n}}b + h = 0. \tag{A.2}$$

For proofs of (1) and (2) see Amari (1977) and see Erlhagen (1997) for a proof of (3). The stability of these equilibrium solutions is determined by the following theorem:

Theorem A.2 (Stability of relevant equilibrium solutions) [1] *With the same assumption as in theorem A.1 and* $W_{\text{m}} = \max_{\psi>0} W(\psi) = l_{\text{coop}}k_{\text{p}}/2$, *and* $W_{\infty} = \lim_{\psi \to 2\pi} W(\psi) = k_{\text{p}}l_{\text{coop}}/2 - k_{\text{n}}(\pi - l_{\text{coop}}/2) < 0$ *it follows:*

[1] Stable equilibrium solutions are patterns of activation which the field can retain persistently under a constant stimulation level. It should be noted that "stable" implies "wave-form stable" in the more strict sense.

(1) The $\emptyset$-solution is always asymptotically stable.

(2) The a-solution is asymptotically stable if $dW(a)/da < 0$ (or $w(a) < 0$) and unstable if $dW(a)/da > 0$ (or $w(a) > 0$). An asymptotically stable a-solution exists for $-W_{\mathrm{m}} < h + s_{\mathrm{o}} < 0$.

(3) The N-b solution is asymptotically stable if $dW(b)/db < 0$ and unstable if $dW(b)/db > 0$. An asymptotically stable N-b solution exists for

$$-W_{\mathrm{m}} < -(\mathsf{N}-1)k_{\mathrm{n}}l_{\mathrm{coop}}/2 + h + s_{\mathrm{o}} < 0.$$

For proofs see Amari (1977) and Erlhagen (1997). Note that a stable a-solution implies the existence of a $\emptyset$-solution. This means that the field is bistable. Furthermore, the existence of a stable N-b solution implies the existence a stable a-solution and a $\emptyset$-solution. In this case the field is multi-stable.

These two theorems imply that we can easily check the existence and stability of equilibrium solutions graphically. Figure A.1 depicts the graphical solution of Equations A.1 and A.2 and the stability of the corresponding equilibrium solutions.

A.1.2 Behavior of the field in response to a single-peaked input stimulation

In the following we assume that condition (2) in Theorem A.2 is fulfilled but not condition (3), that is, only one self-stabilized peak of a certain width, a_o can persist within the field.

We first consider the response of the field to a single-peaked stimulus $S(\psi)$ centered at ψ_{input}. When the amplitude of the input peak is very large compared to the non-linear part of the field dynamics described by the integral term, the field behaves as a linear system with the asymptotically stable equilibrium solution $u(\psi) \approx S(\psi) + h$. For our applications this behavior is not useful because the field only reproduces the input pattern. When the strength of the input stimulus is small the pattern of activation that will evolve in the field in response to such input depends on the initial state of activation. Two cases have to be distinguished:

i) The initial state of the field is a stable localized peak of positive activation with width a_o centered at ψ_o. The input peak is centered at ψ_{input} and is wide enough to overlap with the interval $(\psi_o - a_o/2,\ \psi_o + a_o/2)$. In response to the input the peak of activation moves in the direction of increasing stimulus, searching for the maximum of $S(\psi)$. It stops to when the input stimulation at the right and at the left boundary of the positive peak are equal. At the same time the width of the peak of positive activation changes slightly (for more details see Amari, 1977).

   If the input peak is instead positioned such that the two intervals do not overlap then to evolve a new peak centered at field position ψ_{input} the input stimulation at this site has to overcome not only the global inhibition level

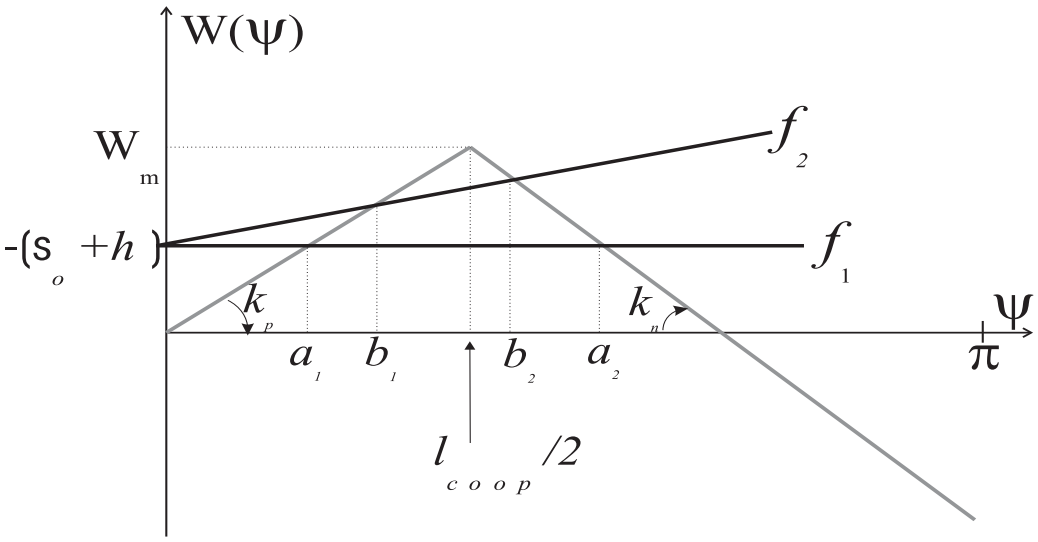

Figure A.1: The solutions of the Equations A.1 and A.2 are the intersection points of curves $f_1(\psi) = -(h + s_\mathrm{o})$ and $f_2(\psi) = (\mathsf{N} - 1)k_\mathrm{n}\psi - h - s_\mathrm{o}$ with $W(\psi)$ respectively. The slope of $W(\psi)$ at the intersection points indicates the stability of the corresponding equilibrium solutions. We interpret the plot: The curve $f_1(\psi)$ intersects the curve $W(\psi)$ at the two points a_1 and a_2. This means that two a-solutions exist. One a-solution with a localized peak of length a_1 (a_1-solution) and another a-solution with a peak of length a_2 (a_2-solution). The slope of $W(\psi)$ at $\psi = a_1$ is positive which indicates that the equilibrium solution a_1-solution is unstable. Conversely, the negative slope of $W(\psi)$ at $\psi = a_2$ denotes that the a_2-solution is stable. The curve $f_2(\psi)$ intersects the curve $W(\psi)$ at the two points, b_1 and b_2. The field has therefore also a N-b solution where the peaks have length b_1 (N-b_1 solution) and a N-b solution where the peaks have length b_2 (N-b_2 solution). $W(\psi)$ has positive slope at $\psi = b_1$ and negative slope at $\psi = b_2$. This reveals that the N-b_1 solution is unstable while the N-b_2 solution is stable.

h but also the additional inhibition ($-k_\mathrm{n}a_o$) created at this site by the peak centered at ψ_o with length a_o. Thus, to guarantee that the field will "delete" the previous peak and that it will evolve a new peak, centered at ψ_input, the input strength $S(\psi_\mathrm{input})$ at this site, must exceed the value $k_\mathrm{n}a_o + h$, i.e. $S(\psi_\mathrm{input}) > k_\mathrm{n}a_o + h$, and the input width has to fulfill the condition $a_\mathrm{input} > a_o$ (Erlhagen, 1997).

ii) When the initial state of the field is the flat solution, $u(\psi) = h < 0$ everywhere, the field can remain in the off-state or it can evolve a localized peak on activation depending of the strength of the input stimulation. The question we have to address is, how much input energy is necessary to bring the system from the $\emptyset$-solution to a stable a-solution? For a mono-modal input the *critical stimulus energy* that triggers this transition depends on the intensity and on the length of the input peak. To get an estimation of this critical energy we consider an uniform input stimulation of intensity $s\prime$ and length $a\prime$. The field

activation converges to a stable a-solution if the following condition is satisfied

$$W(a) = -(h + s\prime). \tag{A.3}$$

The critical length $a(s\prime)$, which depends on the stimulus strength $s\prime$, can be found by inverting the function $W(a)$ in the interval $0 \leq a \leq l_{\text{coop}}/2$, i.e.

$$a(s\prime) = W^{-1}\left(-(h + s\prime)\right) \tag{A.4}$$

which can be accomplished graphically.

A.1.3 Behavior of the field in response to a multi-peaked input stimulation

In our robotic applications we are interested in the $\emptyset$-solution and a-solution only. Thus, we have to tune the parameters of the field to avoid the existence of $\mathsf{N} - b$ solutions. This is accomplished by making the inhibition strength k_n sufficiently large such that the condition (2) in theorem A.2 is satisfied but not condition (3). This way the field exhibits a competition process among various stimulated sites and eventually only one self-stabilized peak of positive activation evolves. The field converges to a a-solution in response to a multi-modal input stimulation.

A.2 Dynamics of the field with a ramp threshold function with saturation

Kishimoto and Amari (1979) have demonstrated that the previous theorems can be generalized to monotonic increasing threshold functions:

$$\Theta(u) = \begin{cases} 0 & \text{for } u < 0 \\ \varphi(u) & \text{for } 0 \leq u \leq \mathsf{TH} \\ 1 & \text{for } u > \mathsf{TH} \end{cases} \tag{A.5}$$

where $\varphi(u)$ is an arbitrary monotonically increasing differentiable function with $\varphi(0) = 0$ and $\varphi(1) = 1$. The ramp threshold function with saturation can be seen as piecewise linear approximation to the class of threshold functions defined by A.5.

To announce the theorems that constrain the existence and stability of the different types of equilibrium solutions we need to introduce the following assumptions:

Let $\Theta_0(\cdot)$ and $\Theta_{\text{TH}}(\cdot)$ be Heaviside functions with different thresholds, respectively,

$$\Theta_0(u) = \begin{cases} 0 & \text{for } u \leq 0 \\ 1 & \text{for } u > 0 \end{cases} \tag{A.6}$$

$$\Theta_{\text{TH}}(u) = \begin{cases} 0 & \text{for } u \leq \mathsf{TH} \\ 1 & \text{for } u > \mathsf{TH} \end{cases} \tag{A.7}$$

Then the monotonic threshold function $\Theta(\cdot)$ (i.e. Equation A.5) satisfies:

$$\Theta_0(\cdot) \geq \Theta(\cdot) \geq \Theta_{\mathrm{TH}}(\cdot) \tag{A.8}$$

Lets call Θ-field a field with a threshold function as defined by Equation A.5, and lets call Θ_0-field and Θ_{TH}-field fields with threshold functions as defined by Equations A.6 and A.7 respectively. Throughout the rest of this section we further assume a constant and stationary input stimulation $S(\psi, t) \equiv s_{\mathrm{o}}$ to the field. Under these assumptions the following theorem determines the existence of a $\emptyset$-solution:

Theorem A.3 (Existence of $\emptyset$-solution) *A Θ-field has the $\emptyset$-solution if and only if the corresponding Θ_0-field has the $\emptyset$-solution.*

Lemma A.1 (Existence of a-solutions) *Both the Θ_0-field and Θ_{TH}-field have a stable and an unstable pattern of activation with a localized positive peak if and only if*

$$\mathsf{TH} - h - W_{\mathrm{m}} < s_{\mathrm{o}} < -h$$

For proofs of see Kishimoto and Amari (1979).

Theorem A.4 (Existence of a-solutions) *If the Θ_0-field and the Θ_{TH}-field have stable localized peak equilibrium solutions $u_0(\psi)$ and $u_{\mathrm{TH}}(\psi)$, respectively, then the Θ-field has a localized peak equilibrium solution satisfying*

$$\Theta_0[u_0(\psi)] \geq \Theta[u(\psi)] \geq \Theta_{\mathrm{TH}}[u_{\mathrm{TH}}(\psi)]$$

Theorem A.5 (Stability of a-solutions) *The Θ_{TH}-field has a stable localized peak equilibrium solution when both the Θ_0-field and the Θ_{TH}-field have a stable one.*

Theorem A.4 can be used to yield an estimation for a lower bound, $m_{\min}$, of the slope m of a ramp threshold function that still guarantees the existence and stability of a self-stabilized peak (i.e. a a-solution). There exist a maximum permitted threshold, $\mathsf{TH} = \mathsf{TH}_{\max}$, in Equation A.7 above which the excitatory forces within the field are not sufficiently strong anymore to trigger the evolution of a stable localized activity distribution. Thus, it follows that $m_{\min}$ and $\mathsf{TH}_{\max}$ are interrelated. Erlhagen (1997) proved that the relationship between these two parameters that guarantees the stability of a a-solution is

$$m_{\min} = \frac{1}{\mathsf{TH}_{\max}}. \tag{A.9}$$

Appendix B

Appendix of Chapter 7: Interval limits

$$
\begin{aligned}
\psi_a &= \psi_{\text{wall}} - \Delta\psi_{\text{w}} - \pi/2 \\
\psi_b &= \psi_{\text{wall}} - \Delta\psi_{\text{w}} + \pi/2 \\
\psi_c &= \psi_{\text{wall}} - \Delta\psi_{\text{w}} + 3\pi/2 \\
\psi_d &= \psi_{\text{wall}} + \Delta\psi_{\text{w}} - \pi/2 \\
\psi_e &= \psi_{\text{wall}} + \Delta\psi_{\text{w}} + \pi/2 \\
\psi_f &= \psi_{\text{wall}} + \Delta\psi_{\text{w}} + 3\pi/2 \\
\psi_g &= \psi_{\text{wall}} + \Delta\psi_{\text{w}} + \pi/2 \\
\psi_h &= \psi_{\text{wall}} + \Delta\psi_{\text{w}} + 3\pi/2 \\
\psi_i &= \psi_{\text{wall}} + \Delta\psi_{\text{w}} + 5\pi/2 \\
\psi_j &= \psi_{\text{wall}} - \Delta\psi_{\text{w}} + \pi/2 \\
\psi_l &= \psi_{\text{wall}} - \Delta\psi_{\text{w}} + 3\pi/2 \\
\psi_m &= \psi_{\text{wall}} - \Delta\psi_{\text{w}} + 5\pi/2
\end{aligned}
$$

Bibliography

[1] S Amari. Dynamics of pattern formation in lateral-inhibition type neural fields. *Biological Cybernetics*, 27:77–87, 1977.

[2] Y Ando, T Tsubouchi, and S Yuta. A reactive wall following algorithm and its behavior of an autonomous mobile robot with sonar ring. *Journal of Robotics and Mechatronics*, 8(1):79–86, 1996.

[3] R C Arkin. Motor schema-based mobile robot navigation. *The International Journal of Robotics Research*, 8(4):92–112, 1989.

[4] R C Arkin. *Behavior-Based Robotics*. MIT Press, Cambridge, 1998.

[5] C Balkenius. *Natural Intelligence in Artificial Creatures*. Lund University Cognitive Studies, 37, 1995.

[6] J Barraquand and J-C Latombe. Robot motion planning: a distributed representation approach. *The International Journal of Robotics Research*, 10, 1990.

[7] G Bauzil, M Briot, and P Ribes. A navigation subsystem using ultrasonic sensors for the mobile robot Hilary. In *First Int. Conf. on Robot Vision and Sensory Control*, pages 47–58, Stratford–upon–Avon, UK, 1981.

[8] R D Beer. A dynamical systems perspective on agent-environment interaction. *The AI Journal*, 72:173–215, 1995.

[9] T Bergener, C Bruckhoff, P Dahm, H Janssen, F Joublin, R Menzner, A Steinhage, and W von Seelen. Complex behavior by means of dynamical systems for an anthropomorphic robot. In *Organization of Computation in Brain-like Systems, 1999 Special Issue of Neural Networks*, October 1999.

[10] T Bergener and A Steinhage. An architecture for behavioral organization using dynamical systems. In C Wilke, S Altmeyer, and T Martinetz, editors, *Abstracting and Synthetesizing the Principle of Living Systems: Proceedings of the Third German Workshop on Artificial Life*, pages 31–42. Verlag Harri Deutsh, 1998.

[11] E Bicho, P Mallet, and G Schöner. Using attractor dynamics to control autonomous vehicle motion. In *Proceedings of the 24th Annual Conference of the IEEE Industrial Electronics Society (IECON98)*, pages 1176–118, Aachen-Germany, Aug/Set IEEE, Piscataway, NJ, 1998.

[12] E Bicho, P Mallet, and G Schöner. Target representation on an autonomous vehicle with low-level sensors. *International Journal of Robotics Research, in press*, 1999a.

[13] E Bicho, P Mallet, and G Schöner. Using attractor dynamics to control autonomous vehicle motion. *IEEE Transaction on Robotics and Automation, submitted*, 1999b.

[14] E Bicho and G Schöner. The dynamic approach to autonomous robotics demonstrated on a low-level vehicle platform. *Robotics and autonomous systems*, 21:23–35, 1997a.

[15] E Bicho and G Schöner. Target position estimation, target acquisition, and obstacle avoidance. In *Proceedings of the IEEE International Symposium on Industrial Electronics (ISIE'97)*, pages SS13–SS20. IEEE, Piscataway, NJ, 1997b.

[16] J Blauert. *Spatial Hearing - The Psychophysics of Human Sound Localization.* MIT Press, Cambridge MA, USA, 1996.

[17] J Borenstein and Y Koren. Real-time obstacle for fast mobile robots. *IEEE Transactions on Systems, Man and Cybernerics*, 19(5):1179–1187, Sep/Oct 1989.

[18] V Braitenberg. *Vehicles. Experiments in Synthetic Psychology.* MIT Press, Cambridge, Mass., 1984.

[19] R W Brockett. Asymptotic stability and feedback stabilization. In *Differential Geometric Control Theory*, number ISBN 3-7643-3091-0. Birkhäuser, 1983.

[20] R A Brooks. Solving the find-path problem by good representations of free space. *IEEE Transactions on Systems, Man and Cybernetics*, SMC-13(3):190–197, March-April 1983.

[21] R A Brooks. A robust layered control system for a mobile robot. *IEEE Journal of Robotics and Automation*, RA-2:12–23, 1986.

[22] R A Brooks. A robot that walks: Emergent behavior from a carefully evolved network. *Neural Computation*, 1(2):253–262, 1989.

[23] R A Brooks. Intelligence without representation. *Artificial Intelligence*, 47:139–160, 1991.

[24] R A Brooks. New approches to robotics. *Science*, 253:1227–1232, 1991.

[25] R A Brooks. Artificial life and real robots. In F J Varela and P Bourgne, editors, *Towards a Practice of Autonomous Systems: Proceedings of the first European Conference on Artficial Life*. The MIT Press, 1992.

[26] R A Brooks. From earwigs to humans. *Robotics and Autonomous Systems*, 20:291 – 304, 1997.

[27] R A Brooks and J H Connell. Asynchronous distributed control system for a mobile robot. *SPIE, Mobile Robots*, 727:77–84, 1986.

[28] C Bruckhoff and P Dahm. Neural fields for local path planning. In *Proceedings of the International Conference on Intelligent RObotic Systems (IROS 98)*, pages 1431–1436, October 1998.

[29] W H Cade and E S Cade. Male mating sucess, calling and searching behavior at high and low densities in the field cricket, gryllus integer. *Animal Behavior*, 43:49–56, 1992.

[30] S Cameron. Motion planning and collision avoidance with complex geometry. In *IECON 98, 24th Annual Conference of the IEEE Industrial Electronics Society*, volume 2, pages 2222–2226, Aachen-Germany, Aug 31 - Sep 4 1998.

[31] R Chatila. Representations + reason + reaction → robot intelligence. In T Kanade and R Paul, editors, *Robotics Research — Tthe Sixth International Symposium*, pages 387–397. The International Foundation for Robotics Research, Cambridge, MA, U.S.A., 1994.

[32] T M Chen and R C Luo. Development and integration of multiple behaviors for autonomous mobile robot navigation. In *IECON 98, 24th Annual Conference of the IEEE Industrial Electronics Society*, volume 2, pages 1146–1151, Aachen-Germany, Aug 31 - Sep 4 1998.

[33] R Chipalkatti and M A Arbib. The prey localisation model: A stability analysis. *Biological Cybernetics*, 57:287–299, 1987.

[34] J H Connell. *Minimalist Mobile Robotics*. Academic Press, 1990.

[35] C I Connolly, J B Burns, and R Weiss. Path planning using Lapalce's equation. *IEEE Robotics and Automation*, pages 2102–2106, 1990.

[36] I Cox. Blanche-an exprimental in guidance and navigation of an autonomous robot vehicle. *IEEE Transactions on Rotocis and Automation*, 7(2):193–204, 1991.

[37] I J Cox and G T Wilfong, editors. *Autonomous robot vehicles*. Springer Verlag, Berlin, 1990.

[38] J D Crawford. Introduction to bifurcation theory. *Reviews of Modern Physics*, 63(4):991–1037, 1997.

[39] P Dahm and C Bruckhoff. Autonomous decision making in local navigation. In *From Animals to Animats 5: Proceedings of the Fifth International Conference on Simulation of Adaptive Behavior (SAB 98)*, pages 229–233. MIT Press, August 1998.

[40] P Dahm, C Bruckhoff, and F Joublin. A neural field approach to robot motion control. In *Proceedings of the 1998 IEEE International Conference on Systems, Man, and Cybernetics (SMC'98)*, pages 3460–3465, 1998.

[41] O Duda. Auditory localization demonstrations. *Acustica - Acta Acusticca*, 82(2):346–355, Mar 1996.

[42] C Engels and G Schöner. Dynamic fields endow behavior-based robots with representations. *Robotics and autonomous systems*, 14:55–77, 1995.

[43] W Erlhagen. *Lokalisierte, stationäre Verteilung in neuronalen Feldern (Localized stationary distribuitions in neural fields)*. Harri Deutsch, Frankfurt, 1997.

[44] J P Ewert. The neural basis of visually guided robots. *Sci. Am.*, 230:34–42, 1974.

[45] D Feng and B Krogh. Satisficing feedback strategies for local navigation of autonomous mobile robots. *IEEE Transactions on Systems, Man and Cybernetics*, 20(6):476–488, November-December 1990.

[46] A Fujimori, P N Nikiforuk, and M M Gupta. Adaptive navigation of mobile robots with obstacle avoidance. *IEEE Transactions on Robotics and Automation*, 13(4):596–602, August 1997.

[47] M A Giese. *Dynamic neural model for motion perception*. Kluwer Academic, 1999.

[48] G Giralt. An integrated navigation and motion control system for autonomous multisensory mobile robots. pages 191–214. The International Foundation for Robotics Research, Cambridge, MA, U.S.A., 1984.

[49] G Giralt. Robot autonomoy and mashine intelligence: Trends and critical issues — A post-symposium report. In T Kanade and R Paul, editors, *Robotics Research — Tthe Sixth International Symposium*, pages 363–370. The International Foundation for Robotics Research, Cambridge, MA, U.S.A., 1994.

[50] K Y Guentchev and J Weng. Learning-based three dimensional sound localization using a coplanar array of microphones. In *Intelligent Environments Symposium*, Proc. 1998 AAAI Spring Symposium Series, Stanford University, Mar 23-25 1998.

[51] D H House. A model of the visual localization of prey by frog and toad. *Biological Cybernetics*, 58:173–192, 1988.

[52] H Hu and M Brady. Dynamic path planning with uncertainty for mobile robots in manufacturing. *IEEE Transactions on Robotics and Automation*, 13(5):760–766, October 1997.

[53] J Iijima, S Yuta, and Y Kanayama. Elementary functions of a self-contained robot YAMABICO 3.1. In S J et al. Hanson, editor, *Proc. 11th Int. Symp. Ind. Robots*, pages 211–218, Tokyo, 1993. The MIT Press.

[54] J Jones and A M Flynn. *Mobile Robots – Inspiration to implementation.* A K Peters, 289 Linden Str., Wellesley, MA 02181 USA, 1993.

[55] K Kedem and M Sharir. An automatic motion planning system for a convex polygonal mobile robot in 2-dimensional polygonal space. In *Proceedings of the 4th Annual Symposium on Computational Geometry*, pages 239–340. Association for Computing Mashinery, 1988. reprinted in Cox and Wilfong (eds.) (1990).

[56] O Khatib. Real-time obstacle avoidance for manipulators and mobile robots. *International Journal Robotics Research*, 5:90–98, 1986.

[57] B K Kim and K G Shin. Minimum-time path planning for robot arms and their dynamics. *IEEE Transactions on Systems, Man and Cybernetics*, SMC-15(2):213–223, 1985.

[58] K Kishimoto and S Amari. Existence and stability of local excitations in homogeneous neural fields. *Journal of Mathematical Biology*, 7:303–318, 1979.

[59] K Kopecz and G Schöner. Saccadic motor planning by integrating visual information and pre-information on neural, dynamic fields. *Biological Cybernetics*, 73:49–60, 1995.

[60] D Y Kortenkamp, R P Bonasso, and R Murphy. *Artificial Intelligence and Mobile Robots.* AAAI Press, Cambridge, 1998.

[61] J R Koza. Evolution of a subsumption architecture that performs a wall following task for an autonomous mobile robot. In S J et al. Hanson, editor, *Computational Learning Theory and Natural Learning Systems.* The MIT Press, 1994.

[62] Y Kuwana and I Shimoyama. A pheromone-guided mobile robot that behaves like a silkworm moth with living antennae as pheromone sensors. *International Journal of Robotics Research*, 17(9):924–933, 1998.

[63] E W Large, H I Christensen, and R Bajcy. Scaling the dynamic approach to path planning and control: Competition amoung behavioral constraints. *International Journal of Robotics Research*, 18(1):37–58, 1999.

[64] J C Latombe. *Robot Motion Planning*. Kluwer Academic Publishers, 1991.

[65] J P Laumond. Motion planning for mobile robots: From academic to practical issues. In *Robotics Research, the sixth International Symposium, The International Foundation for Robotics Research*, pages 21–27, Cambridge, USA, 1993.

[66] M Liggins, I Kadar, and V Vannicola. Distributed fusion architectures and algorithms for taeget tracking. In *Proc. of the IEEE*, volume 85, January 1997.

[67] T Lozano-Perez and W A Wesley. An algorithm for planning collision free paths among polyhedral obstacles. *Communications of the Association for Computing Mashinery ACM*, 22(10), 1979.

[68] V J Lumelsky and A A Stepanov. Dynamic path planning for a mobile automaton with limited information on the environment. *IEEE Transactions on Automatic Control*, AC-31(11):1058–1063, November 1986.

[69] V J Lumelsky and A A Stepanov. Path planning strategies for a point mobile automation moving amidst unknown obstacles of arbitrary shape. *Algorithmica*, 1987.

[70] H H Lund, B Webb, and J Hallam. A robot attracted to the cricket species *Gryllus bimaculatus*. In P Husbands and I Harvey, editors, *Fourth European Conference on Artificial Life*, pages 246–255. MIT Press, 1997.

[71] H Mallot, H Bülthoff, J J Little, and S Bohrer. Inverse perspective mapping simplifies optical flow computation and obstacle detection. *Biological Cybernetics*, 64:172–185, 1991.

[72] M J Mataric. A distributed model for mobile mobile robot environment-learning and navigation. In *Technical report, AI-TR-1288*, MIT Artficial Intellligence Laboratory, 1990.

[73] M J Mataric. Behavior-based control: Main properties and implications. In *Proceedings of Workshop on Intelligent Control Systems, International Conference on Robotics and Automation*, pages 169–175, Nice, France, May 1992.

[74] M J Mataric. Behavior-based robotics as a tool for synthesis of artificial behavior and analysis of natural behavior. *Trends in Cognitive Sciences*, 2(3):82 – 87, 1998.

[75] J McCarthy, M Minsky, N Rochester, and C Shannon. A proposal for the darthmounth summer research project on artificial intelligence. August 1955.

[76] Q Meng, D Liu, M Zhang, and Y Sun. Wall-following by an autonomously guided vehicle (agv) uisng a new-fuzzy-I(integration) controller. *Robotica*, 17:79–86, 1999.

[77] A Mills. Auditory localization. *Foundations of Modern Auditory Theory*, 2:301–348, 1972.

[78] H Neven. *Dynamics for vision-guided autonomous mobile robots*. Fortschrittberichte, Düsseldorf, 1997.

[79] H Neven and G Schöner. Neural dynamics parametrically controlled by image correlations organize robot navigation. *Biological Cybernetics*, 75:293–307, 1996.

[80] N J Nilson. A mobile automation: An application of artficial intelligence techniques. In *Proceedings of 1st Int. Joint Conf. on Artificial Intelligence*, pages 509–520, washigton, DC, 1969.

[81] L Perko. *Differential Equations and Dynamical Systems*. Springer Verlag, Berlin, 1991.

[82] A Pruski. Robots mobiles autonomes. *Traité Mésures et Contrôle des Techniques de l'Ingénieur*, R7(850):1–18, 1999.

[83] E Rimon and D E Koditschek. Exact robot navigation using artificial potential functions. *IEEE Transactions on Robotics and Automation*, 8(5):501–518, 1992.

[84] S J Ross, J M Daida, C M Doan, T F B Begey, and J McClain. Variations in evolution of subsumption architectures using genetic programming: The wall following robot revisited. In JR Koza, D E Goldberg, D B Fogel, and Riolo R L, editors, *Proceedings of the First Annual Conference*, July 1996.

[85] E R Scheinerman. *Invitation to Dynamical Systems*. Prentice Hall, 1996.

[86] H Schöne. *Spatial Orientation – The spatial control of behavior in animals and man*. Princeton University Press, Princeton, NJ, 1984.

[87] G Schöner and M Dose. A dynamical systems approach to task-level system integration used to plan and control autonomous vehicle motion. *Robotics and Autonomous Systems*, 10:253–267, 1992.

[88] G Schöner, M Dose, and C Engels. Dynamics of behavior: Theory and applications for autonomous robot architectures. *Robotics and Autonomous Systems*, 16:213–245, 1995.

[89] J T Schwartz and M Sharir. On the piano movers' problem: I. the case of a two-dimensional rigid polygonal body moving amidst polygonal barriers. *Communications in Pure and Applied Mathematics*, 36:345–398, 1983.

[90] S Shama, N Shen, and P Gopalawamy. Stereausis: Binaural processing without neural delays. *Journal of the Acoustical Society of America*, 86:989–1006, Mar 23-25 1989.

[91] K.G. Shin and N. D. McKay. Minimum-time control of robotic manipulators with geometric path constraints. *IEEE Transactions on Automation and Control*, AC-30(6):531–541, June 1985.

[92] J S Singh and M D Wagh. Robot path planning using intersecting convex shapes. *IEEE Transactions on Robotics and Automation*, RA-3:101–108, 1987.

[93] T Smithers. What the dynamics of adaptive behaviour and cognition might look like in agent-environment systems. In *Presented at the workshop: On the Role of Dynamics in Representation in Adaptive Behaviour and Cognition, 9/10 December 94, San Sebastian, Spain*, 1994.

[94] A Steinhage. *Dynamical Systems for the Generation of Navigation Behavior*. Shaker Verlag, Aachen, 1998.

[95] A Steinhage and G Schöner. Self-calibration based on invariant view recognition: Dynamic approach to navigation. *Robotics and Autonomous Systems*, 20:133–156, 1997.

[96] R Takahashi and R J Schilling. Motion planning in a plane using generalized voronoi diagrams. *IEEE Transactions on Robotics and Automation*, 5(2):143–150, April 1989.

[97] P Turennout, G Honderd, and L J Schelven. Wall-following control of a mobile robot. In *Proceedings of the 1992 IEEE International Conference on Robotics and Automation*, pages 280–285, Nice, France, May 1992.

[98] W G Walter. *The living brain (reprinted 1963)*. Norton, New York, 1953.

[99] B Webb. Using robots to model animals: a cricket test. *Robotics and Autonomous Systens*, 16:117–134, 1995.

[100] H R Wilson and J D Cowan. A mathematical theory of the functional dynamics of cortical and thalamic nervous tissue. *Kybernetik*, 13:55–80, 1973.

[101] T Yata, L Kleeman, and S Yuta. Wall following using angle information measured by a single ultrasonic transducer. In *Proceedings of the 1998 IEEE International Conference on Robotics and Automation*, pages 1590–1596, May 1998.

[102] R Zapata, P Lepinay, and P Thompson. Reactive behaviors of fast mobile robots. *Journal of Robotic Systems*, 11(1):13–20, 1994.

Index